The Hashemite Kingdom of Jordan
Scientific Research Support Fund
The Hashemite University

JJEES

Jordan Journal of Earth and Environmental Sciences

Volume (11) Number (2)

Cover photo © Dr. Ahmed Gharaibeh

JJEES is an International Peer-Reviewed Research Journal

ISSN 1995-6681 jjees.hu.edu.jo June 2020

Jordan Journal of Earth and Environmental Sciences (JJEES)

JJEES is an International Peer-Reviewed Research Journal, Issued by Deanship of Scientific Research, The Hashemite University, in corporation with, the Jordanian Scientific Research Support Fund, the Ministry of Higher Education and Scientific Research.

Editorial Board:

Associate Editorial Board: (Arranged Alphabetically)

International Advisory Board: (Arranged Alphabetically)

Editorial Board Support Team:

Submission address:

Manuscripts should be submitted electronically to the following e-mail:

jjees@hu.edu.jo

For more information and previous issues:

www.jjees.hu.edu.jo

Hashemite Kingdom of Jordan

Scientific Research Support Fund

Hashemite University

Jordan Journal of Earth and Environmental Sciences

JJEES

An International Peer-Reviewed Scientific Journal

Financed by the Scientific Research Support Fund

Volume 11 Number (2)

http:// jjees.hu.edu.jo/

ISSN 1995-6681

Cover page photo: "Jebel Ammar, Late Ordovician glacial deposits in southern Jordan"
Photographed by Senior Geologist Dr. Ahmed Gharaibeh, Ministry of Energy and Mineral Resources, Jordan

JJEES
Jordan Journal of Earth and Environmental Sciences

JJEES

JJEES (2020) 11 (2): 77-85
ISSN 1995-6681

Jordan Journal of Earth and Environmental Sciences

The Minimal Significance of State Responsibility Concept in Resolving Environmental Disputes

Rehab Barnawi

Princess Nourah bint Abdulrahman University, College of Business Administration, Department of Law, Saudi Arabia.

Received 14th May, 2019; Accepted 29 June, 2019

Abstract

The objective of this article is to show that the principle of state responsibility is significant in theory, but not in practice in resolving environmental disputes. This may be attributed to the following reasons: the principle is not well-established in environmental law. Moreover, it needs to be designed in a single instrument that is solid and clear to be considered by the arbitrators, and this instrument should define the principle and its parameters, in addition to its procedural aspects. The explored defects of this principle leading to its insignificance include: the extent of liability, the magnitude of the harm, the forms of reparation, the required standard of care and some enforcement issues. This article also presents several sections to determine the principle's efficiency-i.e., whether it is modified or not in terms of invocation and enforcement, with reference to environmental case law. This study also provides some suggestions and an alternative to this principle.

Keywords: State responsibility, Civil liability, Environment, Environmental law, Transboundary environmental damage.

1. Introduction

Since the emergence of environmental law at the international level, international bodies have acknowledged the need for effective procedures to encourage states to implement environmental treaties. Despite the presence of some general procedures of compliance such as setting targets for the state parties to achieve -as the 1998 Kyoto Protocol adopted- or subjecting infringing states to monetary penalties, there have been infringements by some states leading to interstate disputes. The broadest instrument-establishing mechanism for settling interstate disputes is Art.33 (1) of the UN charter 1945 which states that:

> "The parties to any dispute, the continuance of which is likely to endanger the maintenance of international peace and security, shall, first of all, seek a solution by negotiation, enquiry, mediation, conciliation, arbitration, judicial settlement, resort to regional agencies or arrangements, or other peaceful means of their own choice."

One of the important approaches to tackle international disputes is by relying on the concept of state responsibility. In environmental law, it has been mostly invoked in cases involving transboundary pollution damages. The essence of state responsibility arises from states undertaking obligations set in either form of treaties or acknowledged as customary law.

States are bound by any treaty if they have manifested a form of direct or indirect consent, ratification, or an undertaking to implement the treaty in domestic law and ensuring compliance of the terms by all bodies of the state. By taking these steps, states are generally bound by the treaty- that is to say, should any state party fails to implement it effectively or monitor its bodies efficiently, or should any state's organs or non-state organs under the direct control of the state party fail to comply with any of the required terms, state responsibility may be invoked by the injured party, thus international responsibility accumulates over the state in breach.

One of the main reasons of treaties' violation – especially those concerned with the environment- is that most of the treaties only lay down a framework or general principles, and require state parties to take the necessary measures they see fit. For example, the 1979 Convention on Long Range Transboundary Air Pollution necessitates further actions to be taken by state parties to enrol it into their national systems; however, perceptibly not all states would be efficient or punctual in doing so. The only solution to this issue is the inclusion of implementation measures within the treaty itself or at least some procedural aspects or standards to be followed when implementing the treaty. This has been successfully adopted in UNCLOS and has been proven to be clear and efficient. (Hart, 2008) comments on agreements by the state parties saying:

> "[The] Implementation Agreement could add real value by giving substance to these provisions of UNCLOS, improving co-ordination between sectors, and clarifying responsibilities to 'protect and preserve' based on modern developments".

In addition to the international treaties, a state is responsible under customary international law, the rules that have been practiced by the state and supported by opinio juris -the belief of a legal obligation to do such acts- provided that the state is not a persistence objector to the rule as the case of Libya v Malta (1985) indicates. There are some complications in enforcing customary law in the case law due to the non-codification of this kind of law. In cases dealing with environmental disputes, many states have rejected responsibilities over breaching customary rules. For

* Corresponding author e-mail: rabarnawi@pnu.edu.sa

example, the USSR in the Chernobyl incident asserted that it was not bound by or in breach of customary law when it failed to provide information or notify the affected states.

It is apparent now that modern environmental law conventions largely focus on preventing environmental damages, conservation of the natural resources, and encouraging states to refrain from performing or permitting activities potentially leading to environmental damages instead of repairing the harm after it is done. In the case of a state failure to adhere to its environmental obligations and thus causing harm to other states, there is a requirement upon the perpetrators to repair, restitute, compensate, satisfy or formally apologise to the affected bodies or states for the environmental wrong. These requirements are called liabilities, and the liabilities of states or any international organization have been defined by Goldie (1985) as:

> "[The] consequences of a failure to perform [a] duty, or to fulfil the standards of performance required. That is, liability connotes exposure to legal redress once responsibility and injury arising from a failure to fulfil that legal responsibility have been established".

State responsibility is, perhaps, a misleading term because it does not only refer to states alone, as may some believe; rather, it has emerged at a time when states alone were considered the subjects of international law. In practice, any international body or person under the rules of international law can be subject to responsibility, and thus become liable. The application of state responsibility in environmental disputes is strongly connected to the International Law Commission's [ILC] Draft Articles on the Responsibility of States for Internationally Wrongful Acts which mainly codify customary international law. These articles been widely accepted and applied by international arbitrators to the extent that they are accepted by the international community. Art.1 of this Draft states that 'every internationally wrongful act of a state entails the international responsibility of that State'. This is the starting point of establishing the principle.

The upcoming sections would explore the application of the concept of state responsibility in environmental case law, and how it appears to be effective only in theory. Nonetheless, in practice the concept did not appear as significant in resolving the disputes as it should be. Cases of environmental disputes are mostly pointing to the role of civil liability proceedings in transboundary environmental wrongs. Perhaps seeking civil liability should be the perfect replacement to the establishment of state responsibility in such cases. In civil liability, the victims are most likely interested in remedies for the wrongs suffered than in state responsibility actions.

2. Theoretical Significance of State Responsibility

The notion of state responsibility is strongly significant in resolving environmental disputes, given that it is effectively set and applied. It applies widely to many situations, such as transboundary air or toxic pollution, acid rains, and damages as a result of hazardous or non-hazardous activities, hence, states often have a choice to resort to it. Indeed, states have acknowledged the significance of this principle; there had been several calls to enact an international set of rules dealing with such liabilities. For example, Principle 22 of The Declaration of the United Nations Conference on the Human Environment (Stockholm, 1972) recognized the gap in the law concerning environmental responsibility and urged that

> States shall cooperate to develop further the international law regarding liability and compensation for the victims of pollution and other environmental damage caused by activities within the jurisdiction or control of such States to areas beyond their jurisdiction.

There has not been any significant progress in the area until The United Nations Conference on Environment and Development (Rio, 1992) reaffirmed the need for international law generating liability for damages to the environment in Principle 33:

> States shall develop national law regarding liability and compensation for the victims of…. environmental damage. States shall also cooperate in an expeditious and more determined manner to develop further international law regarding liability and compensation for adverse effects of environmental damage caused by activities within their jurisdiction or control to areas beyond their jurisdiction.

Unfortunately, as Sands (2003) agrees there is no single instrument which establishes the generally applicable international rules with regard to state responsibility and liability in Environmental Law. The previous instruments- Rio and Stockholm conventions- set non-binding legal principles; they are only designed to commit governments to ensure environmental protection and developments of rights and responsibilities. Rules on liability of states may be found under different conventions, some ILC reports and customary law are applied by judges in international case law, yet not all conventions and ILC reports are legally binding to every state.

Generally, state practice shows unwillingness to establish a single instrument of international liability; Sands (2003) contends that this might give rise to the fear of imposing excessive costs on them; nonetheless, states would normally gather to produce internationally binding instruments if they regard the matter in question as necessary. Surely, they are not taking the principle as a matter of high importance in resolving their disputes neither do they observe its advantages. State responsibility says that states will act with due diligence in matters affecting their neighbouring states; they would place high scrutiny on their agents, and would notify the neighbouring states in case of potential harms, which in effect would reduce transboundary harm disputes and help find consensus or solutions among the states.

Another advantage of state responsibility is that it works as a deterrent; the injured state is able to subject all of the wrongdoers to trials and get compensated from each one in accordance to Art.47 ILC Rep. on State Responsibility, so no entity can escape liability. It can also as Art.48 elaborated have a standing in behalf of the community as a whole, or groups of the injured, many breaches indeed will be committed without fear of litigations if such rules do not exist. This contention has been firstly rejected by the Court asserting it was early for Environmental Law to accept such claims in Behring Sea Fur Seals Arbitration (1999) when the USA argued that it has the right to protect Fur Seals even if

they are outside the three mile limit of its territorial water, the tribunal rejected the claim and exercised its powers in enacting a binding regulation. If this occurs nowadays, there is no reason why it should not be acceptable as both states' practice and the ILC Report on State Responsibility permits states to initiate claims on behalf of the community as a whole.

It might be maintained that Art.48 may give rise to politically-motivated invocation and may allow counter measures to take place. However, by observing Art.54 of the same report, one could assume that this would rarely materialise in practice, the Court would only allow countermeasures that it sees as lawful to be taken, such as the collective measure taken by states against Iraq's invasion of Kuwait in 1990 to freeze Iraqi's assets under the authorisation of the Security Council. Besides, no state would like to incur costs by initiating international litigations unless the matter is of grave concern to it.

Accordingly, various elements have to be established for the state responsibility principle. There should be an environmental damage as a result of an act or omission of states, or actions of individuals attributable to those states, as Professor Eagleton (1928) puts it: '[a] State owes at all times a duty to protect other States against injurious acts by individuals from within its jurisdiction'. Moreover, locus standi should be established, material damages and causation should also be proven and parties have to consent to the jurisdiction of the ICJ or the arbitrator. Although these requirements are effective in not opening the floodgate of litigations to the ICJ and in regulating the mechanism of invocation, they place hardships, cost money and time to be applied, and potentially leave some injured parties without effective remedies.

The main issue of the principle is the absence of guidance in interpreting its elements; they can only be explained by observing the Court's practice and some of the enacted treaties; deficiencies of this principle are explored below.

3. Practical Deficiencies of States' Responsibility

Issues hindering the popularity of the state responsibility in environmental law are the difficulties facing the international community in defining its parameters such as: the extent of liability, the magnitude of the harm, the forms of reparation, the required standard of care and some enforcement issues. Indeed, these differ from one case to another; for instance, nuclear damages are mostly hard to repair compared with oil spillage incidents causing sea pollution which can be cleaned. Each element is discussed below in details.

3.1 Damages

The existence of environmental damage is the main criterion to initiate state responsibility claims. Several definitions of the environment exist; the widest is mostly easier to adopt as The World Commission on Environment and Development stated 'the environment is where we live'. The problem is based on the meaning of the term Damage and the degree of harm required accumulating liability. Should there be an adverse effect? Should there be pollution or would depletion of natural resources be sufficient? Should the harm be significant? Should it be proven beyond reasonable doubt and what is the threshold? The knowledge of such requirements is essential for the wronged party prior to initiating a proceeding based on state responsibility before the Court.

The Trail Smelter Case established that only apparent harm should be compensated. The Canadian lawyers managed successfully in the case to narrow down the definition of the compensated damage, by excluding the invisible harm and harm that is not proven or 'even if [proven], too indirect and remote to become the basis, in law, for an award of indemnity'. In the case, economic injury to the properties and livestock along with the injury to the businesses, and to the cleared and uncleared lands were put forward by the USA to be measured. Most injuries were rejected by the tribunal; firstly, there was a lack of proof in regard to the economic injury. Secondly, injury to business enterprises was considered too remote, and for the cleared and uncleared land, the reduction of value and production was indemnified; nevertheless, a definition of damage in a pure sense was not provided by the judges.

The scope of damage has been expanded in the case of water pollution of Ciudad Juarez in 1961. A case where Mexico complained about offensive odors from two American companies who were said to be polluting the air with fumes and throwing fetid offal in the Rio Grande, causing both physical and economical damage to the residents of Ciudad Juarez. The USA accepted responsibility of the companies' acts and had taken measures to control the odors. As a result of this ruling, according to (Lester, 1963) damage currently includes 'any artificial change in the natural quality of any particular natural [resources]-water hereto- rather than a more narrow definition in terms of use or damage'.

Prior to the case of Ciudad Juarez, the tribunal in The Lake of Lanoux Arbitration recognised the possibility of environmental damage to water; nevertheless, it rejected the Spanish claim about the potential damage to its environment if France decided to divert the waters of a shared water source flawing from Lake Lanoux as part of a hydroelectric project. The ruling assumes that in the absence of the proof of damage, a state could not bring a claim. This makes state responsibility a reactive rather than a preventive principle as it hinders states from initiating claims for potential damages.

The case law implies that it is for the Court to determine the parameters of damage and when to award indemnities, since the ICJ is not bound by the doctrine of precedents; a state cannot be sure whether it is going to be indemnified and what is the form or amount of damage it is going to obtain. States might be discouraged from invoking claims and enduring costs in the absence of a general standard for measuring the damages and with the possibility of getting it being imprecise or minimal.

In the absence of an international agreement for establishing the threshold of the damage, state practice assumes that damages have to be substantial to trigger liabilities. It suggests that claims are justified if the injury leaves serious consequences -this is apparent in the Trail Smelter Arbitration (1939), or the damage caused is irreparable in Nauru v. Australia case, or if it is more than minimal in Hungary v Slovakia (1997). The major difficulty

arises in cases of nuclear damages. For example, after the Chernobyl accident, several instruments established different thresholds to the requisite level of radioactivity such as the International Commission on Radiological Protection; several individual states also adopt their own radioactive dose limits affecting human bodies, farms, and businesses. Despite the efforts, these divergent thresholds are impractical for states, and are likely to create controversy among litigants.

To conclude, according to case law and state practice, there is no clear interpretation and threshold of damage incurring international liability. Each case has been resolved according to its circumstances. There is no harmony in the law, thus, injured states might be affected internationally; it might not get indemnified- and might be domestically subject to litigations by its individuals. The latter has been manifested in the Chernobyl incident when several states had to compensate their affected individuals as a result of the radiation such as the UK, Germany, and Sweden.

3.2 Liabilities

When it comes to liability, debates are on whether it should be subjective or objective in nature. The ILC Report on State Responsibility requires faults to establish responsibility; since this leaves the uncovered environmental harm caused without fault, it created a parallel basis for remedies calling them liabilities. Therefore, a state can be liable even if it acted in a manner not violating environmental law but causing a non-tolerable injury to other states, this is specified in Art. 2 of the ILC Draft Articles on the Prevention of Transboundary Harm from Activates. Liabilities help fulfil the purpose of state responsibility, and ensures reparation. In cases involving liabilities, states are likely to raise the standard of care requirement which could be seen as a mitigating factor in case law. Generally, in environmental disputes, due diligence is not an easy standard to administer in the absence of binding international standards. Arbitrators are unlikely to accept it a s a defence, and even if they did, they would place a heavy burden of proof on the party trying to rely on it -mostly the source state.

The reasons why an injured party brings claims include seeking cessation of the act, reparation, or compensation either for a pure environmental damage or a consequent damage to health and properties. In order to attain that, the court would initially distinguish between ultra-hazardous and non-hazardous activities. Absolute liability should be imposed on the former. Since the source state is aware of the nature and the risks involved in carrying out activities such as nuclear plants, it should be absolutely liable for harm if it occurs, and a proof of fault should not be required.

It might be argued that strict liability -in which various defences might be available- could be imposed in some cases where the source state has been due diligent. However, it should not completely exempt it from liability, and damage should be minimally payable. For example, in the Trail Smelter Arbitration (1939), the USA tried acting with due diligence by increasing the height of the plants' stacks albeit worsening the situation more than the lower stacks. Damage was indeed payable, but the act has been taken into consideration by the tribunal.

Furthermore, it must be asserted that fault-based liability should not be considered in environmental cases because it would require the court to set standards of care, and would also add more burdens to the injured state. If the source state managed to prove an absence of fault, the injured party would be left without a remedy, and this is not acceptable as it undermines the principle of state responsibility. The source state should rather reduce the probability of environmental interstate disputes by undertaking mitigating factors prior to its actions, namely, notification of the harms, and consultation on preventative measures to the likely being injured states.

The ILC Articles on the Prevention of Hazardous Harm includes initiative procedures to prevent environmental harms; nevertheless, they are lengthy in time and lack incentives and binding aspects that would induce states to employ them. For example, Art.11 -setting certain procedures in the absence of notification- requires the likely to be affected state to send a written request asking for information under Art.8 if the source state failed to send a notification. Upon receiving the request and when the source state decided not to notify, both had to enter into consultation -Art.9- to reach a consensus.

By the time resolutions are reached, the damage might have already accrued or worsened; a requirement of cessation of the act during negotiation should be imposed rather than merely urging the source state to arrange feasible measures to minimize the risk under Art.11 (3).

3.3 Reparation

Forms of reparations are varied under state responsibility, the ILC on State Responsibility in Art. 34-39 elaborates the forms of restitution, compensation, and satisfaction. It has to be said that these forms of reparations seem effective and attainable theoretically; nonetheless, in reality they are not so as the case law shows. For example, in the Trail Smelter case, the payment to the USA was late and the amount was minimal. In other incidents, reparation might not be feasible due to the severity of the harm such as in the Fukushima incident, while in others, the source state cannot be sued or coerced to pay for the damages such as in the case of the USSR in the Chernobyl incident.

One issue regarding reparation is that it cannot be easily managed. For instance, in the case of compensation, it is mostly hard to quantify environmental damage in monetary values, and thus disputes might be ignited again. Similarly, restitution is almost hard in many cases, as completely wiping out environmental damages may not be feasible. In Canada Claim against the Union of the Soviet Socialist Republics for Damage Caused by Soviet Cosmos 954, the Canadian soil was rendered unfit for use as a result of the satellite crash, restitution was impossible and, therefore, compensation was paid upholding Canada's right to make additional claims since the damage cannot be determined precisely in nuclear contamination.

Satisfaction seems as the easiest and last resort form of reparation as it requires nothing from the source state except acknowledgment of the breach and a formal apology. However, most states are reluctant to express their regret for the wrongful act. They either regard it as an act affecting

their sovereignty and status at the international level, or they may consider it as embarrassment and humiliation.

3.4 Standing Issues

There are several elements to be elaborated to determine if a state is able to have a standing at the international level to the point of invoking claims. The state has to be injured as a result of another country's act as Art.42 ILC's on State Responsibility stressed. A state is injured if it was individually affected by the breach, which normally occurs in bilateral agreements, or if the breach affected every other state to which the obligation is owed such as the breach to the Treaty of Antarctica, or if the invoking state is significantly affected by the breach and is distinguished from all injured states.

Where the breach of one state affects every other state party, all should be equally injured, and thus should have a standing as long as it is feasible to do so. Nevertheless, the source state might not be factually able to compensate all injured parties, thus, there should be distinctions between primary and subsidiary litigations as Crawford (2001) elaborated: the treatment of collective damage should distinguish between primary beneficiaries and those states with legal interests in compliance, accordingly some states might not even be compensated.

Standing issues mostly arise if a third party is involved in the proceeding. Deciding a case might necessarily get a third party involved and affect its rights; hence, the third party intervenes to protect itself. This has been problematic as recent history shows that the ICJ has accepted third-party intervention only in two incidents. In Land, Island and Maritime Frontier Dispute (1990) and in the case of Cameroon v. Nig. This potentially renders the effected party without reparation especially if one of the parties involved is not consenting to the jurisdiction of the ICJ. For example, in the Monetary Gold Case, in a dispute between Italy on one side, UK, France, and the USA on the other side, the Court declared it is without jurisdiction to adjudicate upon the merits of the claim because doing so would require the Court to decide whether Albania wronged Italy and Albania was not consenting to the Court's jurisdiction.

Additionally, even if the injured state is likely to be granted locus standi and to succeed by invoking the principle of state responsibility, most states are reluctant to do so. (Stephens, 2009) added that they are greatly reluctant even if the environmental damage is so severe. Recent practices demonstrate that states prefer other means to solve their problems; either by negotiation, mutual agreements, or diplomatic consensus. This has been apparent even in regional instruments that have a clear mechanism of state responsibility such as Art.259 TFEU giving member states the right to bring actions for infringement of the EU legislations against other parties. The article had been rarely used by states. Only six cases have been brought so far, and none invoked an environmental issue, and only three of the former five have been closed by a final judgment.

An Additional reason for the reluctance of invoking the principle is the fear of countermeasures or relationship tensions between the states in dispute. These reasons can be extracted from the Chernobyl disaster in which the explosion of the nuclear power plant reactor produced a radioactive cloud that flew over several countries including Sweden, Germany, and Switzerland. None of the states initiated any claim against the USSR, rather, they offered to cooperate, and no obligation was imposed upon the USSR. It was suggested that they feared being in the same situation in the future and might be held liable as well. Their reaction could also be seen through the lens of sympathy to the affected state.

Another obstacle in locus standi is that the ICJ cannot give a ruling or even an advisory opinion if the state in question does not consent to its jurisdiction. In Status of Eastern Carelia (1923), the PCIJ refrained from issuing an advisory opinion on the interpretation of disputed bilateral treaty between Finland and Russia over East Karelia, for the reason of Russia's refusal to participate in the proceedings and its non recognition of the jurisdiction of the League or the Court itself -stated in the Advisory Opinion, 1923 PCIJ (ser. B) No. 5. As a result, many environmental issues cannot be resolved at the international arena under the concept of state responsibility.

3.5. Enforcement

The final hurdle of the principle of state responsibility is the absence of enforcement mechanisms. Nothing can be done if the source state refrains from abiding by the arbitral ruling, and states cannot be coerced to compensate if they refrain from doing so. It could be contended that the injured state can rely on Art. 22 of the ILC's Report on State Responsibility by countermeasures against the responsible state in order to compel it to cease the unlawful act or repair the injury. However, this contention is not feasible in practice as it seems only to work with powerful states. If the injured state is weaker than the source state, countermeasures may worsen the situation rather than solve the problem. It may lead to more economic or diplomatic tensions, thus, most of the weak injured states prefer not to use such a tool.

Another suggestion is subjecting the source state to penalties in the event of failure to comply with the judgments, but this is also hard to administer considering the number of states. Moreover, this solution has been adopted by the EU, and proved the potentiality of unfairness. For instance, states may still not pay for the only detriment is them being in debt, and the injured party gets nothing.

As a result of these impediments to the principle of state responsibility, an easier regime that is not connected to politics and governments must be employed. A system that is practical in time and money and ensures fairness and compensation, and a mechanism for the injured be it a state, an international or national body or even an individual must be employed. This is provided by a civil liability regime which is already employed in nuclear cases, and should be considered in transboundary environmental damages in general.

4. Civil Liability in Nuclear Cases

Customary law established state responsibility in civilian nuclear energy in Cosmos 954. This has not proved popular as the Chernobyl incident clearly showed the refusal of states to accept liabilities for nuclear transboundary harms. Prior to the Chernobyl incident, states applied

different principles in relation to nuclear power. Assuming the importance of the field and the associated risks which are seen as barriers for development, they realized that both the public and the operators needed protection. Victims have to be assured that sufficient protection and compensation are provided. Similarly, operators must not be discouraged from investments due to financial debilitating liabilities. Accordingly, neither ordinary tort rules exposing investors to unlimited liabilities and involving technical complexity in allocating wrongdoers, nor international liability are sufficient hereto. Therefore, a regime of a civil third-party liability with states being responsible as guarantors of the operator's strict liability with the accumulated residual liability on them has been internationally established. Acknowledged principles for the liability of nuclear damage have been adopted in these instruments such as the strict and exclusive liability upon the operator who has to be insured limiting the liability in time and amount.

Since a single nuclear incident would attract several litigations, different national courts may apply different laws if civil liability is adopted. This establishes the need for a united instrument ruling the area. For instance, in The Japanese Fishermen Case, the USA subjected several Japanese fishing vessels to excessive level of radiation and contaminated a number of fishing boats and men as a result of unlawful hydrogenic bomb testing in the Marshall Island Trust Territory. Although a tribunal has been established to determine the extent of the damage, the USA managed through diplomatic means to pay two million dollars as compensation to Japan. If the matter has not been diplomatically settled, the tribunal might have to award. If the incident happened between different countries, the calculation of the damage may also be different in the absence of a guiding international instrument to calculate the nuclear damages.

This article deals with two categories of nuclear damages. First, where the source state carries an internationally wrongful activity causing nuclear pollution such as atmospheric nuclear tests, for which objective standards should be applied; state responsibility under customary law mostly invoked by the injured parties. For example, in Australia v. France and New Zealand v. France, the two states objected to France carrying out nuclear weapon tests in the Pacific Ocean as being contrary to international law and creating anxiety and fear of environmental and health damages to the nations of both countries. Even though the case has ceased to exist when France announced a termination of conducting the tests, judge Ignacio-Pint asserted:

> "I see no existing legal means in the present state of the law which would authorize a state to come before the court asking it to prohibit another state from carrying out on its own territory such activities, which involves risks to its neighbour."

This establishment is controversial as it renders states as with no power to stop each other from operating activities which might cause transboundary damages in the absence of certain evidence. States desire a preventative system along with remedial one.

An additional example is dumping radioactive substances into a territorial sea causing damages to other states. The 1958 USA pacific Nuclear Tests shed further light on the state responsibility principle. Fortunately during that period, the USA government announced responsibility to compensate any damages or economic losses caused by the tests while taking all precautionary measures required. It even allowed Japan to initiate compensation claims after the tests if any evidence displaying economic loss was presented. Such situations required state responsibility and did not prove controversial.

A third important example is when a state uses nuclear weapons against another. This indeed should not be justified even if it is for self-defence. The Hiroshima atomic bombing on Japan by the USA caused devastating environmental, property and health harm, yet the USA was not sued or condemned by the international community. State responsibility should be imposed in such situations to regulate the use of power. In fact, the court used its discretion to reject giving an advisory opinion requested by the World Health Organization (1996) in the Legality of the Use by a State of Nuclear Weapons in Armed Conflict, invoking lack of jurisdiction in the matter. In the advisory opinion to the same question requested by the General Assembly, the Court could not conclude the unlawfulness of the use or the threat of use of nuclear weapons in the extreme circumstances of self-defence, which places high anxiety on the states and more demands to regulate such powers.

The second category is where the source state operates nuclear plants on its territory. This carries the risk of nuclear disasters occurring either through technical or human error, thus neighbouring states are always threatened by a potential harm. Absolute liability is always applicable as a mean of solving inequities between nuclear and non-nuclear states.

Customary law limited the doctrine of sovereignty -allowing lawful activities resulting in extra territorial damages- by the good neighbourliness doctrine bringing state responsibility into operation, even though this is questionable in nuclear cases. Numerous nuclear incidents have taken place in different nuclear energy countries. The 1986 Chernobyl incident in Ukraine and the 2011 Fukushima plant incident in Japan created unlimited international reactions.

Prior to the incidents, states promoting peaceful use of nuclear power recognized the need to establish a regulating instrument to provide legal certainty, eliminate discrimination and subject all claimants of state parties to similar laws. Two major nuclear civil liability instruments have been concluded, namely the 1960 Paris Convention on Third Party Liability in the Field of Nuclear Energy and the 1963 Vienna Convention on Civil Liability for Nuclear Damage. Both incorporated similar fundamental principles; nevertheless, parties of the Paris convention added two supplementary public funds in the Brussel's convention after recognizing the impossibility of the operator to compensate damage or loss to any person or property in cases of accidents; one was from the source state and the second was a contribution from the state parties. The Chernobyl incident resulted in motivating states to merge the two conventions together to provide more protection to the largest number of

victims and regulate the operators' interests.

Despite the international efforts to attract as many states as possible to join in, both of the Paris and Vienna Convention systems have suffered from relatively limited participation. In fact, most of the nuclear plants are located in non-convention parties such as Canada, China, India, and the USA, and most of them are also among the most populated countries in the world. This poor participation could be ascribed to the unpopularity of certain terms of the conventions such as the limited liability, for states may not see the reason for restricting compensation of their victims. However, these terms would at least guarantee some sort of compensation even if it is minimum as in reality and individual victims may get nothing from the source state similar to Chernobyl. Another reason could be that the conventions may benefit transboundary victims more than nationals; this appears to be true as professor Lamm in 1998 remarked:

> [After] the Chernobyl accident, the then Soviet Union refused to pay compensation to any foreign victims, some people believed that if the Soviet Union had been a party to the Vienna Convention, foreign victims would at least have had a chance to receive some compensation.

Since both Chernobyl and Fukushima incidents show states' refrainment from initiating claims, civil liability –which has been called for by nuclear conventions- is the ultimate solution for nuclear cases to avoid complexities and insure compensation. In the case of Chernobyl, the USSU was internationally liable for the damage caused as a result of the negligence of the workers in the plant if actual damage and causation were proved by the injured states. Initially, a flurry of litigations threatened the USSR, but have been soon dropped recognizing the uncertainties of indemnities and the impossibility of enforcing payment (Malone, 1987).

Reasons for such hesitations include: the direct and indirect damage materialized was severe and non-calculable in monetary terms. The USSR itself experienced life losses, health issues, and serious contamination rendering large areas unfit for inhabitancy. The Chernobyl incident highlighted several deficiencies in the applicable law. The standards for determining liability are not clear. Should these standards be faults as a result of negligence or recklessness, or strict liability as a result of transboundary ultra hazardous harms, or liability for the unreasonable interference in the natural resources of another state; state responsibility normally applies to the latter. Secondly, there is uncertainty of the recoverable damages in terms of subsequent economic loss and injuries to properties and businesses. Lastly and more importantly is the lack of means of enforcement. The USSR is not a party in any international liability or compensating regime. It is not consenting to the ICJ as an arbitrator, even if there was a litigation, decisions of the ICJ were only enforceable through the Security Council of the UN in which the USSR has the veto power.

Another highlighted issue is the absence of global early warning system of nuclear incidents, and the absence of obligation to inform the states if such incidents occur. The USSR failed to notify other states in adequate time alleging that there is no international obligation to inform other states in events of accidents. Moreover, in the absence of safety standards for the nuclear plants at that time, the Chernobyl plant used an outmoded graphite reactor which was abandoned by many countries after the fire in 1957 at Britain's Windscale graphite reactor, yet there was no consequence. If civil liability was adopted, it will be hard for operators to escape liability easily in such situations.

The recent Fukushima incident did not attract international liability claims because transboundary damage was minimal causing no threat to people, livestock or corps in other states due to the location of the incident. However, domestic damage was substantial. If there has been interstate litigation, it will be beyond the financial capacity of Japan as the government had to assess TEPCO by paying $1.16 billion only for domestic litigants. Whether states' supplementary funding would suffice if transboundary harm was caused is even questionable. International reaction was more humanitarian in the case; however, further deficiencies of the current state of nuclear law have been highlighted. The leakage of contaminated water which was used to cool the operators caused severe water pollution. Accordingly, the marine life emigrating to the Japanese coast is and will continue to be exposed to radioactive substances. However, (Stephen, 2011) thought and we agree that the impact of these substances is not yet clear, and at worst it would not only affect Japanese people.

There is indeed much work done at the international arena to regulate nuclear energy as a result of the previous incidents, such as the 1994 IAEA Convention on Nuclear Safety, and the two 1986 Conventions Relating to Early Notification of Nuclear Accidents and the assistance to the countries affected by such accidents. International community response has been a compromise; indeed they should cooperate to channel legal liability and encourage other state to become parties of relevant conventions which seem to provide clear rules for individuals, states, and operators.

Despite these efforts, Fukushima demonstrated a lack of enforcement. The Japanese plant was not up to the standards required by the 1994 Vienna convention. The design and operational features adopted by TEPCO were no longer the standards requires by the convention. Thus, in theory Japan violated the convention and the consequences of such violation were not apparent. It can be suggested that the consequences of breaching the nuclear conventions cannot be determined as the international community continues to encourage states to become parties rather than add more burdens on them. Nuclear cases require designated rules, and state responsibility is not significant because the major concern currently is the protection of the human population; it can, therefore, be achieved through regulated civil liability actions.

5. Conclusions: an Alternative Regime to State Responsibility

Since state responsibility does not guarantee that individual victims will be compensated in transboundary harms, civil liability regime does. The difference between state responsibility and civil liability is that the former refers to the liability of a state under public international law and the latter means the liability of natural or legal person under

the domestic legislation including the legislation established to implement the provisions of international treaty obligations. Civil liability should be in a better place to deal with transboundary harms. It is not profoundly burdensome for national courts to ensure that several forms of protection of the public are devised and liability is imposed on the wrongdoer. Since transboundary damages would still occur however diligent the state has been in regulating harmful activities, the ILC took an initiative step publishing the 2006 Principles on the Allocation of Loss in the Case of Transboundary Harm Arising out of Hazardous Activities which adopts a civil liability regime.

Civil liability converts transboundary cases into a national matter. It enables victims to gain an effective access to national courts of the source state and sue the polluter. Also, it allows them to have the choices of both forum and the applicable law. Since most pollution is caused by individuals rather than states, civil liability applies the polluter pays principle, which is more forward than the state responsibility principle which involves lengthy and risky procedures to be taken by their states.

For the regime to operate effectively, equal access to information, equal access to national courts and remedies should be available to the foreign individuals without any discrimination on the base of nationality, geographical location, or residence. This has been called upon by the ILC on the 2006 report, and has also been adopted by the Organisation for Economic Co-operation and Development (1977) in Recommendation on Implementation of a Regime of Equal Right of Access and Non-Discrimination in Relation to Transfrontier Pollution, Para.4 (a):

> Countries of origin should ensure that any person who has suffered transfrontier pollution damage or is exposed to a significant risk of transfrontier pollution, shall at least receive equivalent treatment to that afforded in the country of origin in cases of domestic pollution and in comparable circumstances, to persons of equivalent condition or status.

Civil liability has also played an important role in different countries' constitutions such as Spain and France, and proved effective. For example, Sandoz chemical spillage in Rhine has been resolved successfully without international proceedings, and should Canada adopt civil liability, the Trail Smelter Arbitration (1939) would be nationally solved. Individuals are already trying to resolve transboundary environmental disputes by other lengthy means such as Human Rights' Conventions which require local remedies to be exhausted and whose benefits are mostly restricted to the individuals who suffer losses not to the community at large.

Indeed, there are obstacles in the civil liability regime; however, they can be overcome. Firstly, the availability of international law in the source state depends on the extent of the incorporation of international law into the domestic law. This can be overcome by encouraging states to incorporate international instruments domestically. Another obstacle involves the wide discretions of national courts. Some jurisdictions deny access to cases involving foreign entities or might claim denial as a result of foreign courts being in a better position to deal with the claim. A suggested solution is when courts adhere to the forum non conveniens maxim requiring courts to consider relevant factors such as damage assessment and compensation to decide what legal system are in a better position to deal with the case.

Additionally, there are difficulties facing litigants in terms of language differences and unfamiliarity with legal systems. In some cases, they might face difficulties in the choice of law, or they might also be forced to one forum if access has been denied in their preferred forum. Moreover, sufficient procedural rights and environmental protection might not be guaranteed. These obstacles can be maintained by different means. In the case of unfair denial to access or remedy, violation of human rights' conventions may be invoked. The civil liability regime is easier to maintain as many conventions are linked to each other, thus, individuals would eventually be compensated. The major obstacle of this regime is the prevention of justice due to civil wars, corruption, or intimidation by the state, even though these rarely occur and can be solved by invoking international conventions. All in all, the civil liability regime will ensure compensation to the injured, in addition to the efficiency in time and procedures and the ability to solve interstate environmental disputes. It is already available to deal with internal environmental damage, yet there is only a need to extend it to include transboundary claims.

Acknowledgement

This research was funded by the Deanship of Scientific Research at Princess Nourah bint Abdulrahman University through the Fast-track Research Funding Program.

References

Bering Sea Fur Seals Arbitration (UK v. USA) 1 Int. Env. L. Reps (1999) 43

Crawford, J.R. (2001). Responsibility to the International Community as a Whole. Indiana Journal of Global Legal Studies, pp.303-322.

Declaration of the United Nations Conference on the Human Environment (Stockholm) (16 June 1972) UN Doc. A/CONF/48/14/REV.1. 21st plenary meeting Chap.11

Eagleton, C. (1928). The Responsibility of States in International Law (1928). New York. (Reprint, Kraus, 1970) P 83–84. 14. Moore, Vol. 6, pp. 811–815. 15. Wharton

Gabc˘íkovo-Nagymaros Dam Case (Hungary v Slovakia) [1997] ICJ Reps 7

Goldie, L.F.E. (1985). Concepts of strict and absolute liability and the ranking of liability in terms of relative exposure 1 to risk. Netherlands Yearbook of International Law, 16, pp.175-248.

Hart, S. (2008). Elements of a possible implementation agreement to UNCLOS for the conservation and sustainable use of marine biodiversity in areas beyond national jurisdiction (Vol. 2). Gland: IUCN.

Lamm, V. (1998). The protocol amending the 1963 Vienna Convention. Nuclear Law Bulletin, pp.7-24.

Land, Island and Maritime Frontier Dispute, Application to Intervene (1990) ICJ REP. 92 & Maritime Boundary Between Cameroon and Nigeria (Cameroon v. Nig.), Application to Intervene (1999) ICJ REP. 1029

Lester A. P. 'River Pollution in International Law' (1963) 57 Am. J. Int'l L.

Libya v Malta (1985) ICJ Reports [13], ILR 239

Malone, L.A. (1987). The Chernobyl accident: a case study in international law regulating state responsibility for transboundary nuclear pollution. Colum. J. Envtl. L., 12, p.203.

Organisation for Economic Co-operation and Development (OECD). (1977). Recommendation on implementation of a regime of equal right of access and non-discrimination in relation to transfrontier pollution. (17 May 1977), C(77)28.

Paris Convention on Third Party Liability in the Field of Nuclear Energy (July 29 1960) 1041 UNTS 358

Protocol, K. (1998). The Kyoto Protocol to the framework convention on climate change. URL: http://un. org./ru/ documents/decl_conv/conventions/pdf/kyoto. pdf.

Sands, P. (2003). Principles of International Law. 2nd edn, Cambridge, CUP.

Status of Eastern Carelia, Advisory Opinion (1923) PCIJ (ser. B) No. 5, at 6 (July 23). The contemporary spelling of the name of the territory is Karelia.

Stephen L.K. (2011). 'International Law Lessons From the Fukushima Nuclear Disaster' (2011) New York Law Journal, April 29. <http://www.clm.com/publication.cfm?ID=324> accessed 26th Dec 2017

Stephens, T. (2009). International Courts and Environmental Protection, CUP, 2009.

Trail Smelter Arbitration (US v. Canada) 33 Am. J. Int'l L. 182 (1939), 35AJIL (1941) 684

JJEES

JJEES (2020) 11 (2): 86-92
ISSN 1995-6681

Jordan Journal of Earth and Environmental Sciences

Agronomic Evaluation of Manure Ashes: Effect on Soil Reaction and Electrical Conductivity

Azeez Jamiu[1], Adeyemo Eyitomilayo[1], Olowoboko Toyin[1*], Afolabi Tahjudeen[2]

[1]Department of Soil Science and Land Management, Federal University of Agriculture, Abeokuta, Nigeria
[2]Department of Chemistry, Federal University of Agriculture, Abeokuta, Nigeria

Received 19 March 2019; Accepted 2 December 2019

Abstract

Manure ashing seeks to concentrate manure nutrients and reduce their bulkiness. This study is conducted to evaluate the effects of dried manure and their ashes on soil pH, electrical conductivity (EC). The study includes laboratory-incubation, screen house [both completely randomized] and field [randomized complete block design] experiments. Treatments which are control (CON), dried poultry manure (DPM), poultry manure ash (PMA), dried cattle manure (DCM), cattle manure ash (CMA), and dried goat manure (DGM), goat manure ash (GMA) and NPK 15-15-15 were applied at 120 kg P ha^{-1} to soil. Soils taken fortnightly were analyzed for pH and EC. Results showed that averagely, across the weeks of study, the soil incorporated with manure ash had higher pH values relative to the soil with the dried manure treatments. Manures and their ashes increased soil pH, and the incorporation of poultry manure ash led to significant increase in EC when compared to the incorporation of dried manure across the weeks in the incubation experiment. In the field experiment, the application of cattle manure ash led to significant increase in soil pH and EC over the weeks of observation. The study concludes that the effects of manure ashes on soil pH and EC are comparable to those of dried manures thus showing the potential of a good liming material. Hence, the use of animal manure ash in place of dried manures is highly recommended by this study.

Keywords: Animal manure ash, Electrical conductivity, Soil reaction.

1. Introduction

In recent times, the use of organic manures with or as an alternative to inorganic fertilizers in sustainable agricultural practice has increased worldwide, because it improves soil structure and stimulates the biological processes in the soil that help to build fertility (Ano and Agwu, 2005). Olatunji et al. (2006) opined that the application of organic manure has higher comparative economic advantages over the use of inorganic fertilizers.

The quantity of livestock waste generated in Nigeria is large (Nwajiuba and Chimezie, 2000), most of which have potential for use in the maintenance of soil fertility. Irrespective of the massive manure production potential, very little amount of the available animal manure is being utilized for crop production because animal manure is bulky and is not aesthetically pleasing to handle thereby reducing its economic value, which has accounted for a substantial portion of it being disposed of as a waste product.

Kimbi et al. (1992) observed that in extensive livestock grazing systems only about 1% of farmers apply animal manure on land, indicating serious underutilization of such resources. This is mainly due to the lack of scientific basis for enlightening farmers on appropriate application rates, storage techniques, and application methods (Gabriel, 1998). However, as animal production shifts toward fewer but larger operations, the number of confined animals has increased in some geographical locations, resulting in more manure produced than can be assimilated by the available farmland where the animals are raised and the disposal of such manures becomes a major problem.

Due to its bulkiness and unpleasant aesthetics, animal manures have been disposed as waste in tropical countries. There has been, however, a need to determine alternative ways of processing and handling animal manures. The charring or burning of manure has become an alternative method of processing manures. It involves the turning of manure to ash for the purposes of concentrating the nutrients in the manure, reducing the bulkiness, and presenting the nutrient elements in a form that is readily available to the plants.

Masto et al. (2007) showed that the application of manure has a significant effect on the chemical properties of soil, and many of these effects are due to the increased organic matter. Soil pH is the measure of soil acidity or alkalinity. It is an important indicator of soil health. A number of researchers have suggested that organic residues (e.g., animal manures) might be used as alternative liming materials and that their application can increase plant growth in acidic soils by ameliorating aluminum (Al) toxicity (Pocknee and Sumner, 1997; Mokolobate and Haynes, 2002).

Soil pH affects crop yields, crop suitability, plant nutrient availability, and soil micro-organism activity which influence key soil processes. The solubility and availability of most nutrients in soils are determined by the soil pH (Azeez and Van Averbeke 2012). Electrical conductivity (EC) is a measure of soil salinity. Manures added to the soil mineralize and release the nutrients and salts to the soil. Soil electrical conductivity serves as a measure of soluble

* Corresponding author e-mail: rachy_blare26@yahoo.com

nutrients and indirectly shows the mineralization of organic matter in the soil (De et al., 2000).

The search for sustainable soil fertility replenishment techniques is ongoing in which most studies concentrated on the use of dried animal manure; however, limited information on the use of animal manure ash is available. Animal manure is bulky, and not aesthetically pleasing to handle resulting to the substantial portion of it being disposed of as a waste product. The recent practice of converting the dried waste to ashes is a new way of recycling the manure and concentrating the nutrients to reduce its bulkiness: however, there is paucity of data on the agronomic evaluation of animal manure ash in respect to some soil chemical properties. Consequently, the objective of this study is to evaluate the effect of dried animal manure and manure ash on soil reaction and electrical conductivity in incubation, screen house, and field experiments.

2. Materials and Methods

2.1. Soil Sample Collection, Preparation and Analysis

Top soil samples (0-20cm) were collected from four locations in Ogun state based on their different parent materials. The locations are: Alabata and Osiele from basement complex parent materials; Itori and Papalanto from sedimentary parent materials. The soils were air-dried and passed through a 2mm-diameter sieve. The physical and chemical properties of the soils were determined as follows: pH in water using a glass electrode pH meter; particle size distribution, using the hydrometer method (Bouyoucos, 1965). Available phosphorus was determined using Bray-1 procedure. Exchangeable acidity was determined in a 1.0M KCl extract as described by Page et al. (1982). Exchangeable bases were extracted with 1N NH_4OAc buffered at pH 7. Sodium and K in the extract were determined by flame photometer, while Ca and Mg were determined using Atomic Absorption Spectrometry. Soil Fe was analyzed using atomic absorption spectroscopy after HNO_3-H_2O_2-HCl digestion.

2.1.2. Manure Collection, Preparation, Analyses and Experimental Treatment and Design

Cured cattle dung, goat manure without beddings and poultry manure (battery cage) were obtained from Federal University of Agriculture, Abeokuta farm. The manures were air-dried; and some were burnt in an open air to produce ash at temperature 320–450 °C. The dried manure ashes used were digested with nitric and perchloric acid (2:1) (Watanabe et al., 2013). The digests were analyzed for pH, available P, Calcium, Magnesium, Potassium, Sodium, exchangeable acidity, copper, zinc, iron and texture using standard procedures (Kaira and Maynard, 1991).

Incubation and screen house experiments were laid in a completely-randomized design while the field experiment was laid in a randomized complete block design with three replications. Treatments were control, dry cattle manure, cattle manure ash, dry goat manure, goat manure ash, dry poultry manure, poultry manure ash, and NPK 15-15-15 at a rate of 120 kg P ha^{-1}. The control was the soil without manure, the inorganic fertilizer was used as a check.

2.3. Experimentations

In the incubation experiment, two soils each from basement complex (Alabata, Osiele) and sedimentary (Itori and Papalanto) parent materials were used. Plastic containers containing 100g of soil were labeled appropriately with treatments applied individually after which distilled water was added. Soil amendment mixtures were incubated in a dark cupboard for eight weeks. Treatments were applied as above. Sub-samples were taken at two week- intervals for eight weeks (0, 2, 4, 6 and 8 weeks) and analyzed for pH, and electrical conductivity. In the screen house experiment, one soil each from basement complex (Alabata) and sedimentary (Papalanto) were used for this study involving two cycles of maize growth. Plastic buckets were filled with 5kg of the respective soil samples with dried manures applied two weeks before planting and manure ashes and NPK applied two weeks after planting. Water was added to the treated pots bringing them to the field capacity for two weeks to achieve equilibrium before sowing three seeds of maize (BR-9928-DMR-SR-Y) which were thinned to 1 seedling per pot at two weeks after planting. Soil samples were taken from the treatment pots at 0, 4 and 7 weeks for the first cycle and 0, 4 and 6 weeks for the second cycle after planting. The collected soil samples were analyzed for pH, and electrical conductivity according to the method mentioned earlier. The field experiment was done at the Federal University of Agriculture, Abeokuta ($7^0 12^1$ to $7^0 20^1$ N and $3^0 20^1$ to $3^0 28^1$). The field was cleared mechanically, ploughed, harrowed and divided into experimental plots. The size of the field was 22.0m x 26.0m, plot size was 3m x 4m and net plot size was 1.5m x 2m. Dried manures were applied two weeks before planting. Three seeds of maize were planted per hole with a space of 75 cm x 25 cm after which it was thinned to two plants per stand at two weeks' after planting, manure ashes and NPK were applied two weeks after planting to their respective plots. The plants were monitored on the field for twelve weeks. Soil samples were collected at 0, 2, 4, 6, 8 and 10 weeks after planting (WAP) and analyzed for pH, and EC according to the aforementioned method.

2.4. Data Analysis

Data collected were subjected to analysis of variance (ANOVA). The significant treatments were separated using Duncan Multiple Range Test (DMRT) at $p \leq 0.05$. The analysis was carried out using statistical analysis system (SAS).

3. Results

3.1. Characterization of Soils, Dried Manures and Manure Ash

The pH of the soils are shown in Table 1; they ranged from 6.75 in the soil from Osiele to 7.63 in the soil from Itori. The highest pH, available phosphorus, calcium, sodium, and iron were found in the soil from Itori, while the soil from Osiele had the highest magnesium and exchangeable acidity. The characteristics of dried manures and manure ashes are also presented. There was a significant increase in the pH, total P, and exchangeable bases in manure ashes compared with the dried manures. The iron content of these manures also increased after ashing although a significant increase was only observed for the dried cattle manure and dried goat manure after ashing. The highest pH, potassium, sodium, and carbon nitrogen ratio were observed in the goat manure ash, while the total P, calcium, and magnesium were observed to be the highest in the poultry manure ash. The order of total P content was as follows: poultry manure ash > goat manure

ash >cattle manure ash >dried poultry manure > dried goat manure > dried cattle manure.

3.2. Effect of Dried Manures and Manure Ash on Soil pH

The application of poultry manure ash increased pH significantly in the soils from Alabata and Osiele, while the dried goat manure resulted in a significant increase in the soils from Itori and Papalanto in the incubation experiment (Table 2). The dried-manure-amended soils differed from manure-ash-amended soils across the weeks. In the soil from Alabata, the highest pH was found at two weeks after treatment incorporation (2WAI). However, at 0WAI and 2WAI, manure ash did not yield any differences compared to dried manures. At 4, 6, 8WAI, a significant increase and decrease in pH were observed, respectively for DGM and DCM in comparison to their manure ashes. At 0WAI, a significantly lower pH was observed in the control soil and the manure ashes of poultry and cattle had significant effects on pH when compared to their dried manures. At 2WAI, the NPK amended soil had a significantly lower pH than other treated soils, although manure ashes, except GMA, showed similar effects. At 4 and 8WAI, application of CMA and GMA led to a significant increase and decrease in the soil pH compared to their manure counterparts.

Table 1. Some properties of soils and manures

Soil	pH	EC	Avail. P	Ca	Mg	K	Na	Fe	Al+H	Texture
		dSm^{-1}	$mgkg^{-1}$			$cmolkg^{-1}$		$mgkg^{-1}$	$cmolkg^{-1}$	
Alabata	7.16	0.38	10.26	5.13	1.05	0.27	0.47	6.70	0.04	Loamy sand
Osiele	6.75	0.43	9.33	4.06	2.25	0.25	0.47	8.75	0.07	Loamy sand
Itori	7.63	0.73	21.30	6.71	1.34	0.34	0.60	15.45	0.05	Loamy sand
Papalanto	6.84	0.26	6.84	2.56	1.71	0.18	0.31	8.25	0.06	Sandy
Funaab	6.83	0.40	4.98	3.56	1.27	0.47	0.56	7.75	0.05	Loamy sand

Manures	pH	Total P	Ca	Mg	K	Na	Cu	Zn	Fe	C/N
				$cmolkg^{-1}$					$mgkg^{-1}$	
Dried poultry manure	8.20f	14.7d	44.10b	30.70c	15.20e	15.20e	111b	1248b	4556b	14.75cd
Poultry manure ash	10.45b	30.50a	75.50a	63.00a	55.50b	58.40b	209a	237a	6978b	12.73d
Dried cattle manure	8.70e	2.20f	30.10d	15.00d	10.20f	10.40f	57c	372e	3654a	15.65cd
Cattle manure ash	10.15c	22.30c	33.70c	43.00b	21.90d	22.40d	112c	746c	9325a	20.43ab
Dried goat manure	9.60d	4.60e	17.80f	20.00d	38.70c	38.40c	25d	598d	2829c	15.65cd
Goat manure ash	10.90a	28.10b	25.30e	42.00b	75.20a	76.80a	77c	722c	9304a	22.52a

Means with the same letter in each column are not significantly different at $p \leq 0.05$

Table 2. Effect of manure amendments on soil pH in incubation study.

Treatment	Alabata					Osiele				
kg/ha	0 WAI	2 WAI	4 WAI	6 WAI	8 WAI	0 WAI	2 WAI	4 WAI	6 WAI	8 WAI
CON	6.75ab	7.77a	7.12abc	7.05cd	7.22ab	6.52d	7.50a	7.08bc	6.63a	7.30a
DPM	6.44b	7.30d	7.25ab	7.30ab	7.27a	6.61bc	7.38a	7.14bc	6.63a	7.20b
PMA	6.62ab	7.65abc	7.60a	7.40a	7.85b	6.95a	7.33ab	7.13bc	6.77a	7.13bcd
DCM	7.17a	7.70ab	7.17cd	7.12bcd	7.22ab	6.75bc	7.43ab	6.93bc	6.62a	7.08cd
CMA	7.25a	7.73ab	7.70a	7.15d	7.28a	6.90a	7.40abc	7.43a	6.83a	6.88e
DGM	6.72ab	7.47cd	7.27bcd	7.20bc	7.02c	6.70bc	7.40abc	7.45ab	6.15a	7.52a
GMA	6.95ab	7.53bc	6.92d	6.75e	6.90d	6.52d	7.07d	6.78d	6.82a	7.07cd
$NPK_{(15\text{-}15\text{-}15)}$	6.95ab	7.72ab	7.50abc	6.70e	7.27a	6.77b	7.18cd	7.35ab	6.60a	7.15bc
	Itori					Papalanto				
CON	7.00b	7.55bc	7.43b	6.93f	6.85e	6.80de	7.63ab	7.20bcd	6.90ab	7.32b
DPM	7.23ab	7.60b	7.47b	7.07de	7.05c	6.97c	7.23b	6.98de	6.83bc	7.13d
PMA	7.07b	7.23d	7.60ab	7.37b	6.77f	6.72e	7.65ab	7.22bc	6.88ab	7.20c
DCM	7.32a	7.75ab	6.97d	6.85f	6.93d	7.48a	7.33ab	6.88e	6.95ab	7.28b
CMA	7.10ab	7.30cd	7.85a	7.20c	7.15b	7.13b	7.36ab	7.05cde	6.82bc	7.17cd
DGM	7.17ab	7.87a	7.73a	7.57a	6.90de	7.18b	7.30ab	7.50a	7.12a	7.72a
GMA	7.31a	7.52bc	7.02cd	6.95ef	7.30a	7.42a	7.35ab	6.88e	6.62c	7.38a
$NPK_{(15\text{-}15\text{-}15)}$	7.23ab	7.33cd	7.20c	7.18cd	7.12bc	6.90cd	7.37ab	7.28ab	6.87b	7.18cd

Means with the same letter in each column are not significantly different at P<0.05
DPM = Dry poultry manure, PMA = Poultry manure ash, DCM = Dry cattle manure, CMA = Cattle manure ash, DGM = Dry goat manure, GMA = Goat manure ash, CON = Control.

The application of DGM significantly increased the pH of the soil from Itori at 2, 4 and 6WAP than other treatments. However, significant decreases and increases were observed respectively at 2 and 4, 6WAP for PMA and CMA in comparison to their dried manure counterparts, while GMA significantly decreased pH in comparison to its dried manure. At 8WAP, the treatment effects were significant since the control soil had significantly lower pH than other treated soil. CMA and GMA increased pH compared to their dried manures, while the contrary was the trend in the soils treated with PMA. In the soil from Papalanto, the treatment effect was not significant at 2WAP.

At 4, 6 and 8WAP, the highest pH was observed in the DGM treated soils, which was significantly different from the pH in the manure-ash-amended soil. In the screen house experiment (Table 3), the soil pH at 0 and 7WAP was significantly increased with the single application of DGM and DPM, respectively. However, at 4WAP, PMA and DGM significantly increased the pH of the soil from Alabata and Papalanto, respectively. At 4WAP, the soil from Alabata, showed a significantly lower pH for the NPK-amended-soil; however, other treatment effects, did not differ from the control soil. At 7WAP, dried manures and the manure ashes of goat and cattle showed similar results; however, a significant decrease in pH was observed in PMA-amended-soil relative to the DPM-amended-soil. In the soil from Papalanto, treatment effects at 0WAP were only observed for DCM and DCM in comparison with other treatments and control soils. It was also observed that the application of dried cattle manure significantly increased the electrical conductivity of soils used in the screen-house experiment. At 0 and 4WAP, regarding the soil from Alabata, the control soil recorded the lowest EC, while the dried manure-amended-soil had a significantly higher EC relative to the manure-ash-amended soil. In the soil from Papalanto, a significantly lower EC was observed across the weeks for the control soil, and the dried manures significantly increased the soil EC compared to their manure ashes.

Table 5 shows the effects of the treatments on the soil pH during the field evaluation. The application of cattle manure ash led to a significantly higher pH corresponding to other treatments at all weeks of evaluation. At 0WAP, dried manures and manure ash were similar in their effect on soil pH; however, the lowest pH was recorded in the DPM-amended soil. A similar sequence was observed at 2WAP although the GMA-amended soil had the lowest pH which significantly differed from its ash-amended soil. Conversely, the single application of CMA and GMA led to a significant increase and decrease in pH compared to their dried-manure counterparts at 4WAP. At 6, 8 and 10WAP, the application of GMA allowed for a significantly lower pH relative to other amendments. However, at 6 and 10WAP, PMA and GMA did not differ from their dried-manure counterparts, while a significant decrease in pH was observed or PMA and GMA relative to their dried manures at 8WAP.

Table 3. Effect of manure amendments on soil pH and electrical conductivity in the screen house experiment

Treatment	Alabata						Papalanto					
kg ha^{-1}	0 WAP	4 WAP	7 WAP	0 WAP	4 WAP	6 WAP	0 WAP	4 WAP	7 WAP	0 WAP	4 WAP	6 WAP
Soil pH												
	Cycle 1			Cycle 2			Cycle 1			Cycle 2		
CON	7.48bc	6.92ab	7.28c	7.28c	7.12b	7.67ab	7.15b	6.65b	6.95c	6.95c	7.12b	7.67ab
DPM	6.87d	7.07ab	7.78a	7.78a	7.13b	7.75a	7.33b	6.40bc	7.58ab	7.58ab	7.13b	7.76a
PMA	7.36c	7.17a	7.52b	7.52b	7.43ab	7.30c	7.17b	6.38bc	7.70a	7.70a	7.43ab	7.30c
DCM	7.70ab	6.85b	6.50d	6.50d	7.43ab	7.73a	7.73a	6.47bc	7.30b	7.30b	7.43ab	7.70a
CMA	7.42c	7.12ab	6.48d	6.48d	7.42ab	7.70a	7.27b	6.62bc	6.87cd	6.87cd	7.42ab	7.73a
DGM	7.88a	6.83b	7.38bc	7.28c	7.73a	7.53ab	7.72a	7.05a	7.52ab	7.52ab	7.73a	7.47bc
GMA	7.70ab	7.82b	7.28c	7.38bc	7.48ab	7.47bc	7.20b	6.27c	6.60d	6.60d	7.48ab	7.53ab
NPK $_{(15\text{-}15\text{-}15)}$	7.45c	6.30c	7.42bc	7.42bc	6.38c	7.72a	6.73c	6.35c	6.72cd	6.72cd	6.38c	7.72a
Soil Electrical Conductivity												
CON	0.63g	0.46f	0.44c	0.44c	1.28e	0.58cd	1.04h	1.09h	0.31f	0.31f	1.28e	0.58cd
DPM	3.76b	0.89e	0.35e	0.35e	1.11e	0.84c	2.05e	3.77b	0.45c	0.45c	1.11e	0.84c
PMA	0.85g	0.36g	0.40g	0.40g	0.80f	0.31d	1.67g	3.13d	0.29f	0.29f	0.80f	0.31d
DCM	5.38a	3.34a	1.02a	1.02a	3.92a	6.48a	5.75a	5.55a	1.14a	1.14a	3.92a	6.48a
CMA	1.63e	1.02d	0.32f	0.32f	1.88d	0.77c	1.86f	1.68f	0.83b	0.83b	1.88d	0.77c
DGM	2.68c	2.04c	2.04c	2.04c	3.40b	0.85c	3.89b	1.22g	0.44cd	0.44cd	3.40b	0.85c
GMA	2.06d	0.94e	0.46c	0.46c	2.24c	1.28b	2.15d	3.45c	0.42d	0.42d	2.24c	1.28b
NPK $_{(15\text{-}15\text{-}15)}$	1.30f	3.15b	0.42cd	0.42cd	2.08cd	1.59b	3.42c	1.76e	0.36e	0.36e	2.08cd	1.59b

Means with the same letter in each column are not significantly different at P<0.05
DPM = Dry poultry manure, PMA = Poultry manure ash, DCM = Dry cattle manure, CMA = Cattle manure ash, DGM = Dry goat manure, GMA = Goat manure ash, CON = Control

3.3. Effect of Treatment on Soil Electrical Conductivity

Table 4 shows the effects of the amendment on soil EC during the incubation experiment. The application of DCM significantly increased the electrical conductivity of the soils at all weeks of incubation except at 0WAI for the soil from Alabata, and at 4 and 6WAI for the soil from Osiele and Papalanto. Regarding the soil from Alabata and Osiele, the control soil had significantly lower EC compared to other treated soil at all weeks except at 4WAI. Dried-manure-amended soil had higher EC compared to the manure-ash amended soil from Alabata. However, in the soil from Osiele, the incorporation of poultry-manure ash led to a significant increase in EC compared to its dried manure across the weeks while the contrary trend was observed for other manure ashes only that a significant increase was observed for EC in the CMA-amended soil when compared to its dried manure at 4WAI. In the soil from Itori and Papalanto, the application of dried manures showed a significant effect on EC compared to the manure ash.

Table 4. Effect of manure amendments on Soil Electrical Conductivity (EC) in incubation

Treatment	Alabata [EC (dSm^{-1})]					Osiele [EC (dSm^{-1})]				
kg ha^{-1}	0 WAI	2 WAI	4 WAI	6 WAI	8 WAI	0 WAI	2 WAI	4 WAI	6 WAI	8 WAI
CON	0.61e	0.34h	0.44e	0.29f	0.46de	0.73d	0.31h	0.48c	0.26g	0.31g
DPM	1.04c	0.44f	0.56c	0.58d	0.54c	0.90cd	0.39f	0.43d	0.50d	0.58c
PMA	0.74de	0.38g	0.36f	0.41e	0.42e	0.97cd	0.80b	0.48c	0.81a	0.64b
DCM	1.35b	1.04a	0.83a	1.03a	0.89a	1.81a	0.89a	0.46cd	0.71b	0.90a
CMA	1.07c	0.61c	0.57c	0.68b	0.51cd	1.11bc	0.40e	0.79b	0.62c	0.42f
DGM	1.68a	0.71b	0.76b	0.70b	0.72b	1.22b	0.55c	0.87a	0.43e	0.65b
GMA	0.81d	0.49e	0.47d	0.40e	0.41e	0.90cd	0.36g	0.47cd	0.32f	0.54d
NPK $_{(15\text{-}15\text{-}15)}$	0.76de	0.57d	0.56c	0.63c	0.70b	1.20b	0.42d	0.39e	0.69b	0.48e
	Itori [EC (dSm^{-1})]					Papalanto [EC (dSm^{-1})]				
CON	1.13cd	0.67d	0.86b	0.63e	1.23a	0.80c	0.40d	0.61abc	0.36c	0.47c
DPM	1.23bcd	0.63e	0.64d	0.79cd	0.86c	0.94c	0.42d	0.86ab	0.43c	0.46c
PMA	1.05d	0.57f	0.55f	0.66de	0.61d	0.70c	0.42d	0.37a	0.44c	0.43c
DCM	2.03a	1.14a	1.68a	1.88a	1.29a	3.09a	0.63a	0.75ab	0.59c	0.82a
CMA	1.32bc	0.55g	0.92a	0.99b	0.89c	0.97bc	0.44c	0.60abc	0.56c	0.68b
DGM	2.19a	0.87b	0.93a	0.90bc	1.05b	1.05bc	0.55b	0.45bc	0.39c	0.35d
GMA	1.37b	0.55g	0.61e	0.56e	0.63d	0.90c	0.34f	0.50bc	0.40c	0.36d
NPK $_{(15\text{-}15\text{-}15)}$	1.30bc	0.82c	0.88b	0.87bc	0.93c	1.37b	0.38e	0.40c	0.40c	0.48c

Means with the same letter in each column are not significantly different at $p \leq 0.05$
DPM = Dry poultry manure, PMA = Poultry manure ash, DCM = Dry cattle manure, CMA = Cattle manure ash, DGM = Dry goat manure, GMA = Goat manure ash, CON = Control.

Table 5 shows the effect of the amendments on soil EC in the field experiment. The application of cattle-manure ash led to a significant increase in the soil EC at weeks of observation except 0WAP. At 0WAP, significantly lower EC was observed in the control soil; the highest EC was observed with DCM. At 2WAP, the application of manure ashes significantly increased EC in comparison to their dried manures, and the lowest EC was recorded in the NPK-amended soil. A similar response was observed at 4WAP only that GMA and DGM did not differ. At 6 and 10WAP, only the manure ash of poultry and cattle led to a significant increase in EC in comparison to their dried manures.

Table 5. Effect of amendments on soil pH and electrical conductivity in field evaluation

Treatment	Soil pH						Soil EC (dSm^{-1})					
(kg ha^{-1})	0WAP	2 WAP	4 WAP	6 WAP	8WAP	10 WAP	0WAP	2 WAP	4 WAP	6 WAP	8WAP	10 WAP
CON	6.75ab	7.02d	7.43b	6.90ab	7.22ab	7.30b	0.73d	0.48c	0.54b	0.57c	0.44d	0.46e
DPM	6.44b	7.28bcd	7.47b	6.83bc	7.27a	7.20b	0.90cd	0.43d	0.42c	0.59c	0.54c	0.50d
PMA	6.61ab	7.33abc	7.60ab	6.88ab	7.15b	7.13bcd	0.87cd	0.48c	0.59b	0.64b	0.42e	0.71b
DCM	7.17a	7.43ab	6.97d	6.95ab	7.22ab	7.08cd	1.81a	0.46cd	0.44c	0.42e	0.51cd	0.62c
CMA	7.25a	7.52a	7.73a	7.12a	7.28a	7.75a	1.11bc	0.87a	0.86a	0.90a	0.89a	0.80a
DGM	6.72ab	7.40abc	7.50ab	6.82bc	7.02c	7.05d	1.22b	0.47cd	0.39c	0.65b	0.72b	0.43e
GMA	6.95ab	7.01d	7.02cd	6.62c	6.90d	7.07cd	0.90cd	0.79b	0.40c	0.54c	0.41e	0.32f
NPK $_{(15\text{-}15\text{-}15)}$	6.95ab	7.18cd	7.20c	6.87b	7.27a	7.15bc	1.20b	0.39e	0.40c	0.48d	0.70b	0.69b

Means with the same letter in each column are not significantly different at $p \leq 0.05$
DPM = Dry poultry manure, PMA = Poultry manure ash, DCM = Dry cattle manure, CMA = Cattle manure ash, DGM = Dry goat manure, GMA = Goat manure ash, CON = control

4. Discussion

It is well established that crop production on acid soils can be improved greatly when soil pH is adjusted to near neutral. Soil pH affects nutrient solubility and influences the sorption or precipitation of nutrients with Al and Fe (Hue, 1992). The pH of the soils were slightly acidic to neutral. The fertility of the soils was generally low to moderate, hence, a specific response to the application of organic manure would be expected. The soils had organic carbon levels above 11 g kg^{-1} indicating a moderate to high organic matter. The available P content ranged from low to moderate (1 – 20 mg kg^{-1}). The available P content of the acid soil is lower than that of the neutral soil. This indicates that Fe ions and Al ions will form complexes with phosphate, therefore making the release of P for plant use higher in the neutral soil than the acidic soil. Manuring is a practice that helps increase the organic carbon content of soils, which may induce better water infiltration, increased capacity to retain nutrients. The alkaline pH observed in the manures indicates the presence of excess basic cation at the expense of acidic ones. Equally, the acidic nature of some of the soils was expected to be controlled by the cations supplied by the manure that was alkaline in reaction and generally high in macro and micronutrients. The composition of micro nutrients in poultry for this study conformed to the findings of Azeez and Averbeke (2010) that feed additives including antibiotics and growth stimulants in poultry diet could be responsible for the increased micronutrients in the poultry litter, with a large quantity metabolized in the body of the birds and the excess excreted as wastes. The trends of nutrient distribution in manures vary. This reflects the differences in the feed composition of the animals. The higher P concentration in the manure ash resulted from the elimination of the carbon during the burning of the ash. The exchangeable bases in the manure ash are more than those in the dried manure. Lal and Ghuman (1989) reported that the conversion of biomass to ash increased the levels of cations and other nutrient elements.

The highest pH values were observed in the amended soils because the addition of organic waste wastes (animal manures) to acidic soils is potentially a reliable strategy for increasing soil pH. Also, this could be attributed to the high content of exchangeable bases in the manures. Other studies have reported a similar effect on soil pH after the application of fresh or composted soil animal manure (Eghball 1999). Ano and Ubochi (2007) reported that animal manures significantly increased the soil pH from 4.6 to values above 5.6. The pH of the ash-manure-amended soil was higher than that of the soil amended with dried manures. This could be attributed to the fact that the initial pH of ash manures was higher than that of the dried manure in addition to the higher amount of exchangeable bases. Ash manures have a high content of calcium hence increasing the liming properties. Adekayode and Olojugba (2009) reported that exchangeable bases were significantly higher in plots treated with wood ash compared to plots treated with other amendments. Electrical conductivity (EC) was significantly increased in the amended soils, in comparison to the EC value obtained in the control. The increase can be explained by the input of nutrients and salt contained in the manure. Goff (2006) reported that salts in manures are sourced from feed additives. Dried manures had higher EC than ash manures. This could be a result of the low carbon nitrogen content of dried manures which allows them to mineralize faster than their ash and hence releasing greater amount of cations that form salts. Azeez and Van Averbeke (2012) found that the electrical conductivity of the soils significantly increased with the application of poultry, cattle, and goat manures, and the potential manure-induced soil salinization was very high in the poultry manure compared with the cattle manure.

5. Conclusions

The present study concludes that the effects of manure ashes on soil pH and EC was comparable to those of the dried manures, thus showing a great potntial as a good liming material. However, the manure ash performed better in terms significant increase in soil pH and EC in comparison to the control and the dried manures. Hence, the use of animal manure ash in place of dried manures is highly recommended for use.

References

Adekayode, F.O., and Olojugba, M.R. (2010). The utilization of wood ash as manure to reduce the use of mineral fertilizer for improved performance of maize (Zea mays L.) as measured in the chlorophyll content and grain yield. J. Soil Sci. Environ mgt 1(3):40-45.

Ano, A.O., and Ubochi, C.I. (2007). Neutralization of soil acidity by animal manure. Mechanism of reaction. African J. Biotech. 6(4):364-368.

Ano, A.O., and Agwu, J.A. (2005). Effect of animal manures on selected soil chemical properties. Nig. J. Soil Sci. 15:14-19.

Azeez, J.O., Van Averbeke, W. (2012). Dynamics of soil pH and electrical conductivity with the application of three animal manures. Comm. Soil Sci. Plant Anal. 43(6):865–874.

Azeez J.O., Van Averbeke, W. (2010). Nitrogen mineralization potential of three animal manures applied on a sandy clay loam soil. Biores. Tech. 101:5645–5651.

Bouyoucos, C.J. (1965). Hydrometer method improved for making particle size analysis of soils. American Proceeding Soil Sci. Soc. 26: 464-465.

De, N. S., Van De Steene, J., Hartman, R., Hofman, G. (2000). Using time domain reflectometry for monitoring mineralization of nitrogen from soil organic matter. European J. Soil Sci. 51:295 –304.

Eghball, B. (1999). Liming effects of beef cattle feedlot manure or compost. Comm. Soil Sci. Plant Anal. 30 (19-20): 2563–257

Gabriel, B.L.M. (1998). Utilization and management of animal manures for crop production. The case of UrbanMorogoro and Kilosa Districts. BSc. (Agriculture) Special Project. Sokoine University of Agriculture,Morogoro. Tanzania.

Goff, J.P. (2006). Macromineral physiology and application to the feeding of the dairy cow for prevention of milk fever and other peripaturient mineral disorders. Animal Feed Sci. Technol. 126: 237-257.

Hue, N.V. (1992). Correcting soil acidity of a highly weathered Ultisol with chicken manure and sewage sludge. Comm. Soil Sci. Plant Anal. 23: 241–264.

Kaira, Y.P. and Maynard, D.C. (1991). Methods manual for forest soil and plant analysis. Inf. Rep. NOR-X-319. Edmonton, Albert: Forestry Canada, Northwest Region, Northern Forestry Center.

Kimbi, G.G., Rutachokizibwa, V., Mollel, N.M., Simalenga, T.E., Ngetti, M.S., Biswalo, P.L. (1992). Identification of SUA-TU Linkage Project needs assessment: A preliminary survey. Report submitted to SUA-TU Linkage Project. Institute of Continuing Education, 13-45. Tanzania: Sokoine University of Agriculture Press.

Lal, R., and Ghuman, B.S. (1989). Biomass burning in windows after clearing a tropical rain forest: Effect on soil properties, evaporation and crop yields. Field Crop Res. 22(4): 247-255.

Masto,R.E., Chhonkar, P.K., Singh, D., Patra, A.K. (2007). Soil quality response to long-t erm nutrient and crop management on a semi-arid Inceptisol. Agric. Ecosys. Environ.118: 130-142.

Mokolobate, M.S. and Haynes, R.J. (2002). Comparative liming effect of four organic residues applied to an acid soil. Biol. Fert. Soils 35:79–85

Nwajiuba, C. and Chimezie, P. (2000). The use of livestock wastes in soil fertility regeneration in Imo state of Nigeria. In Nwokocha, U. and Odi A. (Eds.). Proceedings of the first annual conference of the college of Agriculture and Veterinary medicine, (pp 137-140). Umahia, Abia: Abia State University

Olatunji, O., Ayuba, S.A., Oboh, V.U. (2006). Growth and yield of okra and tomato as affected by pigdung and other organic manures: Issues for economic consideration in Benue state. In: Ojeniyi, S. O. (Ed.). Proceedings of the 30th Annual Conference of the Soil Science Society of Nigeria, (pp.91-98.). Makurdi, Benue: University of Agriculture.

Page, A.L., Miller, R.H., Keeney, D.R. (Eds.) (1982). Methods of soil analysis; 2. Chemical and microbiological properties, 2. Aufl. 1184 S., American Soc. Of Agronomy (Publ.), Madison, Wisconsin, USA, gebunden 36 Dollar.

Pocknee, S. and Sumner, M.E. (1997). Cation and nitrogen contents of organic matter determine its liming potential. Soil Sci. Soc. America J. 61:86–92.

Watanabe, P. H., Thomas, M.C., Pascoal, L.A.F., Ruiz, U.S., Daniel, E., Amorim, A.B. (2013). Manure production and mineral excretion in faeces of gilts fed ractopamine. Maringa: Acta Sci. Animal Sci. 35(3): 267–272.

JJEES

JJEES (2020) 11 (2): 93-97
ISSN 1995-6681

Jordan Journal of Earth and Environmental Sciences

Risk Assessment of Traditional Faecal Pollution Markers in Three Streams in a Suburb of Akure, Nigeria

Olalemi Adewale*, Ogundare Temitope, Yusuff Olanrewaju, Ajibola Temitope

Federal University of Technology, School of Sciences, Department of Microbiology, Nigeria

Received 12 August 2019; Accepted 3 December 2019

Abstract

This investigation was carried out to determine the concentration of faecal indicator bacteria (***Escherichia coli*** and faecal coliforms) in water samples collected from three streams in Akure, Nigeria at different times of the day. This risk assessment is of great significance to human health protection against waterborne diseases. Results revealed high concentrations of *E. coli* (1.20×10^3 colony forming unit per 100 milliliters 'cfu/100 ml') and faecal coliforms (8.50×10^2 cfu/100 ml) in the water samples. In addition, the levels of *E. coli* exhibited positive relationship with total dissolved solids, turbidity, dissolved oxygen, electrical conductivity, and negative relationship with temperature, pH, and alkalinity. The findings from this study suggest that effective faecal pollution control specific procedures may include the improvement of the quality of residential buildings with adequate sanitation in the area surrounding the streams, direction of sewer channels away from the streams, construction of ridges around agricultural farm lands to prevent runoff, campaigns against direct defecation and indiscriminate disposal of animal wastes from poultry birds, cattle, sheep, goats and domestic dogs. These faecal pollution control actions may offer improved ways to protect human health.

Keywords: Faecal indicator bacteria, human health, surface water, sustainable development goals, waterborne diseases

1. Introduction

The number six goal highlighted in the United Nation's new 2015 Sustainable Development Goals (SDGs) is to provide clean water and sanitation by 2030. To achieve this goal, reliable and accessible methods are needed to measure the concentration of *E. coli* and other faecal coliforms in water (Sobsey, 2016). Understanding and monitoring water quality of a region remains a better tool towards promoting sustainable development of water resources and the prevention of waterborne diseases (Aderibigbe et al., 2008; Hiremath et al., 2011). Drinking water should contain less than one *E. coli* or faecal coliform CFU/100 ml, whereas water intended for bathing, recreation or aquaculture should contain less than or equal to 100 *E. coli* or faecal coliforms CFU/100 ml (CEU, 2006). The human health is under tremendous threat due to undesired changes in the physical, chemical, and the biological characteristics of water. Increase in human population, industrialization, use of fertilizers, and anthropogenic activities result in the pollution of water with different harmful contaminants (Patil et al., 2012). This study is aimed at determining the concentration of faecal indicator bacteria (*E. coli* and faecal coliforms) in water samples collected from three streams in Akure, Nigeria at different times during the day. These water sources are prone to faecal contamination especially from direct defecation, close proximity to sewer channels, and runoff from agricultural farm lands during wet periods. In addition, the outbreak of waterborne diseases such as diarrhoea and dysentery have been reported in the vicinity of these water sources. Therefore, this risk assessment was conducted to gain a better understanding of the microbial quality of the streams which may help in identifying specific targets for effective pollution-control actions in a bid to meeting the United Nation's new 2015 Sustainable Development Goals of bringing microbially safe and clean water to all.

There are many places worldwide where humans suffer and die from waterborne diseases, because the water (drinking water, recreational water, crop irrigation water, pond water, shellfish growing and harvesting water, untreated or partially-treated wastewater) (Shittu et al., 2008, Olalemi et al., 2016a) is not protected from, treated against, or tested for faecal microorganisms (Sobsey, 2016). The continuous use of faecally-contaminated water for domestic purposes presents a significant risk to human health, because it may contain pathogenic microorganisms such as viruses and bacteria mostly members of the family *Enterobacteriaceae* that are aetiological agents of many human diseases such as typhoid, cholera, dysentery etc. (Exner, 2015). Generally, the microbial quality of water deteriorates as a result of direct discharge of untreated or partially-treated wastewater into rivers and streams, and the inefficient management of closed and protected water distribution and storage systems. Microbially contaminated water has critical impact on all biotic components of the ecosystem and this could affect its use for drinking, bathing, irrigation, purposes etc.

Globally, about 80% of all diseases and deaths in low-income and lower-middle-income countries are water-related as a result of polluted water (WHO, 2014). Often, these waters are obtained from wells, boreholes, streams, rivers and they may not be pure chemically and/or microbially safe. For

* Corresponding author e-mail: waleolas2002@yahoo.com

instance, rain water which flows into streams may contain dissolved materials from the air and suspended dusts that microorganisms are attached to, and may also lead to urban or agricultural runoffs into the streams. The assessment of human activities (such as sewage disposal, sanitation, and hygiene practices etc.) capable of affecting the quality of water within an area is important. This is necessary, since the demand for water is increasing while accessibility to available freshwater is on the decrease because of pollution from point and non-point sources.

2. Materials and Methods

2.1 Description and Selection of the Study Area

Three different streams located in Aba (sampling point A 'stream 1') and Apatapiti (sampling points B 'stream 2' and C 'stream 3') in Akure, Nigeria were used for the study. The streams are approximately 1.2 – 2.5 meters wide and 0.9 – 1.5 meters deep. The streams are tributaries of River Ala which has a total length of about 57 km flowing downwards from the North to the South of Akure metropolis (Figure 1). The sampling sites were selected based on anthropogenic activities (that included animal rearing involving poultry birds, cattle, sheep, goats, and domestic dogs), direct defecation, close proximity to sewer channels and agricultural farm lands.

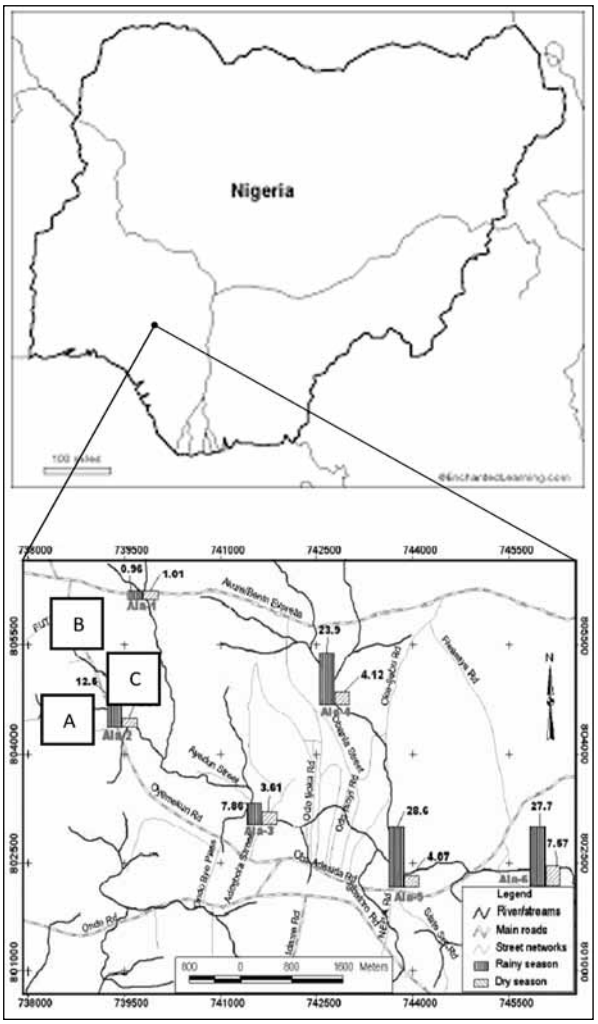

Figure 1. Locality map showing the streams and the sampling points (A, B, C) in Akure, Nigeria.

2.2 Collection of Water Samples

Water samples were collected from the three streams for five consecutive weeks. All water samples were collected at a depth of about 20 – 30 cm below the water surface at the midstream in the direction of flow using sterile, screw-capped 500 ml plastic bottles in the morning (8 – 10 am) and afternoon (1 – 3 pm). A total of 60 grab samples of water were taken from the three streams (i.e., 20 water samples were collected from each stream, of which ten water samples were taken in the morning and the other ten samples were taken in the afternoon). Water samples were coded with names on-site, and then transported to the laboratory in a cool box within one hour.

2.3 Enumeration of Faecal Indicator Bacteria in the Water Samples

Faecal indicator bacteria (faecal coliforms and *E. coli*) were examined using standard microbiological methods. Using the membrane filtration method (ISO 9308-1) (Anon., 2014), a measured volume of the water sample (1 ml) was diluted in one-fold (9 ml) of peptone water and filtered through 0.45 µm cellulose acetate membrane filters in a set-up connected to a vacuum pump that allows easy filtration of the water. The filters were, thereafter, placed on freshly-prepared selective media (Membrane faecal coliform agar 'm-FC' and Membrane lauryl sulphate agar 'MLSA'). The plates were incubated at 37˚C for twenty-four hours (MLSA) and 44˚C for twenty-four hours (m-FC). Yellow colonies on MLSA were sub-cultured onto Eosin methylene blue agar 'EMB' plates and incubated at 37˚C for twenty-four hours to confirm the presence of *E. coli*. Bacterial colonies were counted and expressed as CFU/ 100 ml.

2.4 Determination of Physicochemical Properties of the Water Samples

The physicochemical parameters inherent in the water samples from the three streams were measured using standard methods and recorded appropriately (Anon., 2012). These include temperature (Celsius), pH, alkalinity (milligrams per litre), salinity (milligrams per litre), turbidity (nephelometric turbidity units), electrical conductivity (microsiemens per centimeter), dissolved oxygen (milligrams per litre), and the total dissolved solids (milligrams per liter).

2.5 Statistical Analysis

Data obtained were examined using descriptive statistics and single factor analysis of variance (ANOVA) at 95 % confidence level, while significant means were separated with the Duncan's New Multiple Range Test (DNMRT). Further statistical analyses were undertaken to determine whether there were positive correlations between the concentration of the faecal indicator bacteria and physicochemical properties of the water samples from the streams.

3. Results

3.1 Detection of Faecal Indicator Bacteria in the Water Samples

The concentration of *E. coli* ranged from 0.4×10^2 to 4.3×10^2 cfu/100 ml in stream one, 1.0×10^2 to 1.2×10^3 cfu/100 ml in stream two and 0.6×10^2 to 5.3×10^2 cfu/100 ml in stream three. In general, the concentration of *E. coli* appeared to be higher in the samples collected in the morning compared to those collected in the afternoon, although with a few exceptions i.e., 60%, 10%

and 10% of the water samples from streams one, two, and three respectively, showed higher concentration of *E. coli* in the afternoon samples than in the morning samples (Figure 2).

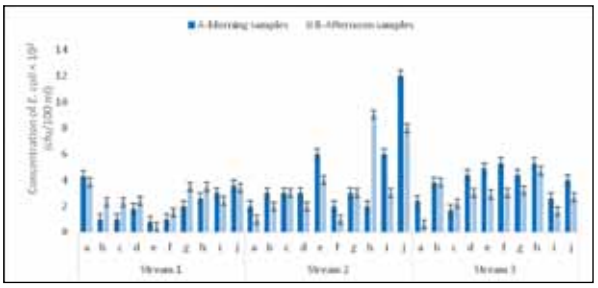

Figure 2. Mean concentration of *E. coli* in water samples from the three streams over the period of study

Key: Water quality standard – Drinking water should contain less than one E. coli CFU/100 ml (CEU 2006)

The concentration of faecal coliforms ranged from 0.7 × 10^2 to 8.5 × 10^2 cfu/100 ml in stream one, 2.0 × 10^2 to 13.0 × 10^2 cfu/100 ml in stream two and 0.9 × 10^2 to 7.2 × 10^2 cfu/100 ml in stream three. Similarly, the concentration of faecal coliforms appeared to be higher in samples collected in the morning compared to those collected in the afternoon, with the exception of stream one where 50% of the samples showed higher concentration of faecal coliforms in the afternoon samples than in the morning samples (Figure 3).

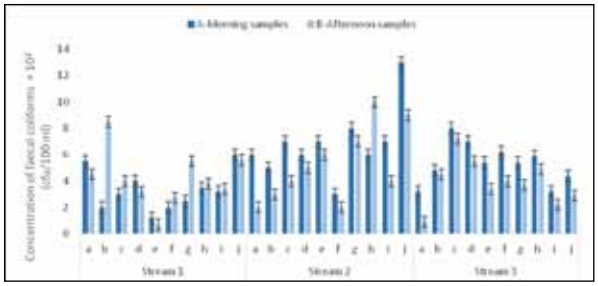

Figure 3. Mean concentration of faecal coliforms in water samples from the three streams over the period of study

Key: Water quality standard – Drinking water should contain less than one faecal coliform CFU/ 100 ml (CEU 2006)

3.2 Physicochemical Characteristics of the Water Samples

In stream one, water temperature ranged from 28 to 31 ˚C, while pH ranged from 6.9 to 7.1, whereas electrical conductivity ranged from 4.4 × 10^2 to 5.5 × 10 µS/cm. In stream two, alkalinity ranged from 6.9 to 25.7 mg/l, while salinity ranged from 24.9 to 63.7 mg/l. The total dissolved solids ranged from 0.1 to 0.5 × 10^2 mg/l and the amount of dissolved oxygen ranged from 2.2 to 6.3 mg/l. Similarly, in stream three, water temperature ranged from 28 to 31 ˚C, while pH ranged from 7.0 to 7.6 and electrical conductivity ranged from 3.9 × 10^2 to 6.0 × 10 µS/cm (Table 1).

Table 1. Physicochemical characteristics of the water samples from the three streams over the period of study

Physicochemical parameters	Stream 1	Stream 2	Stream 3
Temperature (˚C)	29.9 ± 0.9 (28.0-31.0)	29.5 ± 0.4 (27.0-32.0)	29.5 ± 0.4 (28.0-31.0)
pH	7.0 ± 0.0 (6.9-7.1)	7.4 ± 0.1 (7.2-7.8)	7.3 ± 0.2 (7.0-7.6)
Salinity (mg/l)	34.2 ± 0.7 (24.0-49.7)	39.1 ± 0.5 (24.9-63.7)	55.8 ± 12.9 (30.0-79.8)
Total Dissolved Solids ×10^2 (mg/l)	0.2 ± 0.1 (0.1-0.5)	0.3 ± 0.12 (0.1-0.5)	0.4 ± 0.1 (0.2-0.7)
Dissolved oxygen (mg/l)	3.2 ± 0.7 (2.0-4.8)	3.5 ± 0.17 (2.2-6.3)	3.8 ± 0.6 (1.6-6.3)
Alkalinity (mg/l)	13.4 ± 0.3 (9.1-25.7)	11.1 ± 0.20 (6.9-21.4)	15.6 ± 0.3 (9.4-25.7)
Electrical conductivity ×10 (µS/cm)	4.8 ± 0.3 (4.4-5.5)	4.9 ± 0.50 (4.4-6.0)	5.53 ± 0.7 (3.9-6.0)

Key: Values are expressed as Mean ± Standard Deviation (n = 20) (Range: Minimum - Maximum)

3.3 Relationship between Observed Physicochemical Characteristics and Faecal Indicator Bacteria in the Water Samples

The relationship between the concentrations of *E. coli* and those of the physicochemical properties of the water samples were analyzed using scatter plots. Levels of *E. coli* in stream three demonstrated a negative relationship with temperature (R^2 = 0.2211) (Figure 4), whereas levels of *E. coli* in stream two showed a positive relationship with turbidity (R^2 = 0.2579) (Figure 5).

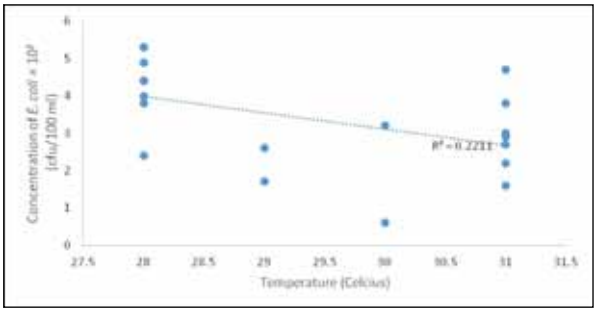

Figure 4. Negative relationship between temperature and mean concentration of *E. coli* in water samples from stream three

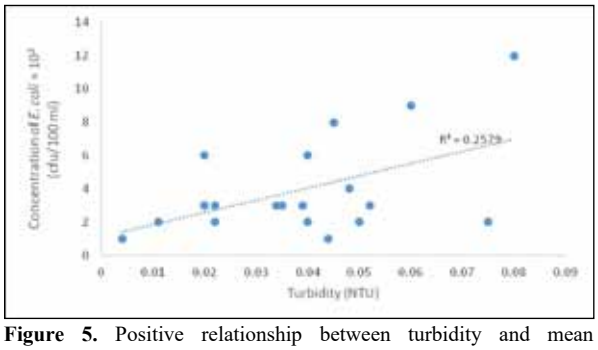

Figure 5. Positive relationship between turbidity and mean concentration of *E. coli* in water samples from stream two

4. Discussion

The first step in microbial risk assessment (hazard evaluation) was carried out by examining the concentration of faecal indicator bacteria in water samples collected from three different streams in Apatapiti and Aba area, Akure, Nigeria at different times of the day. Understanding the microbial quality of the streams is important to identify specific targets for effective pollution control actions in order to achieve one of the goals set by the United Nation

in the new 2015 Sustainable Development Goals that is, providing clean water for all by 2030.

In this study, stream two appeared to be the most contaminated because it contained very high levels of *E. coli* and faecal coliforms compared to streams one and three. Clearly, the waters from the three streams do not meet the acceptable limit of *E. coli* and faecal coliforms in water quality standards, where drinking water should contain less than one *E. coli* or faecal coliform CFU/100 ml, whereas water intended for bathing, recreation, or aquaculture should contain less than or equal to 100 *E. coli* or faecal coliforms CFU/100 ml (CEU, 2006). Waterborne pathogens from faecal pollution continue to be a major cause of infectious disease in many parts of the world. The incidences of these infections are higher in low- and middle-income countries than in high-income countries as a result of inadequate water, sanitation and hygiene (WHO, 2014). The high concentration of *E. coli* and faecal coliforms in the three streams in this study, may be as a result of anthropogenic activities (that included animal rearing, as well as close proximity of the streams to agricultural farm lands. It may also be as a result of surface runoffs following rain and storm events that carry faecal wastes into the streams, thus, increasing the level of microbial pathogens and ultimately impacting the sanitary quality of the stream negatively (Wilkes et al., 2013). There is also the likelihood of indiscriminate discharge of partially-treated or untreated wastewater into the flowing streams, including seepage from poorly functioning septic tanks from close residential buildings. These identified point and non-point sources of faecal contamination of the streams may best be described to originate from both human and non-human sources.

Physicochemical parameters were investigated to determine their contribution to the fate and survival of the faecal indicator bacteria in the streams. Water temperature values exhibited a negative relationship with the concentration of *E. coli* in the streams. Bacteria of enteric origin have been reported in many studies to be inactivated by solar radiation (Chandran and Hatha, 2003; Olalemi, 2015). This may be responsible for the observed trend in this study, where the concentration of *E. coli* appeared to be higher in samples collected in the morning compared to those collected in the afternoon. Alkalinity also showed a negative relationship with the levels of faecal coliforms in the streams. The results obtained in this study, showed that the level of turbidity demonstrated a positive relationship with the concentration of *E. coli* in the streams. This is in agreement with Pommepuy et al. (1992) who observed that enteric bacteria are able to survive for longer period of time in highly turbid waters. The values of electrical conductivity and total dissolved solids showed a similar trend. In all of the streams, counts of faecal indicator bacteria increased with the increase in turbidity and reduced with the increase in temperature. This is in agreement with the observation of many previous studies (Diston et al., 2012; Wilkes et al., 2013; Olalemi et al., 2016b) demonstrating that physicochemical parameters may provide useful information in water quality monitoring for human health protection.

Whilst the United Nations Millennium Development Goals (MDGs) of reducing the number of people worldwide lacking access to microbially-safe water by 2015 was effective to a large extent. Today, many people still lack access to microbially-safe water, most especially in low- and middle-income countries (Sobsey, 2016). Hence, the high burden of waterborne diseases (including diaorrhea) which lead to ill health, morbidity, and mortality in these countries. With the United Nations new 2015 Sustainable Development Goals (SDGs), it is hoped that microbially safe water will be accessible to all by 2030.

5. Conclusions

The sources of faecal contamination of the streams originate mainly from anthropogenic activities (that included animal rearing involving poultry birds, cattle, sheep, goats, and domestic dogs), direct defecation, and runoff from agricultural farm lands. The findings from this study suggest that specific targets for an effective faecal pollution control may include the improvement of the quality of residential buildings with adequate sanitation in the area surrounding the streams, direction of sewer channels away from the streams, construction of ridges around agricultural farm lands to prevent runoff, advocate against direct defecation and indiscriminate disposal of animal wastes from poultry birds, cattle, sheep, goats, and domestic dogs. These faecal pollution control actions may offer improved ways to protect human health.

Acknowledgements

The authors are grateful to the Department of Microbiology, School of Sciences, Federal University of Technology, Akure for providing a conducive environment for the research.

References

Aderibigbe, S. A., Awoyemi, A. O., Osagbemi, G.K. (2008). Availability, adequacy and quality of water supply in Ilorin metropolis, Nigeria. European Journal Scientific Research 23:528-536.

Anon (2012). Standard methods for the examination of water and wastewater (22nd ed.) APHA/AWWA/WEF: Washington DC, USA.

Anon. (2014). ISO 9308 – 1. Water Quality. Detection and Enumeration of Escherichia coli and Coliform Bacteria – Part 1: Membrane Filtration Method for waters with low bacterial background flora. Geneva, Switzerland: International Organization for Standardization.

Chandran, A. and Hatha, A.M. (2003). Survival of Escherichia coli in a tropical estuary. The South Pacific Journal of Natural and Applied Sciences 21 (1): 41-46.

Commission of the European Union (CEU 2006) Council Directive 2006/113/EC of 12 December 2006 on the quality required of shellfish waters (codified version). Official `Journal of the European Communities, L 376: 14–20.

Diston, D., Ebdon, J.E., Taylor, H.D. (2012). The effect of UV-C radiation (254 nm) on candidate microbial source tracking phages infecting a human-specific strain of Bacteroides fragilis (GB124). Journal of Water and Health 10 (2): 262-270.

Exner, M. (2015). The discovery of the aetiology of cholera by Robert Koch 1883. In Bartram et al. (Eds.) Routledge Handbook of Water and Health. London and New York, Routledge, pp. 648-657.

Hiremath, S.C., Yadawe, M.S., Pujeri, U.S., Hiremath, D.M., Pujar, A.S. (2011). Physicochemical analysis of ground water

in Municipal Area of Bijapur (Karnataka). Current World Environment 6: 265-269.

Olalemi, A. (2015). Bacteriophages as surrogates of viral pathogens: a novel tool for the shellfisheries industry. PhD Thesis. University of Brighton, Brighton, UK.

Olalemi, A., Baker-Austin, C., Ebdon, J., Taylor, H. (2016a). Bioaccumulation and `persistence of faecal bacterial and viral indicators in Mytilus edulis and Crassostrea `gigas. International Journal of Hygiene and Environmental Health 219(7): 592-598.

Olalemi, A., Purnell, S., Caplin, J., Ebdon, J., Taylor, H. (2016b). The application of phage-`based faecal pollution markers to predict the concentration of adenoviruses in mussels `(Mytilus edulis) and their overlying waters. Journal of Applied Microbiology 121: ` 1152-1162.

Patil, P.N., Sawant, D.V, Deshmukh, R.N. (2012). Physicochemical parameters for testing of water – A review. International Journal of Environmental Sciences 3(3): 1194-1207.

Pommepuy, M., Guillaud, J.F., Dupray, E., Derrien, A., Le Guyader, F., Cormier, M. (1992). Enteric bacteria survival factors. Water Science and Technology 25(12): 93-103.

Shittu, O.B., Olaotan, J.O., Amusa, T.S. (2008). Physicochemical and bacteriological analysis of water used for drinking and swimming purposes in Abeokuta, Nigeria. African Journal of Biomedical Research 2: 285-290.

Sobsey, M.D. (2016). Advances and innovation to achieve microbially safe and sustainable water: Detection, treatment, and risk management. National Water Research Institute 2016 Clarke Prize Lecture, Fountain Valley, California, USA.

WHO (2014). Preventing diarrhoea through better water, sanitation and hygiene: exposures and impacts in low- and middle- income countries. World Health Organization, Geneva (2014).

Wilkes, G.1., Brassard, J., Edge, T.A., Gannon, V., Jokinen, C.C., Jones, T,H., Neumann, N., Pintar, K.D., Ruecker, N., Schmidt, P.J., Sunohara, M., Topp, E., Lapen, D.R. (2013). Bacteria, viruses, and parasites in an intermittent stream protected from and exposed to pasturing cattle: Prevalence, densities, and quantitative microbial risk assessment. Water Research 47(16): 6244-6257.

JJEES

JJEES (2020) 11 (2): 98-102
ISSN 1995-6681

Jordan Journal of Earth and Environmental Sciences

Measurement of Radon Levels in the Groundwater of Al-Rusaifah City in Zarqa Governorate Using Liquid Scintillation Counter

Sura Al-Harahsheh[1*], and Mohummad Al-Dalabeeh[2]

[1]*Al al-Bayt University, Institute of Earth and Environmental Sciences, Department of Applied Geology and Environment, Jordan.*
[2]*Energy and Minerals Regulatory Commission*

Received 13 July, 2019; Accepted 30 December 2019

Abstract

Groundwater wells in Al- Rusaifah in central Jordan were investigated for radon (^{222}Rn) levels during the winter season using a liquid scintillation counter (LSC). ^{222}Rn was detected in eighteen groundwater samples from six different wells. The concentrations of radon varied from 151.9 to 253.1 Bq/L. The upper concentration limit of ^{222}Rn for drinking water is 11 Bq/L based on the Jordanian Standards for Drinking Purposes. This indicates that ^{222}Rn levels in all groundwater samples exceed the permissible threshold. The health impact assessment of ^{222}Rn showed that for all samples, the total population-weighted average annual effective dose was 3.147mSv/y, which is greater than the maximum value of the general annual effective dose from radon of 0.1 mSv/y, according to the WHO and the European Council.

Keywords: Radon, Al- Rusaifah, Liquid Scintillation Counter, Annual Effective Dose, Zarqa Governorate, Jordan

1. Introduction

Water for human consumption should be free of chemical, microbiological, and radiological contamination (Garba et al., 2008).

Groundwater has more radioactive contents than surface water, since it passes through rocks and soil formations, dissolving many compounds, minerals, and radioactive materials (Mohsen et al., 2016).

^{222}Rn is a naturally-occurring radioactive inert gas, which is a descendent of the uranium decay series and represents the important radon isotopes. It has no taste, smell, or color and its melting point is 202 k (-71C°), boiling point 211.3 k (-61.7 C°), and density at 293 k is 9.73 g/cm^3. Chemically, Radon is unreactive with most materials, so it travels and moves easily through very small spaces (Al-Zubaidy and Mohammad, 2012).

In natural water, Radon originates from the dissolution of radium (^{226}Ra) in groundwater from bed rocks. It doesn't react with any minerals.

Most people do not know that the greatest radiation exposure is caused by natural radiation sources. It is well-known that more than half of the radiation dose is caused by radon and its progeny (^{218}poand ^{214}po) (UNSCEAR, 1993).

Radon and its daughters, especially polonium-218 and polonium-214, are radioactive nuclei that emit alpha particles with energies of 6.003 and 7.678 MeV, respectively (polonium-214, are radioactive nuclei that emit alpha particles).

Radon exists in three natural isotopes, (^{219}Rn, Actinon) and (^{220}Rn, Thoron) and (^{222}Rn, Radon) which are formed by the decay of different isotopes of radium found in the decay chains of ^{235}U, ^{232}Th and ^{238}U, respectively. Actinon and Thoron have very short half-lives (3.96 and 55.6 seconds, respectively).

Radon gas (^{222}Rn) comes from the decay of Radium- 226 in the Uranium-238 decay chain, and has a half-life of 3.82 days. It is an emitter of alpha particles with the energy of 5.4 MeV.

Generally, the Earth's crust is the production site of Radon element that is later dispersed within soil particles in a gaseous state which will be released finally to the atmospheric layers. Radon can tolerate this long journey due to its noble chemical properties. It has been estimated that the radon soil content ranges from 10000 Bq/m^3 to 50000 Bq/m^3(WHO, 2009).

The presence of Radon in natural water and air is due to the ingrowths of ^{226}Ra occurring in the geological materials and water. This process, where radon escapes from the solid materials, is called Emanation process. Because radon is a noble gas, it is freed from any chemical bonds associated with it, and can move over a long distance enough to reach the groundwater or the air.

Jordan is rich in uranium deposits found in phosphate rocks being processed into fertilizers. In its decaying to Lead (^{206}Pb), Uranium generates Radon which is a moderately short-lived element with a life-span of approximately 3.825 days. Phosphate mines in Jordan, are located in relatively highly populated areas (e.g. Ruseifa town, a suburb of Zarqa city). They form potential threats to the public health of those residents living in close proximity to phosphate mines. Additionally, there exist other sources of natural and industrial radioactivity scattered throughout Jordan. (Ragheb, 2010).

The residents of Al-Rusaifa city usually depend on groundwater sources that are pumped through the water distribution system for drinking, cooking, and other uses. Furthermore, the area is rich in phosphate ores.

Radon may cause cancer, and may be found in drinking

* Corresponding author e-mail: sura@aabu.edu.jo

water and indoor air. People who are exposed to radon through drinking water may have an increased risk of cancer over the course of their lifetime, especially lung cancer (EPA, 2005). Radon in the soils under homes is the biggest source of indoor radon, and presents a greater risk of lung cancer than the radon in drinking water. As required by the Safe Drinking Water Act, the EPA has developed proposed regulations to reduce radon in drinking water that has a multimedia mitigation option to reduce radon in indoor air (EPA, 2005).

The International Agency for Research on Cancer (IARC) had classified radon (^{222}Rn) as a mutagenic and carcinogenic substance to human beings. It has also been identified as a public health concern when present in drinking water. The World Health Organization (WHO) suggests that radon causes up to 15% of lung cancers worldwide (EPA, 2005)

The Maximum Contaminant Level (MCL) for the concentrations of radon is 11.1 Bq/L (about 300 pCi/L) in drinking water and in dwellings of 150 Bq/m^3 (about 4.05 pCi/L) (EPA, 1986).

2. Material and Methods

2.1. Study Area

The study area is Al-Rusaifah City at Zarqa governorate in central Jordan. It is one of the biggest cities in terms of population density, with more than half a million people living in a 38 km2 area (15,000 people per square kilometer), which makes it the fourth largest city in Jordan (Al-Ruseifah Manucipality, 2015).

Al-Rusaifah is part of the Amman–Zarqa Basin, one of the most important groundwater basins in Jordan. The renewable groundwater averages 88 million cubic meters per year in this basin (Salameh and Bannayan, 1993). The following are the most outcropping lithostratigraphic units in the study area:

1- ***Amman Silicified Limestone Formation (Santonian–Campanian):***

This formation is of varying thickness in different locations of Jordan. It is distinguished by hard, massive chert beds that form a steep cliff above the pale weathering chalks of the Umm Ghudran formation in central and north Jordan (Powell, 1989; Abed, 2009; Diabat, 2015).

2- ***Al-Hasa Phosphorite Formation (Late Campanian–Early Maastrichtian):***

The top of the Amman formation is usually distinguished by the first appearance of the thick phosphorite beds of the Al-Hasa phosphorite formation (Diabat, 2015). This formation consists of a heterogeneous lithology of medium-thick beds of phosphorite, which are intercalated with thin-medium bedded chert, marl, chalky marl, microcrystalline limestone, and oyster-coquina grain stones (Powell, 1989; Abed, 2009; Diabat, 2015).

The thickness of the phosphate beds ranges from 1.25 m to 3 m. The Upper Cretaceous sediments in Al-Rusaifah form a large basin within the generally eastward dipping sequence. Minor asymmetric folds occur, and faults are rare, consisting mainly of step faults (Jallad et al., 1989).

Many factors affect the formation and movement of radon in the ground: uranium content, grain size, and permeability of the host rock and the nature and extent of fracturing in the host rock. These factors also affect the amount of radon in groundwater (Bodansky et al., 1989). Figure (1) shows the study area.

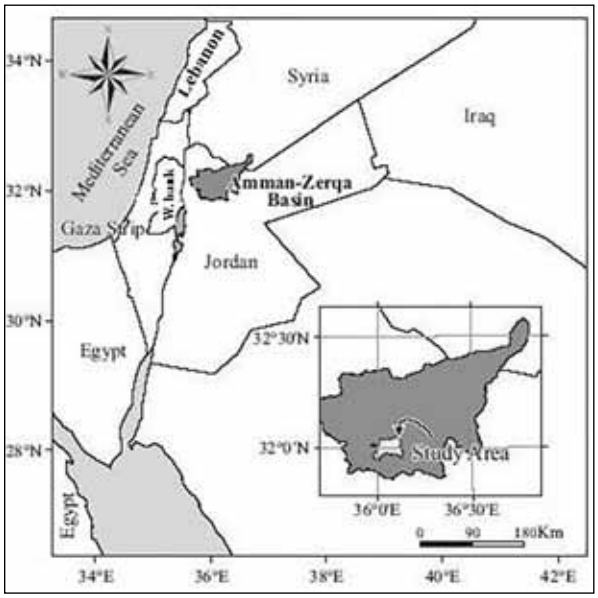

Figure 1. Study area locations.

2.2. Liquid Scintillation Counting

Liquid scintillation counting (LSC) is the most sensitive and widely used technique for detecting and quantifying radioactivity. It is a simple method for determining ^{222}Rn in natural water. Cocktail is first added to the vial, then another 10 ml of water sample was taken with a disposable syringe, ensuring that there is no aeration of the sample, and the water sample is injected at the bottom of the vial, below the immiscible scintillation solution with tightly secured vial's cap. Then the vial was shaken rapidly to ensure that the radon is fully dissolved in the organic solvents, such as toluene. Radon-222 will be extracted from the water phase to the organic scintillate solution. The time and date of mixing the water samples with the liquid scintillation solution will be recorded, and then the mixture will be stored for three hours so that the short-term decay products of ^{222}Rn can grow, attaining a secular equilibrium.

The LSC technique measured the activity of radon and decay products from the rate of photons emitted from the scintillation fluid. In this paper, the Tri-Carb Liquid Scintillation Counter is utilized to determine the counting efficiency of each sample, which then utilized to calculate the disintegration per unit minute (DPM). The main operation principle of the counter is that it depends on the interaction between the emitted beta from the radionuclide and a scintillator, which results into the production of light photons. The generated photon intensity during the scintillation is proportional to the initial energy of the beta particle (PerkinElmer Life and Analytical Sciences, 2008). The scintillation counter can measure photon intensity when the vial containing the radionuclide and the scintillation is placed into the instrument detector.

After that, the light emitted from the sample vials will be amplified via the photosensitive device. The output

amplified signal is then converted to pulses of electrical energy, which are recorded as counts. The accumulated counts are then sorted into individual channels (keV) into which the counts are sorted. The sample spectrum is finally produced from these collected and sorted counts. For further details and operation method of the counter, one may refer to (PerkinElmer Life and Analytical Sciences, 2008). From this spectrum, the system is capable to execute distinct count correction calculations and determine counts per minute (CPM) for every sample.

The instrument also determines the counting efficiency of each sample. Also, it compares the quenching index to the quench index for the samples from the so-called quenching curve, in order to obtain the sample counting efficiency and afterwards calculate DPM for the unknown samples (PerkinElmer Life and Analytical Sciences, 2008).

Using this spectrum, the system can perform various count correction calculations and determine counts per minute (CPM) for each sample. To calculate disintegrations per minute (DPM), the instrument will find the counting efficiency of every sample. By utilizing the quench curve, the instrument is capable to compare the quench index for the samples to the quench index for the quench standards to determine sample counting efficiency and subsequently calculate DPM for the unknown samples https://www.proz.com/profile/970169,https://researchpark.spbu.ru/en/equipment-geomodel-eng/2266-geomodel-experimentalnoe-modelirovanie-eng).

2.3. Annual Effective Dose

The obtained annual effective doses (AED) received by the human body for all drinking water samples (in units of mSv/y) are divided into two parts as follows:

1. The annual dose of radiation resulting from ingestion of radon in drinking water (D_{eff}) in terms of mSv/y, measured by using the following formula (Kozlowska et al., 2010):

$$\mathbf{D_{eff}(mSv/y) = 1000\ A_c W_d\ V}$$

where A_c is the concentration of radon in water in Bq/l; W_d is the radiation dose (conversion factor), which is equal to 1×10^{-8} mSv/Bq; and V is the amount of drinking water consumed by the individual per year, which is equal to 182.5 l/y.

2. The annual dose of radiation resulting from radon which has escaped from drinking water supply, inhalation (H_{eff}) (Kozlowska et al., 2010):

$$\mathbf{H_{eff} = A\ F\ \gamma f\ d\ Q\ C_w}$$

where A is a constant representing the number of working levels (WL); **F** is the equilibrium factor between radon and its daughters and equal to (0.3); **Y** is the equivalent occupational working months per year for a member of the population allowing for residency time and breathing rate, equal to 18 M/y; **f** is the transfer factor of radon gas from water into the air of the dwelling, which is equal to 10^{-4} in air per 1 Bq/l in water; **d** is the dose conversion coefficient factor of radon progeny in the respiratory region, which is equal to 5 mSv/WLM; **Q** is the quality factor for α-particles, which is equal to 20; and $\mathbf{C_w}$ is the radon concentration in water in Bq/L.

To calculate the total annual dose resulting from both the ingestion and inhalation of radon gas from consuming water for drinking and washing purposes is given by H_{eff}+D_{eff}.

2.4. Estimating the lung cancer risk factor

Radon gas can diffuse and escape from water during showering or washing into indoor air at a rate of 10^{-4} per 1 Bq/l in water as proposed by Gesell and Prichard (1975). The lung cancer risk factor from natural radiation is assumed to be 36×10^{-4} per 1 pCi/L as proposed by Cross (1992).

3. Results and Discussion

Table 1 presents the overall radon concentration levels and their annual effective dose exposure for each well. The spatial variations in radon concentration could be a function of the geological structure of the area, depth of the water source, and differences in climate and geohydrological processes occurring in the area (PerkinElmer Life and Analytical Sciences, 2008).

Table 1. Minimum and maximum average radon concentrations, average effective dose, and increase of cancer for water samples in Al-Rusaifah City.

Well	No. of samples	C. min (Bq/L)	C. max (Bq/L)	C. average (Bq/L)	AED mSv/y	Increase of cancer
BASATEEN(A1)	3	165.8±17.6	204.6±22.9	191.1±20.8	3.135±0.363	0.0019
BASATEEN(1)	3	171.8±19.1	188.9±20.9	182.4±19.9	2.992±0.290	0.0018
WELL(8)	3	181.8±21.7	188.9±20.9	186.6±21.3	3.062±0.311	0.0018
MUNICIPAL(4)	3	151.9±16.4	167.6±18.0	159.7±17.2	2.619±0.251	0.0015
OFFICE(2)	3	240.3±25.9	253.1±26.9	248.0±27.4	4.069±0.399	0.0024
WELL(9A)	3	194.3±23.9	209.6±22.6	203.7±22.8	3.007±0.322	0.0020
TOTAL	18			195.3±27.4	3.147±0.399	0.0019

The overall average of radon gas concentration in the drinking water wells sample is 195.3±27.4 Bq/l, where the minimum average radon concentration is 159.7±17.2 Bq/l for the Municipal 4 well water samples, and the maximum average radon concentration is 248.0±27.4 Bq/l for the Office 2 well water samples. The residents of this area are forty times more exposed to radon with higher probabilities of developing cancer or other health-related impacts. This is about 1900 per million inhabitants, which is more than the WHO (2012) estimate of 1000 per million inhabitants. These results are shown in Figure 2.

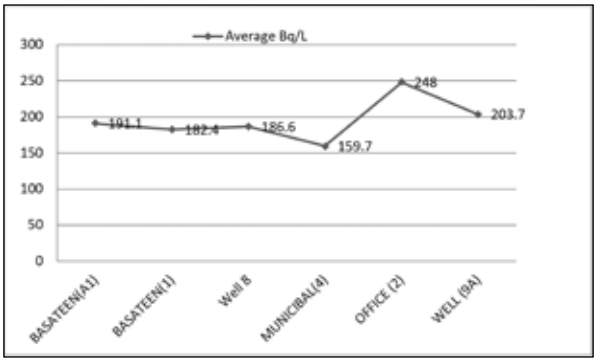

Figure 2. Average radon concentration in Al-Rusaifah City.

Table 2 shows the results of radon concentrations in the present study compared with others. Several national and international health organizations assigned the acceptable action limits for radon concentrations as follows: The EPA (1999) defined a value of 11.1 Bq /l for radon concentration in water; the UNSCEAR (2012) set it at 40 Bq/l; and the WHO (2012) set a value of 100 Bq/l as an action limit.

It seems that our results are much greater than the results obtained by Al-Bataina et al. (2003), Ismail et al. (2008), Aleissa et al. (2012), Rafat (2013), and Mohsen et al. (2016).The high radon concentration values in our study could be attributed to the presence of phosphate mines, which plays a major role in providing an enormous source of radon in the study area. Another plausible source of difference is the use of various detectors in each study.

Table 2. Comparison of 222Rn levels in spring water with results from other workers.

Sample number	Country	Year	Average radon concentration Bq/l	Detection method	Reference
1	Jordan (Al-Karak)	2003	1.854±0.17	CR-39	AL-Bataina et al. (2003)
2	KSA (Riyad)	2012	1.01±0.10	LSC	Aleissa et al. (2013)
3	Iraq (Irbil)	2007	4.693±2.213	CR-39	Ismail et al. (2007)
4	Libya (South Region)	2013	3.46±1.76	CR-39	Rafat (2013)
5	Saudi Arabia (Buraydah City)	2016	4.73±0.84	γ -ray spectrometry	Mohsen et al. (2016)
6	Our study	2016	195.3±27.4	LSC	Current study

4. Conclusions and Recommendations

Eighteen groundwater samples from wells collected from Rusaifah City were investigated for ^{222}Rn concentrations through LCS. It is found that these samples exhibited higher radon concentrations in water than the maximum contamination level of 11.1 Bq/l, as recommended by the EPA (2005).

The highest concentration of radon gas in groundwater in Rusaifah was found in Office 2 (253.1 Bq\l), and the lowest concentration level was in Municipal 4 (151.9 Bq/l). For all samples, the total average of the annual effective doses was found to be larger than the maximum value of the general annual effective dose (0.1 mSv/y) according to the WHO (2004) and the European Council (EC, 2001).

Based on the results, the groundwater in the study area poses a risk to residents, as they are exposed to radon radiation via drinking water (ingestion and inhalation). We recommend that the water of the Rusaifah wells, which contains radon gas with free water, be diluted before distributing it to the people. In addition, we recommend the aeration and filtration of water after pumping from the well and before it is distributed to the public network and the use of treatment plants such as reverse osmosis and/or other electrodialysis processes along with aeration. Finally, more epidemiological public health studies in the area are recommended to find any potential linkage between radon concentrations and incidences of cancer among the inhabitants.

References

Abed, A. (2009). Geology of Jordan, its Environment and Water, Scientific Series 1, Publications of Association of Jordanian Geologists, (in Arabic) Jordan, pp 571.

Al-Bataina, B.A, Tarawneh, S., and Lataifeh, M.S. (2003), measured Radon Concentration in Water and Building Aggregate Samples in Al-Karak, Jordan Abhath Al-Yarmouk. Basic Sciences and Engineering, 12(1): 221-230.

Aleissa, K.A., Alghamdi, A.S., Almasoud, F.I., Islam, M.S. (2013). Measurement of radon levels in groundwater supplies of Riyadh with liquid scintillation counter and the associated radiation dose. Radiat Prot Dosimetry. 154(1):95-103. doi: 10.1093/rpd/ncs140.

Al-Ruseifah Manucipality, Open files, accessed February, 2015.

Al-Zubaidy, N.N., and Mohammad, A.I. (2012). Health Effects on Public of Malka Region due to Radon Gas, Using (CR-39) Detector. Adv. Theor. Appl. Mech., 5(2): 61-67.

Bodansky D., Maurice, A.R., David, R.S. (1989). Indoor Radon and its Hazards. Univ. of Washington Press Seattle and London, second edition, printed in the U.S.A.

Cross, F.T. (1992) Indoor radon concentration and lung cancer: Reality or Mith. Twenty-ninth Hanford on Health and Environmental, BeGelle Press. Columbus, 27-29.

Diabat, A. (2015). Structural and Stress Analysis of the Area between Al-Akeider and Mughayer As-Sirhan, Northwestern Badia- Jordan, Jordan Journal of Earth and Environmental Sciences, 7(1): 37-48.

EC (2001). European Union commission recommendation on the protection of the public against exposure to radon in drinking water supplies, 2001. Brussels, Belgium: Official Journal of the European Communities.

EPA (2005). United States Environmental Protection Agency Office of Water http://www.epa.gov/, (2005).

EPA (1986). United States Environmental Protection Agency Office of Water, A citizen's guide to radon: What it is and what to do about it. United States Environmental Protection Agency. OPA-86-004. U.S. EPA and US. Department of Health and Human Services.

EPA (1999). United States Environmental Protection Agency Office of Water: 40 CFR Parts 141, and 142: National Primary Drinking Water Regulations; radon-222: proposed rule. (US Environmental Protection Agency, [Washington, D.C.], 1999).

Garba, N.N., Rabi'u, N., Yusuf, A.M., Isma'ila, A. (2008). Radon: Its consequences and measurement in our living environs. J. Res. Phys. Sci., 4(4): 23–25.

Gesell, T.F., and Prichard, H.M. (1975). The technologically enhanced natural radiation environment. Health Phys., 28:361-366.

Ismail, A.H, and Haji, S.O. (2008). Analysis of Radon Concentrations in Drinking Water in Erbil Governorate (Iraqi Kurdistan) and its Health Effects. Tikrit Journal of Pure Science, 13(3):2008.

Jallad, I.S., Abu Murry, O.S., Sadaqah, R.M. (1989). Upper Cretaceous phosphorites of Jordan, in: Phosphate Deposit of the World, Vol. 2, Phosphate Rock Resources (A. J. G, Notholt, R. P. Sheldon and D. F. Davidson, eds.), pp. 344-351, Cambridge Univ. Press.

Kozlowska, B., Walencik, A., Dorada, J., Zipper, W. (2010). Radon in ground water and dose estimation inhabitants in spas of the study Mountain area, Poland, Applied radiation and isotopes. PP: 854-857.

Mohsen, B., Atteyat, A., El-Taher, A. (2016). Measurements of Radon Levels in Ground Water by Ray Spectrometr. Arab Journal of Nuclear Science and Applications, 94 (1): 21-27.

PerkinElmer Life and Analytical Sciences (2008). QuantaSmart™ for Tri-Carb® Liquid Scintillation Analyzers Getting Started Guide, Copyright © 2008, PerkinElmer, Inc. https://researchpark.spbu.ru/en/equipment-geomodel-eng/2266-geomodel-experimentalnoe-modelirovanie-eng)

Powell, J. (1989). Stratigraphy and sedimentation of the Phanerozoic rocks in central and south Jordan, parts A and B. Natural Resources Authority (NRA), geology Directorate, Geological mapping Division, Bull.11.

Rafat, M.A. (2013). Evaluation of radon gas concentration in the drinking water and dwellings of south-west Libya, using CR-39 detectors, (IJES), 4(4): 484-490.

Ragheb, M., and Khasawneh, M. (2010). Uranium fuel as byproduct of phosphate fertilizer production. 1st International Nuclear and Renewable Energy Conference.

Salameh, E., and Bannayan, H. (1993). Water Resources of Jordan, Present Status and Future Potentials. Friedrich Ebert Stiftung, Amman, 183 p.

UNSCEAR (1993). Sources, Effects and Risks of Ionizing Radiation. United Nations scientific committee on the effects of atomic Radiation, Report to the General Assembly on the effects of Atomic Radiation, New York, United Nations.

UNSCEAR (2012). Sources and effects of ionizing radiation. United Nations, New York.

WHO (2004). Drinking water Director, Radiation Aspects. World Health Organization (Chapter 9).

WHO (2009). Handbook on Indoor Radon: A Public Health Perspective, Edited by Hajo Zeeb, and Ferid Shannoun, ISBN 978 92 4 154767 3.

WHO (2012) Progress on Drinking Water and Sanitation. World Health Organization, Geneva.

JJEES

JJEES (2020) 11 (2): 103-112
ISSN 1995-6681

Jordan Journal of Earth and Environmental Sciences

Calcareous Nannofossil Biostratigraphy and Carbon Isotopes from the Stratotype Section of the Middle Eocene Wadi Shallala Formation, Northwestern Jordan

Fayez Ahmad[1*], Mahmoud Faris[2], Sherif Farouk[3]

[1]*The Hashemite University, Faculty of Natural Resources and Environment, Department of Earth and Environmental Sciences, Jordan*
[2]*Geology Department, Faculty of Science, Tanta University, Egypt*
[3]*Egyptian Petroleum Research Institute, Nasr City, Egypt*

Received 17 November 2019; Accepted 19 January 2020

Abstract

The stratotype section of the Wadi Shallala Formation in northwestern Jordan has been studied in this work by means of calcareous nannofossils and isotopes for the first time. In addition, the present study discusses the most important Middle Eocene calcareous nannofossil bioevents and biostratigraphy. The study section includes the upper part of Umm Rijam Chert Limestone Formation and Wadi Shallala Formation. Forty-two calcareous nannofossil species which belong to the *Nannotetrina fulgens* (NP15/CP13) Zone were recorded in the study section, and this stratotype section was assigned to the Middle Eocene age, although some previous works have assigned the lower part of this section to the Paleocene Epoch. The Umm Rijam Chert Limestone/ Wadi Shallala formational boundary is marked by the transition from the well-bedded chalk and limestone with dominated charts to the massive chalk. Chronostratigraphically, the Umm Rijam Chert Limestone / Wadi Shallala formational boundary reflects regional paleoenvironmental changes in Jordan correlatable well with nearby countries such as Egypt.

Keywords: Wadi Shallala Formation, calcareous nannofossils, isotopes, Middle Eocene, Jordan.

1. Introduction

Eocene successions in Jordan are mainly characterized by a wide shallow, open marine-rimmed carbonate platform at the southern margin of the Neo-Tethys Ocean (Powell and Moh'd, 2011). It includes the Eocene Umm Rijam Chert Limestone and Wadi Shallala formations (Figure 1).

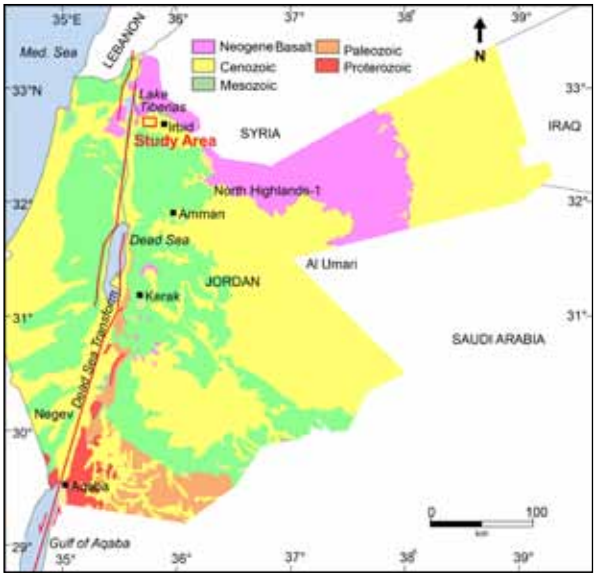

Figure 1. Regional geological map of Jordan showing the location of the study area (Al-Shawabkeh, 1991).

A long-term cooling period started at the end of the Early Eocene Cooling Event (EECO) (e.g., Bijl et al., 2010; Boscolo Galazzo et al., 2014; Hussein et al., 2015) until the Middle Eocene Climatic Optimum (~40.5 to 40 Ma; Boscolo Galazzo et al., 2014). In Jordan, the Umm Rijam Chert Limestone and Wadi Shallala formational boundary have not been previously discussed in details. Therefore, this study adds new information based on carbon isotopes and calcareous nannofossil biostratigraphy. A few previous works have focused on the Eocene microplanktonic stratigraphy of Jordan coupled with $\delta^{13}C$ and $\delta^{18}O$ isotopes (e.g., Farouk et al., 2013, 2015; Hussein et al., 2015). There is presently insufficient information for chronostratigraphy at the boundary between the Umm Rijam Chert Limestone and Wadi Shallala formations. The age assignment by the previous authors of the Umm Rijam Chert Limestone and Wadi Shallala formational boundary is a controversial stratigraphic point. It was dated to the Early-Middle Eocene (e.g., Fadda, 1996; Andrews, 1992; Sharland et al., 2004), while others reported it within the Middle Eocene (e.g., Bender, 1974; Powell and Moh'd, 2011; Farouk et al., 2013).

The main aims of the present study are: 1) to document the main Middle Eocene calcareous nannoplankton biostratigraphy and bioevents events against the $\delta^{13}C$ and $\delta^{18}O$ isotope; 2) to discuss the stratigraphic ranges of some important nannofossil species within the studied interval; and 3) to compare the obtained results with the different sections measured in west central Sinai, Egypt.

* Corresponding author e-mail: fayeza@hu.edu.jo

2. Lithostratigraphy

The exposed studied section at the type-locality of Wadi Shallala area (32°37′49″N, 35°56′23″E) includes the uppermost part of the Umm Rijam Chert Limestone and Wadi Shallala formations (Figure 2A). The Umm Rijam Chert Limestone Formation can be subdivided into three major units (Parker, 1970). The lower unit consists of about 8 m massive bituminous imparts brown-black argillaceous chalk with an unexposed base (Figure 2A). In the present study, this unit is considered to be equivalent to the Paleocene Muwaqqar Chalk Formation which was recorded in the same area by Weisemann and Abdullatif (1963) and Moh'd (2000). The middle unit consists of about 18 m thick limestone with few chert beds and nodules.The third upper unit characterizes the upper most part of the Umm Rijam Chert Limestone Formation (Figures 2B and 3). It consists of 15m thick limestone with chert intercalation. The Wadi Shallala Formation consists of about 8 m grey to white massive chalky limestone with a few chert beds/nodules towards the higher part of the studied section with observed calcium carbonate content (Figure 3). The Umm Rijam Chert Limestone/ Wadi Shallala formational boundary can be drawn above the last chert horizon, and is marked by the transition from the well-bedded chalk and limestone with dominated cherts to the massive chalk. Similar vertical facies changes were noted in Egypt between the limestone with chert of the Thebes Formation and argillaceous marl and limestone of the Darat Formation (Figure 4). The Wadi Shallala Formation is overlain by lower Oligocene limestone of the Tayba Formation in northwest Jordan and Wadi El Ghadaf in the eastern part of Jordan (e.g., Farouk et al., 2013).

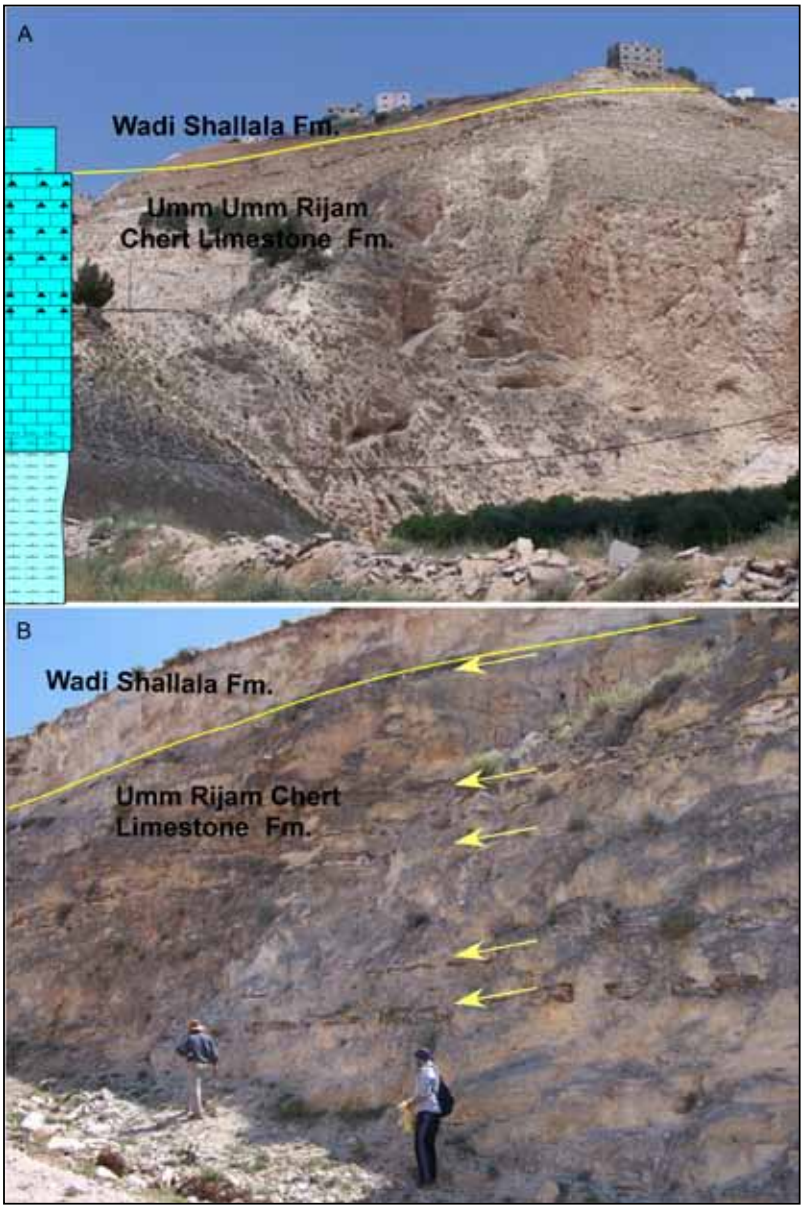

Figure 2. ***A:*** Field photograph showing the three major cycles of Umm Rijam Formation underlying the Wadi Shallala Formation. Fig. ***B:*** Field photograph showing the upper part of Umm Rijam Formation, which is characterized by an increase of bedded chert (arrows show the chert beds) underlying the massive chalk of the Wadi Shallala Formation.

3. Material and Methods

A total of 120 samples were collected, sampled, and examined for nannofossils and $\delta^{13}C$ and $\delta^{18}O$ isotope. Stable isotope analyses of $\delta^{13}C$ and $\delta^{18}O$ were performed on 120 bulk samples at the University of Arizona, Geosciences Department, Environmental Isotope Laboratory using an automated carbonate preparation device (KIEL-III) coupled with a gas-ratio mass spectrometer (Finnigan MAT 252).

Nannofossils slides were examined using the polarizing microscope with a magnification of 1250 x. Abbreviation codes used for the relative abundance of each nannofossil species are A; Abundant (1-10 Specimen/field of view) C; Common (1 Specimen / 1-10 field of view), F: Few (1 Specimen / 11-50 field of view), R: Rare (1 Specimen / 50 -100 field of view); and VR: Very Rare (1 specimen/more than 100 field of view). For preservation, an abbreviation code was used: G = good; individual specimens exhibit little or no dissolution, or overgrowth; diagnostic characteristics of most specimens are preserved and specimens are identifiable at the species level. M = moderate; individual specimens exhibit some evidence of dissolution, or overgrowth; primary diagnostic features are somewhat altered, but most specimens are identifiable at the species level. Biostratigraphic abbreviations used in the present study are: FO=First Occurrence, LO=Last occurrence.

4. Calcareous Nannofossils Biostratigraphy and Bioevents

The calcareous nannofossils in most of the studied samples are abundant to few and are well-diversified; their preservation range from good to moderate. A total of about forty-two taxa has been identified; their relative abundance, and preservation have been plotted (Table 1). Some representative nannofossil species are illustrated in Plates (1 - 2).

The biostratigraphic data obtained from calcareous nannofossils indicate that the whole studied succession is related to the *Nannotetrina fulgens* (NP15/CP13) Zone based on the zonal scheme of Martini (1971) and Okada and Bukry (1980). It is defined as the interval from the first occurrence (FO) of *N. fulgens* to the last occurrence (LO) of *Blackites gladius. Nannotetrina fulgens*, and other species of the genus *Nannotetrina* are used to define the base of the *N. fulgens* Zone (NP15) following the suggestions of Perch- Nielsen (1985). Perch-Nielsen (1985) and Abul-Nasr and Marzouk (1994) have remarked that the genus *Nannotetrina* disappears near the NP15/NP16 zonal boundary.

The LO of *B. infatus* and FO of *N. fulgens* together were used to trace base of *N. fulgens* Zone in the Agost section, Spain (Larrasoana et al., 2008). The FO of *N. fulgens* was used to define base of NP15a (Bown, 2005). The LO of *N. fulgens* and the FO of *Reticulofenestra umbilicus* were previously used to determine base of NP16 Zone (Perch-Nielsen, 1985). On the other hand, the NP15 (*N. fulgens*) Zone includes the interval from the FO to the LO of the nominated species (Shamrock et al., 2012). The CP13 (NP15) was divided previously by Okada and Bukry (1980) into three Subzones (CP13a, b, c).

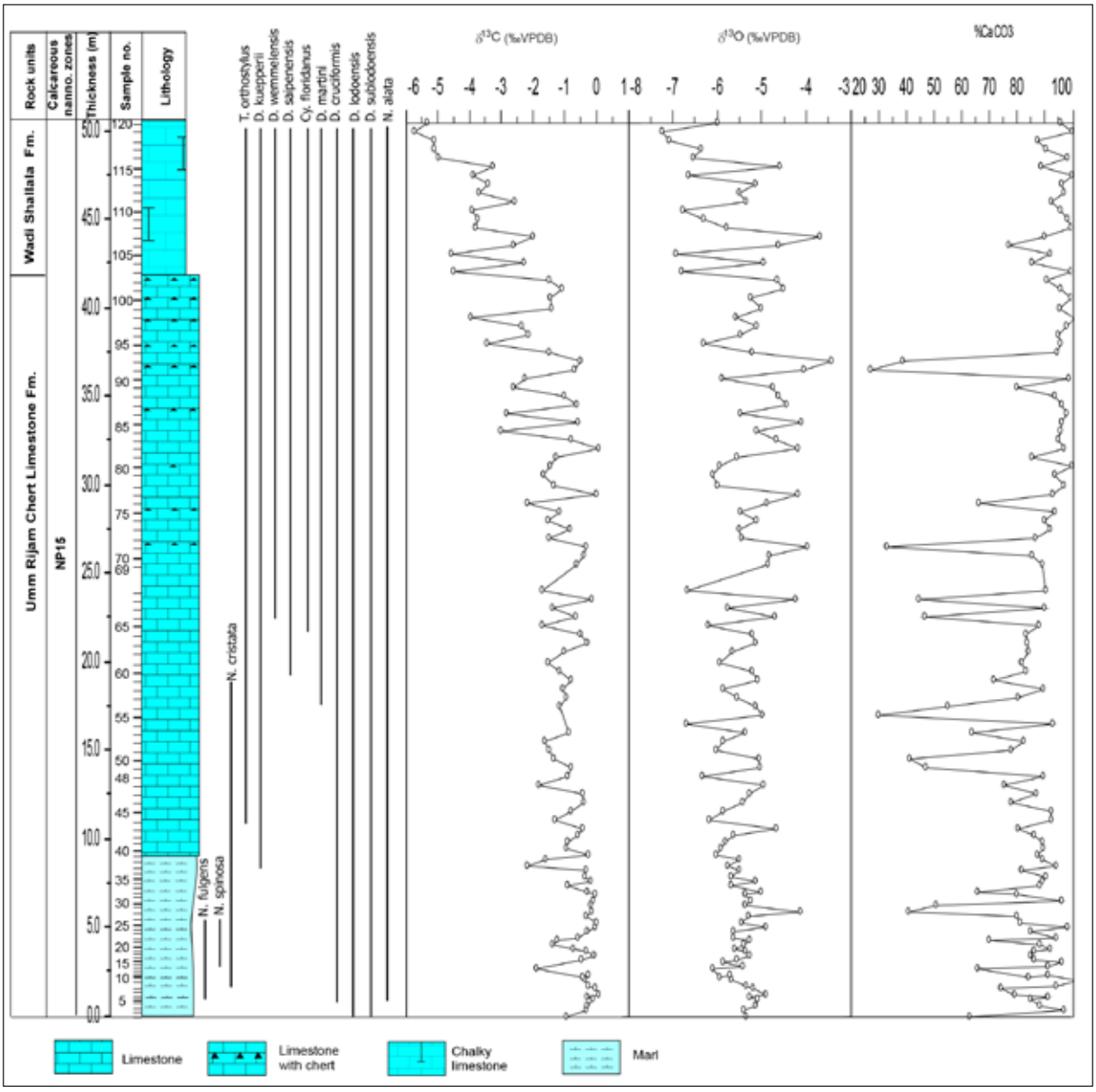

Figure 3. A measured exposed section showing the lithology against the δ13C and δ18O isotope values and CaCO3 values at the type section of Wadi Shallala Formation.

Table 1. Distribution of calcareous nannofossil species in Wadi Shallala section.

Middle Eocene																																								Age
Umm Rijam Chert Limestone Fm.																																								Formation
1	2	3	4	5	6	7	8	9	10	11	12	13	14	15	16	17	18	19	20	21	22	23	24	25	26	27	28	29	30	31	32	33	34	35	36	37	38	39	40	Sample No.
A	A	A	A	C	A	A	A	A	A	A	C	F	F	A	A	A	A	A	A	A	C	A	A	A	A	F	A	A	A	A	A	C	C	F	C	A	A	A	B	Abundance
G	M	M	M	M	M	G	G	G	G	G	G	M	M	G	M	M	G	G	M	G	G	G	G	M	M	M	M	G	G	M	M	M	M	M	G	G	G	G	-	Preservation
NP 15																																								Nannofossil zones
VR			VR	VR	VR	VR	VR	VR	VR	VR	R			VR		R	VR	R	VR	R	R	VR	VR	R	R	VR	VR	R		VR	R	R	R		R	R	VR	VR		*Campylosphaera dela*
VR		VR		VR		VR				VR	VR							VR	VR	VR		VR																		*Chiasmolithus grandis*
F	R	R	R	R	R	F	R	R	R	R	VR			R	VR	F	F	F	R	R	R	R	R	R	R	VR	F	R	F	R	F	F	R		R	F	F	R		*Chiasmolithus solitus*
VR	VR			VR	VR	VR													VR			VR			VR							VR				VR				*Discoaster sublodiensis**
R	R	R	R	R	R	R	R	R	R	F	F	VR	VR	F	F	R	R	F	R	F	F	F	F	R	R	R	F	F	F	F	F	F	F	R	R	R	R	R		*Ericsonia formosa*
VR			VR	VR		VR								VR		VR			VR	VR	VR	VR	VR	VR				VR		VR	VR	VR	VR			VR				*Neococcolithes dubius*
VR			VR			VR	VR		VR	VR					VR	VR	VR		VR	VR	VR	VR	VR	R	R	VR	R	VR	VR		VR	VR			VR	VR	VR			*Pontosphaera exilis*
VR										VR					VR					VR			VR									VR								*Pontosphaera multipora*
VR			VR			VR			VR	VR																	VR	VR	VR					VR				VR		*Pontosphaera pectinata*
VR	VR	VR				VR				VR				R	VR					VR		VR	VR				VR			VR	VR									*Pontosphaera plana*
VR	VR	VR	VR			VR	VR			R	VR			VR											VR			VR									VR			*Helicosphaera seminulum*
VR	VR		VR		VR	VR	VR	VR		VR	VR	VR	VR		VR	VR		VR	VR		VR	VR		VR			VR		VR	VR	VR	VR	VR	VR	R	R	R	R		*Sphenolithus moriformis*
R	R	R	R	VR		R	VR	VR	VR	R	R			VR	VR	R	VR	VR	VR	VR	VR	VR	R	VR	VR	VR	R			VR	VR	VR	VR		VR	VR	R	R		*Sphenolithus radians**
R	R	VR	R	F	R	R								R											VR															*Tribrachiatus orthostylus**
VR	VR	VR						VR	VR		VR			VR	VR										VR		VR								VR					*Nannotetrina alata**
VR		VR				VR					VR																													*Nannotetrina fulgens**
R	VR	VR	VR			VR	VR	VR	VR	VR		VR		VR	VR	VR		R	R	R		VR	VR	VR	VR		VR	VR	VR	VR	R	VR			R	VR	R	R		*Zygrhablithus bijugatus*
	VR			VR		R		VR			R						R	R				VR	VR	VR	VR	VR		VR	VR		VR	R	VR		R			VR		*Discoaster lodoensis**
	VR							VR			VR																													*Nannotetrina cristata**
	VR													VR		VR	VR	VR	VR	VR		VR	VR	VR	VR	VR	VR	VR	R	R	VR	VR	VR	R	R	F	F	F		*Reticulifenestra dictyoda**
		VR	VR			VR				VR																														*Scyphosphaera apsteinii*
		VR	VR				VR	VR										VR	VR	VR	VR		VR	VR	VR	VR	VR									VR				*Pontosphaera pulchra*
			VR			VR			VR		VR											VR											VR		VR		VR			*Sphenolithus editus*
				VR	VR				VR		VR			VR			VR														VR									*Discoaster cruciformis**
				VR		VR			VR		VR																													*Nannotetrina spinosa**
							VR	VR	VR								VR		VR																					*Ellipsolithus macellus*
									VR	VR							*VR*																							*Girgisia gammation*
									VR									VR		VR	VR			VR																*Discoaster barbadensis*
										VR										VR												VR								*Teweius ? crassus*
														VR	VR	VR	VR	R	R																					*Discoaster binodosus*
																R	R	R	R	F	F	F	F	R	R	R	R	R	R	R	F	F	F	VR	R	R	R	R		*Coccolithus pelagicus*
																VR										VR														*Discoaster deflandrei*
																VR	VR	VR		VR	R	VR	R	R	R		R	R	R	VR	VR	VR	R		R	R	R	R		*Helicosphaera lophota*
																	VR			VR	VR	VR		VR	VR		VR			VR		VR			VR		VR	VR		*Coronocyclus nitescens*
																	VR			VR																				*Lophodolithus mochloporus*
																		VR	VR	VR	R		VR											VR						*Discoaster kuepperi**
																		VR																						*Discoaster distichus**
																			VR	VR	VR	VR		VR	VR			VR				VR				VR				*Pontosphaera versa*
																					VR		VR																	*Sphenolithus* sp1
																							VR						VR											*Discoaster* sp1
																								VR	VR		R		R			VR		VR			R	R		*Helicosphaera sp*
																												VR									VR	VR		*Coronocyclus bramlellei*

The CP13a/NP15a includes the interval from the FO of *Nannotetrina fulgens* to the FO of *Chiasmolithus gigas*. The CP13b/NP15b (Total range subzone) represented by the interval from the FO to the LO of *Ch. gigas*. The CP13c/NP15c encompasses the interval from the LO of *Ch. gigas* to the FO of *Blackites gladius* and LO of *N. fulgens*. According to Perch-Nielsen (1985) and Bown (2005) *Discoaster sublodoensis* has its last appearance within the lower NP15 Zone. In the investigated section, *D. sublodoensis* ranges from the bottom of the section to its top (samples 1 to 120; Figure 3 and Table 1); in addition to the absence of *Ch. gigas*, this may indicate that the studied interval belongs to the lower NP15 (CP13a/NP15a).

4.1. Nannofossil Bioevents

In the present study, some nannofossil bioevents have been reported and discussed briefly as follows:

4.1.1. LO of Tribrachiatus orthostylus

The LO of *T. orthostylus* is noted as an unreliable taxon to define the top of NP13 Zone, where it has been reported within *Nannotetrina fulgens*, a marker taxon of NP15 (Perch-Nielsen, 1985; Wei and Wise, 1989). *T. orthostylus* has also been recorded within the lower NP15 Zone of the study section (from sample 1 to 26).

4.1.2. LOs of Discoaster Lodoensis and Discoaster Sublodoensis

The FO of *D. sublodoensis* defines the base of NP12; it disappears at the CP12a/NP12b (=NP14a/NP14b) (Perch-Nielsen, 1985). On the study section, *D. lodoensis* and *D. sublodoensis* ranged from sample 1 to 120, and they occurred in very rare numbers throughout the section. It is necessary to mention that both *D. lodoensis* and *D. sublodoensis* are recorded in the NP15 Zone in many sections in west central Sinai, Egypt (Strougo et al., 2003).

4.1.3. FO Nannotetrina Group

The base of NP15 is marked by the FO *Nannotetrina fulgens*, a secondary taxon used by Perch-Nielsen (1985). The total range of *Nannotetrina fulgens* is sometimes applied to delineate the lower and upper limits of the Zone NP 15

(Perch-Nielsen, 1985).

The FO of *Blackites gladius* is considered as a problematic bioevent in the eastern North Sea Basin, and consequently the upper boundary of Zone NP15 has been placed at the LO of *Nannotetrina fulgens* (Thomsen et al., 2012). The presence of *Nannotetrina fulgens* in sample (CH1) reflects the base of the Zone NP15. *Nannotetrina fulgens*, *N. spinosa, N. alata* and *N. cristata* occur in very rare frequencies throughout the study interval. The FO of *N. fulgens* and the LO of *B. inflatus* were used to trace the base of the NP15 Zone in the Agost section, Spain (Larrasoana et al., 2008)

The first appearance of *Reticulofenestra umbilicus* tentatively approximates the beginning of Zone NP16 (Perch-Nielsen, 1985), but this species does not actually appear to be present in the studied section. The authors tentatively assign the entire sampled section to Zone NP15. On the other hand, following Okada and Bukry (1980), *Chiasmolithus gigas,* is restricted to the middle part of Zone NP 15 (NP15b/CP13b) and does not occur in the samples under study. The *N.fulgens* Zone has been reported in several sections in west central Sinai; Wadi Feiran, Hammam Faraun, and Wadi Wardan, as well as, in El Sheikh Fadl Butte (Minia-Maghagha, east of the Nile Valley) (Strougo et al., 2003).

4.1.4. LO of Discoaster kuepperii

The FO of *D. kuepperii* occurs within NP12 (Perch-Nielsen, 1985), while it's LO occurs within the upper NP14 (CP12b). In the studied section, it occurs within Zone NP15 (Sample 19 to 120). This species is previously recorded from Zone NP15 in many stratigraphic sections in west central Sinai (Strougo et al., 2003).

4.1.5. LO of Discoaster wemmelensis

Discoaster wemmelensis first appears at the base of CP12b (=NP14b), where it disappears within NP16 (Perch-Nielsen, 1985). In the present section, this species occurs within Zone NP15 (Sample 53 to 76). The LO of *D. wemmelensis* appears in the Middle Eocene sediments (NP15 Zone) in some sections in west central Sinai (Strougo et al., 2003).

Table 1. Continue

Middle Eocene																																								Age
Umm Rijam Chert Limestone Fm.																																								Rock Unit
41	42	43	44	45	46	47	48	49	50	51	52	53	54	55	56	57	58	59	60	61	62	63	64	65	66	67	68	69	70	71	72	73	74	75	76	77	78	79	80	Sample No.
A	A	C	A	A	A	A	A	A	F	F	A	F	F	C	A	A	C	A	A	C	F	A	B	C	B	F	C	A	A	A	F	A	A	A	A	A	A	C	C	Abundance
G	G	M	M	G	M	M	M	M	G	G	G	G	G	G	G	G	G	M	M	G	M	M		G		M	G	G	G	G	M	M	G	G	G	M	G	M	M	Preservation
NP15																																								Nannofossil zones
R	VR		R	R	VR	VR	VR	VR			VR				VR	VR	VR		VR	VR	VR	VR				VR	VR	VR	VR	VR		VR	VR	VR	VR		VR			*Campylosphaera dela*
VR			VR			VR	VR	VR										VR											VR		VR				VR		VR			*Chiasmolithus grandis*
F	F	R	R	C	C	C	C	F			R	R		F	VR	R	R	F	R	R	R	F		R		R	VR	VR	F	F	R	R	F	F	F		C		R	*Chiasmolithus solitus*
R	R	R	VR	R	VR	R	VR	VR	VR		VR	VR	VR	VR	VR	F	F	VR	R	VR	VR	R		VR		VR	VR	VR	VR	R	VR	VR	R	R	VR	VR	VR	VR	VR	*Coccolithus pelagicus*
VR	VR				VR	VR		VR			VR			VR	VR	VR	VR	VR	VR	VR	VR					VR		VR	VR	VR		VR	VR				VR			*Discoaster barbadensis*
VR	VR		VR	VR	VR	VR	VR	VR						VR	R			VR		VR	VR						VR			VR				VR						*Discoaster sublodoensis**
F	R	R	R	R	R	R	R	R	R	R	C	F	F		R	R	R	F	R	F	R	F		F		R	F	R	R	R	R	R	F	F	R		R	R	R	*Ericsonia formosa*
VR	VR		VR	R			VR	VR			VR			VR										R																*Helicosphaera sp*
R	VR		VR	R	R	VR	VR											VR																						*Helicosphaera lophota*
VR			VR	VR	VR		VR				R	VR			VR	VR		VR		VR							VR	VR												*Pontosphaera pulchra*
VR			VR	VR	VR		VR								VR	VR					VR	VR					VR		VR	VR		VR	VR		VR		VR			*Pontosphaera versa*
F	F	F	C	F	C	F	F	F	F	R	R	R	VR		VR	R	R	F	F	VR	VR	F		R		VR	F	F	R		VR	R	R	R	R	VR	F	F		*Reticulifenestra dictyoda**
VR		VR	VR	VR		VR	VR	VR	R	R	VR	R			VR	VR		VR		VR	VR	VR		VR		VR	VR			VR	VR				VR	VR			VR	*Sphenolithus moriformis*
VR	VR	R	R	VR	VR	VR	R		R	R	VR	R			R	R	R	R	R	R		R		R			R	VR	VR	VR		VR		VR	R		VR	VR	R	*Sphenolithus radians**
VR	VR				VR	VR	VR	VR			R				VR		VR											VR	VR	VR	VR	VR	VR	VR	VR					*Pontosphaera exilis*
VR	VR					VR	VR																					R												*Helicosphaera bramlettei*
VR			VR	VR	VR	VR	VR	VR						VR	VR	VR	VR	VR	VR	VR	VR	VR					VR		VR	VR			VR		VR		VR		VR	*Neococcolithes dubius*
VR			VR	VR					VR							VR	VR											VR												*Nannotetrina alata*
VR	VR	VR	VR		VR		VR								VR				VR	VR							VR	VR	VR	VR		VR	VR		VR				VR	*Zygrhablithus bijugatus*
	VR					VR						R					VR									VR						VR	VR	VR						*Discoaster binodosus*
VR	VR			VR	VR	VR	VR									VR												VR		VR										*Discoaster cruciformis**
	VR			VR	VR	VR	VR	VR	VR		VR		VR	VR	VR	VR	VR	VR	VR		VR	VR		VR				VR	VR	VR		VR			VR	VR	VR	VR	VR	*Helicosphaera seminulum*
		VR		VR			VR							VR	VR			VR	VR	VR							VR			VR		VR	VR	VR	VR				VR	*Discoaster kuepperi**
			VR	VR	VR	VR					VR				R											VR		VR												*Pontosphaera multipora*
			VR	VR																																				*Discoaster martinii*
			VR														VR																							*Nannotetrina cristata*
			VR	VR	VR	VR	VR	VR							VR					VR								VR	VR	VR	VR	VR	VR							*Pontosphaera pectinata*
				VR		VR		VR																		VR			VR											*Discoaster gemmifer*
				VR			VR			VR					VR	VR													VR	VR		VR	VR	VR	VR		VR			*Pontosphaera plana*
				VR				VR			VR				VR		VR		VR																					*Discoaster saipanensis**
				VR			VR																																	*Neococcolithes minutus*
					VR									VR	VR			R																						*Sphenolithus sp1*
					VR			VR																													VR			*Discoaster deflandrei*
					VR																					VR			VR	VR						VR				*Discoaster sp*
					VR										VR		VR	VR	VR	VR	VR			VR				VR	VR	R	R	R	VR	R	R		R			*Discoaster lodoensis**
						VR											VR																							*Discoaster cruciformis*
						VR												VR										R	R	VR				VR			VR			*Blackites tenuis*
						VR		VR																						VR										*Discoaster distichus**
												VR						VR																	VR					*Discoaster wemmensis*
												VR		VR	VR			R	R																			VR	VR	*Sphenolithus sp2*
																VR		R	R			VR		R			F	F	R	R					R	VR	F	R	R	*Cyclicargolithus floridanus*
																		VR											VR	R			VR		VR		VR		VR	*Blackites sp*
																		VR											VR	VR						VR	VR		VR	*Blackites spinous*
																		VR	VR																					*Nannotetrina spinosa*
																		VR																						*Tewelus crasus*
																			VR		VR							VR	VR				VR							*Coronocyclus nitescens*
																			VR										VR				VR		VR					*Micronstholithus attenuatus*
																				R																				*Pontosphaera multipora*
																								VR					VR											*Discoaster strictus**
																								VR																*Girgisa gammation*
																											VR	VR	VR	R		VR	R	VR						*Braarudosphaera bigelowii*
																													VR											*Lophodolithus mochloporus*
																													VR											*Coronocyclus bramelttei*
																														VR		VR	VR		VR					*Chiasmolithus grandis*
																																VR								*Lophodolithus nascens*

Table 1. Continue

Age	Middle Eocene																																							
Rock Unit	Umm Rijam Chert Limestone																						Wadi Shallala Fm.																	
Sample No.	81	82	83	84	85	86	87	88	89	90	91	92	93	94	95	96	97	98	99	100	101	102	103	104	105	106	107	108	109	110	111	112	113	114	115	116	117	118	119	120
Abundance	C	A	A	A	C	B	A	A	A	A	A	VR	C	A	A	A	A	A	A	C	A	A	R	B	F	C	C	C	C	C	C	C	VR	F	C	R	C	F	R	R
Preservation	M	G	G	G	G		G	G	M	G	G	M	M	G	G	G	G	G	G	G	G	G	M		G	G	G	G	G	G	G	M	M	M	G	M	M	M	M	M
Nannofossil zones	NP15																																							
Blackites sp	VR		VR	VR				VR	VR	VR	VR			VR	VR	VR			VR		VR	VR					VR													
Chiasmolithus solitus	R	F	C	F	R		R	R	F	C	F		F	F	F	F	F	F	R	C	C	C	VR		R	F	F	F	F	F		VR		VR	R	VR	F			
Coccolithus pelagicus	VR	VR	R	R	VR		VR	VR	VR	VR	R	VR	R	F	R	R	R	F	VR	VR	VR	VR	VR		VR	R	F	F	F	R	R	F	VR	F	R	R	F	F	R	R
Discoaster barbadensis	VR	VR	VR				VR	VR		VR								VR	VR		VR	VR					VR	VR		VR	VR	VR	VR	VR	VR	VR		VR		R
*Reticulifenestra dictyoda**	F	C	F	F	C		F	F	F	F	F		R	F	F	F			R	F	F	F	R		F	F	F	F	F	C	F	F		R	R		F		R	
*Discoaster kuepperi**	VR																	VR												VR										R
Ericsonia formosa	R	R	R	R	VR		R		R	R	F	VR	F	F	F	F	F	F	R	R	F	F	R		F	F	F	F	F	R	R	R		R	F	F	R	R	R	VR
Neococcolithes dubius	VR	VR	VR	VR			VR	VR	VR	VR				VR	VR		VR		VR		VR	VR				VR	VR	VR	VR	VR										
Cyclicargolithus floridanus	A	A	F	F	F		F	F	F	F	F		R	F	F	F	F	R	R	F	R	R	R		R	F	F	R	R	F	F	F		F						
Girgisa gammation	VR																																							
Coronocyclus nitescens		VR	VR	VR			VR									VR						VR					R	VR				R		VR	VR	VR	VR	VR	VR	
Chiasmolithus grandis		VR	VR	VR			VR	VR		VR	VR			VR	VR	VR	VR	VR	VR	VR	VR							VR			VR			VR	VR	VR				
Pontosphaera exilis			VR	VR				VR	VR					VR		VR			VR		VR																			
*Discoaster saipenensis**			VR																VR									VR	VR											VR
Helicosphaera lophota			VR						VR	VR			VR	VR	VR	VR			VR			VR				VR	VR													
Blackites spinosus			VR							VR	VR			VR	VR				VR		VR	VR																		
Helicosphaera seminlum			VR	R			VR	VR	VR	VR			VR	VR	VR	VR	VR	VR	VR	VR	VR	VR						VR												
*Discoaster sublodoensis**				VR					VR	VR	VR				VR	VR				VR		VR	VR						VR	VR	VR	VR			VR	R	VR			VR
Pontosphaera pectinata			VR	VR				VR	VR	VR	VR				VR		VR		VR	VR	VR	VR																		
*Sphenolithus radians**			R				VR		VR	VR					VR			VR		VR	VR				VR	VR		VR		VR		VR		VR						
Zygrhablithus bijugatus			VR	VR			VR			VR	VR				VR	VR	VR	VR	VR	VR	VR	VR			VR	VR	R			VR	VR	VR								VR
Lophodolithus mochloporus			VR																																					
Pontosphaera versa			VR							VR	VR			VR	VR	VR			VR		VR	VR																		
Pontosphaera pulchra			VR																VR			VR																		
Ellipdolithus lajollaensis			VR											VR	VR						VR	VR																		
Campylosphaera dela			VR	VR			VR				VR		VR	VR	VR							VR				VR	VR	VR												
*Discoaster lodoensis**			VR	VR			VR	VR	VR				VR		VR	VR			VR		VR						VR	VR	VR		VR				VR					VR
Ellipsolithus macellus			VR																																					
Chiasmolithus consuetus			VR																																					
Cyclicargolithus luminis					VR	VR															VR																			
Sphenolithus sp1					VR			VR																		VR														
Coronocyclus bramlettei							VR	VR	VR	VR							VR		VR	VR	VR	VR						VR												
Discoaster deflandrei								VR					VR					VR																VR						VR
*Discoaster distichus**								VR	VR																															
Discoaster gemmifer								VR																																
Discoaster binodosus								VR	VR	VR			VR									VR																		
Pontosphaera multipora									VR							VR						VR																		
Pontosphaera plana									VR				VR		VR				VR	VR		VR																		
Discoaster sp										VR						VR			VR															VR						VR
*Discoaster strictus**										VR									VR		VR	VR																		
Helicosphaera sp											VR					VR																								
Braarudosphaera bigelowii														VR											VR	VR					VR	VR								VR
Blackites tenuis														VR	VR	VR					VR	VR																		
Chiasmoluthus sp															VR																									
Lophodolithus nascens																VR			VR	VR																				
Sphenolithus moriformis																VR			VR	VR	VR				VR									VR			VR		VR	
Micronstholithus sp.																	VR								VR	VR														
Discoaster martini																			VR																					
*Discoaster cruciformis**																					VR							VR												VR
Neococcolithes minutus																					VR						VR	VR						VR						
Helicosphaera bramelttei																						VR																		
Nannotetrina alata																												VR												VR
*Discoaster wemmelensis**																																		VR						VR

4.1.6. FO of Discoaster saipanensis

The FO of *D. saipanensis* occurs at the base NP15 (Perch-Nielsen, 1985). It rarely occurs, and has a sporadic distribution throughout the study samples. This species has been recorded in Zone NP15 from many sections in west central Sinai (Strougo et al., 2003).

4.1.7. LO of Discoaster cruciformis

The LO of this taxon occurs around the CP12a/CP12b (NP14a/b) (Perch-Nielsen, 1985). This species has a sporadic occurrence throughout the studied samples, and its last appearance was in the topmost sample 120 (Table 1). In the west central Sinai sections, this species was previously recorded from the NP15 Zone (Strougo et al., 2003).

4.1.8. FO of Cyclogargolithus floridanus

This species is recorded from Subzone NP14b by Bown (2005). It is recognized to belong to the Middle Eocene Zone NP15 of the study section.

4.1.9. FO of Discoaster martini

The first appearance of *Discoaster martini* occurs in the lower part of Zone NP15 (Perch-Nielsen, 1985). In the present section, it first appears within Zone NP15. *D.martini* was recorded from Zone NP15 in several sections in west central Sinai (Strougo et al., 2003).

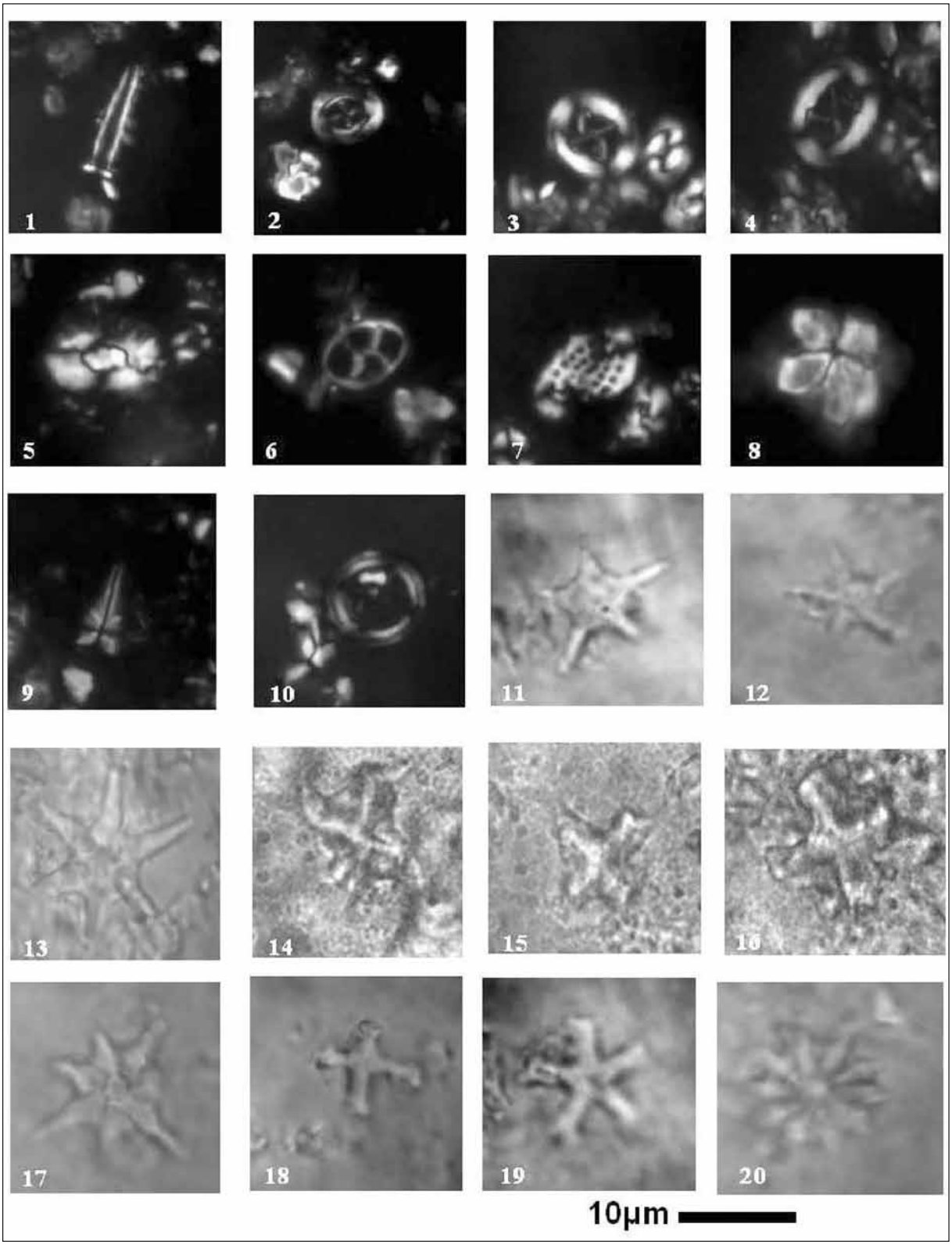

Plate 1. 1. *Blackites spinosus* (Deflandre and Fert, 1954) Hay and Towe (1962), Sample 101; 2. *Campylosphaera dela* (Bramlette Sullivan, 1961) Hay and Mohler (1967) Sample 171; 3-4. *Chiasmolithus solitus* (Bramlette and Sullivan, 1961) Locker (1968), Sample78; 5. *Helicosphaera lophota* Bramlette and Sullivan (1961), Sample 99; 6. *Neococcolithes dubius* (Deflandre, 1954) Black (1967), Sample 78; 7. *Pontosphaera multipora* (Kamptner, 1948) Roth (1970), Sample 83; 8. *Sphenolithus moriformis* (Bronnimann and Stradner, 1960) Bramlette and Wilcoxon (1967), Sample 71; 9. *Sphenolithus radians* Deflandre in Grasse (1952), Sample 59; 10. *Coronocyclus nitescens* (Kamptner, 1963) Bramletle and Wilcoxon (1967), Sample 89; 11-12. *Discoaster sublodoensis* Bramlette and Sullivan (1961); 11. Sample 1; 13. *Discoaster lodoensis* Bramlette and Riedel (1954), Sample 101; 14-15. *Nannotetrina cristata* (Martini, 1958) Perch-Nielsen (1971); 14: Sample 12; 15: Sample 2; 16. *Nannotetrina alata* (Martini, 1960) Haq and Lohmann (1976), Sample 69; 17. *Discoaster saipanensis* Bramlette and Riedel (1954), Sample 101; 18. *Discoaster cruciformis* Martini (1958), Sample 45; 19. *Discoaster martini* Stradner (1959), Sample 45; 20. *Discoaster barbadiensis* Tan (1927), Sample 102.

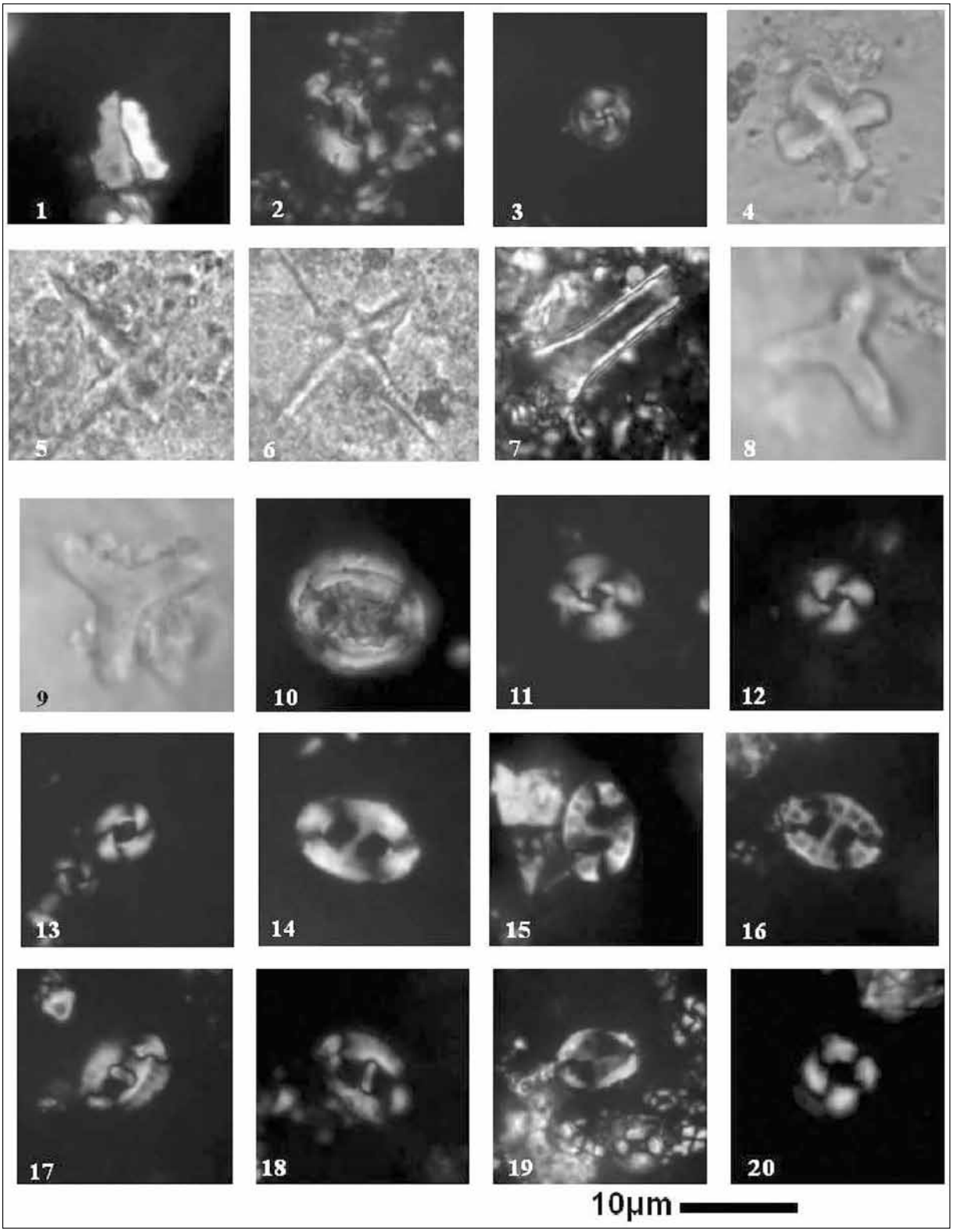

Plate 2. 1. *Zygrhablithus bijugatus* (Deflandre in Deflandre and Fert, 1954) Deflandre (1959) Sample 96; 2. *Helicosphaera bramlettei* Muller (1970), Sample 47; 3. *Girgisa gammation* (Bramlette and Sullivan, 1961) Varol (1989), Sample 10; 4. *Nannotetrina alata* (Martini, 1960) Haq and Lohmann (1976), Sample 9; 5-6. *Nannotetrina fulgens* (Stradner, 1960) Achuthan and Stradner (1969), Samples 6 and 3; 7. *Scyphosphaera apsteinii* Lohmann (1902), Sample 3; 8-9. *Tribrachiatus orthostylus* Sharmrai (1963), Samples 7 and 9; 10. *Chiasmolithus grandis* (Bramlette and Riedel, 1954) Radomski (1968) Sample 71; 11. *Cyclicargolithus floridanus* (Roth and Hay in Hay et al., 1967) Bukry (1971), Sample 83; 12-13. *Reticulofenestra dictyoda* (Deflandre in Deflandre and Fert, 1954) Stradner in Stradner and Edwards (1968); 12: Sample 42; 13: Sample 57; 14. *Pontosphaera exilis* (Bramlette and Sullivan, 1961) Romein (1979), Sample 11; 15-16. *Pontosphaera pulchra* (Deflandre in Deflandre and Fert, 1954) Romein (1979); 15: Sample 44; 16: Sample 102; 17-18. *Helicosphaera seminulum* Bramlette and Sullivan (1961); 17: Sample 61; 18: Sample 47; 19. *Pontosphaera versa* (Bramlette and Sullivan, 1961) Sherwood (1974), Sample 44; 20. *Ericsonia formosa* (Kamptner, 1963) Haq (1971), Sample 49.

5. $\delta^{13}C$ and $\delta^{18}O$ isotope

The $\delta^{13}C$ and $\delta^{18}O$ isotope record in the Wadi Shallala section shows pronounced variability on long- and short-term time scales, with $\delta^{13}C$ values ranging from -5.1‰ ‰ to 0 , while the $\delta^{18}O$ values ranged from -7 24‰ to -3.44‰ (Figure 3). The high negative values of $\delta^{13}C$ and $\delta^{18}O$ recorded in the studied section are interpreted as a late diagenetic overprint of the carbonates with no significant correlation between $\delta^{13}C$ and $\delta^{18}O$ (R^2=0.26). The $\delta^{13}C$ and $\delta^{18}O$ values decreased from -1.5 ‰ to -5.71‰ and -4.96% to -7.24% respectively, whereas the $\delta^{18}O$ records show a notable decrease near the base of the Wadi Shallala Formation. Hussein et al. (2014) reported the same negative trend for $\delta^{13}C$ and $\delta^{18}O$ isotope curves in the Jordan due to burial diagenesis as a result of observed granular calcite and drusy cements and enriched organic matter intervals.

6. Discussion and Conclusions

The calcareous nannofossil assemblage is well-diversified, and the preservation varies from good to moderate. The standard schemes of Martini (1971) and Okada and Bukry (1980) were used in this study. About forty-two nannofossil species were identified from the Middle Eocene interval of the study section including the Umm Rijam Chert Limestone and Wadi Shallala formations, which were exposed in the type-locality of Wadi Shallala, northwestern Jordan. These can be safely assigned to the *Nannotetrina fulgens* Zone (NP15) for the whole stratigraphic section. The abundance of nannotetrinids is very rare throughout the study interval with a discontinuous distribution. Okada and Bukry (1980) have divided Zone CP13 (=NP15) into three subzones (a, b and c). The lowest Subzone CP13a includes the interval from the FO of *N. fulgens* to the FO of *Chiasmolithus gigas*. The middle Subzone CP13b includes the total range of *Ch. gigas*, and the younger Subzone CP13c occupies the interval from the LO of *Ch.gigas* to the LO of *N. fulgens*. Owing to the entire absence of *Ch. gigas* (a marker of subzone CP13b) and *R. umbilicus* (marker of base NP16), and the continuous presence of *D. lodoensis*, *D. sublodoensis* throughout the samples studied (samples from 1 to 120), it can be concluded that the section under study can be assigned to the Subzone NP15a. Some of the Middle Eocene nannofossil events of Martini (1971) and Okada and Bukry (1980) have been recognized. The stratigraphic ranges of some important nannofossil markers are also briefly discussed. In the present study, the Umm Rijam Chert Limestone and the overlying Wadi Shallala formational boundary occurs the nannofossil NP15 /CP13 Zone. A vertical facies change is assignable within Zone NP15 either in Egypt and Jordan covering a wide disruption which reflects a eustatic sea-level change. So, the upper part of the Umm Rijam and the Wadi Shallala formations in the study area are well-correlated with the upper part of the Thebes Formation (similar to the lithology of Umm Rijam Chert Limestone Formation) and overlying Darat Formation (which consists of argillaceous limestone with marl) in west Sinai of Egypt (Figure 4).

At the Wadi Shallala section, the $\delta^{13}C$ and $\delta^{18}O$ isotope values show a clear negative excursion in $\delta^{13}C$ and $\delta^{18}O$ measurements near the lower part of the Shallala Formation implying a different diagenetic process.

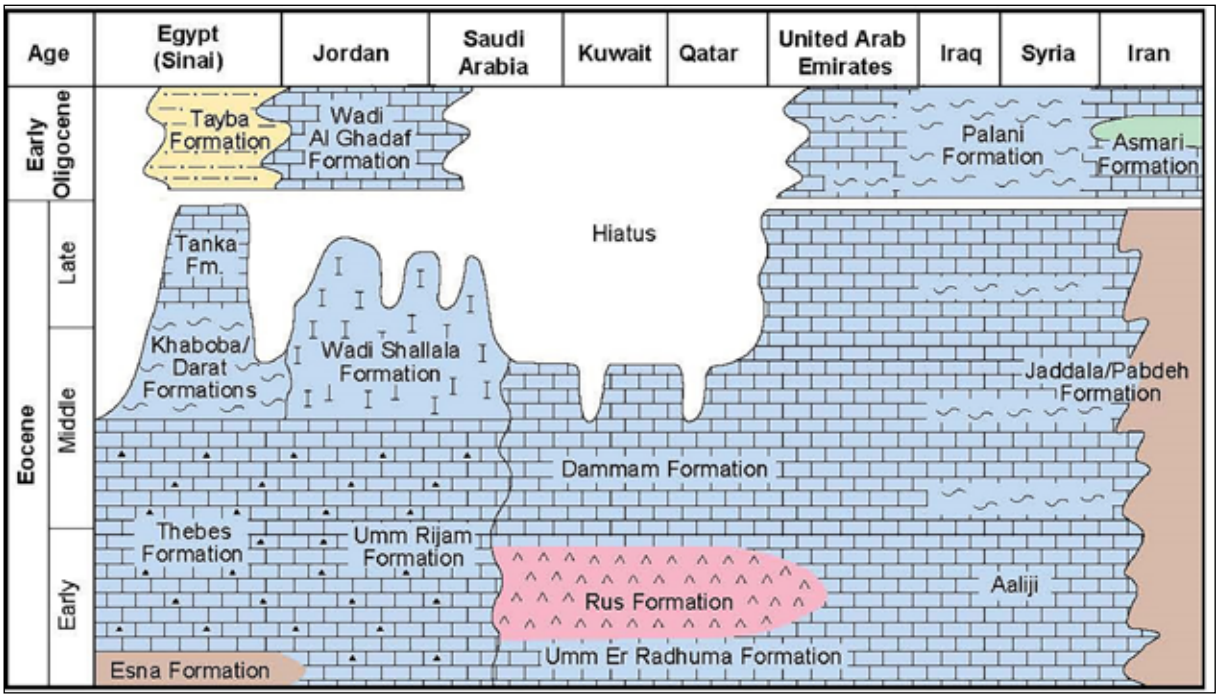

Figure 4. Comparison of Umm Rijam and Wadi Shallala formations with others lithostratigraphic schemes for the Paleogene succession across the African/Arabian plates (modified after Sharland et al., 2001; Farouk et al., 2013 and 2015).

Acknowledgements

The financial support provided by The Hashemite University to Dr. Fayez Ahmad is gratefully acknowledged. Comments by three anonymous reviewers greatly improved an earlier draft of the manuscript.

References

Abul-Nasr, R.A. and Marzouk, A.M. (1994). Eocene biostratigraphy of Wadi Wardan, Sinai, with especial Emphasis on calcareous nannofossils. M.E.R.C. Ain Shams Univ, Earth Sci. Ser. 8:178-187.

Al-Shawabkeh, K. (1991). The geology of the Adir area. Map sheet no. 3152 II. Bull. 18, Amman.

Andrews, I. J. (1992). Cretaceous and Paleogene lithostratigraphy in the subsurface of Jordan. Natural Resources Authority Subsurface Geol. Bull. 5, P. 60.

Bender, F., (1974). Geology of Jordan. Gebrueder Borntraeger, Berlin, P. 196 p.

Bijl, P. K., Houben, A. J. P., S. Schouten, S., Bohaty, S. M., Sluijs, A., Reichart, G. J. J. S. Sinninghe Damsté, J. S. S., Brinkhuis, H. (2010), Transient middle Eocene atmospheric CO2 and temperature variations. Sci. 330 (6005): 819–821.

Boscolo Galazzo, F., Thomas, E., Pagani, M., Warren, C., Luciani, V., Giusberti, L. (2014). The middle Eocene climatic optimum (MECO): A multiproxy record of paleoceanographic changes in the southeast Atlantic (ODP Site 1263, Walvis Ridge). Paleoceanogr. 29: 1143-1161.

Bown, P.R. (2005). Palaeogene calcareous nannofossils from the Kilwa and Lindi areas of coastal Tanzania (Tanzania Drilling Project 2003-4). Jour. Nannoplankton Res. 27(1): 21-95.

Fadda, I. (1996). The Geology of Wadi El Ghadaf Area Map Sheets No. 3353-II. The Hashemite Kingdom of Jordan, Natural Resources Authority, Geological Mapping Division, Bull. 34 p. 26.

Farouk, S., Ahmad, F., Smadi, A. (2013). Stratigraphy of the middle Eocene – lower Oligocene successions in northwestern and eastern Jordan.-Jour. of Asian Earth Sci. 73: 396–408.

Farouk, S., Faris, M., Ahmad, F., Powell, J. (2015). New microplanktonic stratigraphic data and sequences across the Middle-Late Eocene and Oligocene boundaries in eastern Jordan. GeoArabia 20 (3): 145-172.

Hussein, M.A., Alqudah, M., Blessenohl, M., Podlaha, O., Mutterlose, J. (2015). Depositional environment of Late Cretaceous to Eocene organic-rich marls from Jordan. GeoArabia 20 (1):191-210.

Hussein, M.A, Alqudah, M., Boorn, S., Kolonic, S., Podlaha, O., Mutterlose, J. (2014). Eocene oil shales from Jordan -their petrography, carbon and oxygen stable isotopes. GeoArabia 19 (3): 139-162.

Larrasoana, J.C., Gonzalvo, C., Molina, E., Monechi, S., Ortiz, S., Tori, F., Tosquella, J. (2008). Integrated magnetobiochronology of the Early/Middle Eocene transition at Agost (Spain): Implications for defining the Ypresian/ Lutetian boundary stratotype. Lethaia 41 (4): 395-415.

Martini, E., (1971). Standard Tertiary and Quaternary calcareous nannoplankton zonation. In: Farinacci, A. (Ed.): proceeding II Plan Conf, Roma, 1970, 2: 739-785.

Moh'd, B. (2000). The geology of Irbid and Ash Shuna Ash Shamaliyya (Waqqas) map sheet no. 3154-II and 3154-III. Natural Resources Authority, Geol. Mapping Division, Bull. 46.

Okada, H. and Bukry, D. (1980). Supplementary modification and introduction of code numbers to the low latitude coccolith biostratigraphic zonation (Bukry, 1973; 1975). Marine Micropaleontol. 5: 321-325.

Parker, D.H., (1970). The hydrogeology of the Mesozoic-Cenozoic aquifers of the western highlands and plateau of east Jordan. UNDP/FAO, AG 2: SF (No. 2). Jordan 9, Technical report.

Perch-Nielsen, K. (1985) Cenozoic Calcareous Nannofossils. In: Bolli, H.M., Sanders, J.B. and Perch-Nielsen, K. (Eds.), Plankton Stratigraphy, Cambridge University Press, Cambridge, 427-554.

Powell, J.H. and Moh'd, B.K. (2011). Evolution of Cretaceous to Eocene alluvial and carbonate platform sequences in central and south Jordan. GeoArabia 16 (4): 29-82.

Shamrock, J.L., Watkins, D.K., Johnston, K.W. (2012). Eocene biogeochronologyand magnetostratigraphic revision of ODP Hole 762C, Exmouth Plateau (Northwest Australian Shelf). Stratigraphy 9 (1): 55–75.

Sharland, P.R., Archer, R., Casey, D.M., Davies, R.B., Hall, S.H., Heward, A.P., Horbury, A.D., Simmons, M.D. (2001). Arabian Plate Sequence Stratigraphy. GeoArabia Special Publication 2, P. 371.

Sharland, P.R., Casey, D.M., Davies, R.B., Simmons, M.D., Sutcliffe, O.E., (2004). Arabian plate sequence stratigraphy revisions to SP2. GeoArabia 9 (1): 199–214.

Strougo, A., Faris, M., Basta, R.K. (2003). Dating the "Cardita Limestones" and the lower "Green Beds" of west central Sinai by calcareous nannofossils. M.E.R. C. Ain Shams Univ. Earth Sci. Ser. 17:87-114.

Thomsen E, Abrahamsen N, Heilmann-Clausen C, King C, Nielsen O. B. (2012). Middle Eocene to earliest Oligocene development in the eastern North Sea Basin: Biostratigraphy, magnetostratigraphy and palaeoenvironment of the Kysing-4 borehole, Denmark. Palaeogeogr. Palaeoclimatol. Palaeoecol. 350–352:212–235. doi: 10.1016/j. palaeo.2012.06.034.

Wei, W., and Wise S.W. Jr. (1989). Paleogene calcareous nannofossil magnetobiochronology: results from South Atlantic DSDP site 616. Mar. Micropaleontal. 14:119–152.

Weisemann, G., and Abdullatif, A. (1963). Geology of the Yarmouk area, North Jordan. GGM report, P. 81.

JJEES

JJEES (2020) 11 (2): 113-125
ISSN 1995-6681

Jordan Journal of Earth and Environmental Sciences

Zagros Metamorphic Core Complex: Example from Bulfat Mountain, Qala Diza Area, Kurdistan Region, Northeast Iraq

Kamal Haji Karim[1*] and Mayssaa Al-Bidry[2]

[1]University of Sulaimani, Collage of Science, Department of Geology, Iraq
[2]University of Technology, Department of Petroleum Technology, Iraq

Received 17 November 2019; Accepted 3 February 2020

Abstract

Bulfat (Kele Mountain is located northeast of the Qala Diza town at the northeast of Iraq near the border with Iran. The mountain was previously considered as an igneous complex (Bulfat Igneous Complex) of extreme mineralogical, petrological, and structural heterogeneities at the outcrop, hand-specimen and microscopic scales. In previous studies, tens of igneous rocks are indicated in the Complex such as basalt, meta-basalt, gabbro, syenite, metadiabases, diorite, peridotite, serpentinites, nepheline syenite, granitoid-gabbro association, troctolite, olivine gabbro, old gabbro, new gabbro, amphibole-pyroxene gabbro, pegmatites and others. All of these rocks are highly affected by deformations on small and large scales such as folding, normal faulting, ptymagtic folding, mylonitization, crystal bending and crystal boundaries suturing in addition to foliation. Field and lab observations in the present study don't aid the presence of the abovementioned "igneous" rocks and ophiolite on the mountain (in the Bulfat Ophiolite Complex). The present study concludes that all the above mentioned rocks are mixtures of different types of metamorphosed volcaniclastic sandstones, conglomerate, siltstones (greywakes) and shale. These sediments are derived originally from volcanic arcs (Urumieh-Dokhtar Magmatic Arc) with subsidiary amounts of limestone and plutonic igneous rocks clasts. From the remote volcanic arcs, the sediments were transported by turbidity currents to a basin of deposition in the Qaladiza and Bulfat area (as a part of the Sanandij-Sirjan Zone) during the Paleocene-Eocene age. Many evidences are found to prove the sedimentary origin of the rocks of the Complex such as the transition from fresh volcaniclastic sandstones to their mild and intense metamorphosed counterparts, the preservation of planner beddings, sharp erosional surfaces, laminations, grains sorting-roundness, folding, bending of pervious gabbros around marble, submarine channels filled with metamorphosed coarse sandstones. Other evidences are absence of dykes, pillow basalts and volcanic flows, contact metamorphism, hydrothermal mineralization. These sedimentary rocks are regionally metamorphosed to greenschist, amphibolite and pyroxenite facies which can be called schists, mafic-felsic gneisses or granulites and rare migmatite rocks. As parent rocks, all these sedimentary rocks, are deeply buried by tectonic thickening during Eocene, and were partially or totally crystallized by diagenesis and regional metamorphism. Later, during the late Miocene-Pliocene, they were uplifted as a Bulfat Core Complex. Therefore, according to the analysis and discussion of all aforementioned information, the origin of the Complex is formulated in a single model of the core complex, and the deposition of the sedimentary rocks is illustrated by paleogeographic and tectonic models. All previous studies are critically and objectively evaluated and compared to the results of the present study which does not support the occurrence of ophiolites and volcanic rocks in the Bulfat (Qaladiza) area.

Keywords: Bulfat Mountain, Zagros Orogenic Belt, Metamorphic Core complex, Mafic Gneiss, Granulite, Migmatite, Walash-Naoperdan Series, Volcaniclastic Sandstones, Greywackes

1. Introduction

The Bulfat Mountain is located in the northeast of Qala Diza town in northeastern Iraq and trends NW-SE parallel to the Iranian border. Its northwestern part is located inside Iran, and has the width, length, and elevation of 5km, 25 km, 2000m respectively (Figure 1). Tectonically, it is located in the Thrust Zone of Buday (1980), Suture Zone of Jassim and Goff (2006) which is equivalent to the outer part of Sanandij-Sirjan Zone (Ruttner and Stocklin, 1968) in Iran. The mountain has more or less an oval shape, and is surrounded from all sides nearly by sedimentary rocks. According to previous studies, the grade of metamorphism and the igneous rocks increase toward its center.

The Bulfat Mountain was subjected to extensive geological investigations from the late fiftieth of last century till now. According to these investigations, geologically, the mountain is the most complex succession in Iraq. Therefore, geologists applied many geological terms to name the geological setting of the mountain such as the "Bulfat Thrusted Block" Bolton (1958); "Bulfat Igneous complex" (Pshdari, 1983; Buday and Jassim, 1987; Buda, 1993); Bulfat massif (Jassim et al., 1982). Others used terms such as, "The Bulfat block" and "Bulfat Group" (Jassim et al., 2006); Bulfat Complex (Elias and Al-Jubory, 2014). "Bulfat Compex" is used in the descriptions and discussions of the present study.

Researchers have divided the rocks of the mountain into two types; the first type consists of thermally and regionally metamorphosed sedimentary rocks (carbonate and pelites),

* Corresponding author e-mail: kamal.karim@univsul.edu.iq

while the second includes igneous rocks such as basalt, intermediate, basic and ultra-basic intrusive igneous rocks. The origin of the rocks of the complex are controversial, and includes basaltic arc theoleiite and calc-alkaline basalt (Aziz, 1986), volcano-sedimentary of geosynclinal units Jassim et al. (1982); Oceanic intra-arc rift setting (Ali, 2017); Paleocene Oceanic volcanic-arc (Aswad et al., 2016); low-K calc-alkaline magma of basaltic arcs affinity (Aqrawi and Sofy, 2007). Other origins are volcanic arc granite with a dual subduction-zone system (Aswad et al., 2013); rocks of the active margin of the Iranian microcontinent represented by Sanandaj-Sirjan rocks (Elias and Al-Jubory, 2014); subduction-zone system in Iraqi Zagros Zone (Ali, 2015).

The age determination by K/Ar method indicates 40- 45 Ma as the age of the cooling of the intruded basic igneous rocks, but they may have intruded over a somewhat earlier period (Jassim et al., 1982). They added that regional metamorphism affects only Cretaceous rocks or older rocks which makes one presume that they occurred together within the folding in the Laramide orogeny (Upper Cretaceous).

The present study is aimed at presenting several field and lab evidences that would exclude the presence of basalts and plutonic igneous rocks (ophiolite) in the Bulfat Complex. The authors consider that all these rocks are a result of the metamorphism of volcaniclastic sandstones and greywackes, and other sediments derived from volcanic and plutonic igneous rocks. The processes of deposition, burial, diagenesis, and regional metamorphism and uplift are discussed in the framework of a Metamorphic Core Complex model.

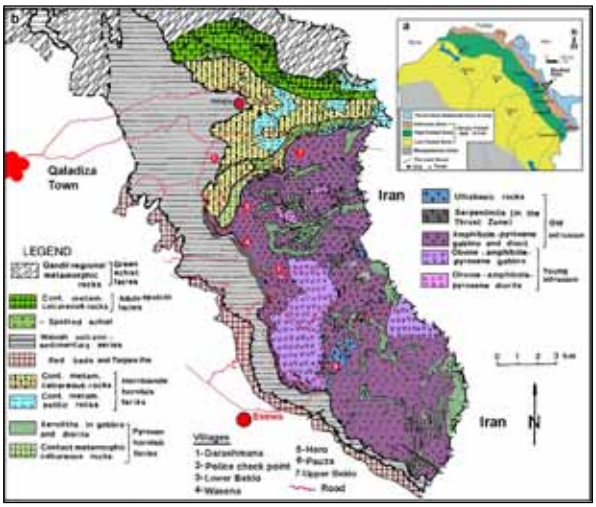

Figure 1. a). Location map (Jassim and Goff, 2006). **b).** Geological map of the Bulfat Mountain area showing the distributions of metamorphic and igneous rocks (Buda, 1993).

1.1. Methodology

The study of the Bulfat Complex is based on fieldwork and microscopic studies. During the years 2010 to 2019, several field trips were conducted to the different parts of the mountain to understand its geomorphology, structure, rock types, their field relations, boundary condition (local and regional geological relations of the complex with neighboring units and complexes) and tectonic setting. During these trips, a total of thirty samples were collected from previously described rocks such as volcanic rocks, metavolcanic rocks, hornfelses, gabbros, syenite, diorite and peridotites. The samples were collected along the paved and unpaved roads that are shown in red line in (Figure 1). Thin sections were prepared for a petrographic study under polarized and stereo-microscopes. The huge published previous data were studied, evaluated, and compared with each other and with the present study. The boundary conditions of the complex were studied on a scale of tens kilometers including the whole northeastern Iraq, and we linked of the obtained boundary conditions to the internal geology of the complex extracting the differences and similarities with other complexes in term of petrology, structure, stratigraphy, and tectonics. As a result, the present study has been set in serious disagreements with previous studies based on the aforementioned attributes of the Complex and its boundaries. These disagreements are justified by field and laboratory evidences and are discussed in detail in several sections.

2. Results

2.1. Absence of volcanic rocks in the Bulfat Complex

According to Jassim et al. (1982), part of the Bulfat Complex consists of ocean-ridge volcanic and sedimentary sequences, which were regionally metamorphosed during Mesozoic. They added that the igneous rocks (metadiabases, basalt, metabasalts, acidic volcanic tuffs, metaandesites and andesite have been metamorphosed at the ocean bottom and preserved their original porphyritic, amygdaloidal textures, in spite of the extensive recrystallization. Aziz (1986) studied spilitized and metamorphosed basalts and andesites inside the Walash-Naoperdan Series (or group) in the Qaladiza area at the southern and western boundaries of the Complex. Ali (2015) studied the same rocks (metabasalts and metaandesite) in detail both petrographically and geochemically in the same area especially around the Halsho and Darashmana villages, and he concluded that they belong to the calc-alkaline basalt of the island- arc setting.

The present field and petrographic studies oppose the presence of volcanic rocks around and on the Bulfat Mountain. There are clear signals that all the above mentioned volcanic rocks are fresh or slightly to moderately metamorphosed volcaniclastic sandstones, conglomerates (greywackes) and shales (Figure 2). These sediments were derived from different mafic and felsic igneous source areas (mainly basaltic terrains) with possible subsidiary limestone sources. These source areas supplied the basin with volcaniclastic sandstones rich in feldspars, pyroxene, and olivine with minor quartz and possible limestone clasts. The fresh sedimentary rocks (greywakes) are exposed to the south of Beklo, Darashimana, Halsho and Gira villages in addition to the area around Darwina, Badin and Shodan villages.

The first signal is gradation from unmetamorphosed volcaniclastic sediments to slightly and then to moderately metamorphosed ones when one walks from the southern boundary to the core of the Bulfat Complex (Figure 3). In spite of mild or intense metamorphism, the traces of the original textures (sorting and roundness of the grains) and structures (laminations and beddings) are preserved in most rocks (Figures 5-6). These rocks are affected, more or less, by regional metamorphism which is imparted schistosity and

foliation in pelitic rocks but not to the degree of destroying the original depositional structures and textures. Due to the preservation, the metamorphosed laminated sediments look like mafic and felsic hornfels (Andrew, 1984), schists, basic or acidic gneisses while they are similar to gabbro or peridotite when the structures are destroyed.

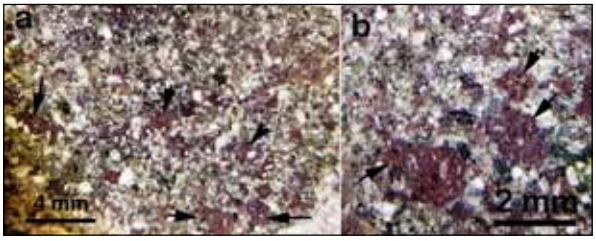

Figure 2. The rock previously claimed as basalt (under stereomicroscope) consists of volcaniclastic sandstone which shows some degrees of sorting and roundness, the volcanic clasts are indicated by black arrows.

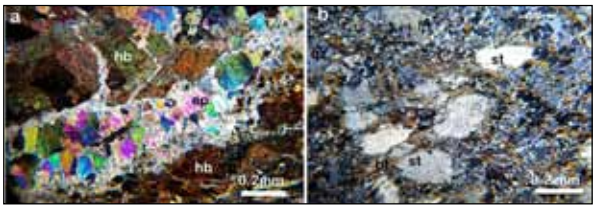

Figure 3. Medium grade metamorphic rocks (schists) under XPL in Shilana valley along the old unpaved road to the Peak of Bulfat Mountain. **a).** Epidote-hornblende schist, s. no. 2, 500 west of Police station. **b).** Staurolite- biotite- muscovite schist, s. no.4, 200m to the west of the police station.

The second is a clear preservation of beddings and laminations of the sedimentary parent rocks (Figures 4-5). In the hand specimens and in thin sections, the white and dark laminae are clearly visible which represent feldspar and hornblende or pyroxene rich bands. The third signal for the sedimentary origin is the textures of thin sections of the metabasalt of Aziz (1986, p.32) and Ali (2015, p.248) which show clear sorting and roundness of the grains of the "metabasalt" rocks without any evidence of basaltic flow textures. It can be observed in (Figures 7a-b) that the rock is a medium-grade metamorphic rock (amphibolite facies) and consists of hornblende and plagioclase. Nearly all grains (clasts) have approximately the same size (mechanically-sorted) with rounded edges but irregular (mechanically abraded) boundaries, and they are neither euhedral nor subhedral. The same properties are observable from the two thin sections of Mohammad and Aziz (2013) of Pauza ultramafic rock. The first one exhibits an irregularly broken periphery of a coarse hornblende clast which is surrounded by finer ones in schistose texture (Figure 7c). The second shows granular anhedral olivine clasts with fine matrix of same mineral in surrounding areas (Figure 7d). Mafic or felsic granulite (Gorayeb et al., 2017) is the types of metamorphic rocks that can be considered for some rocks on the mountain. This later article included photos of granulites (p.335) that are similar to those published by Ali (2015) and Mohammad and Aziz (2013) for metabasalt and ultramafic rocks.

These characteristics include the preservation of original sandstone grains in which rock textures are preserved during metamorphism. In Figure (7a), the interstitial spaces between the grains are filled with irregular and anhedral hornblende crystals resembling the irregular intergranular cement of sandstone. These crystals are metamorphosed from a fine-grain matrix which was derived from a volcanic arc and filled the interstitial spaces between clasts. In this connection Dietrich (1960) referred to the possibility of the distinction of some sedimentary clastic-grain shapes in gneisses. Many thin sections of the quartz rich metamorphic rocks are compared with other volcaniclastic sandstones in other parts of the world (see Sharp and Robertson, 2002; Schmincke and Von Rad, 1979). The results were very comparable in the view of roundness, sorting and irregular boundaries (Figure 8). Before metamorphism, the sedimentary grains already acquired a parallel diagenetic orientation due to compaction and the intense tectonic stress in the synorogenic stress of the Zagros Belt. These diagenetic orientations enhanced the further development of the schistosity, foliation, and banding during the regional metamorphism.

Figure 4. Metamorphosed volcaniclasitc greywakes and shale. **a).** preserved original bedding. **b).** preserved millimetric sedimentation laminae on the head of Shilana Valley 300 m to the north of police check point at latitude and longitude of 36o 11' 32.89" N and 45o 17' 00.86" E.

Figure 5. Horizontal alternation of metamorphosed fine- and coarse-grains of volcaniclastic sandstones (greywackes) beds and marls beds. Previously, these rocks were treated most possibly as volcanic siliceous tuff. They are located at the latitude and longitude of 36° 9' 17.56" N and 45° 14' 41.51" E.

Figure 6. Same alternation at vertical attitude at latitude and longitude of 36° 9' 17.5 6" N and 45°14' 41.51" E, between Darashimana and Lower Beklo villages.

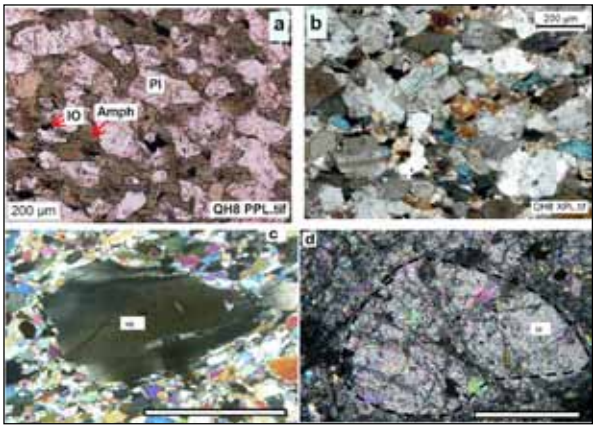

Figure 7. Two thin sections of metabasalt of Ali (2015), the authors think that they show the sorting, and roundness of the cloudy crystals of plagioclase and sutured contacts; **a).** The inter-granular matrix of (possible silt-size volcanic grains) is recrystallized to anhedral hornblende. **b).** Sorting and the anhedral characteristics of the grains of the original volcaniclastic sandstone derived from the erosion of porphyritic volcanic source area. c and d). Thin section photos of ultramafic rock of Pauza (Bulfat Mountain) (Mohammad and Aziz (2013), **c).** The authors think this shows an abraded boundary, granular, anhedral and schistose texture, **d).** Granular and anherdal olivine grains with a fine matrix of the same minerals.

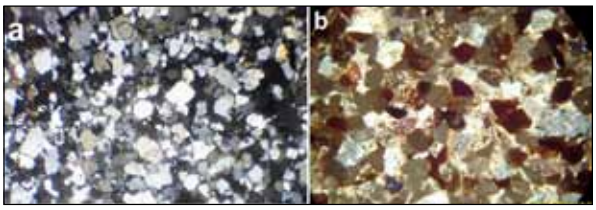

Figure 8. a). metamorphosed quartz rich sediments of Bulfat Complex, s.no.8 XPL, quartz overgrowth can be seen in the upper center. It is compared with; **b).** sandstone of Tanjero Formation) the results are both very comparable in the view of roundness, sorting, grain- interlocking and irregular boundaries, XP light, the lengths of the two photos are 1.5mm.

The forth is the rocks that are claimed to be igneous rocks can be seen in horizontal, oblique and vertical tilted conditions in the same area; they underwent the same folding directions and intensities of the marbles and fresh volcaniclastic rocks that are at the boundary of the complex (Figures 4-7). Therefore, if these rocks are volcanic or plutonic rocks, they must be of a synsedimentary eruption or intrusion, which must show a basaltic flow, pillow basalts, volcanic cone, ropy and amygdaloid and dilatation (local swell between sediments) structures in addition to glassy texture and contact metamorphism. During field work, the present authors did not find any of these structures. Additionally, they found two types of successions (rocks). The first includes fresh thick successions of volcaniclastic sandstone described in the previous paragraphs. The second is a successions dominated by marl with a subordinate impure sandstone (now changed to light and dark metamorphosed greywackes); these successions are very similar to the acidic tuff recorded in previous studies, especially the marl, in most places, is a friable easily-weathered and slightly-metamorphosed with a light grey color resembling wood ashes (Figures 6-7).

The fifth evidence is the presence of large lensoidal bodies, bedding, lamination and erosional surfaces in the previous gabbros and peridotites on the Bulfat Mountain. The lensoidal bodies have a length of 4-40 and a thickness of 0.2-6 meters of volcaniclastic coarse sandstones which were metamorphosed and recrystallized to coarse-grained basic gneisses (Figure 9). Hamasalh (2004) considered these rocks as ultramafic rocks, while Mohammad and Aziz (2013) studied the exsolution lamellae in the orthopyroxene of lherzolite from the Pauza ultramafic rocks; they concluded that the lamellae are formed in a deep mantle.

Some of the rocks (previously claimed to be igneous rocks) exhibit large lensoidal shapes reflecting the submarine channels in which they were deposited (Figure 9). While most others are regularly bedded, laminated, cross-bedded and show sharp erosional surfaces between fine-grain mafic beds and coarse-grain felsic beds (Figure 10a). The paleocurrent can be predicted from the lensoidal shape of the channels which is pointing nearly towards the south. The same types of channels are found near the Waras village on the Mawat Complex where the rocks previously considered as volcanic rocks. The abovementioned south direction of the paleocurrent can be observed from the Waras channel too (Figure 10b).

The strongest evidence (the sixth evidence) for the sedimentary origin of the previous Bulfat ophiolite is the clear gradation between fresh volcaniclastic sandstones (greywackes), around the Complex, and their low and high grades of metamorphosed equivalents in the center of the Bulfat Complex. Geologists can see this gradation (zoning) while walking from the boundary to the core. Due to the stacking of tens of different sedimentary rocks and the intense folding, the metamorphic zoning does not have a certain shape or regular boundaries. Therefore, it is difficult for most geologists to delineate easily the boundaries of zoning of the complex but the progressive metamorphism is very clear from the boundary to the center of the complex.

Figure 9. Submarine channels filled with coarse-grained metamorphosed volcaniclastic sandstones directly to the south of Pauza village on Bulfat Mountain. These rocks are considered as mafic igneous rocks in the previous studies.

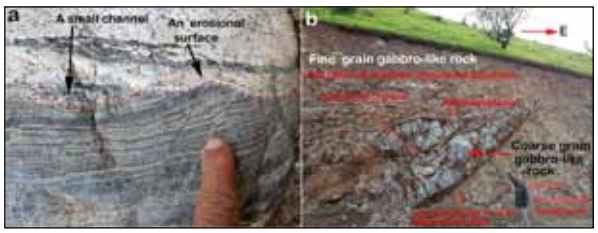

Figure 10. a). an erosional surface, a small channel and laminations in the metamorphosed volcaniclastic sandstone (previously considered as a gabbro), a section of road cut at 1km north of Ganau village east of Esewa town, Bulfat Mountain. **b).** Submarine channel filled with metamorphosed coarse-grain volaniclastic sandstones scored in metamorphosed fine-grain volaniclastic sandstones at the 500 m southwest of Waras village, at the latitude and longitude 35° 47' 13.87'' and 45° 30' 18.41''respectively. Previously, its location was believed to be the volcanic rocks.

2.2. Absence of dykes and bosses

Buday and Jassim (1987) reported the intrusion of various small size pegmatitic dykes and boss-like bodies into the calcareous and pelitic rocks of Bulfat Complex. They added that the dykes consist of white coarse-grained feldspar, and they cut across older intrusions and country rocks. Buda (1993, p.36) recorded many white feldspar-rich pegmatite dykes in the plutonic and metamorphic rocks. He added that they have different composition depending on their occurrences, and that the feldspar dykes in the pyroxene-amphibole gabbro and diorite are rich in sodium (An32). He further added that Dykes, in olivine gabbro or diorite are rich in calcium (labradorite, An56), which commonly has been altered to zoisite and prehnite.

The present authors, has not observed dykes and bosses in the Bulfat Complex and in the whole Northern Iraq. In the complex, they observed two types of bodies, the first one is a succession of a dark coarse-grain alternation of felsic and mafic volcaniclastic sandstones which are tightly and isoclinally folded during tectonic deformations, and they look like small dykes or bosses. This succession is now metamorphosed regionally to rocks which resemble gabbro or diorite. In the folds, the white (feldspars) and dark (pyroxenes) sedimentary laminations are bending 180 degrees, this bedding is true for the associated marble and calcsilicate layers (Figures 11a and 12). A close look revealed that there is not even one millimeter of contact metamorphism between the rocks claimed to be gabbro and the marble in the fold. If the succession in the photo is restored to a horizontal condition before deformation, it would look exactly like the contact between Kolosh and Sinjar Formations as appear from the photos (11b) at 500 m southwest of the Kalk Smaq village in the Dokan Area. The interesting fact is that both successions of Kalka Smaq (near the Low Foded Zone) and Bulfat Complex are of the same age (Paleocene-Eocene) (Figures 11a and b). Most of the metamorphosed limestone occurs as pure calcite marble, while it contains silicate minerals in the core of the Complex where metamorphism is maximum (Figure 11b).

The second type constitutes are faulted large and small veins in all metamorphosed volcaniclastic and marble rocks of the studied area which most probably and incorrectly were identified previously as dykes. These veins extend for several meters cutting across layering, and generally have a wedge-shape since they become narrower at one end (Figure 13). These veins are originally fractures generated before metamorphism during tectonic burial and deformationa. Later, they were filled with calcite and were then replaced predominately by plagioclase, quartz with subordinate amphiboles or pyroxene during regional metamorphism. During metamorphism, they were transformed to coarse-grain rocks similar to granitoids or dioritic rocks. In this regard, Spotl et al. (1999) mentioned replacement of calcite by plagioclase (albite) under high temperatures and in deep burial diagenetic environments (in presence of brine fluid). They added that the replacement ranges from high-grade diagenesis (150-200 °C) to lower green schist facies (300-350 °C), and in the siliciclastic sediments, the replacement began earlier and on a large scale.

Korh et al. (2011) recorded many albite veins in greenschist facies metabasites or in sheared and banded volcano-sedimentary rocks with sharp contacts with their host rocks, without alteration haloes. They added that they are, generally, centimeteric to decimetric wide, and in some places can be traced for several meters. Albite veins are monomineralic or may occur in association with quartz. They further added that the albite is coarse-grained (up to 1 cm) and well- crystallized, without preferential orientation, and the veins were often emplaced in the shear zones' postkinematic phase.

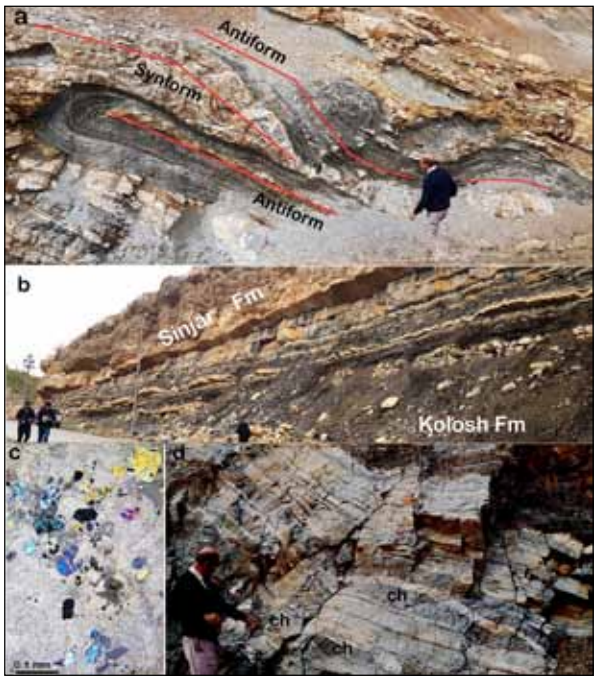

Figure 11. a). Intensive deformation limb-on-limb antiforms and a synforms (bended 180 degrees and overturned toward southwest, the red lines are traces of axial plain of folds. It is regionally metamorphosed volcaniclastic sandstone (greywacke) overlain by marble (limestone) without contact metamorphism. They were considered previously as layered gabbro, a section along the road cut at latitude and longitude of 36° 9' 55.18" N and 45°15' 9.64" E on the paved road to Kele Border Check point. **b).** If the succession in the photo (a). is restored to a horizontal condition before deformation, it would look exactly like the contact between Kolosh and Sinjar Formations as appears from the photos (b) at 500 m southwest of Kalk Smaq village Dokan area. The rocks of both photos nearly have the same ages (Paleocene-Eocene). **c).** Calc-silicate rock with olivine (colored grains) and calcite (grey) near the Iranian border on the paved road on the top of the Bulfat Mountain, s.no.11, XPL. d) The alternation of the felsic and mafic-rich layers of volcaniclastic sandstones with small channels (ch) at 300 m west of Beklo village. These rocks were previously considered as gabbro and diorite.

There are many evidences to prove the absence of dykes; the first is the lack of a sign of dilatation among hundreds of the inspected claimed intrusions, which is expected to be the main evidence of the forceful intrusion of igneous rocks into sedimentary or igneous rocks (Figure 12). The second is the absence of cross-cutting relations of the claimed basic or granitic dykes with layers of host rocks (volcaniclastic, calcareous and pelitic rocks) (Figure 11). In contrast, all of the claimed basic and ultrabasic claimed dyke-like bodies always extend parallel to the original layers of the volcaniclastic sandstones (Figures 11-12). The third is the

absence of a chilled border and metamorphism across the boundaries of the rocks claimed to be dykes; if they were hot and magmatic materials, they must have chilled borders of fine-grain hornfels or have gradation boundaries. The forth is the record of Buda (1993) in which he mentioned that dykes cut both plutonic igneous and metamorphic bodies. This record is important since it means that the dykes ascended after the intrusion of main igneous bodies and the metamorphism. This statement debilitates the idea of the igneous dykes and sustains the idea of the calcite and plagioclase veins and fractures, since the dyke commonly bifurcated from (or associated with) igneous intrusions and predate main metamorphism.

2.3. Presence of para-gneiss, granulite and migmatite

Many evidences can be presented to manifest the occurrence of paragneisses and granulite on the Bulfat Mountain. One of these evidences is the frequent presence of coarse-grain rocks regularity banded with light and dark colored minerals (Figure 14). In addition to banding, all linear and platy minerals have parallel arrangements forming foliation and lineation. These rocks were considered as gabbros in many localities of the mountain by previous studies; however, Aswad et al. (2013, p.111) observed a rhythmic layering in the gabbro (in the Rashid valley) which consisted of labradorite (light) and dark (mafic) minerals of augite and hornblende. Additionally, they described one type of gabbro as "pseudogranitoid gneiss" due to the foliation of pyroxene which is equivalent to the present para-gneiss.

Figure 12. A tilted sequence of felsic and mafic beds of metamorphosed volcaniclastic sandstone (plagioclase and hornblende rich layers) on Bulfat Mountain with marble at the top, at the latitude and longitude of 36° 10' 37.02" N and 45°16' 32.89" E. The marble is originally a shallow reefal carbonate of Naoperdan Formation.

Figure 13. Metamorphosed coarse-grained mafic volcaniclastic sediments (dark background) (previous gabbro) cut by several white discordant and concordant faulted veins (possibly earlier calcite veins), which are regionally metamorphosed to dominant white plagioclases, quartz and amphiboles. Location: at the latitude and longitude of 36° 11' 21.07" N and 45°17' 07.68" E.

The second evidence is the recording of possible migmatite which is an incipient local melting of the gneiss or granulite rocks (Figures 15b and 16). These migmatite bodies have uneven boundaries (surfaces) and irregular aerial distributions; at some places, they are 3 meters long and 2 meters thick. The bodies are not intrusions since they have no connection, from any sides, to the surroundings and are encircled by relatively finer-grain granulite from all sides. The migmatites are extremely coarse-grained with dominant plagioclase and miner amounts of hornblende or nepheline. In these migmatites, the crystals are randomly distributed (Figure 15). But we do not excluded a deformed channel (filled with coarse felsic grains), as origin of these bodies, since the areas of their occurrences are intensely deformed and their shapes are more or less lensoidal.

The third evidence is the published geological map by Buda (1993) which shows many long and zig-zag bending bodies of the xenoliths inside the claimed igneous rocks of the complex in the central and southeastern part of the Bulfat Complex. These xenoliths are numerous and cover half of the outcrop of the previous gabbros and diorites (Figure 1b). These voluminous and numerous bodies (now exist as low- or medium-grade metamorphosed volcanoclastic sediments) are unusual, and need further explanations than the previous ones. The explanation provided by this study refers to the common origin of the host gneisses (or granulites) and xenoliths, each one is part of different lithologies of the same volcaniclastic succession. The porous coarse-grain greywackes are metamorphosed to gabbros or diorites-like rocks, while the siltstones and marls are partially metamorphosed and remained as the xenoliths. The shallow burial of the xenoliths (sedimentary successions) is possible; therefore, they are mildly metamorphosed as the cover rocks of the Complex, while the deeper buried rocks changed to paragneiss or granulite. Another possibility for the origin of the xenoliths is the preservation of some depositional properties of the original thermally-resistive rocks of the sedimentary successions (laminated impervious beds after metamorphism). In contrast, the non-resistive associated sedimentary rocks changed to felsic and mafic gneisses which are treated by many authors as gabbros (Figure 14a).

The fourth evidence is the inability of the petrology (under microscope in mm scale) and geochemistry to solve the controversy of the origin of the Bulfat metamorphic and igneous rocks due to their high diversities as recorded by the previously mentioned authors. These two methods cannot show if the rocks' constituents (such as olivine, pyroxene, and plagioclase grains or crystals) are transported for long distance from their sources or they are indigenous (home-grown) and crystallized in the Bulfat area from magma. But our fieldworks inside and outside the complex (boundary condition studies) decoded the origin of these rocks, that are previously studied, as peridotite, serpentinite–matrix mélange, serpentinite, granitoids, melanocratic gabbro, Nepheline syenite, diorite, granitoid-gabbro association, xenoliths in gabbro and diorite, pseudogranioid, troctolite, olivine gabbro, old gabbro, new Gabbro, amphibole-pyroxene gabbro, metadiabases, basalt, metabasalts, andesite, meta- and acidic tuff. In their study, Al-Hamed et al. (2019)

recorded five types of pegmatites in the Complex.

The metamorphic rocks are also numerous too, and include many types of hornfelses-like rocks and schists. One may ask how and why all these rocks do coexist over several square killometers and are exposed as thousands of beds (layers)? The present study answers this question via suggesting a simple common origin for all of these metamorphic and igneous-like rocks. The answer is the suggestion of a sedimentary origin which can solve the mystery of the rocks swarming of the Bulfat Mountain. The sedimentary origins can group them all in one geochronological, geochemical, tectonical, and petrological framework which is the Metamorphic Core Complex. The mineralogy of both exposed metamorphic rocks and their parent sedimentary rocks were nearly similar; they were derived from the erosion of remote igneous source terrains (basaltic arc) far inside the Iranian territory. The detritus from the arc were transported to the Bulfat area during Paleocene-Eocene by turbidity currents, and were deposited in the deep basin. The water energy and hydraulic activities were separated and increased the concertation of certain minerals as vast beds or as localized lensoidal channels. After the metamorphism, they yielded different rocks; therefore, the metamorphism to gabbro-like or peridotite-like and other rocks was possible especially with the availability of all essential materials, porosity, entrapped seawater, and the different mixtures of volcaniclastic clasts of mafic and felsic mineralogies.

Therefore, the progressive metamorphism of units such as the Walash-Naoperdan Series will give all types of metamorphic and "igneous rocks" since they contain all types of silicate and carbonate sediments that produce different types of the igneous-like rocks, gneisses, ganulites and marble, and calcsilicate rocks when thermally or regionally metamorphosed. The progressive metamorphism of pure and impure sandstones (greywakes) and shales will produce felsic and mafic gneisses or granulites. Their content of marl and calcareous shale will produce a rock similar to the siliceous tuff by low-grade metamorphism, while by high-grade they remain as layered xenolith because they are resistive to thermal metamorphism relative to other rocks.

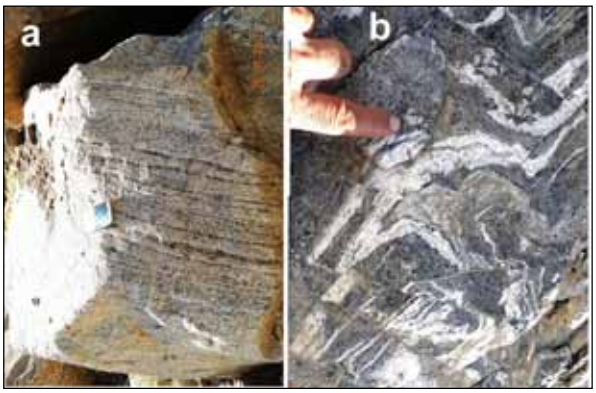

Figure 14. a). Gneiss on Bulfat Mountain at the eastern boundary of the Hero Village. **b).** possible partial melting inside metamorphosed mafic volcaniclastic forming felsic migmatite but a felsic-rich layer is not excluded.

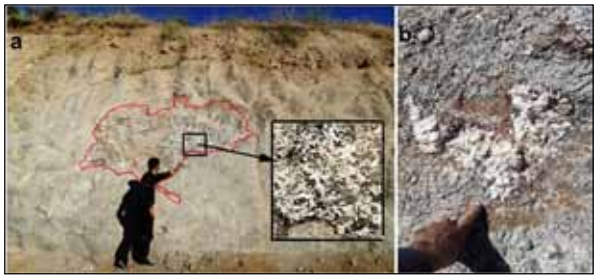

Figure 15. a). A possible migmatite body in side granulite or gneiss with irregular boundaries and isolated from all sides, a section along a road cut at the peak of Bulfat Mountain at 200 m east of the police check point. **b).** A small pegmatite body inside gneiss on the Bulfat Mountain at 300m south of the police checks point on the peak of the mountain. In both photos, channels filled by coarse-grain felsic sandstone are not excluded.

The fifth evidence is the highly-deformed (sheared and foliate) and cloudy textures of the most rocks claimed to be diorite, gabbros and peridotites which appear, under polarizer microscope, as stressed and sutured grains (Figure 16). The cumulate and adcumulate textures of the igneous rocks (Wager et al. (1960) are not observed in all of the inspected thin sections. The stressed and deformed rocks which are claimed to be mafic and ultramafic rocks (especially around Pauza village) are discussed in detail by Hamasalh (2004). In thin sections, most of the texture of these rocks shows foliations, but non-foliated granular and coarsely-crystallized textures are not rare especially at the center of the Complex; they are composed of plagioclase, pyroxene and olivine (Figure 16). Mafic granulite (Yu et al., 2019 and Gorayeb et al., 2017) is the best name to be used for these granular and high-grade facies which are lacking crystal zoning and cumulate textures.

The Walash-Naoperdan Series occurs around the Bulfat and Mawat complexes (at least, at the south, southwest and southeast) apparently below the Red Bed Series, and consists (as previously indicated) of a mixture of volcanic rocks, sedimentary rocks, and carbonate sediments. But the present study inferred that the series does not contain volcanic rocks; instead, it consists of volcaniclastic sandstone, shale and greywacke (Figure 17) that was derived mainly from the volcanic (basaltic arc) source areas. These sediments can produce the gabbro or diorite-like rocks after metamorphism and crystallization.

Between Beklo and Wasena villages and on the eastern side of the unpaved road, a clear succession of a metamorphosed coarse-grained dark volcaniclastic succession can be observed about 10m thick (Figure 17); it was considered by Buda (1993) as gabbro. This succession is very similar to the fresh and coarse sandstone successions near Darawena and 1 km south of Darashmana villages. The same succession occurs in the south Mawat Complex between the Bard Pan and Gabara villages, and consists of a thick succession of fresh volcaniclastic sandstones; that is very similar to the metamorphosed succession near the Belko village on the Bulfat Mountain in outcrop alternation (Figures 17-19).

Figure 16. coarse crystalline previous gabbro (present mafic granulite resulted from metamorphosed coarse-grain volcaniclasts sandstones which have sutures boundaries (red arrows) and no cumulate texture 500m to the west of the Iranian police station on the border on the Bulfat Mountain, s.no.12, XPL

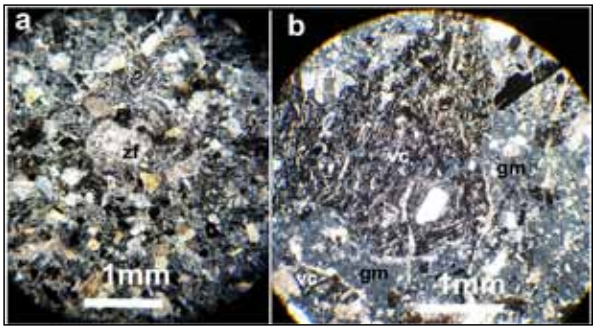

Figure 17. a). Volcaniclastic sandstone of Walash-Naoperdan Series (in Mawat area) derived from volcanic source area and mostly consists of zoned plagioclase (zf) volcanic clasts under XP light, S.no. 15. **b).** The same sandstone shows large clast (grain) (vc) of volcanic rocks with fine-grained groundmass (gm).

Figure 18. a). Metamorphosed succession of well-bedded and laminated volcaniclastic sandstone composed mainly of hornblende and plagioclase, exposed between the Beklo and the Wasena village at the latitude and longitude of 36° 9' 2.74" N and 45° 16' 0.32" E. **b).** A close-up photo of the laminated bed in the red circle shows regular and parallel laminations, the present study assumes that they are originally sedimentary and belong to the Walash-Naoperdan Series.

Figure 19. Comparison between: **a).** stacking pattern of the layered hornfels-like rocks (near the Beklo village) and **b).** Fresh the volcaniclastic sandstone (greywacke) of the Walash-Naoperdan Series at 3km east of Mawat town on the road to the Gabara village.

The sixth evidence is the well-known idea of the open-system processes and the multiple-sources of the intruded gabbroic magma of the Wadi Rashid gabbro by Aswad et al. (2013). This idea supports our sedimentary origin theory of the Bulfat Complex and the presence of gneiss rocks, since most complete open system is a sedimentary basin, which was supplied at different times and places by different sediments from tens of source areas and environments. However, this open system of the sedimentary rocks hosts possible small localized closed systems due to the sandwiching of different rocks by others of different mineralogical and textural properties. These closed systems produce unexpected metamorphic rocks in small areas where, in some cases, several metamorphic rocks can be seen along few meters a head (Figure 12). In contrast to the present study, Elias and Al-Jubory (2014) studied the provenance and tectonic setting of the metapelites deposits in the Bulfat Complex, and concluded that pelites may have been originally derived from an old post-Archean granitic upper continental crust.

The seventh evidence is the diversities of the age determination of the different rocks of the Bulfat Complex which implies the same ages of the rocks claimed as igneous and the metamorphic rocks. Nearly, all the determined ages by radioactive methods ranged between 33 and 45 million years. The age determination (by the ^{40}Ar /^{39}Ar method) of the metamorphism of the pelitic rocks far from the bodies (claimed as igneous) by Karo et al. (2018) is 35 Ma, while the age determination of igneous rocks crystallization by Karo, (2015), Ali (2017) and Jassim et al. (1982) is 41, 39, and 40- 45 Ma, respectively.

From these ages, two facts are clear, the first is a difference in the age of the crystallization of igneous rocks, and the second is the age similarity of the metamorphic rocks that are far from and close to the claimed intrusions. A 10 Ma difference in age implies metamorphism and magmatism are not related in particular if the same method was used on the same minerals.

In the magma, the biotite is last mineral that crystallizes, so its age must be younger than the country rocks which crystallize when the magma is near its peak temperature. Furthermore, the age of biotite reflects the age of the closure temperature of biotite with regard to the isotopes used.

3. Discussion

3.1. Possible Metamorphic Core Complex (MCC)

The previous tectonic models of the Ophiolite Complex cannot answer all questions about the origins of the diverse rocks that are arranged in successions of thousands of layers in a small geographic area with cross beddings, erosional surfaces, and tens of thousands of laminations. Additionally, there is a clear gradation between pure (unmetamorphosed) greywackes and their low- or high-grade metamorphic equivalent rocks (basic and felsic gneisses and granulites). This is true about the controversy and discrepancy regarding their types and geologic settings. The field and lab observations as well as the literature reviews convinced the present authors to propose a new tectonic model which is Metamorphic Core Complex (MCC). This model can probably solve the problems regarding the mixture of numerous dissimilar sedimentary, metamorphic, and igneous-like rocks in highly sheared and uplifted small areas.

Ring (2014) defined MCC as a rock complex which resulted from a horizontal lithospheric extension; it forms in the low-viscosity lower crust when the extension occurs at high rates and deformations occur within the upper crust in localized detachment faults. They are oval-shaped and usually updomed (anticlinal) structures in which mid-

crustal basement rocks of higher metamorphic grade have been tectonically juxtaposed against low-grade upper crustal rocks.

According to Coney (1980), metamorphic core complexes are normally characterized by a heterogeneous, older metamorphic-plutonic basement terrain overprinted by low-dipping lineated and foliated mylonitic and gneissic fabrics. Furthermore, a sedimentary cover terrain is typically weakened and sliced by numerous subhorizontal younger-on-older faults. He further added that between the basement and the cover terrains is a detachment fault and/or steep metamorphic gradient with much brecciation and kinematic structural relationships indicating sliding or detachment. MCC is defined by Lister and Davis (1989) as a crust structure which resulted from major continental extension, when the middle and lower continental crust is dragged out from beneath the fracturing, extending the upper crust. Deformed rocks in the footwall are uplifted through a progression of different metamorphic and deformational environments, producing a characteristic sequence of (overprinted) meso- and microstructures.

Huet et al. (2011) mentioned that the development of MCC corresponds to a mode of lithospheric continental stretching that follows collision. They added that the rheological layering of the crust inherited from collision is a first-order parameter controlling the development of extensional structures in post-orogenic settings. 'Cold' MCC can develop, if the crust is made of a strong nappe thrust on the top of weaker metamorphic cover and basement units. Okay and Satir (2000) summarized MCC in the mountain belt of western Turkey Kazdağ mountain range which is associated with a rapid exhumation in which gneiss, amphibolite, and marble are metamorphosed at 5kb and 640 C°. They added that the unmetamorphosed cover rocks, ductile shear Zone, mylonite and normal fault (brittle deformation) occurred at an upper level.

These characteristic features can be observed on the Bulfat Mountain including the ductile deformation (Figures 9 and 17), the foliated mylonitic, and the gneissic texture (Figures 14 and 21) and surrounding of Metamorphoc rocks by unmetamorphed sediments (Figures 1 and 16 see Walash Series, Red Bed Series and Tanjero Formation).

Figure 20. Intense deformation of the metamorphosed greywacke (with sedimentary felsic and mafic-grain-rich laminae), a) as ptygmatic folding of previous fractures, b) folding of white and black laminae in form of synforms and antiforms. These folds are deformed before metamorphism during tectonic burial.

The MCC occurs in different tectonic settings such as extension, compression, and shields settings. According to DeCelles (2004) and Crittenden et al. (1980), the Cordillera belt is a fold thrust belt that was developed during Jurassic-Tertiary. They added that the belt contains more than twenty-five large bodies of MCCs, and extends from Canada to Mexico passing through central USA. In these MCCs, Vanderhaeghe et al. (1999) discussed the role of partial melting in generation of migmatites and granitic bodies (Figure 15a) which later underwent late-orogenic collapse, and exhumation of high-grade rocks in the hinterland of a thermally mature orogenic belt. As for the Zagros orogenic belt, Alizadeh et al. (2010, p.338) discussed geochronology in a metamorphic core complex (or gneiss dome).

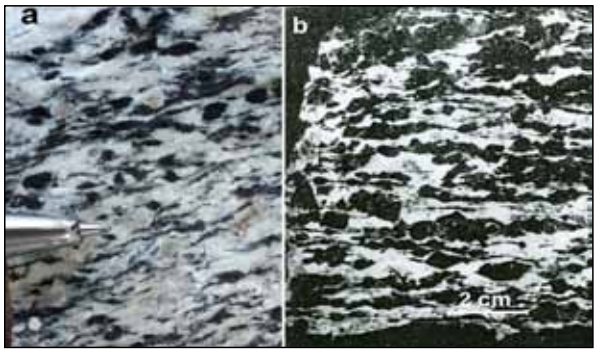

Figure 21. a). Augen and foliated gneiss (mylonitic gneiss) on Bulfat Mountain 400 m to the east of the police check point. **b).** the same type of rock was reported by Jassim et al. (1982) near Beklo village and is considered by them as Pyroxene amphibole gabbro.

The overall shape, rock types, and tectonic position (location) of the latter MCC are very similar to those of the Bulfat and Mawat MCC, only being older (77 my). The Bulfat MCC is associated with extension and normal faulting both locally and regionally. On a local scale, many normal faults can be seen which occurred after metamorphism (during uplifting) (Figure 22). On a regional scale, Karim, (2006) discussed in details the occurrence of a normal fault (Mawat fault) at the south eastern boundary of the Complex (Figure 23). At the northern boundary of the Complex, Mohajjel and Rasouli (2014, p.68) drew a normal fault which extends tens of kilometer inside Iran parallel to the Complex long axis. In the past, Karim et al. (2009, p.61) considered the Bulfat Mountain as horst, and drew two normal faults at its northwest and southwest boundaries (Figure 23a). All other works on MCC agreed that it has a domal shape (anticline); these include Coney (1980, p12), Daczko et al. (2009) and Charles et al. (2012); previously, Jassim et al. (2006, p.304) has shown the Bulfat Mountain as an anticline.

Figure 22. A normal fault (as a sign of extension) in the metamorphosed greywacke and felsic sandstone overlain by limestone (marble) at the southwestern boundary of the Bulfat Complex at the latitude and longitude of 36° 10' 36.92" N and 45° 16' 32.49" E.

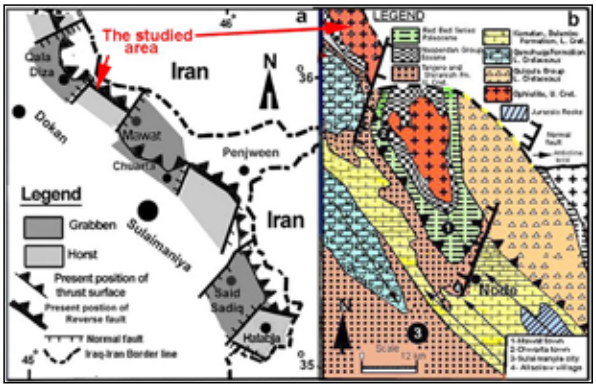

Figure 23. Two maps showing the Bulfat Mountain bounded by two normal faults (horst) from the northwest and the southeast. a) Karim et al. (2009) and b) Karim (2006).

3.2. Depositional Basin of the sediments of the Bulfat Core Complex

According to Aswad et al. (2016), the plutonic rocks of the Bulfat Complex were emplaced into the ophiolite bearing terrain (Albian-Cenomenian) shortly after the 45Ma. They added that the Walash-Naopurdan volcanic activity and the intrusion of the multiphase Bulfat Complex indicate the presence of a dual subduction-zone system in the Iraqi Zagros Zone. Based on geochemical signatures, Ali (2017) attributed the dikes in the Bulfat area to an extensional tectonic environment, such as an intra-arc rift. Karo (2015) considered the Bultat metapelites as a probable derivation from the active continental margin (with an arc affinity) of the Sanadaj-Sirjan Zone.

The sediments of the Bulfat metapelites were derived from the active margin of Iranian microcontinent of the Sanandaj-Sirjan Zone (Elias and Al-Jubory, 2014). The Igneous intrusion in the Bulfat area occurred during the final stage of the primary Cretaceous folding (i.e. most probably in the Laramide orogeny) and the metamorphism affected only Cretaceous rocks (Jassim et al., 1982). Aqrawi, and Sofy, (2007) attributed Bulfat igneous intrusions to a volcanic arc basalt affinity.

The field and lab works in the present study disagree with the above suggested origins of the rocks of the Bulfat Complex. Conversely, indicate that the rocks of the Bulfat MCC are metamorphosed volcaniclastic sandstones (greywackes) and shales. They were deposited after continental collision and the generation of the foreland basin. Their source areas were a terrestrial land consisting mainly of basaltic and andesitic sources (with possible plutonic ones) of the Urumieh-Dokhtar Magmatic Arc. These sources include old and uplifted sediments derived during earlier ages from the arc (Figure 24). After erosion, these sediments were transported and deposited in the Zagros Foreland basin during Paleocene-Eocene by turbidity currents. The model in the latter figure illustrates the Paleocene morphology of the depositional features of the submarine turbidity fan which consists of submarine canyon, gulleys, different type of channels, levees and lobs surface. According to Deptuck and Sylvester (2018), each feature of the submarine fan has its sediment types ranging from silts to conglomerates. Therefore, by this model, the reasons behind the different type of the sediments in mineralogy and caliber can be explained in the Bulfat area. In the channels, different types of clean-coarse sandstones (arenite) of a single or several minerals were deposited, while on the lobe surfaces and levees clay, silt and fine-grain dirty sandstone (greywackes) were lain down. In the channels, the hydraulic sorting of the grain was active due to density and grain-shape sieving. Therefore, in some channels, the gravity sorting induced placer deposits of clasts consisting of olivine or spinel chromium or pyroxene or iron ore which are not rare in the Bulfat, Mawat and Penjween complexes.

During Paleocene-Eocene, the foreland basin, in which the volcanclastic sediments of the Bulfat Complex are deposited, occupied part of the Sanandij-Sirjan Zone of Iran and the whole Iraq. The collision occurred during Campanian and Maastrichtian when the Arabian and Iranian plates collided; consequently, at the first stage, the radiolarites and limestone uplifted close to Arabian Passive Margin and were followed by volcaniclastic sediments (rocks) uplift during. These latter rocks started erosion and provided sediments to the basin (Sanandij-Sirjan Zone) including Bulfat area during Paleocene-Eocene. In the same time, the influx of sediments from the arc (Urumieh-Dokhtar volcanic arc) was continuous too (Figure 24). According to Karim (2004) and Karim and Surdashy (2005) these uplift (obductions) led to the subsidence of the Arabian Passive Margin and the generation of foreland basin during Early Maastrichtian.

During the Paleocene-Eocene age, a thick succession of volcaniclastic sandstones and shales was deposited in the highly subsiding foreland basin. Stratigraphically, they were called in Iraq the "Walash-Naoperdan Series," which consists of clastic and carbonate sediments without volcanic rocks. Later, they were buried deeply by the tectonic loading (thickening) of the crust, and due to this burial, they were intensely deformed both brittlely and ductilely (Figures 19-20).

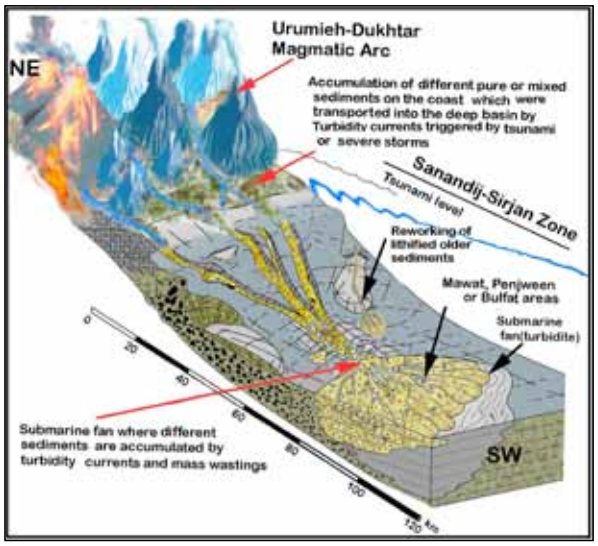

Figure 24. Simplified paleogeographic and tectonic model of the depostion of mafic and felsic valcaniclastic sandstones (and other sediments) by turbidity currents sourced mainly from Urumieh-Dokhtar Magmatic Arc and trassported to the Iraqi part of the Sanandij-Sirjan Zone (Bulfat and Mawat areas). In future works, a more realistic model will be considered.

The deep subsidence had buried and metamorphosed all the sediments regionally under different temperatures

and stresses. The deeper parts were metamorphosed up to amphibolite and granulite facies rocks such as gneisses and granulites in addition to rocks similar to hornfels (Figures 18b and 20) which are previously called gabbros, peridotites or syenite. The shallow buried part is characterized by green schist facies which were previously called metabasalts. These rocks grade upward to unmetamorphosed volcaniclastic sediments and limestone which were previously considered as volcanic rocks and xenoliths respectively (Figures 1-2); they are mainly exposed around the MCC. During the Upper Miocene-Pliocene, the Metamorphic Core Complex was uplifted, and was then exposed weathering and erosion (Figures 25-26). This erosion had supplied huge quantities of conglomerates and sandstone to the progressive southward withdrawal of the Upper Miocene-Pliocene Upper Bakhtiary Basin.

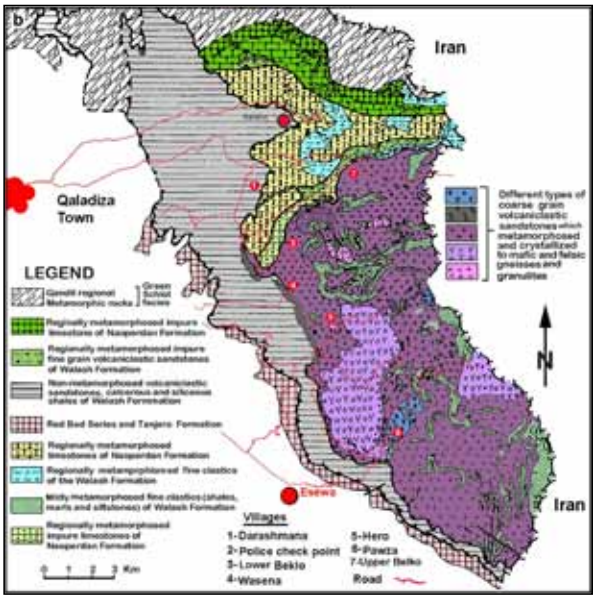

Figure 25. A geological map of the Bulfat Metamorphic Core Complex on which the rock names of the metamorphosed volcaniclastic sandstones and other sedimentary rocks of the present study are plotted. In the future, the rock boundaries need more accurate mapping.

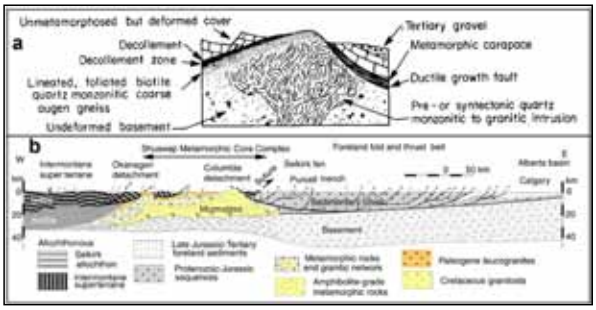

Figure 26. Two Tectonic Models of Metamorphic Core complexes. a). Davis and Coney (1979) and b). Vanderhaeghe et al. (1999).

4. Conclusions

1- The previous "Bulfat Ophiolite Complex" is changed to the Bulfat Metamorphic Core Complex, and the presence of ophiolite and volcanic rocks in the Bulfat and Qaladiza areas is not supported.

2-All exposed rocks in the Complex consist of either fresh volcaniclastics sediments (sandstone, conglomerate, greywackes and shale) or their regional metamorphosed equivalents rocks.

3- Basalts, metabasalt, and plutonic igneous rocks of previous studies are not found on the Bulfat Complex.

4- Most metamorphosed rocks preserved their original sedimentary structures and textures such as the planar beddings, laminations, cross beddings, folding, cross bedding, erosional surfaces, and their granular textures.

5- The Complex consists of thousands of layers of more than ten rock types which all metamorphosed regionally to green schists and amphibolite facies, and locally to gneisses and granulites.

6- Due to the preservation of sedimentary structures (laminations), the metamorphic rocks look like different types of hornfels.

7- All of the rocks previously described as dykes are neither dyke nor sill; rather, they are metamorphosed coarse-grain felsic or mafic sandstones deposited in the submarine channel.

8- The origins of the rocks of the Bulfat Complex are sediments that were originally transported to the Bulfat area from the Urumeh-Dokhtar Magmatic (basaltic) Arc by turbidity currents during Paleocene -Early Eocene. During the Late Eocene- Miocene, they were buried and metamorphosed; however during the Late Miocene-Pliocene they were uplifted.

Acknowledgment

The authors deeply express their thanks to Dr. Ibrahim Qasm Al-Asaadi for reading an earlier version of the manuscript and for this valuable comments and kind encouragement throughout the present study. The works and great efforts of the previous authors, about the Bulfat Complex, must be praised since their ideas and data have been very beneficial to the present study.

References

Al-Hamed S.T., Aswad K.J., Aziz N.R. (2019). Classification of Composite Pegmatite via Staining and Digital Image Processing in the Bulfat Complex, Qala Deza, NE (Iraq). In: Doronzo D., Schingaro E., Armstrong-Altrin J., Zoheir B. (Eds.). Petrogenesis and Exploration of the earth's Interior. CAJG 2019. Advances in Science, Technology & Innovation (IEREK Interdisciplinary Series for Sustainable Development). Springer, Cham.

Ali, S.A. (2015). Petrogenesis of metabasalt rocks in the Bulfat Complex, Kurdistan region, Iraqi Zagros Suture Zone, Kirkuk University Journal, Scientific Studies (KUJSS) 10 (3): 242-258.

Ali, S.A. (2017) 39 Ma U-Pb zircon age for the Shaki-Rash gabbro in the Bulfat Igneous complex, Kurdistan Region, Iraqi Zagros Suture Zone: rifting of an intra-Neotethys Cenozoic arc, Ofioliti 42 (2): 69-80.

Alizadeh, A., Martınez M.L., Sarkarinejad, K. (2010). 40Ar-39Ar Geochronology in a gneiss dome within the Zagros Orogenic Belt, Comptes Rendus Geoscience 342: 837–846.

Andrew, A.S. (1984). P-T-X (CO,) conditions in mafic and calc-silicate hornfelses from Oberon, New South Wales, Australia, J. metamorphic Geol 2: 143-163.

Aqrawi, A.M., and Sofy, M.M. (2007). Petrochemistry and Petrogenesis of Bulfat Mafic Intrusion, Qala Dizeh, Iraqi National Journal of Earth Sciences 7(1): 33-60.

Aswad, K.J., Ali, S.A., Al-Sheraefy, R.M., Nutman, A. P.,

Buckman, S., Jones, B.G., Jourdan, F. (2016). 40Ar/39Ar hornblende and biotite geochronology of the Bulfat Igneous Complex, Zagros Suture Zone, NE Iraq: New insights on complexities of Paleogene arc magmatism during closure of the Neotethys Ocean, Lithos 266–267: 406-413.

Aswad, K.J., Al-Sheraefy, R.M., Ali, S.A. (2013). Pre-collisional intrusive magmatism in the Bulfat Complex, Wadi Rashid, Qala Deza, NE Iraq: geochemical and mineralogical constraints and implications for tectonic evolution of granitoid-gabbro suites. Iraqi National Journal of Earth Sciences 13 (1): 103-137.

Aziz, N.R. (1986). Petrochemistry, petrogenesis and tectonic setting of spilitic rocks of Walash volcanosedimentary Group in Qala Diza area, NE Iraq. Unpub. M. Sc. Thesis, Univ. of Mosul, 181pp.

Bolton, C.M.G. (1958). The geology of the Raniya area. Site Inv. Co. report, S. O. M. library, report no. 271, Baghdad.

Buda, G.Y. (1993). Igneous petrology of the Bulfat area (North-East Iraqi Zagros Thrust Zone) Acta Mineralogica-Petrographica, Szeged 34: 21-39.

Buday, T., (1980). Regional Geology of Iraq: Vol. 1, Stratigraphy (Eds.). Kassab, I.I.M and Jassim S.Z.D. G. Geol. Surv. Min. Invest. Publ. 445 p.

Buday, T. and Jassim, S.Z., 1987. The Regional Geology of Iraq: Tectonism Magmatism, and Metamorphism. I.I. (Eds.). Kassab, I.I.M and Abbas, M.J. Baghdad, 445 p.

Charles, N., Gumiaux, C., Augier, R., Chen, Y., Faure, M., Lin, W., Zhu, R., (2012). Metamorphic core complex dynamics and structural development: field evidences from the Liaodong Peninsula (China, East Asia). Tectonophysics 560–561:22–50.

Coney, P.J. (1980). Cordilleran metamorphic core complexes: An overview, in Crittenden, M.D., Coney, P.J., Davis, G.H. (Eds.). Cordilleran metamorphic core complexes: Geological Society of America Memoir 153: 7-13.

Crittenden, M.D., Coney, P.J., Herbert Davis, G., Hamilton Davis, G., (1980). Cordilleran Metamorphic Core Complexes, Geological Society of America, memoir 153, 490p.

Daczko, N.R., Caffi, P., Halpin, J.A., Mann, P. (2009). Exhumation of the Dayman dome metamorphic core complex, eastern Papua New Guinea J. metamorphic Geol. 27: 405-422.

Davis, G.H., and Coney, P.J. (1979). Geologic development of the Cordilleran metamorphic core complexes, Geology 7: 120-124.

DeCelles, P.G. (2004). Late Jurassic to Eocene evolution of the Cordilleran Thrust Belt and Foreland Basin System, Western U.S.A. American Journal of Science 304:105–168.

Dietrich, R.V. (1960). Banded Gneisses, Journal of Petrology 1(1): 99-120.

Deptuck M.E., and Sylvester Z (2018). Submarine Fans and Their Channels, Levees, and Lobes. in: Micallef, A., Krastel, S., Savini, A. (Eds.). Submarine geomorphology: Cham, Switzerland, Springer, p. 273–299, http://doi.org/10.1007/978-3-319-57852-1_15.

Elias, E.M., and Al-Jubory, Z.J. (2014). Provenance and tectonic setting of the metapelites deposits in the Bulfat Complex, NE-Iraq, Arabian Journal of Geosciences 7(9): 3589–3598.

Gorayeb, P. S.S., Pimentel, M.M., Armstrong, R., Galarza, M.A. (2017) Granulite-facies metamorphism at ca. 570-580 Ma in the Porangatu Granulite Complex, central Brazil: implications for the evolution of the Transbrasiliano Lineament, Brazilian Journal of Geology 47(2): 327-344.

Hamasalh, F.R. (2004). Petrochemistry, petrogenesis and tectonic setting of the Pauza Ultramafic rocks, Bulfat Complex, Northeast Iraq, Kurdistan region, MSc. Thesis, University of Sulaimani. P.115.

Huet, B., Le Pourhiet, L., Labrousse, L., Burov, E., Jolivet, L. (2011). Post-orogenic extension and metamorphic core complexes in a heterogeneous crust: the role of crustal layering inherited from collision. Application to the Cyclades (Aegean domain) Geophys. J. Int. 184: 611–625.

Jassim, S.Z., Buda, G., Neuzilová, M., Suk, M. (1982). Metamorphic development of the Iraqi Zagros Ophiolite Zone, Kryst. Alinikum 16:21-40.

Jassim, S.Z. Suk. M. and Waldhausrova, J. (2006). Magmatism and metamorphism in the Zagros Suture in Jassim and Goff, Geology of Iraq. Published by Dolin, Prague and Moravian, p.298-325.

Karim KH (2004). Basin analysis of Tanjero Formation in Sulaimaniya area, NE-Iraq. PhD thesis, University of Sulaimani University, 135p.

Karim, K.H. (2006). Some sedimentary and structural evidence of possible graben in Chuarta-Mawat area, Sulaimanyia area, NE-Iraq. Iraqi, Jour. Earth Sci. 5 (2): 9-18.

Karim, K.H. and Surdashy, A.M. (2005). Tectonic and depositional history of Upper Cretaceous Tanjero Formation in Sulaimanyia area, NE-Iraq. Journal of Zankoy Sulaimani 8(1): 1-20.

Karim, K.H., Fatagh, A.I., Azad Ibrahim, A., Koy, H, (2009). Historical development of the present day lineaments of the Western Zagros Fold-Thrust Belt: A Case study from Northeastern Iraq, Kurdistan Region. Iraqi Journal of Earth Sciences 9 (1): 55-70.

Karo, N.M. (2015). Metamorphic evolution of the Northern Zagros Suture Zone (NZSZ), Dissertation, zur Erlangung des akademischen Grades, Doctor rerum naturalium (Dr. rer. nat.) in der Wissenschaftsdisziplin “Mineralogie Institut für Erd- und Umweltwissenschaften Mineralogie, 127p.

Karo, N.M., Oberhänsli, R., Aqrawi, A.M., Elias, E.M., Aswad, K.J., Sudo, M. (2018). New 40Ar/39Ar age constraints on cooling and unroofing history of the metamorphic host rocks (and igneous intrusion associates), the Bulfat Complex (Bulfat area), NE-Iraq, Arabian Journal of Geosciences 234: 1-11.

Korh, A.E., Schmidt, S.T., Vennemann, T., Ulianov, A. (2011). Trace Element and O-Isotope composition of polyphase metamorphic meins of the Ile de Groix (Armorican Massif, France): Implication for fluid flow during HP Subduction and Exhumation Processes, in: Dobrzhinetskaya, L. F., Faryad, S.W., Cuthbert, S. (Eds.). Ultrahigh-Pressure Metamorphism, Elsevier Inc.: 243-291.

Lister, G.S., and Davis, G.A. (1989). The origin of metamorphic core complexes and detachment faults formed during Tertiary continental extension in the northern Colorado River region, U.S.: Journal of Structural Geology 11: 65–94.

Mohajjel, M., and Rasouli, A. (2014). Structural evidence for superposition of transtension on transpression in the Zagros collision zone: Main Recent Fault, Piranshahr area, NW Iran, Journal of Structural Geology 62: 65-79.

Mohammad, Y.O., and Aziz, N.R.H. (2013). Exsolution lamellae in orthopyroxene of lherzolite from the Pauza ultramafic rocks, NE Iraq: evidence of deep mantle signature in the Zagros Suture Zone, International Journal of Geography and Geology 2 (9):102-115.

Okay, A.I., and Satir, M. (2000). Coeval plutonism and metamorphism in a latest Oligocene metamorphic core complex in northwest Turkey. Geol. Mag. 137 (5): 495–516.

Pshdari, M. (1983). Mineralogy and geochemistry of contact rocks occurring around Hero and Asnawa, NE-Iraq. Unpub. M. Sc. Thesis, Mosul University. 139p.

Ring, U. (2014). Metamorphic Core Complexes, Encyclopedia of Marine Geosciences Springer Science DOI 10.1007/978-94-

007-6644-0_104-4.

Ruttner, A., and Stocklin, J. (1968). Generalized tectonic map of Iran, ca. 1:10 000 000: IN: Stocklin, J. Structural history and tectonics of Iran: A review. American Association of Petroleum Geologists Bulletin 52 (7): 1229-1258.

Schmincke, H.U., and Von Rad U. (1979). Neogene evolution of Canary Island volcanism inferred from ash layers and volcaniclastic sandstones of DSDP site 397 (LEG47A), Initial report of the Deep Sea Drilling Project, volume XLVII part 1, Washington.

Sharp, T.R., and Robertson, A.H.F. (2002). Petrography and provenance of volcaniclastic sands and sandstones recovered from the Woodlark rift basin and Trobriand forearc basin, Leg 180. In Huchon, P., Taylor, B., and Klaus, A. (Eds.). Proc. ODP, Sci. Results 180, 1–58.

Spotl, C., Longstaffe, F.J., Ramseyer, K., Dinger, B. (1999). Authigenic albite in carbonate rocks - a tracer for deep-burial brine migration? Sedimentology (1999) 46: 649-666.

Vanderhaeghe, O., Teyssier, C., Wysoczanski, R. (1999). Structural and geochronological constraints on the role of partial melting during the formation of the Shuswap metamorphic core complex at the latitude of the Thor–Odin dome, British, Columbia, Can. J. Earth Sci. 36: 917–943.

Wager, L.R., Brown, G.M., Wadsworth, W.J., (1960). Types of Igneous Cumulates, Journal of Petrology 1(1): 73-85.

Yu, S., Li, S., Zhang, J., Sun, D., Peng, Y., Li, Y. (2019). Linking high-pressure mafic granulite, TTG-like (tonalitic-trondhjemitic) leucosome and pluton, and crustal growth during continental collision, GSA Bulletin 131 (3-4): 572–586.

JJEES

JJEES (2020) 11 (2): 126-145
ISSN 1995-6681

Jordan Journal of Earth and Environmental Sciences

Paleocene-Eocene Thermal Maximum Record of Northern Iraq: Multidisciplinary Indicators and an Environmental Scenario

Ahmed N. Al-Fattah[1], Ali I. Al-Juboury[1], Imad M. Ghafor[2]

[1]Geology Department, Mosul University, Mosul, Iraq
[2]Geology Department, Sulaimaniya University, Iraq

Received 20 October, 2019; Accepted 1 March 2020

Abstract

In order to trace the environmental response of the PETM record in northern Iraq, three outcropping sections are selected at Sinjar, Dohuk, and Shaqlawa areas which included the Aaliji and Kolosh Formations. Lithologically, the fresh lithological color change was a distinctive field feature of PETM lithosomes. Biostratigraphically, the Paleocene/Eocene boundary is assigned by foraminfera in the prepared study at the same locations. Sedimentologically, PETM evidences are extrapolated through petrography (high micritic matrix ratio, magnetosomes, appearance of green algae (Dasycladacean) and early dolomitization). Facies analysis results are supported by the minor sea level rise (third or fourth order cycle) at the earliest Eocene as a one of the PETM indications. Clay mineral assemblage variations of formations referred obviously to warm, arid-seasonal climate conditions, which are consistent with the climatic trend of the southeastern Tethys region.

Geochemically and by using various methods, evidences of stable isotopes values in both formations give important hints for PETM. X-ray fluorescence analyses as geochemical indices fixed and confirmed the PETM environmental conditions, particularly anoxic or euxinic state and the rate of siliciclastic influx or the terrestrial input. Total organic carbon (TOC) and calcium carbonate weight percent variations present other signs regarding productivity nature, organic carbon preservation, and lysocline response during the PETM.

Multi-geoindicators and the integrated relationship among them suggested that the northern Iraq region was affected by the PETM climatic environmental perturbation in the marine realm within an epicontinental foreland basin.

Keywords: PETM, Paleocene, Eocene, Multidisciplinary study, Iraq

1. Introduction

The Paleocene-Eocene Thermal Maximum (PETM) represents a major climatic excursion of global nature that took place about 55.9 Ma. Global temperatures increased by ~ 6°C during a few thousand years, and the PETM is estimated to be approximately (~170) k.y. in duration (Zachos et al.,1993; Röhl et al., 2007; Harding et al., 2011; Zeebe and Lourens, 2019). The (PETM) was a geologically brief, rapid, abrupt, intemperate episode of global warming representing a significant impact on both marine and terrestrial ecosystem and is marked by a global temperature rise (5-8 °C) associated with a prominent negative carbon isotope excursion (CIE) ($\delta^{13}C$) (Sluijs et al., 2007).

There were multiple events within the late Paleocene and early Eocene, which imply a unique and non-singular trigger causing or leading to the release of huge and catastrophic or chronic fluxes of amounts of isotopically light CO_2 and/or CH_4 into the exogenic (ocean-atmosphere) that generated perturbations in the carbon cycle (Sluijs et al., 2007; Zhang et al., 2019; Elling et al., 2019). There are many causes suggested for the PETM such as the release of marine gas hydrates, Igneous Province activity, Permafrost thawing, Bolide impact (Dickens et al., 1995; Kent et al. , 2003; Svensen et al., 2004; DeConto et al., 2012; Zeebe, 2013; Schaller et al., 2016; Jones et al., 2019). Although such causes of the PETM remain controversial (Hupp et al., 2019), Methane release from clathrates is currently the most agreed upon cause which explains the PETM event (Khozyem et al., 2014; Hupp et al., 2019).

Bowen et al. (2006) maintained that rapid and extreme changes in the earth system may be triggered by natural carbon cycle perturbation even at times of globally-warm climates and in an ice-free world, and the PETM phenomena was the obvious indicator of that perturbation. They mentioned that an array of changes in the atmosphere, geosphere, hydrosphere, and biosphere have been documented during the PETM.

To bridge a gap in information related to the Paleocene Eocene thermal maximum succession locally and regionally, the current work presents a comprehensive study of the PETM event in Iraq through dealing with various geo-indicators and submitting a conceptual environmental model of climatic evolution of this warming event in Iraq.

In order to trace the geological responses in detail of the Iraqi geological record, three outcrop sections are selected carefully to represent the northern part of Iraq in Sinjar, Dohuk, and Shaqlawa areas, which contain the Aaliji and Kolosh formations (Figure 1). During the Paleocene and Eocene epochs these areas were located as a part of Tethys marine environments realm between paleolatitude (25-30°) N, (Scheibner and Speijer, 2008).

The samples were analyzed by adopting a multidisciplinary approach as the recent mode in paleoclimatic recognition.

* Corresponding author e-mail: alialjubory@yahoo.com

This included traditional petrography and scanning electron microscopy (SEM), major and trace elements by X-ray fluorescence (XRF) geochemistry, accompanied by stable isotopic geochemistry and clay mineralogy using X-ray diffraction (XRD). The multidisciplinary approaches of sedimentology, chemostratigraphy and clay mineralogy show the realm of climatic and paleoenvironmental evolution during the PETM from northern Iraq.

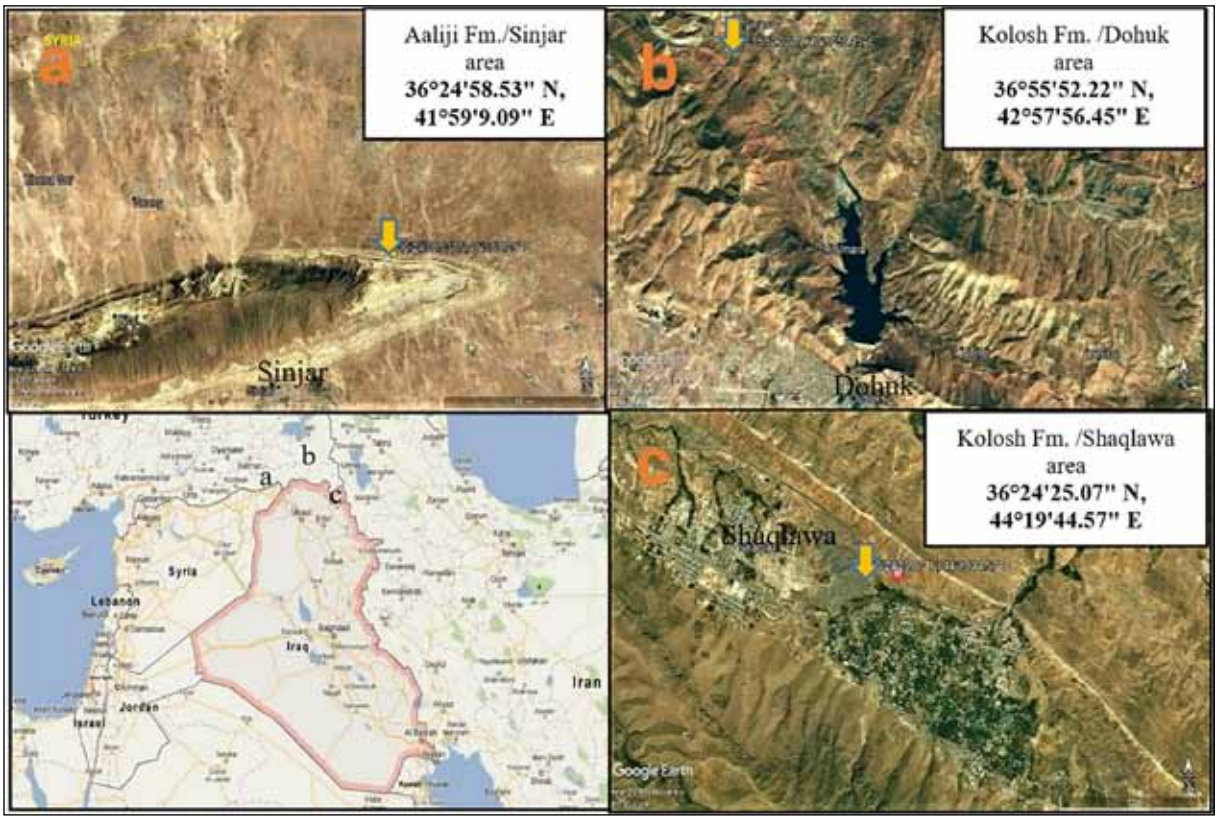

Figure 1. Location map of the studied areas.

2. Geological Setting

The middle Paleocene- Eocene megasequence (AP10) was deposited during a period of renewed subduction and volcanic activity associated with the final closure of the NeoTethys. The products of this subduction in Iraq are volcanics of the Walash Group (island arc setting) and the clastic-dominated Naopurdan Group (forearc setting) (Jassim and Buday, 2006).

During the Paleocene-Eocene period, Iraq was located between paleolatitudes 10-25° N (Sharland et al., 2001). These sediments were deposited in a NW-SE trending basin (70 km wide) in NE Iraq. This narrow basin extends longitudinally to Syria and Turkey, and SE Iran (Aqrawi et al., 2010). In the basin center and toward the Mesopotamian and Foothill Zones (Aaliji Formation) they were deposited in an offshore open marine or outer shelf basinal environments.

The Kolosh Formation, on the other hand, was deposited within narrow rapidly subsiding trough in marginal marine environments bordered to the NW-SE ridge by shallow water reef and lagoonal environments represented by Sinjar and Khurmala Formations in northern Iraq (Jassim and Buday, 2006).

The history of the early Paleogene continental shelf of most of Arabia is the reverse of much of the Mesozoic, with its extensive shallow-water (subtidal-supratidal) inner shelf carbonates (Umm Er Radhuma Formation), giving way to evaporites of lagoonal sabkha environments on a stable shelf (Rus Formation).The evaporates were replaced by carbonate-shelf conditions at about the turn of the lower to middle Eocene, when the beds of the (Dammam Formation) were deposited (Al-Sharhan and Nairn, 2003); Figure (2).

3. Materials and Methods

Field work and sampling have been achieved accurately in the outcrops; samples were measured and described lithologically. They were taken at least within 0.5 m intervals depending on bed thickness and lithological variations. Generally, the expected Paleocene- Eocene transition area of Aaliji and Kolosh Formations is distinguished in the field by thin and frequent limestone beds (5-25 cm) and/or black-gray high organic silty or marly shale beds, as well as yellowish, brownish, or a lighter rock color estimated in the early Eocene rocks.

3.1 Paleontological proxies

Analysis of foraminifera has been carried out firstly on three-five test samples located on a long interval space within the Paleocene/Eocene expected position for each section. The results enabled the resaerchers to constrain the upper Paleocene/lower Eocene spanning samples approximately. These samples exist between A15-A35 in Sinjar section (Aaliji Formation), D20-D35 in Dohuk section and Q15-Q35 in Shaqlawa section (Kolosh Formation), see Figures (3 A - C). Foraminifera were extracted from most of the indurated marl and limestone using the washing method (Brasier, 1980; Lirer, 2000).

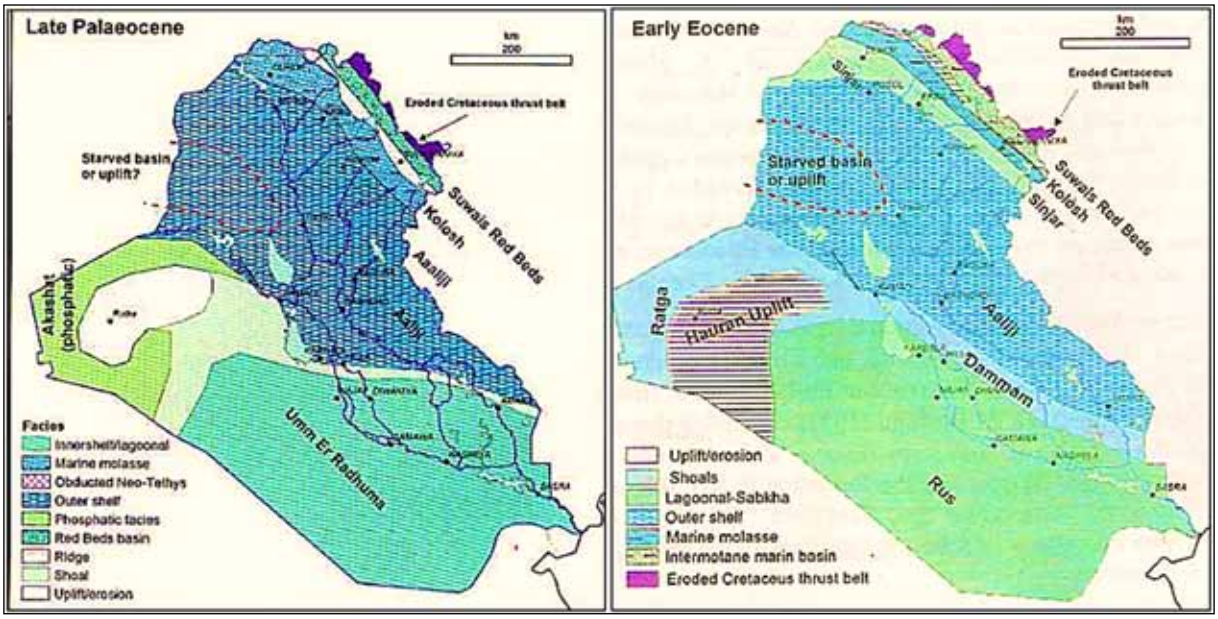

Figure 2. Late Paleocene –Early Eocene paleogeography and facies distribution of Iraq from Jassim and Buday (2006).

3.2 Mineralogical Proxies

Sixty thin sections were studied petrographically by the Vickers polarized microscope at the Earth Science Department, Royal Holloway, University of London.

SEM for identification and description of the clay mineral phases were carried out with magnifications between 100X and 16000X with gold-coated samples. Analysis was carried out at the scanning microscope unit of Royal Holloway, University of London using the Hitachi S-3000N scanning electron microscope.

A representative portion of each sample was manually ground to a fine powder using a ceramic mortar and pestle. The powder was packed into a recessed plastic holder and preferred orientation was minimized. The samples were analyzed using a Philips X-ray diffractometer (PW3710) scanning from 4º to 40º 2θ. Peak identification was enabled using PDF/ICCD database and quantification was done through Rietveld analysis using commercial software program Siroquant (Sietronics, Australia). Analysis was done at laboratories of the Department of Earth Sciences, Royal Holloway, University of London.

3.3 Geochemical proxies

X-ray fluorescence analysis of the major and trace-element geochemistry of the selected samples was performed (using AXIOS spectrophotometer made by PANalytical) at the laboratories of the Department of Earth Sciences, Royal Holloway, London University. Sample preparation includes two steps; fused glass disc and pressed pellets preparations. Pellets are then dried in an oven overnight at 80˚C before being analyzed.

For carbon and oxygen isotope measurements of bulk carbonate samples, ~300 to 1000 µg of the powdered samples (obtained by drilling fresh rock surfaces or of the samples crushed with a pestle and mortar) were first roasted in a vacuum oven for one hour at 200˚C to drive off residual water and volatiles. For carbon- and oxygen-isotope measurements of foraminifera, ~100 to 300 µg of foraminifera were picked and cleaned with methanol before being oven dried at 70˚C. Foram tests were then crushed using a glass rod. All samples were analyzed by continuous-flow mass spectrometry using a Gas bench connected to a Thermo-Finnegan Delta +XP mass spectrometer. All isotope data were measured in the Bloomsbury Environmental Isotope Facility (BEIF) at the University College London and were reported in ‰ deviation from Vienna Peedee belemnite (PDB). One standard deviation error on internal standards was better than ±0.1‰ for both $\delta^{13}C$ and $\delta^{18}O$ during the analysis of the samples.

Bulk rock samples were analyzed for their Total Organic Carbon (TOC) and $CaCO_3$ contents. Samples for (TOC) analyses were crushed to a fine powder, then weighed (~60 to 100 mg) and decarbonated with ~10% HCl in silver foil cups. Once decarbonation was complete, the samples were left to dry. The samples were weighed (~10 to 30 mg) in tin cups for Total Carbon (TC) analysis. All samples were analyzed by combustion in a Thermo Finnegan Flash Elemental Analyzer (EA). Reproducibility of an internal standard was better than 0.1 wt. %. $CaCO_3$% was calculated by subtracting TOC from TC, multiplying it by 8.33333 (recurring). All analyses were achieved at the University College London (UCL), UK.

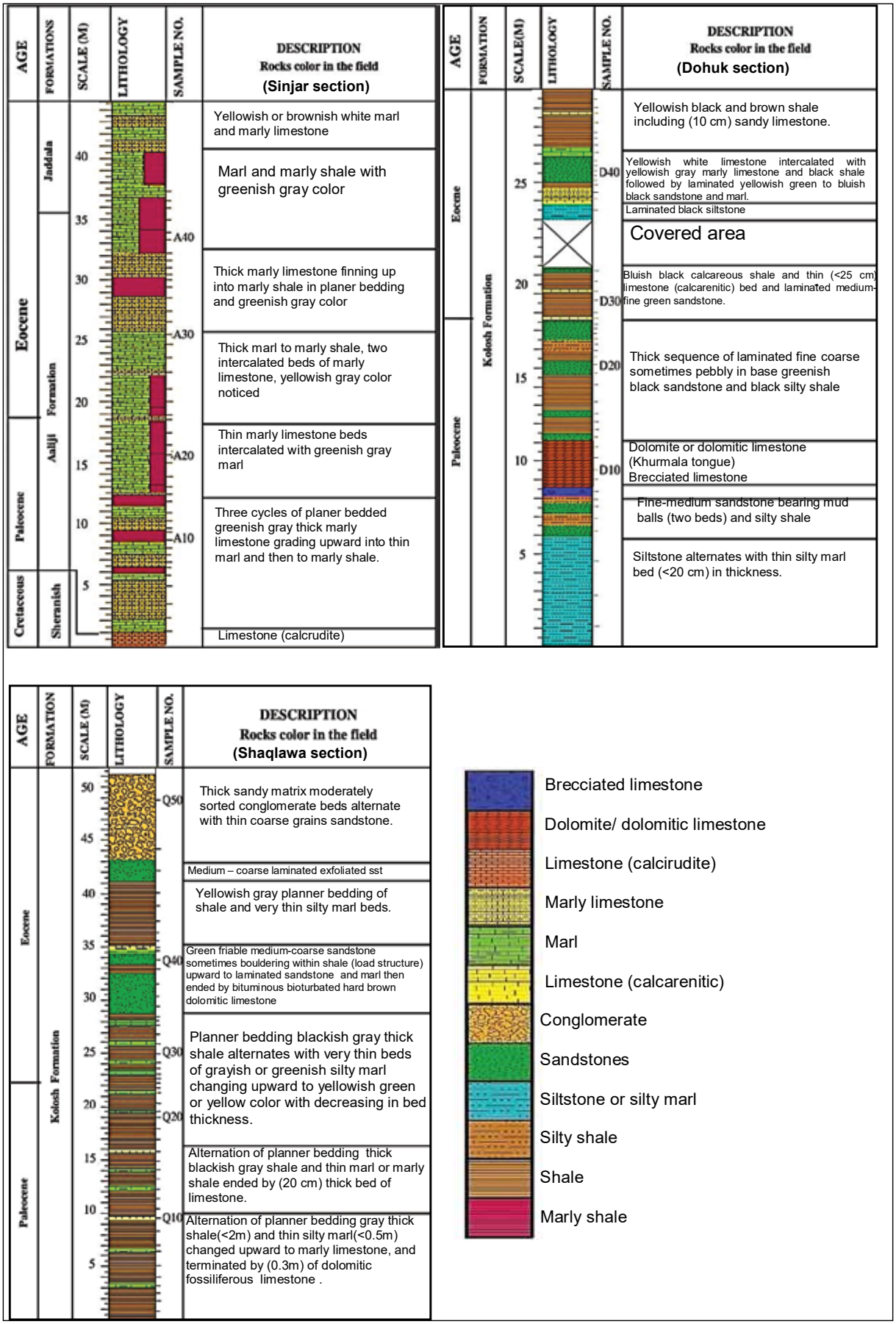

Figure 3. Lithostratigraphy and age assignment of Aaliji Formation and Kolosh Formation at Dohuk and Shaqlawa area.

4. Results

4.1 Lithostratigraphy

The expected Paleocene-Eocene transition area of the Aaliji and Kolosh formations is distinguished in the field by thin and frequent limestone beds (5-25 cm) and/or black-gray high organic silty or marly shale beds, as well as yellowish, brownish, or lighter rock color estimated in the early Eocene rocks.

In the Aaliji Formation, the studied succession is composed mostly of marly limestone, marlstone, and calcareous shale. The Paleocene interval is mostly made up of thinning upward marly limestone beds associated with thickening upward marlstone and calcareous/marly shale. At the upper Paleocene-lower Eocene lithesome, the intercalation of the thin-bedded calciturbidites the marly limestone (4-10 cm thickness) beds become more frequent, interestingly accompanied by color change from greenish-gray dominated facies to yellowish and /or brownish-gray dominated facies, Plate (1 A and B).

The Kolosh Formation (Dohuk and Shaqlawa sections) exhibit other field physical properties, which are considered as a clue to PETM lithosome. In the Dohuk section, an abrupt transition from clastic turbidite Bouma sequence mode deposits to calcarenitic tempestite sequence mode deposits (eventstone) attracts the attention. Also, there is an abnormal event particularly when the main sequence color changes from green to a yellowish white color in addition to the presence of shells (tempestite beds), Plate (1 C).

On the other side, yellowish marl and reddish brown bands as well as high organic- matter-rich black shales charecterize the PETM lithesome at Shaqlawa section (deep marine Kolosh facies), Plate (1 D).

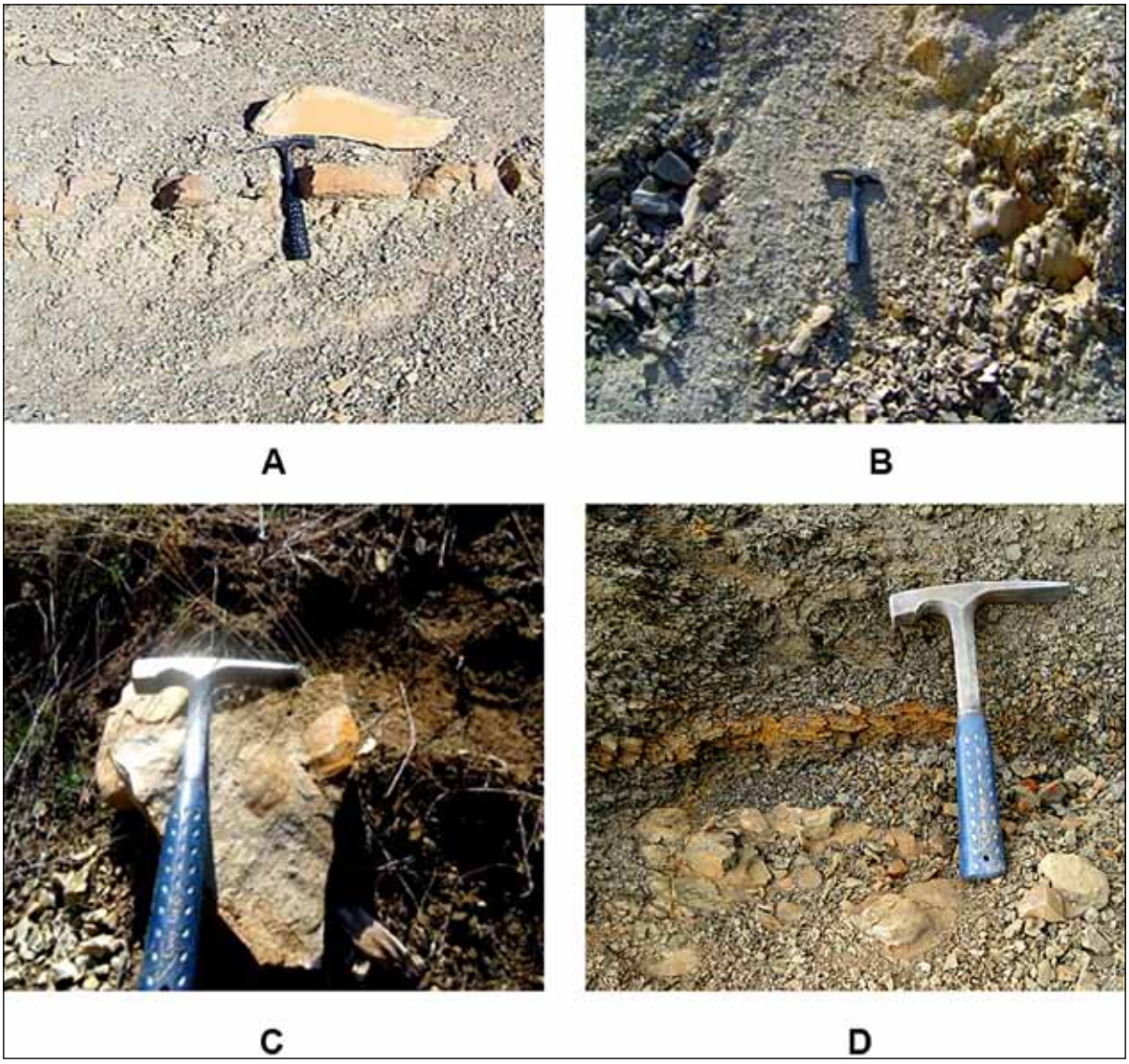

Plate 1. A. Calciturbidite thin beds of marly limestone, **B.** color defference at Paleocene-Eocene transition facies of Aaliji Formation at sinjar anticline. **C.** yellowish white calcarenitic limestone (Tempestite) in Dohuk section. **D.** yellowish marl and reddish brown band in the black shale of Shaqlawa section.

4.2 Biostratigraphy

Adopting Berggren and Pearson (2005), the Paleocene-Eocene biostratigraphic boundary of Aaliji Formation delimited at Last Appearance Datum (LAD) of Morozovella velascoensis (sample A23) and First Appearance Datum (FAD) of Acarinina sibaiyaensis (sample A24) Figure (3 A), (AL Fattah et al., in press).

In the Kolosh formation at Dohuk and Shaqlawa, the last recorded occurrence of Angulogavelinella avnimelechi in sample (D28) and sample (Q24) respectively close the uppermost Paleocene time, in turn the early Eocene time is characterized by deep-water agglutinated foraminifera (DWAF) assemblages that are recorded in samples (D31, Q25) Figure (3 B,C) (AL Fattah et al., in press).

Planktonic foraminifer's assemblages respond to PETM environmental conditions represented by species reorganization (decline, abundance) and morphological optimal adaptation (shape, size). While the benthic foraminifera respond was represented by the benthic extinction event (BFEE) (in deep locations) with a general decrease in the generic diversity of photoautotrophic (oligotrophic conditions) larger foraminifera followed by abundance stage (in shallow locations) (AL Fattah et al., in press).

4.3 Chemostratigraphy

Isotope composition ($\delta^{13}C$ and $\delta^{18}O$)

Carbon stable isotope values of bulk rock samples range from (- 1.09 ‰ to 0.65 ‰) in the Aaliji Formation with an average of (0.03 ‰) and a negative magnitude of the highest peak (about - 1.1 ‰) Figure (4 A). In turn, they range between (-6.99 ‰ to 0.64 ‰) with an average of (-2.24 ‰) and a negative magnitude of (-1‰ around Paleocene-Eocene boundary) in the Kolosh Formation (Dohuk section) Figure (4 B), and between (-37.01 ‰ to -1.81 ‰) with an average of (-10.13 ‰) and a negative magnitude of (-13‰ around Paleocene-Eocene boundary) in the Kolosh Formation (Shaqlawa section), Figure (4 C).

Although these results seem to be affected by diagenesis, particularly in the Kolosh Formation, distinctive hints observed for a negative excursion (CIE) in both Formations coincided with the early Eocene. These hints are main peaks, a negative trend line of values, abrupt shifting and magnitude of highest peak occur within the accepted (CIE) range of marine environments Figures (4 A - C).

The peak amplification may be a result of the reworking of depleted siliciclastics (Höntzsch et al., 2011) (Duhok) or the original signal of carbon isotope overprinted and accentuated by the early diagenetic dolomitization due to the bacterial sulfate reduction and/or more likely by the high organic-matter content (Bolle et al., 2000; Mazzullo, 2000) as (Shaqlawa) section.

The early Eocene peak magnitude values approximation between Kolosh (Dohuk) and Aaliji Formations confirmed confidently that those values are likely true especially at the Aaliji Formation because it is comprised of limestones and marls that have been indurated or compacted during the early diagenesis, and have a high ratio of calcite/organic matter; thereby they may represent closed systems with respect to carbon isotopes (retaining original signals) according to Schmitz et al. (1997).

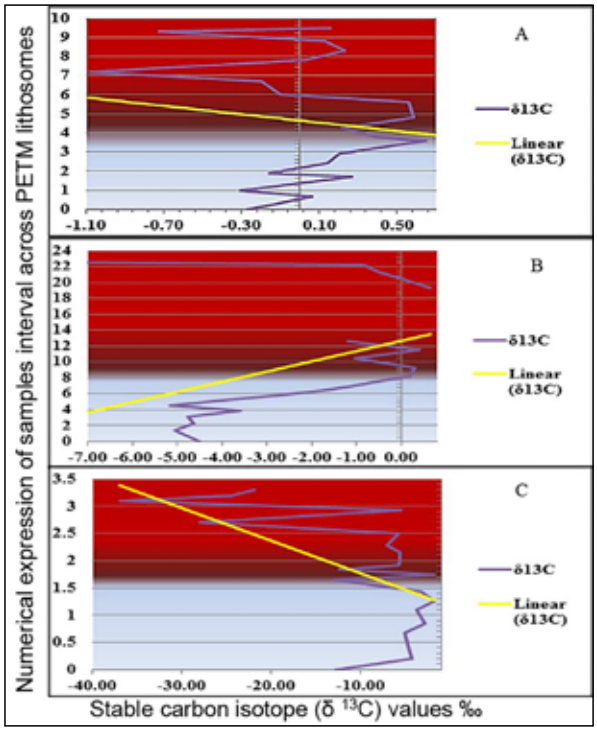

Figure 4. TStable carbon isotope ($\delta^{13}C$) behavior taken from bulk samples across PETM lithosomes of the studied sections, **A.** Aaliji Formation at Singar section **B.** Kolosh Formation at Dohuk section, **C.** Kolosh Formation at Shaqlawa section, the contact between two colors corresponds to the Paleocene / Eocene contact.

Isotopic analysis of $\delta^{13}C$ for the Aaliji Formation mixed planktonic foraminifera ranged between (0.8 ‰ and 1.4 ‰) and they are represented by two peaks after the Paleocene/ Eocene contact with a peak magnitude of less than (< 0.5 ‰). These positive values can be interpreted as a result of the recrystallization diagenetic process (dissolution and reprecipitation of calcite) on the foraminiferal tests, where the recrystallization causes "smoothing" of the original or bulk samples isotope signals (Veizer, 2009). However, the early Eocene shifts are observed inspite of a lesser magnitude, Figure (5 A).

Oxygen ($\delta^{18}O$) stable isotope is considered as a function to precipitation and temperature as well as salinity variations (Uchikawa and Zeebe, 2010). Foraminferal (mixed species) isotope analysis of $\delta^{18}O$ results for the Aaliji Formation showed values ranging between (-4.3 ‰ and -5.6 ‰) along with two peaks: a low magnitude peak at the Paleocene/ Eocene boundary and a high magnitude peak at early Eocene as well as a negative trend line and a peak magnitude of less than (<1 ‰), Figure (5 B). Bulk sample $\delta^{18}O$ values at the Aaliji Formation fluctuated between (-4.52‰ and -3.36‰) with an average of (-3.75‰). More than one negative peak was observed after the Paleocene/ Eocene boundary (within the early Eocene) with a peak magnitude of (<1‰), Figure (6 A). On the other hand, $\delta^{18}O$ values at the Kolosh Formation in Dohuk section fluctuated between (-5.19‰ and 0.19‰) with an average of (-3.58‰). After the Paleocene Eocene boundary, the samples start to tend towards negative values until they cease in the covered area which is expected to have values that are more negative (a high magnitude peak) Figure (6 B). In the Kolosh Formation and at the Shaqlawa section, $\delta^{18}O$ values fluctuated between (-7.31‰ and -3.79‰) with an

average of (-5.54‰), high magnitude negative peaks were observed around the Paleocene/ Eocene boundary especially in the early Eocene, Figure (6 C).

Despite the role of diagenesis affecting the original $\delta^{18}O$ signal, observed distinctive hints support the partial preservation of the original $\delta^{18}O$ signal suggestion in both of the Aaliji and Kolosh formations. Thus, the general trend of the original $\delta^{18}O$ signal remains preserved particularly in the Aaliji Formation, whereas in the Kolosh Formation, it is expected to be vulnerable to post depositional processes due to a relatively shallow marine environment Figure (5, B) and (6). Briefly, the original $\delta^{18}O$ signal in the Aaliji Formation may be less modified by diagenesis and more preserve than in the Kolosh Formation.

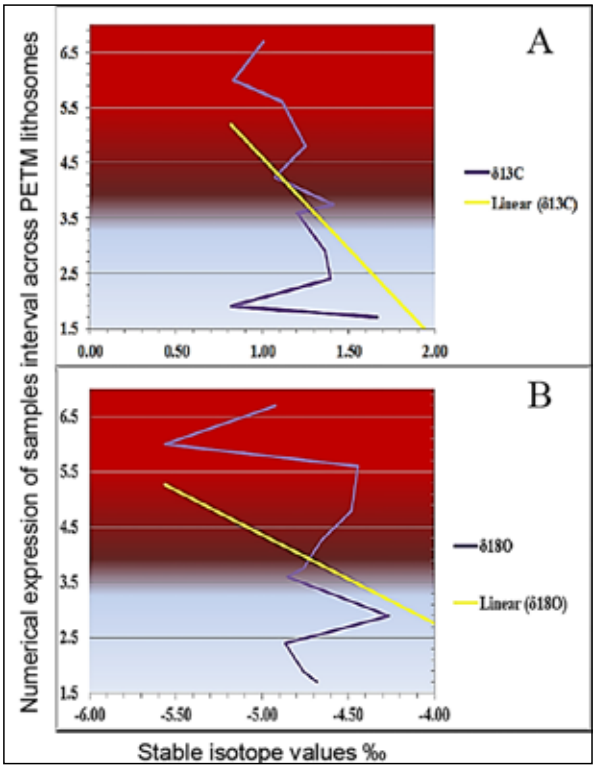

Figure 5. Planktonic foraminifera (mixed species) stable isotope behavior taken across PETM lithosome of Aaliji Formation. **A.** ($\delta^{13}C$) and **B.** ($\delta^{18}O$), the contact between two colors correspond to the Paleocene / Eocene contact.

5. ???????

5.1 Major and Trace-Element Analysis

It is clear that the elemental geochemistry of the PETM Lithosomes at the Aaliji and Kolosh (Shaqlawa section) formations is partly controlled by a bulk mineralogical composition. The dominated clay mineral amount and TOC concentration in the deposits (discussed later) appear to be largely the two major controls on the absolute abundance of many of the elements (Soliman et al., 2011).

In the Aaliji Formation, with the exception of CaO, MnO, P_2O_5, Na_2O, and SO_3, the other major elements oxides increased in the early Eocene and are represented in two phases separated by anomalous values in sample (A27) which is composed of marly limestone. The increased phases coincided with marly shale lithologies as shown in Figure (7). These major element features suggested a slight increase in contribution from detrital materials.

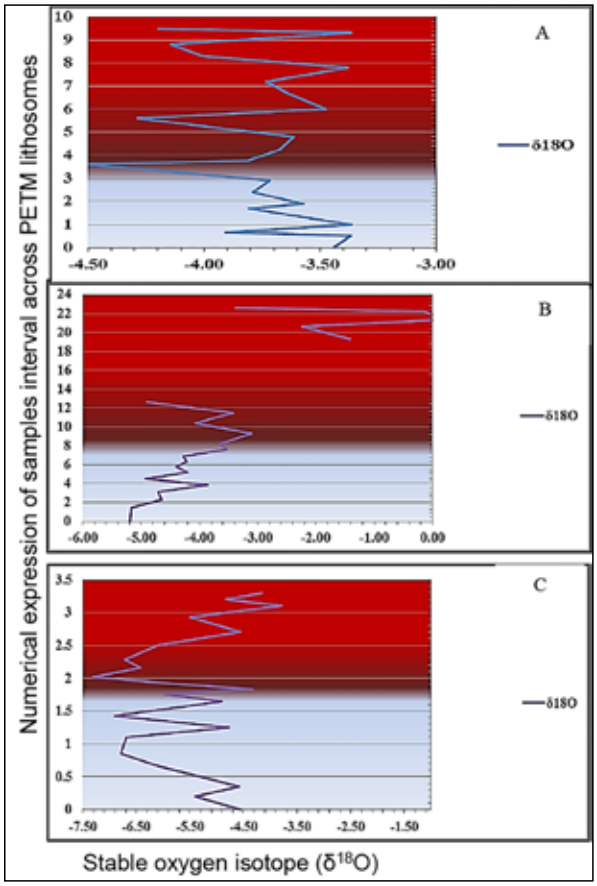

Figure 6. Stable oxygen isotope ($\delta^{18}O$) behavior taken from bulk samples across PETM lithosomes of studied sections. **A.** Aaliji Formation. **B.** Kolosh Formation at Dohuk section. **C.** Kolosh Formation at Shaqlawa section, the contact between two colors correspond to Paleocene / Eocene contact.

The following geochemical indices (Mo/U, Mo/Cr, V/Al, V/Cr, Ni/Co, U/Th, V/V+Ni, Fe/Ti, U/Al, Mo/Al, Si/Al, K/Al, Zr/Al, Rb/Al) are increased, while other indices as (Ti/Al, Mn/Al, Ba/Al, Ni/Al, Mg/Al, Fe/Al) are decreased Figure (8).

These results are interpreted as follows: the variations in paleoredox sensitive indicator ratios increase in (Mo/U, Mo/Cr, V/Al, V/Cr, Ni/Co, U/Th, V/V+Ni, Fe/Ti, U/Al and Mo/Al) and decrease in Mn/Al indicate deposition under anoxic or euxinia conditions (Giusberti et al., 2007; Sluijs et al., 2008 ; Giusberti et al., 2009; Alegret et al., 2010; Schulte et al., 2011a; Dickson et al., 2012; Liu et al., 2012). Similarly, the increase in terrestrial input indicators including (Si/Al, K/Al, Zr/Al, Rb/Al) are recorded. The Si/Al peak is rather related to the high abundance of quartz concurrent with a low level of phyllosilicate abundance reflecting a decrease in the flux of Al (relative to Si); the increased Si/Al ratio is best explained by a relative increase of fine-grained silt-sized quartz. Such a marked increase in the Si/Al ratio and quartz content can reflect significant arid climatic conditions (Schulte et al., 2011a). The overall inverse relationship of K/Al with $CaCO_3$ is a strong evidence of its detrital source and corresponds well with the relatively higher input of illite (K-rich) by fluvial or aeolian transport (Thomas and Bralower, 2005). The zirconium- and titanium-bearing heavy minerals (e.g., rutile, ilmenite, sphene, and zircon) are generally enriched in sandsilt-sized siliciclastic detritus and Al is generally enriched in the clay-size fraction (Fralick and

Kronberg, 1997 and Dypvik and Harris, 2001 in Schulte et al., 2011a). Thus, it is obvious that the high Zr/Al, and Rb/Al ratios as well as the K/Al, ratio document a brief influx of more detrital sediments and suggest that the provenance area was tapped during the rapid sea-level rise (Schulte et al., 2011a; Ver Straeten et al., 2011). Because of the strong resistance of Ti and Al to diagenetic alteration, the Ti/Al ratio has been used as a useful proxy for the occurrence of extraneous material in sedimentary sequences (Lipinski et al., 2003; Schmitz et al., 2004 in Soliman et al., 2011). Likely, this explains the decrease in Ti/Al ratio in the Aaliji Formation. This is attributed to a relative rarity or absence of extraneous material (basinal environments). Low Ti/Al values may coincide with sapropel beds and reflect reduction in the aeolian dust supply (Ver Straeten et al., 2011; Liu et al., 2012). A sharp decline in the Ba/Al ratio that is used as a proxy for biological productivity suggests sharp transition from a eutrophic to an oligotrophic or mesotrophic condition at the early Eocene that is concomitant with the foramineferal evidence. Fe/Al and Ni/Al ratios showed that the strength of sulphate-reducing (i.e. sulphidic) conditions was relatively small (Liu et al., 2012). Finally, the slight decrease in the Mg/Al ratio and its subsequent increase is attributable to the brief dissolution period of the syndepositional dolomite because of CCD shallowing.

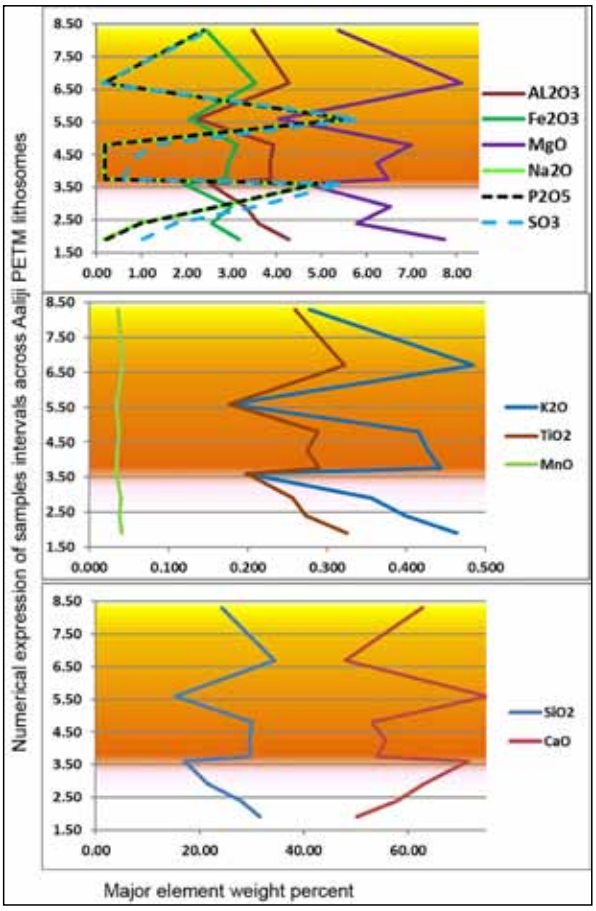

Figure 7. Major elements' behavior across the Aaliji Formation PETM lithosome,the contact between two colors correspond to the Paleocene / Eocene contact.

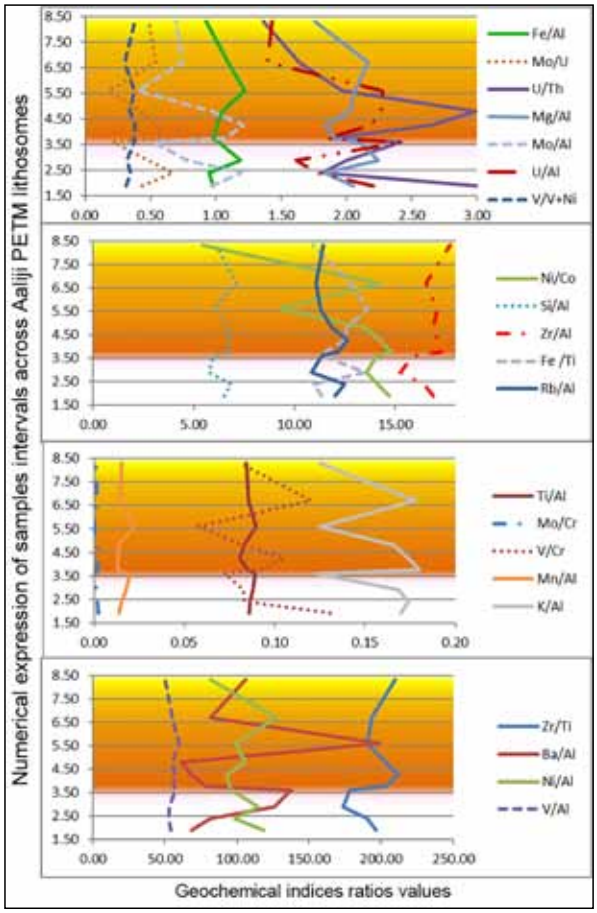

Figure 8. Geochemical indices ratios variations across Aaliji formation PETM lithesome, the contact between two colors correspond to Paleocene / Eocene contact.

In the Kolosh Formation (Shaqlawa), although oscillations in major elements and oxide values are attributed to the alternation of silty marl beds with shale, there are relative increasing trends in all oxides with the exception of CaO and MnO around and after the Paleocene/Eocene boundary Figure (9). This increase is interpretable in shale as a contribution of detrital clay minerals, whereas it may reflect the occurrence of a high silt ratio in silty marl beds after the Paleocen /Eocene boundary.

The geochemical elemental ratios such as (V/Al, Ni/Co, Fe/Ti, Zr/Ti, Mg/Al, Si/Al, Zr/Al, Mn/Al, and Ni/Al), CaO and MnO oxides were low, whereas (Ti/Al, Ba/Al, Fe/Al, K/Al, Mo/Al, U/Al, Mo/U, Mo/Cr, V/Cr, U/Th, V/V+Ni and Rb/Al) ratios were high, Figure (10).

The increase in paleoredox sensitive indicator ratios (Mo/U, Mo/Cr, V/Cr, U/Th, V/V+Ni, U/Al and Mo/Al) as well as the decrease in Mn/Al may be referred to depleted-oxygen (dysoxia or anoxia) environmental conditions. Other paleoredox sensitive indicator ratios that are decreased abnormally (V/Al, Ni/Co, and Fe/Ti) are attributed to the ventilation style which is lower than that in the Aaliji section as evidenced by the low V/Al ratio. In addition, the decrease in Ni/Co ratio is negligible since its value is still above seven (Alegret et al., 2010), whereas a slight decrease in Fe/Ti may interpreted by the high siliciclastic flux at

the Kolosh Formation compared with the Aaliji Formation which is consistent with absence of iron scavenging period from a euxinic water column to form syngenetic pyrite (Schulte et al., 2011a). The terrestrial input indicators (Si/Al, K/Al, Zr/Al, Rb/Al) exhibit an increase in K/Al, Rb/Al and a decrease in Si/Al and Zr/Al ratios. The increased values are interpreted as a reflection of more detrital influx of sediments and mineral phases (largely illite) and during sea level rise conditions (Schulte et al., 2011a). The Zr/Al ratio decrease may be a function of the diminishing sand-sized fractions in the Kolosh clastic sediments (Ver Straeten et al., 2011). A drop in the Si/Al ratio at the onset of the PETM points can be attributed to either the reduced Si input derived from silicic organisms (e.g., radiolarians) or the lowered input of (aeolian?) quartz (Schulte et al., 2011b). Since Ti/Al ratio is used as a useful proxy for the occurrence of extraneous material in sedimentary sequences, its slight high value indicates the occurrence of more extraneous material, and this coordinated with clastic nature of Kolosh Formation. Increase in the Fe/Al ratio can be referred to the strength of sulphate-reducing conditions or may indicate a more intense weathering (Sluijs et al., 2008; Liu et al., 2012). The Ba/Al ratio showed an increased value suggesting prevailed eutrophic conditions with some fluctuations which might be attributed to mesotrophic conditions.

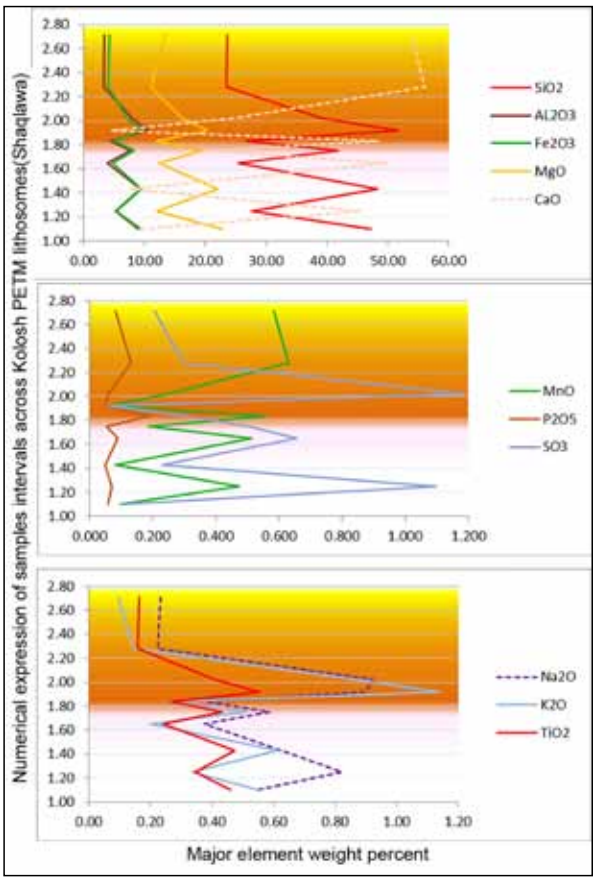

Figure 9. Major elements' behavior across the Kolosh Formation PETM lithesome (Shaqlawa section), the contact between two colors correspond to the Paleocene / Eocene contact.

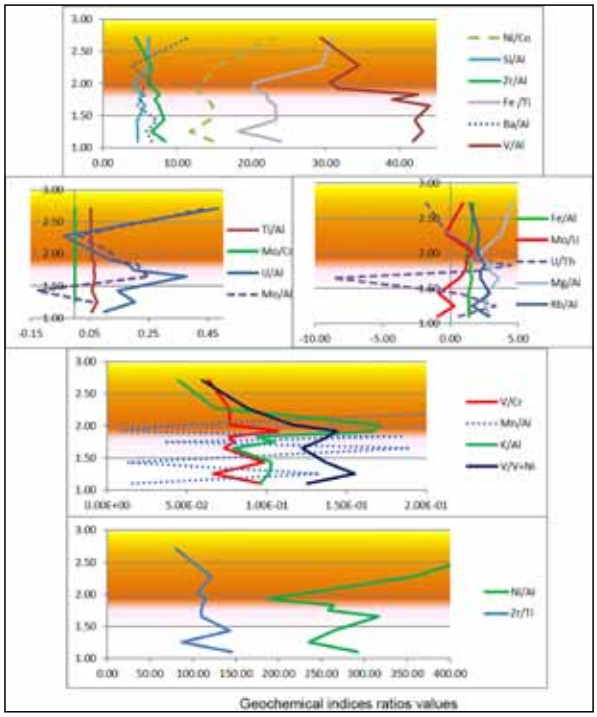

Figure 10. Geochemical indices ratio variations across the Kolosh Formation PETM lithesome (Shaqlawa section), vertical axis represents samples' intervals of PETM lithesome, the contact between two colors correspond to the Paleocene / Eocene contact.

5.2 Total Organic Carbon (TOC)

Total organic carbon ratios of the bulk rock samples range from 0.19 % to 1.14 % with an average of 0.66 at the Aaliji Formation. They range from 0.0496 % to 0.62 % with an average of 0.22 % at the Kolosh Formation (Duhok section), and from 0.058 % to 0.601 % and average of 0.22 % at Kolosh Formation (Shaqlawa) along the PETM lithosomes.

The similarity in average values between the Duhok and Shaqlawa sections supports the idea of a similar source at the Kolosh Formation in these sections. The TOC amounts are high at the early Eocene in all studied sections, and can be related in principle to low sedimentation rates (Aaliji Formation) and/or siliciclastic input materials (terrestrial source of organic matter), and \or elevated organic-matter production. Figure (11).

In general, the change in TOC contents suggests that there was a profound change in the conditions (Meadows, 2008). In many of the continental shelf and epicontinental sections that span the PETM (as the studied sections), total organic carbon (TOC) is high (Cohen et al., 2007).

The increase of organic fluxes to the sea, the increase of primary productivity, and the improved preservation under anoxia conditions (lack of bioturbation) are together probable causes of the TOC enrichment during PETM. (Tremolada and Bralower, 2004; Ernst et al., 2006; Sluijs et al., 2008; Meadows, 2008; Soliman et al., 2011).

Moreover, TOC enrichment in shelf/epicontinental sea settings is considered as an evidence for the transient sea level rise (Arthur and Sageman, 2004). Elements that bond to organic matter or form sulfide compounds are enriched in strata under low dysoxic to anoxic conditions. Briefly, the paleoredox sensitive indicator ratios that suggest deposition under anoxic conditions appear to be linked to the enhanced TOC values and the very finely laminated shales (no

bioturbation) and the transient sea level rise at the PETM lithosomes in the studied sections.

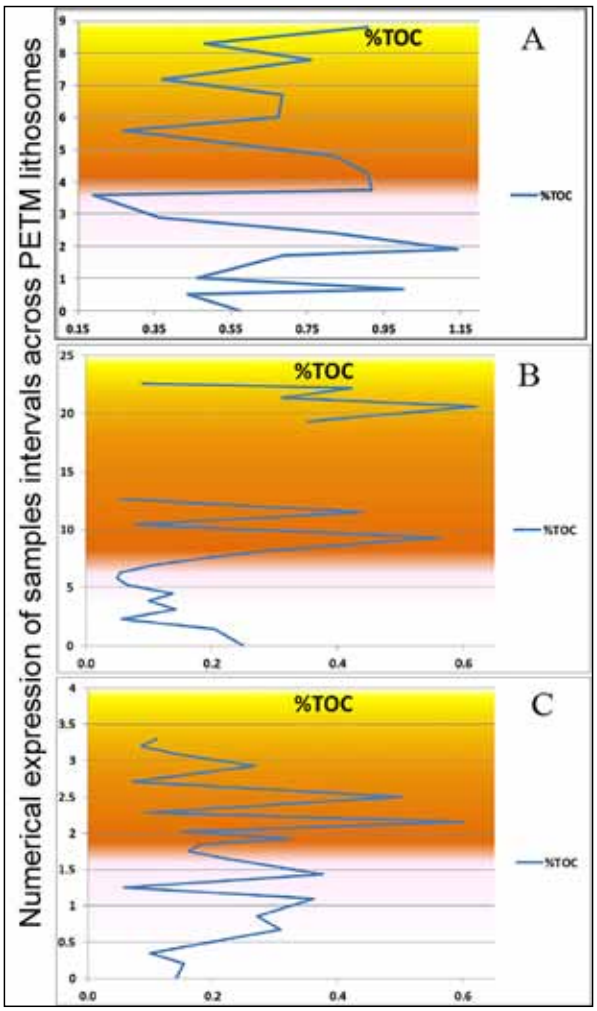

Figure 11. Total organic carbon percentage variations across the PETM lithosomes. **A.** Aaliji Formation. **B.** Kolosh Formation at Dohuk section. **C.** Kolosh Formation at the Shaqlawa section, the contact between two colors correspond to the Paleocene / Eocene contact.

5.3 Calcium Carbonate Ratios

Calcium carbonate ratios fluctuated between 60.74% and 84.31% in an average of 70.04 % at the Aaliji Formation. At Kolosh Formation (Dohuk section), they ranged from, 9.82% to 81.33% with an average of 50.8% and from 5.25% to 67.7% with an average of 37.4% at the Kolosh Formation (Shaqlawa). $CaCO_3$ weight percentage values begin to decline relatively after the base of Eocene at all sections except Dohuk, but they returns to improve upwards Figure (12). This exception may be attributed to the dissolution contrast between deep sea and shelf deposits, where shelf deposits were largely unaffected by dissolution that is originated from the lysocline shallowing during PETM (Zachos et al., 2005; John et al., 2008).

The decrease in $CaCO_3$ accumulation/preservation rates during the PETM was driven primarily by a significant increase in sea floor dissolution, rather than by a major decrease in surface water biological production, or is rather related to siliciclastic dilution (Nicolo et al., 2007; Nguyen et al., 2009). Moreover, the $CaCO_3$-poor sediments are enriched in redox-sensitive trace metals such as Mo, U and V that are indicative of bottom water anoxia, accompanied by increases in TOC and may include surface of maximum flooding (MFS) (Sluijs et al., 2008; Ver Straeten et al., 2011).

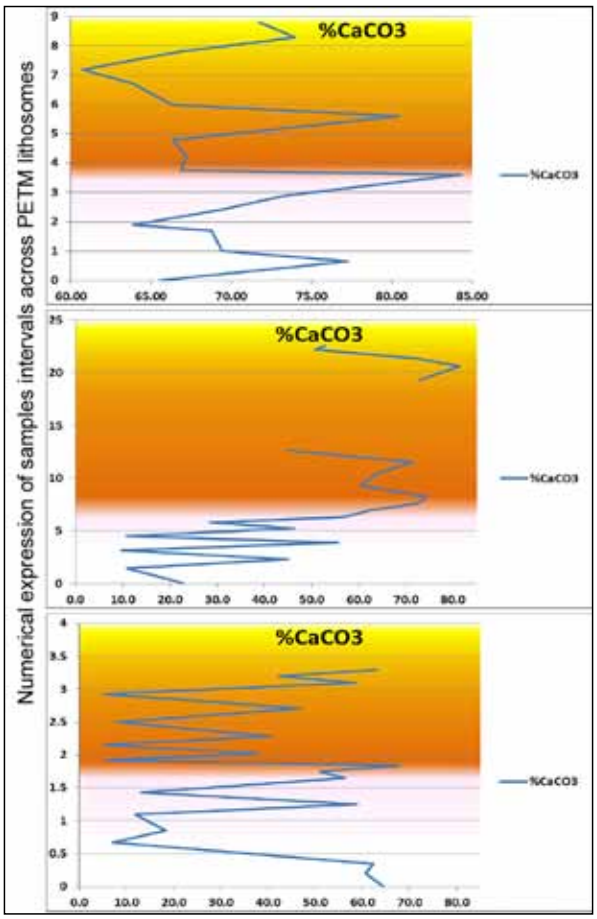

Figure 12. Calcium carbonate ratio variations across the PETM lithosomes. **A.** Aaliji Formation. **B.** Kolosh Formation at Dohuk section. **C.** Kolosh Formation at Shaqlawa section, the contact between two colors correspond to the Paleocene / Eocene contact.

6. Sedimentology

6.1 Petrography and Facies Analysis

PETM facies (facies or lithosome spanning or nearly equivalent to the uppermost Paleocene – mid Early Eocene) are distinguished in all sections by local or perhaps global and minor sea level transgression associated with early Eocene which was confirmed by (Speijer and Wagner, 2002; Baceta et al., 2011; Farouk 2016) and was identified by the change in microfacies' characteristics to the relatively more deep environments compared to the previous facies.

In the Aaliji Formation, the PETM zone revealed a slight increase in: matrix (clays and organic matter), clastic grains, radiolaria ratio (sea level rise), and dissolution porosity as well as paucity in benthic foraminifera especially after (sample A27) (Benthic Foraminifera Extinction Event (BFEE)) compared to pre PETM rocks Plate (2 a - d). Texturally, the facies exhibit dark greenish gray color mudstone and wackestone and sometimes wacke-packstone (sample A27) which may represent the (BFEE bed). Relatively, good sorting and increase in moldic vuggy porosity may be attributed to selective or normal dissolution.

In the Kolosh Formation, at Dohuk area, packages of petrographic features are noticed, where two calcarenite beds (sample D28, D31), perhaps representing (BFEE) and/

or LFT (Larger Foraminifera Turnover)) were deposited with the latest or end of Paleocene to early Eocene (between sample D28 to D32). These beds include bioclast fragments (large miscelanid nummulites, rotalides, less common milliolides, mollusca, bryozoa, bivalves, echinoderm and marine green algae (dasycladacean)), extraclasts, and rare lithoclasts (chert, quartz, feldspar and various rock fragments). The lithoclasts are less common than the bioclasts and all constituents merge in a micritic increasing up matrix, in addition to the magnetite or iron oxides which are arranged horizontally. These features relate to each other in a homogenous micritic matrix and vuggy to channel porosity and may be of a horizontal orientation texture, Plate (3 a, b, c). The Kolosh Formation in Shaqlawa area during the PETM zone has an increased magnetite (perhaps biogenic arranged in lamination or in a series or bullet-shaped), increased micritic or clay matrix (thick shale facies) (samples Q29, Q31), in contrast to other clastic grains, Plate (3 d - f).

Sea level rise hints were recorded and synchronized with the onset PETM stage environmental effects and continued during early Eocene. The rise was minor in the Aaliji Formation, (SMF 3) and continued in general, but the shifting basin ward took place from deep shelf/toe of slope contact environments to deep shelf /basin plain contact environments or (FZ2/FZ1). Because the (SMF3) facies emplaced in both FZ3 and FZ1 facies zones (Flügel, 2004), this small environmental shifting recognized by subfacies change within (SMF3) main facies when the wackstone dominance was replaced upward by a mudstone dominance in addition to the petrographic features mentioned previously.

In the Kolosh Formation at Shaqlawa section, the environmental perturbation was expressed by slowly finning up facies and an increase in calcareous blackish gray shale rather than thin marl. These changes were observed after (sample Q22) and the deepening petrographic features continued upward until the sandstone was revealed. The (SMF 3) with rare and small planktonic forams and more micritic organic matrix appeared in sample (Q29). All these phenomena indicate that environmental deepening or sea level rise was synchronized with PETM stage, thereby a minor shift occurred from (FZ3/FZ4) contact to the deepest end of (FZ 3) or from a slope/toe of the slope environment position (pre PETM) to near toe of slope /deep shelf interrelation environmental position (within outer ramp).

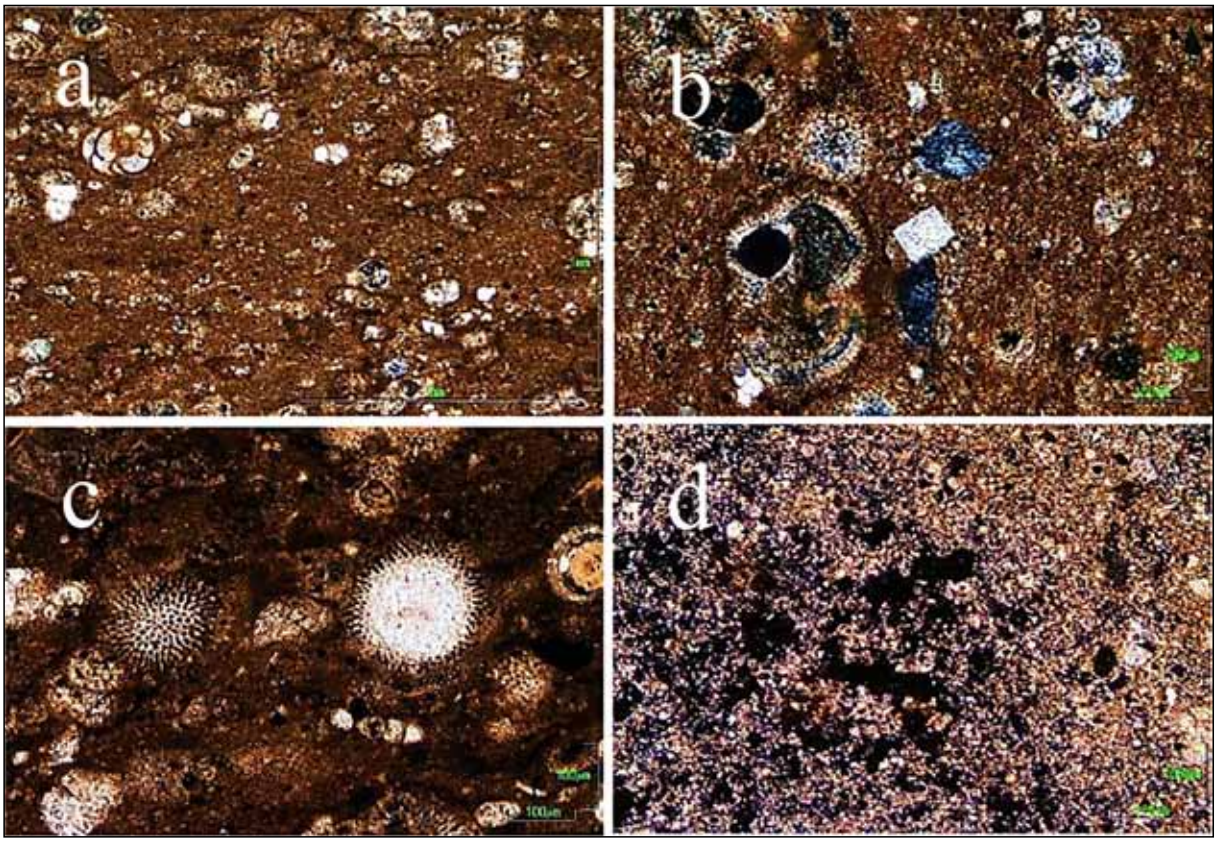

Plate 2. (a). Increasing in micritic or mud matrix (Sample A29). **(b).** Appearing clastic grains of quartz and chert with skeletal components (Sample A27). **(c).** Radiolaria skeletal grains, (Sample A29). **(d).** Spread in vuggy porosity due to dissolution or lysocline shallowing (Sample A24).

In the Kolosh Formation at the Dohuk section, the limited sea level rise make the facies (SMF5) in this stage spending more time within the deep parts of broad zone (FZ4). As sea level begins to rise, storm processes continue to rework and transport a skeletal material basin ward. Depletion of siliciclastics associated with transgression helps to concentrate or increase skeletal material at this time, and only a few large storms influence the deeper areas of the basin. Applying sequence stratigraphic terminology (Sageman, 1996), the packages correspond to lowstand and early transgressive system tracts. The vigorous hurricanes associated with global warming at subtropical platforms was enough to reach deeper areas of the basin slope (FZ4) forming two cycle of tempestite deposits, with the later one represented by (SMF 6) (sample D31). Generally, the PETM stage here is created in a slope or fore reef environment at

or above the storm wave base level. However, the minor transgression observed clearly in this section may be attributed to the continuity forming a slope/ toe slope (mid/ outer ramp) environment at the end, especially when a turbidity character for the upper sandstone bed (sample D33) is obserevd. Although the finishing of the PETM tropical hurricanes effect gives a clue of the PETM decline, it does not necessarily mean the end of a minor transgression effect.

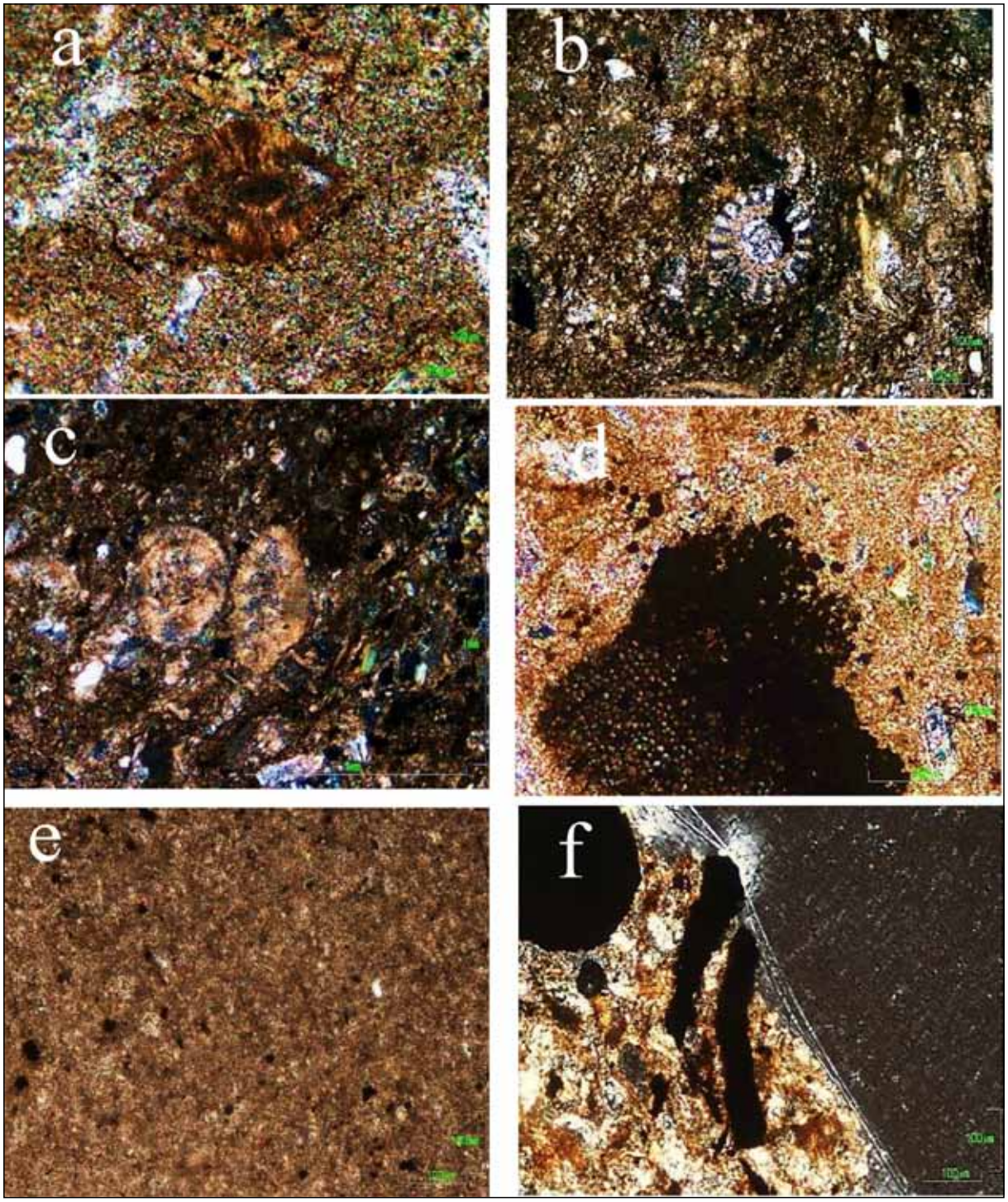

Plate 2. (a). Larger foraminifera Nummulites (Assilina) characterized by radial hyaline tests. Coiling is biconvex planispiral (Sample D28). **(b).** Blue green algal fragments(Dasycladacea) (SampleD29). **(c).** Decrease in clastic materials versus increase in bioclast and micritic matrix (Sample D28). **(d).** Common biogenic iron oxide crystals (Sample Q25). **(e).** Absence of clastic grains and the dominating micritic or mud matrix (Sample Q29). **(f).** Bullet-shaped and elongate chains of biogenic iron oxides (Sample Q27).

6.2 Clay Minerals

Since the Tertiary deposits' thickness within the Tethyan Sea did not exceed 1500 m, sediment did not suffer deep burial diagenesis, Therefore, clay minerals clues or imprint remained in the deposits (Bolle et al., 2000; Bolle and Adatte, 2001).

Generally, the clay mineral assemblages reflect the climatic conditions under which those minerals were weathered (Ghergari and Onac, 2001). Their relative abundance changes provide valuable information and good

indicators about the prevailed climatic conditions such as warmness, aridity, humidity as well as the geoenvironmental conditions including the weathering rate.

XRD investigation has revealed that the following clay minerals are dominant in all of the studied sections; smectite (montmorillonite), illite, kaolinite, and palygorskite, Plate (4). The non-clay minerals are represented by calcite, ankerite, quartz, feldspar, hornblende, and rutile.

There are approximate shifts in clay values at the onset of early Eocene in all sections. In the Aaliji Formation, increases in all clay minerals as well as non- clay ankerite and quartz are recorded in Figure (13 A). In the Kolosh Formation at Dohuk section, the clay-mineral content fluctuates, which may refer to coastal perturbation, where an increase in illite, kaolinite and ankerite versus a decrease in quartz with a constant content in montmorillonite and an absence of palygorskite were observed Figure (13 B). In the Kolosh Formation at Shaqlawa section, there are very high increases in illite compared to montmorillonite, quartz and ankerite increase, conversely, there is a general decrease in kaolinite and paucity in palygorskite (0-0.3 wt. %), Figure (13 C).

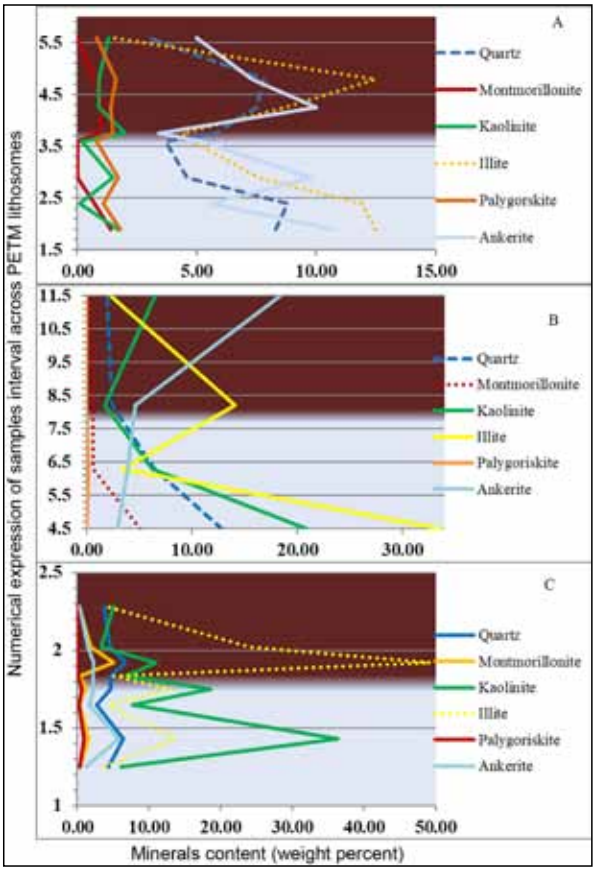

Figure 13. Distribution of clay minerals, Quartz, and Ankerite across the PETM lithosomes of the studied sections. **A.** Aaliji Formation. **B.** Kolosh Formation at the Dohuk section. **C.** Kolosh Formation at the Shaqlawa section, the contact between two colors correspond to the Paleocene / Eocene contact.

7. Discussion

7.1 PETM Geochemical Signatures

Many geochemical measures showed and separated the geochemical signatures that are used in singular or in integration with each other as an indication of environmental conditions that are characterized and associated with the PETM hyperthermal event.

In summary, the obtained geochemical signatures are the proven distinctive hints for carbon negative excursion (CIE), and the $\delta^{18}O$ negative shifts are coincided with the early Eocene, and interpreted by the injection of huge amounts of 13C-depleted carbon into the ocean–atmosphere system, leading to an unusual temperature rise largely expressed by high oxygen (^{18}O) isotope negative peaks.

Major and trace-element analysis gives multi-indications of PETM, where the relative increase trend in most major oxides suggests a slight increase in contribution to the detrital materials (mostly clay minerals). On the other hand, the variations in the geochemical indices of paleoredox sensitive indicator ratios (for example; U/Th, U/Al and Mo/Al) indicate anoxic or euxinia conditions (Yao et al., 2018), while the increase in terrestrial input sensitive indicator ratios such as (Si/Al, K/Al, Zr/Al, Rb/Al) is a strong evidence of the progressive increase in the detrital input source with specific features. Other geochemical indices' variation such as (Ba/Al, Ti/Al, and Fe/Al provides more information about the environmental conditions such as productivity nature. Moreover, high terrestrial organic matter influx to the sea floor and improve its preservation as recorded in Teythan margins (including studied sections) evidenced by the high TOC concentration coordinated with anoxia, transient sea level rise, and the increase of primary productivity conditions.

Finally, the decrease in the $CaCO_3$ accumulation/preservation rates during the PETM was driven primarily by a significant increase in sea floor dissolution (lysocline shallowing) or are rather related to the siliciclastic dilution, while the lysocline deepening was signalled by increases in the $CaCO_3$ percentages (Alegret et al., 2018; Harper et al., 2019).

7.2 PETM Sedimentological Signals

In the Aaliji Formation, the increase in the radiolarian test reflects a good vertical water circulation (upwelling), and a decrease in $CaCO_3$ in the sediments because of the dissolution or CCD and the lysocline shallowing (Flügel, 2004 and 2010). Nevertheless, the increase in the dissolution porosity and the rarity of benthic foraminifera suggest the CCD and lysocline shallowing option as a global signal (Bralower et al., 2018), in addition to preparing for the upwelling process post PETM. The more micritic matrix and darker rock color observed in PETM zones were explained as a response to the sea level rise and high organic matter that may be associated with this high matrix (transient high productivity or eutrophy).

The calcareous tempestites in the Kolosh Formation are calcarenite at the Dohuk section and calcisiltite at the Shaqlawa section. The deposits are thought to be formed by tropical PETM-induced storms and hurricanes as is clear by the green algae (dasycladacean) (Flügel, 2004 and 2010). The presence of these calcareous tempestite shows that the deposition occurred below, but near to the storm wave base, and is mainly coincident with relative sea-level falls (lowstand) and early transgressive system tracts (TST) (Sageman, 1996). The rapid warming associated with the onset of the PETM caused significant changes in

the environmental conditions (such as seasonality and high productivity); these variable environmental conditions would favour the diversification and proliferation of robust organisms adapted to exploit and tolerate periods.

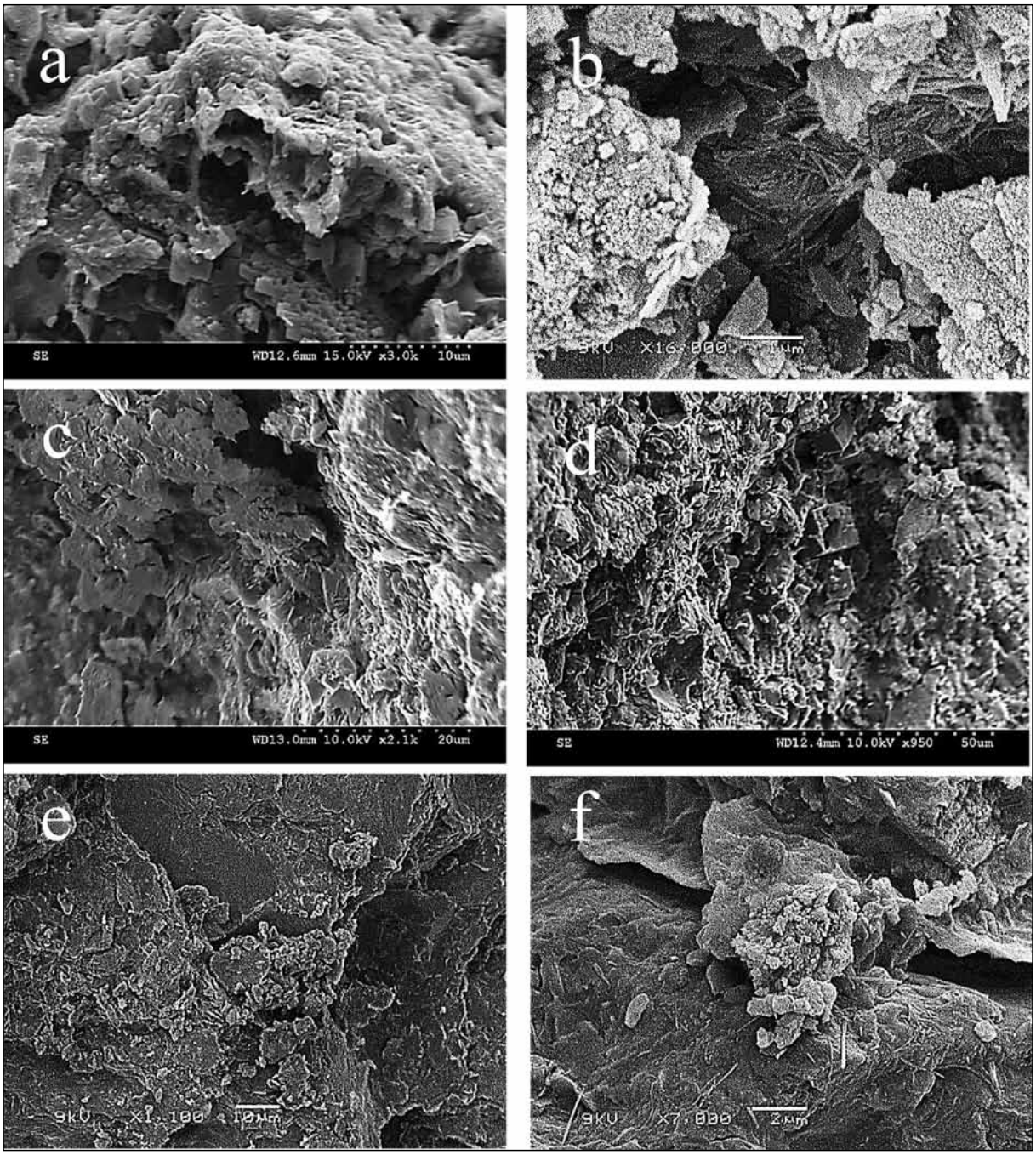

Plate 4. (a) Mostly authigenic montmorillonite (comb structure) (mo), detrital illite flakes (i) with dolomite rhombs (d). (A26). **(b)** Pore filling authigenic acicular palygorskite (p). (A27). **(c)** Spiny illite (i) coating grain or dolomite rhombs (arrows), vuggy micro porosity (mp) with detrital montmorillonite (mo). (D24). **(d)** Degraded illite flakes (arrows), dolomite rhombs partly dissolved (d), degraded kaolinite (k). (D28). **(e)** Degraded detrital kaolinite (k), highly degraded illite flakes (i) of detrital origin. (Q22). **(f)** Spiny palygorskite fibers (p) coating detrital framework grains, scattered carbonated (c). (Q24).

Magnetosomes of crystal shapes may be possibly identified in the Kolosh Formation, see Plate (2, f). They are typically arranged in elongate chains within the cell in order to direct the organism along the magnetic field lines and assist in the organism's search for nutrients. They might even be used as an intracellular energy or iron supply (Lippert, 2008). The environmental conditions spurred the magnetotactic bacteria bloom and the diversification of iron biomineralizing organisms specific to the subtropics in general, (they may also be global), although limited to the shallow continental shelves (Lippert, 2008; Rudmin et al., 2018) as noticed in Dohuk and some how at the Shaqlawa sections.

Vuggy – channel porosity observed in petrographic study could support the early dissolution idea or may be caused by synsedimentary to early diagenetic biogenic methane exhalation originating from the decay of organic matter (Liu et al., 1988 in Flügel, 2004). Both originating methods give a clue about the PETM event effect on sediment diagenesis.

The PETM abnormal paleoenvironmental conditions

controlled the semi-consolidated PETM sediments' zone (early Eocene sediments) during its early diagenetic stage. Relative oxygen depletion or deficiency (not true anoxia), global increase in temperature, and the concentration of benthic food (eutrophic conditions) that prevailed within the sediments in the very shallow surface layer during the PETM show no record of trace fossil producers gradually but rapidly (Rodríguez-Tovar et al., 2011). This conclusion provides an indication of the weak or negligible effect of bioturbation diagenetic processes on the PETM zone sediments. However, the reduction condition and hypoxia are common along the Kolosh and Aaliji rocks, but increase during PETM zone as inferred by the increase of the pyrite authigenesis and TOC content (micritic matrix and dark color shale), absence of ichnofossils, and sediment lamination.

The PETM-induced sea level rise represents an indirect factor for the PETM impact, and possibly had a direct effect on the paleodepositional response, which resulted in originating the PETM depositional expression, tracing it through microfacies interpretation.

In the Aaliji Formation, although (SMF3) is dominated, the shifting basinward took place from deep shelf/toe of slope contact environments to deep shelf /basin plain contact environments. In the Kolosh Formation, at Shaqlawa section, minor shifts occurred from slope / toe of slope contact environments (per PETM) to near toe of slope /deep shelf interrelation. In the Kolosh Formation at Dohuk section, minor transgression was observed, from a slope or forereef environment to slope/ toe of slop transition environments especially when a turbidity character was observed upwards.

The climatic evolution of the Tethys in northern Iraq, as inferred by the clay mineralogy of the study areas had almost the same climatic trend as reported by Bolle and Adatte (2001) for southeastern Tethys. The coexisting of illite, smectite and some kaolinite indicate warm and seasonal (montmorillonite) climate fluctuating between humid (kaolinite) and dry (illite) episodes. This feature is confirmed by Wang et al. (2011) and Kemp et al. (2016). The presence of some authigenic palygorskite indicates an increase of hot conditions and aridity (Khormali et al., 2005).

The results revealed that detrital input is possibly the main source of kaolinite, smectite and illite, while in situ neoformation during the saline and alkaline environment this could be the dominant cause of palygorskite occurrences. Smaller amounts of kaolinite with the presence of smectite indicate the gradual shift to a more seasonal climate. From the late Paleocene to the early Eocene, the gradual decrease of kaolinite in low latitudes was coincident with gradual increases in illite, which indicates the progressive development of aridity and massive dryness and evaporation in the southeastern margins of Tethys (Bolle and Adatte, 2001).

The early Eocene samples are characterized by an increase in quartz grains in both of the Aaliji and Kolosh Formation at Shaqlawa section which is a function of a promoting increase in physical or mechanical weathering, erosion, and runoff. This is due to longer periods of aridity and probably foster less dense vegetation (e.g., Schmitz and Andreasson, 2001). Whereas, the increase of storm-induced tempestite as inferred by the recycled calcarenite beds' deposition explains the relatively detrital quartz-grain paucity in the Kolosh Formation at the Dohuk section Figure (13).

Kaolinite increased obviously at the Aaliji Formation as compared to the Kolosh Formation. The relative variations may be explained by the increasing of suspended kaolinite particles when transported from the nearshore resulting in differential accumulation settling at the offshore setting (Aaliji and occasionally in Kolosh Formation at Shaqlawa section) (Harding et al., 2011). The same cause may be attributed to the decreasing in montmorillonite in the Kolosh Formation at the Dohuk section Figure (13).

Both illite and ankerite increased in all the studied sections during the early Eocene Figure (13), which may suggest an increase in hydrothermal activities' weathering for illite in the source areas and hydrothermal deposition via early cementation or syndolomitization by ankerite; whereas Palygorskite developed and increased at the Aaliji Formation in addition some little increase at the Kolosh Shaqlawa section.

The increase in palygorskite is interpreted to be enhanced in arid, warm, and evaporative conditions, whereas the decreasing palygoriskite in the Kolosh Formation especially at the Dohuk section Figure (13) can be explained by the high terrigenous input, Mg-depletion due to syndolomitization or cementation, or by the Mg –transportation to a deeper sea position that inhibited the palygorskite formation in shallower environments.

7.3 PETM Environmental Scenario

7.3.1 Onset of the PETM

Stratigraphical, sedimentological, and geochemical signatures discussed in the previous sections characterize the onset of the PETM succession at Paleocene/Eocene boundary. The upper Paleocene relative sea-level fall or regression immediately preceding the PETM leads to the infilling of broad submarine channel or channel-like depressions (valley incision), causing erosion of the bordered exposed NW-SE ridge. This condition may be enhanced by earthquakes along major lestric faults (foreland basin) and, in shallow waters, by the effects of storm waves on the sea bed, and significantly induced terrigenous sediment input, gravity mass movement (slope failure), and completed a rapid progradation and/or upbuilding of extensive submarine fans (proximal to distal) that formed the Kolosh Formation deposits.

In addition to global/regional stimulates (e.g. volcanic activities), the Kolosh Formation depositional condition such as the decreasing pressure because slope masses failure and storm waves may largely have worked as a local inducer changing the stable methane clathrates' deposits, which are buried into older Aaliji and Kolosh semi consolidated deposits to unstable methane clathrates as an important source of carbon. The process of methane gas release is thus started increasingly. An input of huge amounts of isotopically light CO_2 and/or CH_4 into the earth system took place synchronizing with global PETM phenomena. Hence, warm climate takes to develop in northern Iraq region rapidly. Subsequently at the earliest Eocene, sea level started to rise responding to an early warming effect (melting of small ice

sheets, sea water expansion or other agents) that is caused by the greenhouse gases' release and concurrent to the onset of deposition of the first PETM event beds or facies.

A progressive increase of weathering/ erosion rates and detrital (fluvial) input is strongly expected during the onset of the PETM as a normal environmental reaction to adjustment and the naturalized warming consequences. Increasing fluvial discharge prepared the sea water to developing primary saline water stratification as well as its thermal stratification. Water column stratification reduced vertical mixing or the upwelling process and immediately affected nutrient availability creating oligotrophic conditions (decrease productivity) with the onset of PETM (Alegret et al., 2018)

The onset of oxygen depletion in the deep sea may have occurred due to either the rapid oxidation of released methane from gas hydrates to carbon dioxide or the expansion and intensification of mostly terrestrial source organic matter zone, where the oxygen demand for the decay of metabolizable organic matter exceeds the rate of oxygen supply, Figures (14 A and B).

7.3.2 Peak phase of the PETM

The peak phase of PETM correspond to CIE peaks at the early Eocene time as the multi-sources release of greenhouse gases and global warming continued in a progressive manner. Certainly, this geologically rapid and chronic continuity affected the earth ecosystems, which responded through generating exceptional interplaying of environmental factors to contribute in the preparation of PETM environmental conditions. The inherent conditions from the onset of the PETM phase developed to become intemperate and severer in this phase.

The high concentration of greenhouse gases imposed excess amounts of CO_2 to be dissolved in marine ecosystems (as assumed in the studied sections paleoenvironment) to create an increase in H_2CO_3. Lowering in pH and $CaCO_3$ saturation (sea water acidification) (Babila et al., 2018), lysocline and CCD shallowing to naturalize acidification and widespread $CaCO_3$ dissolution took place severely reflecting leaching by corrosive waters. These changes were the most important factors in initiating the deposition of detrital clays within the early Eocene at the studied formations. On the other hand, increased temperatures, which intensified the hydrological cycle (Oliva-Urcia et al., 2018) resulted in an increase in humidity and hydrolysis reactions preparing for the next acceleration of weathering and erosion power rates which helped naturalize acidification through the increase of alkalinity as a result of dissolved bicarbonates supplied by fluvial discharge, then by lysocline deepening perhaps reaching its pre PETM original position.

Intense hydrological cycle is most likely associated with higher freshwater influxes that resulted in the establishment of density and /or salinity stratification (Frieling et al., 2018) in addition to weak thermal (low thermal gradient) stratification of the water column that led to extra water stratification and a high reduction in vertical circulation (upwelling) and horizontal circulation. Sea level rise may have shifted or expanded the upwelling regions towards shoreline areas (farther west Iraq) and consequently increased productivity in the photic zone, which also is more promoted by fluvial influx of organic / nutrients-rich sediments.

Relative enhancing in productivity by sea level rise and fluvial influxes, led to a more oxygen consumption within semi- stagnant water (good stratification). These parameters strongly supported the accumulation of organic carbon and promoted development of hypoxia or anoxia tendency state as explained by the presence of the lamination in deposits, and other previous indicators. The oxygen deficiency resulted in inhibited growth and elevated mortality prior to reaching the adult reproductive phase. Therefore, all PETM conditions particularly sea level rise and oxygen deficiency played an important role in restructuring the benthic ecosystem and benthic foraminifera extinction event (BFEE), immediately after the onset of global warming as in Figure (14 C).

7.3.3 The Recovery Phase of the PETM

Although a gradual transition exists between the PETM phase and the recovery phase (Lyons et al., 2019), its characteristic features were sensible after the early Eocene identified by the highest organic carbon (TOC) in concert with evidence and for oxygen-deficiency (such as lamination). The recovery phase was probably characterized by a rapid regrowth of terrestrial and marine organic inventories.

A number of negative feedback processes may have contributed to carbon sequestration including the expansion of continental vegetation with increased terrestrial organic carbon storage and/or elevated surface ocean productivity with increased marine organic carbon burial. Productivity enhancment likely originated through the development of more vigorous circulation due to the intensification of the wind. The enhanced vertical mixing was originatd by the upwelling of nutrient-rich intermediate Tethyan water into the epicontinental basin, and increase nutrient supply by fluvial discharge. However, quantitatively, the most important feedback for permanently sequestering carbon and lowering atmospheric CO_2 levels are the acceleration of silicate-weathering reactions on land.

The weathering mechanism would yield a net positive influx of bicarbonate and soluble cations into the ocean, thereby driving ocean carbonate content toward saturation and enhancing carbonate production/preservation rates until equilibrium was restored. An increase in the rate of carbonate sedimentation inferred by the increase of $CaCO_3$ percentage upward which would be consistent with the enhanced silicate weathering helped to promote a relatively rapid recovery from the CIE and falling global temperatures; the CO_2-triggered increased weathering and bioproductivity feedback effects possibly enhanced the subsequent progressive return to pre-PETM environmental conditions such as changing the waters to become progressively more oxic or (suboxia), Figure (14 D).

Finally, during the late recovery of the PETM, the siliciclastic flux has not returned to pre-event values, the concurrent sedimentary evidence for improved seafloor oxygenation, and excess in carbonate sedimentation considerably may reflect the lower siliciclastic input during a maximum flooding phase Figure (14 E).

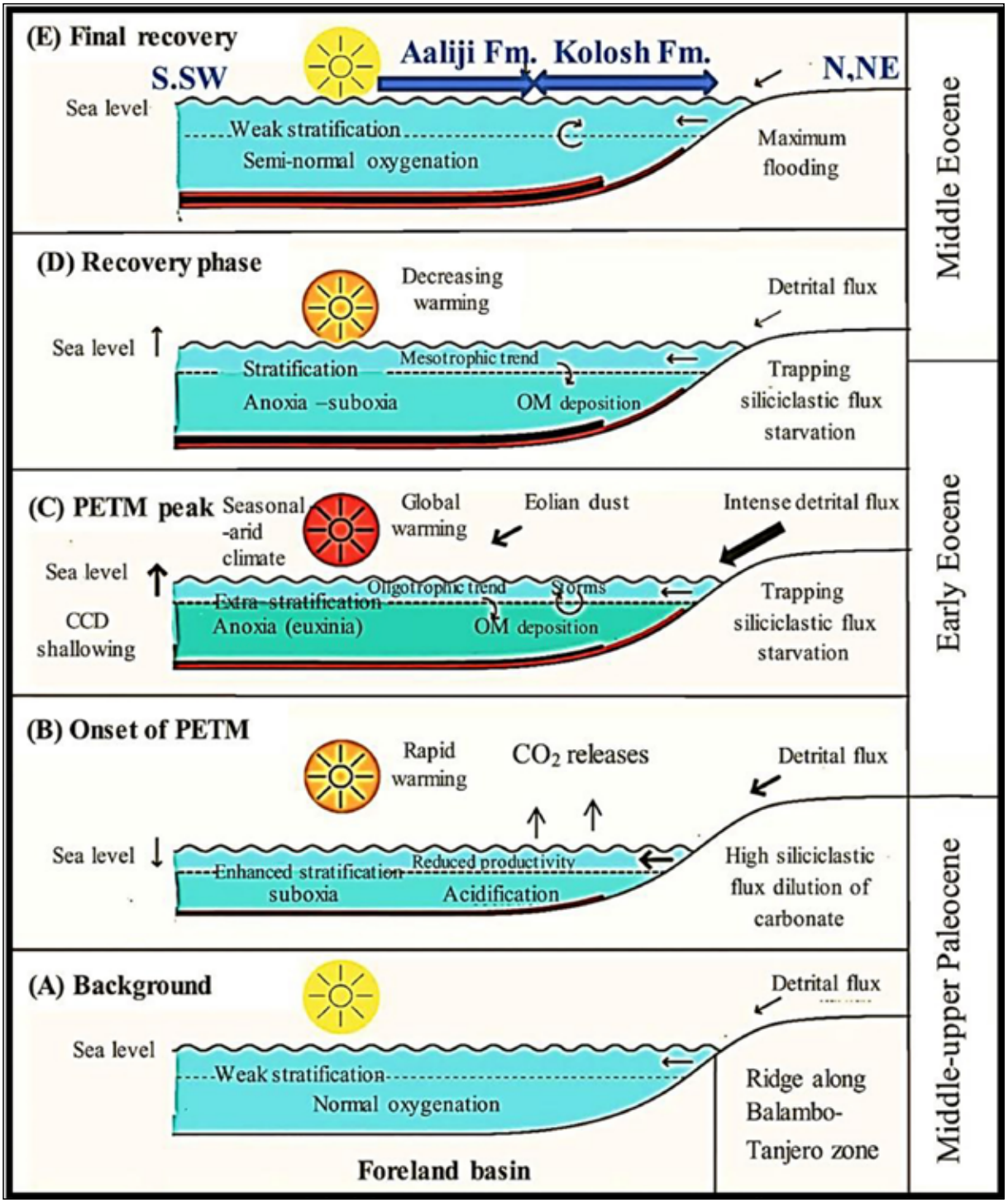

Figure 14. Conceptual model of climatic-environmental interplaying changes during the PETM event illustrated on an imagined paleogeographic cross section extending from N.NE to S.SW of Iraq. **(A).** Background conditions. **(B).** PETM onset. **(C).** PETM peak phase. **(D).** recovery phase, and **(E).** late recovery phase of this hyperthermal event. Modified after Schulte et al. (2011a).

8. Conclusions

1- The direct and indirect sedimentological, and geochemical indicators and the integration relationship among them suggest that during the Paleocene – early Eocene period, the northern Iraq region was affected by PETM climatic event interplayed in the marine realm within the epicontinental foreland basin. Both formations (Aaliji and Kolosh) are included at least in principle in the lithological or sedimentary records of PETM-associated events.

2- The fresh lithological color change to brown or yellowish brown or yellowish white colors is the distinctive field feature to trace the PETM equivalent lithosome in the Aaliji and Kolosh Formation outcrops as well as other field features such as the calciturbidite beds and /or organic matter rich black shale (deep marine) or calcarenitic tempestite beds (shallow marine).

3- There are several petrographic signals for the PETM environmental conditions identified in the Aaliji

and Kolosh Formations such as magnetosomes (bacterial biomineralize), high matrix ratio, appearance of green algae (dasycladacean), as well as lack of bioturbation, early dissolution, and early dolomitization diagenetic process.

4- The PETM- related facies perturbations could be distinguished more obviously in shallow marine environments (Dohuk section) compared to deep marine environments (Aaliji Formation and Shaqlawa section).

5- A Paleoclimate trend (cold or warm) is an important and effective factor in facies model interpretations at least within minor sequence changes (smaller than third order).

6- Clay mineral assemblages and its variations across PETM lithosomes in the Aaliji and Kolosh Formations referred to same climatic trends of the southeastern Tethys region (warm, arid-seasonal climate).

7- The maximum flooding surface (MFS) is included within the PETM interval or lithosomes refering indirectly to the occurrence of transgressive system tracts (TST) associated with PETM effects.

8- The true carbon stable isotope values of sea water were represented more likely in The Kolosh Formation (Dohuk section) and the Aaliji Formation. In contrast, the original Oxygen stable isotope signal in the Aaliji Formation was less modified by diagenesis and was more preserved than in the Kolosh Formation.

9- The geochemical indices or ratios werea sensitive and a highly-valued method for tracing and identifying the anoxic or euxinia conditions and the rates of siliciclastic influx as well as the confirmation of other PETM-associated environmental factors such as the sea level rise and weathering intensity. Moreover, the variations in these ratios are, thus, considered the geochemical expression or responses of PETM-environmental interplaying.

10- The Kolosh Formation receives a siliciclastic flux with more extraneous material higher than the Aaliji Formation.

11- The increase of organic fluxes, increase of primary productivity, and improved preservation under anoxia conditions together caused the TOC enrichment during PETM at the studied sections.

References

Al Fattah, A. N., Al-Juboury, A.I., Ghafor, I. M. (in press). Biostratigraphic significance during the Paleocene-Eocene Thermal Maximum (PETM) in Northern and Northeastern Iraq.

Alegret L., Matíasc, R., Manuela, V. (2018). Environmental instability during the latest Paleocene at Zumaia (Basque-Cantabric Basin). The bellwether of the Paleocene-Eocene Thermal Maximum. Palaeogeography, Palaeoclimatology, Palaeoecology 497:186- 200.

Alegret, L., Ortiz S., Arenillas, I., Molina, E. (2010). What happens when the ocean is overheated? The foraminiferal response across the Paleocene–Eocene Thermal Maximum at the Alamedilla section (Spain). Geol. Soc. Am. Bull. 122:1616–24.

Al-Sharhan, A.S., and Nairn, A.E.M. (2003). Sedimentary basins and petroleum geology of the Middle East. Elsevier Science, Amsterdam, Netherlands P. 843.

Aqrawi, A.A.M., Goff, J.C., Horbury, A.D., Sadooni, F.N. (2010). The petroleum geology of Iraq, Scientific Press Ltd, UK, P.424.

Arthur, M.A., and Sageman, B.B. (2004). Sea-level control on source-rock development. Perspectives from the Holocene Black Sea, the Mid- Cretaceous Western Interior Basin on North America, and the Late Devonian Appalachian Basin. In. Harris, N. B. (Ed.), The Deposition of Organic-Carbon-Rich Sediments. Models, Mechanisms, and Consequences. SEPM Special Publication 82: 35–59.

Babila, T.L., Penman, D.E., Hönisch, B., Kelly, D.C., Bralower, T.J., Rosenthal, Y., Zachos, J.C. (2018). Capturing the global signature of surface ocean acidification during the Palaeocene–Eocene Thermal Maximum. Phil. Trans. R. Soc. A376.20170072. http.//dx.doi.org/10.1098/rsta.2017.0072.

Baceta, J., Pujalte, V., Wright, V.P., Schmitz, B. (2011): Carbonate platform models, sea-level changes and extreme climatic events during the Paleocene-early Eocene greenhouse interval: a basin- platform-coastal plain transect across the southern Pyrenean basin. In: Pree-Meeting Field trips Guidebook, 28th IAS Meeting. Zaragoza (C. Arenas, L. Pomar and F. Colombo, Eds.). Sociedad Geológica de España, Geo-Guías, 7:151-198.

Berggren, W.A., and Pearson, P.N. (2005). A revised tropical to subtropical planktonic foraminiferal zonation of the Eocene and Oligocene. Journal of foraminiferal Research 35: 279 – 298.

Bolle, M.P., and Adatte, T. (2001). Palaeocene–early Eocene climatic evolution in the Tethyan realm. clay mineral evidence. Clay Minerals 36: 249–261.

Bolle, M.P., Tantawy, A.A., Pardo, A., Adatte, T., Burns, S., Kassab, A. (2000). Climatic and environmental changes documented in the upper Paleocene to lower Eocene of Egypt. Eclogae Geologicae Helvetiae 93: 33–51 pp.

Bowen, G.J., Bralower, T.J., Delaney, M.L., Dickens, G.R., Kelly, D.C., Koch, P.L., Kump, L.R., Meng, J., Sloan, L. C., Thomas, E., Wing, S.L., Zachos, J.C. (2006). Eocene Hyperthermal Event Offers Insight Into Greenhouse Warming, EOS, Transactions of the American Geophysical Union 87: 165-169.

Bralower, T.J., Kump, L.R., Self-Trail, J.M., Robinson, M.M., Lyons, S., Babila, T., Ballaron, E., Freeman, K.H., Hajek, E., Rush, W., Zachos, C. (2018). Evidence for shelf acidification during the onset of the Paleocene-Eocene Thermal Maximum. Paleoceanography and Paleoclimatology33:1408-1426. https.// doi.org/10.1029/2018PA003382.

Brasier, M.D. (1980). Microfossils. George Allen and Unwin Ltd., London, 193 p.

Cohen, A.S., Coe, A.L., Kemp, D.B. (2007). The Late Palaeocene-Early Eocene and Toarcian (Early Jurassic) carbon isotope excursions. a comparison of their timescales, associated environmental changes,causes and consequences. Journal of Geological Society London 164:1093—1108.

DeConto, R.M., Galeotti, S., Pagani, M., Tracy, D., Schaefer, K., Zhang, T., Pollard, D., Beerling, D.J. (2012). Past extreme warming events linked to massive carbon release from thawing permafrost. Nature 484, 87-91.

Dickens, G.R., O'Neil, J.R., Rea, D.K., Owen, R.M. (1995). Dissociation of oceanic methane hydrate as a cause of the carbon- isotope excursion at the end of the Paleocene, Paleoceanography, 10, 965–971.

Dickson, A.J., Cohen, A.S., Coe, A.L. (2012). Seawater oxygenation during the Paleocene-Eocene Thermal Maximum, Geology 40 (7): 639–642.

Dickson, A.J., Cohen, A.S., Coe, A.L. (2012). Geochemical facies analysis of fine- grained siliciclastics using Th/U, Zr/Rb

and (Zr+Rb)/Sr ratios. Chemical Geology 181:131–146.

Elling, F.J., Gottschalk, J., Doeana, K.D., Kusch, S., Hurley, S.,J., Pearson, A. (2019). Archaeal lipid biomarker constraints on the Paleocene- Eocene carbon isotope excursion. NATURE COMMUNICATIONS (2019) 10.4519 | https.//doi.org/10.1038/ s41467-019-12553-3.

Ernst, S.R., Guasti, E., Dupuis, CH., Speijer, R.P. (2006). Environmental perturbation in the southern Tethys across the Paleocene/Eocene boundary (Dababiya, Egypt). Foraminiferal and clay mineral records. Marine Micropaleontology 60: 89-111.

Farouk, S. (2016). Paleocene stratigraphy in Egypt. Journal of African Earth Sciences 113: 126-152.

Flügel, E. (2004). Microfacies of carbonate rocks, analysis, interpretation and application, Springer, Berlin P. 976.

Flügel, E. (2010). Microfacies of carbonate rocks, analysis, interpretation and application, 2nd edition, Springer, Berlin P. 984.

Fralick, P.W., and Kronberg, B.I. (1997). Geochemical discrimination of clastic sedimentary rock sources. Sedimentary Geology 113: 111– 124.

Frieling, J., Reichart, G. Middelburg, J. J., Röhl, U., Westerhold, T., Bohaty, S., M., Sluijs, A. (2018). Tropical Atlantic climate and ecosystem regime shifts during the Paleocene–Eocene Thermal Maximum. Clim. Past 14: 39–55. https.//doi. org/10.5194/cp-14-39- 2018.

Ghergari L. and Onac B. (2001). Late quaternary paleoclimate reconstruction based on clay minerals assemblage from preluca tiganului (gutai mountains, Romania), studia universitatis babes- bolyai, geologia, xlvi (1): 15-28.

Giusberti, L., Coccioni, R., Sprovieri, M., Tateo, F. (2009). Perturbation at the sea floor during the Paleocene–Eocene Thermal Maximum. Evidence from benthic foraminifera at Contessa Road, Italy. Marine Micropaleontology 70 (3–4): 102–119.

Giusberti, L., Rio, D., Agnini, C., Backman, J., Fornaciari, E., Tateo, F., Oddone, M. (2007). Mode and tempo of the Paleocene–Eocene Thermal Maximum in an expanded section from the Venetian pre- Alps. Geological Society of America Bulletin 119: 391–412.

Harding, I.C., Charles, A.J., Marshall, J.E.A., Pälike, H., Roberts, A.P., Wilson, P.A., Jarvis, E., Thorne, R., Morris, E., Moremon, R., Pearce, R.B., Akbari, S. (2011). Sea-level and salinity fluctuations during the Paleocene–Eocene thermal maximum in Arctic Spitsbergen, Earth and planetary Science Letters 303: 97- 107.

Harper, D.T., Hönisch, B., Zeebe, R., Shaffer, G., Haynes, L., Thomas, E., Zachos, J.,C. (2019). The magnitude of surface ocean acidification and carbon release during Eocene Thermal Maximum 2 (ETM-2) and the Paleocene–Eocene Thermal Maximum (PETM). Paleoceanography and Paleoclimatology https.//doi.org/10.1029/2019PA003699

Höntzsch, S., Scheibner, C., Guasti, E., Kuss, J., Marzouk, A.M., Rasser, M.W. (2011). Increasing restriction of the Egyptian shelf during the Early Eocene? — New insights from a southern Tethyan carbonate platform, Palaeogeography, Palaeoclimatology, Palaeoecology 302:349–366.

Hupp, B.N., Kelly, D.C., Zachos, J.C., Bralower, T.J. (2019). Effects of size- dependent sediment mixing on deep-sea records of the Paleocene- Eocene Thermal Maximum: Geology, v. 47, p. 749–752, https:// doi .org /10 .1130 /G46042.1.

Jassim, S.Z., and Buday, T. (2006). Middle Paleocene-Eocene Megasequence (AP 10). In Jassim, S.Z. and Goff, J.C. (Eds.). Geology of Iraq. Dolin, Prague and Moravian Museum, Brno, Czech Republic. P. 155-167.

John, C. M., Bohaty, S. M., Zachos, J. C., Sluijs, A., Gibbs, S., Brinkhuis, H., Bralower, T. J. (2008). North American continental margin records of the Paleocene–Eocene thermal maximum. Implications for global carbon and hydrological cycling. Paleoceanography 23, PA2217.

Jones, M.T., Percival, Stokke, E.W., Joost Frieling, J., Mather, T.A., Riber, L., Schubert, B.A., Schultz, B., Tegner, C., Planke, S., Svensen, H.H. (2019). Mercury anomalies across the Palaeocene–Eocene Thermal Maximum. Climate of the Past 15, 217-236, doi: 10.5194/cp-15-217- 2019.

Kemp, S.J., Ellis, M.A., Mounteney, I., Kender, S. (2016). Palaeoclimatic implications of highresolution clay mineral assemblages preceding and across the onset of the Palaeocene–Eocene Thermal Maximum, North Sea Basin. Clay Minerals 51: 793–813.

Kent, D.V., Cramer, B.S., Lanci, L., Wang, D., Wright, J.D., Van der Voo, R. (2003). A case for a comet impact trigger for the Paleocene/Eocene thermal maximum and carbon isotope excursion Earth Planet. Sci. Lett. 211 13– 26.

Khormali, F., Abtahi, A., Owliaie, H.R. (2005). Late Mesozoic-Cenozoic clay mineral successions of southern Iran and their paleoclimatic implications. Clay minerals 40: 191-203.

Khozyem, H., Adatte, T., Keller, G., Tantawy, A.A., Spangenberg, J.E. (2014). The Paleocene-Eocene GSSP at Dababiya, Egypt –Revisited. Episodes, 37 (2): 78-86.

Lipinski, M., Warning, B., Brumsack, H.J. (2003). Trace metal signatures of Jurassic/ Cretaceous black shales from the Norwegian Shelf and Barents Sea. Palaeogeography, Palaeoclimatology, Palaeoecology190: 459–475.

Lippert, P.C. (2008). Big discovery for biogenic magnetite, PNAS, 105, 46:17595-17596.

Lirer, F. (2000). A new technique for retrieving calcareous microfossils from lithified limedeposits. Micropaleontology 46: 365–369.

Liu, Q., Larrasoaña, J.C., Torrent, J., Roberts, A.P., Rohling, E. J., Liu, Z., Jiang, Z. (2012). New constraints on climate forcing and variability in the circum-Mediterranean region from magnetic and geochemical observations of sapropels S1, S5 and S6. Palaeogeography, Palaeoclimatology, Palaeoecology 333-334: 1–12.

Liu, Y.G., Miah, M.R.U., Schmitt, R.A. (1988). Cerium: Achemical tracer for paleo-oceanic redox conditions. Geochimica et Cosmochimica Acta 52 (6): 1361-1371

Lyons, S.L., Baczynski, A. A., Babila,T.L., Bralower, T.J., Hajek, E.A., Kump, L. R., Polites, E.G., Self-Trail, J.M.,Trampush, S.M., Vornlocher, J.R., Zachos, J.C., Freeman, K.H. (2019). Palaeocene– Eocene Thermal Maximum prolonged by fossil carbon oxidation. Nature Geosc ience 12 (1): 54–60. https://hdl. handle.net/10.1038/s41561- 018 0277-3

Mazzullo, S.J. (2000). Organogenic dolomitization in peritidal to deep-sea sediments. Journal of Sedimentary Research 70 (1): 10-23.

Meadows, D.J. (2008). Geochemistry of the Paleocene Tartan Formation in the Great South Basin, New Zealand, Unpublished Diploma Thesis, Victoria University of Wellington, P.108.

Nguyen, T.M.P., Petrizzo, M.R., Speijer, R.P. (2009). Experimental dissolution of a fossil foraminiferal assemblage (Paleocene–Eocene Thermal Maximum, Dababiya, Egypt). Implications for paleoenvironmental reconstructions. Marine Micropaleontology 73:241–258.

Nicolo, M.J., Dickens, G.R., Hollis, C.J., Zachos, J.C. (2007). Multiple Early Eocene hyperthermals. Their sedimentary expression on the New Zealand continental margin and in the deep sea. Geology 35: 699- 702.

Oliva-Urcia, B., Gil-Peña, I., Samsó, J.M., Soto, R., Rosales, I. (2018). A Paleomagnetic Inspection of the Paleocene-Eocene Thermal Maximum (PETM) in the Southern Pyrenees. Front.

Earth Sci. 6:202. Doi: 10.3389/feart.2018.00202.

Rodríguez-Tovar, F.J., Uchman A., Alegret, L., Molina, E., (2011). Impact of the Paleocene–Eocene Thermal Maximum on the macrobenthic community. Ichnological record from the Zumaia section, northern Spain, Marine Geology 282: 178–187.

Röhl, U., Westerhold, T., Bralower, T.J., Zachos, J.C. (2007). On the duration the Paleocene–Eocene Thermal Maximum (PETM). Geochemistry, Geophysics, Geosystems 8 (12): 1-13.

Rudmin, M., Roberts, A.P., Horng, C.S., Mazurov, A., Savinova, O., Ruban, A., Veklich, M. (2018). Ferrimagnetic iron sulfide formation and methane venting across the Paleocene-Eocene thermal maximum in shallow marine sediments, ancient West Siberian Sea. Geochemistry, Geophysics, Geosystems19: 21–42. https.//doi.org/10.1002/2017GC007208.

Sageman, B.B. (1996). Lowst and tempestites. Depositional model for Cretaceous skeletal limestones, Western Interior basin, Geology 24 (10): 888–892.

Schaller, M.F., Fung, M.K., Wright, J.D., Katz, M.E., Kent, D.V. (2016). Impact ejecta at the Paleocene-Eocene boundary Science 354: 225–9.

Scheibner, C. and Speijer, R.P. (2008). Late Paleocene–early Eocene Tethyan carbonate platform evolution — a response to long- and short-term paleoclimatic change. Earth-Science Reviews 90: 71– 102.

Schmitz, B., and Andreasson, F.P. (2001). Air humidity and Lake δ18O during the latest Paleocene–earliest Eocene in France from recent and fossil fresh-water and marine gastropod δ18O, δ13C, and 87Sr/86Sr. Bulletin of the Geological Society of America 113: 774– 789.

Schmitz, B., Asaro, F., Molina, E., Monechi, S., Von Salis, K., Speijer, R. (1997). High-resolution iridium, δ13C, δ18O, foraminifera and nannofossil profiles across the latest Paleocene benthic extinction event at Zumaya, Spain. Palaeogeography, Palaeoclimatology, Palaeoecology 133: 49–68.

Schmitz, B., Peucker-Ehrenbrink, B., Heilmann-Clausen, C., Aberg, G., Asaro, F., Lee, C. T. A. (2004). Basaltic explosive volcanism, but no comet impact, at the Paleocene–Eocene boundary. High-resolution chemical and isotopic records from Egypt, Spain and Denmark. Earth and Planetary Science Letter 225: 1–17.

Schulte, P., Joachim, C., Brumsack, H., Mutterlose, J. (2011b). Element chemostratigraphy across the Paleocene-Eocene thermal maximum at Demerara Rise, Central Atlantic (ABSTRACT), Berichte Geol. B. - A., 85 (ISSN 1017-8880)–CBEP 2011, Salzburg, June 5th – 8th.

Schulte, P., Scheibner, C., Speijer, R. (2011a). Fluvial discharge and sea- level changes controlling black shale deposition during the Paleocene–Eocene Thermal Maximum in the Dababiya Quarry Section, Egypt. Chem. Geol. 285: 167– 183.

Sharland, P.R., Archer, R., Casey, D. M., Davis, R.B., Hall, S.H., Heward, A.P., Horbury, A.D., Simmons, M.D. (2001). Arabian Plate Sequence Stratigraphy. GeoArabia, Special publication, no. 2. P. 372.

Sluijs, A., Bowen, G. J., Brinkhuis, H., Lourens, L.J., Thomas, E., (2007). The Palaeocene-Eocene thermal maximum super greenhouse. Biotic and geochemical signatures, age models and mechanisms of global change. In. M. Williams, et al. (Eds.) Deep time perspectives on Climate Change. Marrying the Signal from Computer Models and Biological Proxies. The Micropalaeontological Society, Special Publications, the Geological Society, London, 323-349.

Sluijs, A., Röhl, U., Schouten, S., Brumsach, H.J., Sangiorgi, F., Sinninghe Damsté, J.S., Brinkhuis, H. (2008). Arctic late Paleocene–early Eocene paleoenvironments with special emphasis on the Paleocene – Eocene thermal maximum (Lomonosov Ridge, Integrated Ocean Drilling Program Expedition 302). Paleoceanography 23, PA1S11. Doi:10.1029/2007PA001495.

Soliman, M.F., Aubry, M.P., Schmitz, B., Sherrell, R.M. (2011). Enhanced coastal paleoproductivity and nutrient supply in Upper Egypt during the Paleocene/Eocene Thermal Maximum (PETM). Mineralogical and geochemical evidence, Palaeogeography, Palaeoclimatology, Palaeoecology 310: 365–377.

Speijer, R., and Wagner, T. (2002). Sea-level changes and black shales associated with the late Paleocene thermal maximum. Organic- geochemical and micropaleontologic evidence from the southern Tethyan margin (Egypt-Israel). Boulder. Geological Society of America, Special Paper 356: 533-549.

Svensen, H.S., Planke, A., Malthe-Sorenssen, B., Jamtveit, R., Myklebust, T., Eidem, S.R. (2004). Release of methane from a volcanic basin as a mechanism for initial Eocene global warming, Nature 429: 542-545.

Thomas, D.J., and Bralower, T.J. (2005). Sedimentary trace element constraints on the role of North Atlantic Igneous Province volcanism in late Paleocene–early Eocene environmental change. Marine Geology 217: 233–254.

Tremolada, F., and Bralower, T.J. (2004). Nannofossil assemblage fluctuations during the Paleocene–Eocene Thermal Maximum at Sites 213 (Indian Ocean) and 401 (North Atlantic Ocean). Palaeoceanographic implications. Marine Micropaleontology 52: 107– 116.

Uchikawa, J., and Zeebe, R.E. (2010). Examining possible effects of seawater pH decline on foraminiferal stable isotopes during the Paleocene–Eocene thermal maximum. Paleoceanography 25, PA2216. doi:10.1029/2009PA001864

Veizer, J. (2009). Carbon Isotope Variations over Geologic Time, in Gornitz, V. (Ed). Encyclopedia of Paleoclimatology and Ancient Environments, Springer P. 1047.

VVer Straeten, C.A., Brett, C.E., Sageman, B.B. (2011). Mud rock sequence stratigraphy.Amulti-proxy (sedimentological, paleobiological and geochemical) approach, Devonian Appalachian Basin, Palaeogeography, Palaeoclimatology, Palaeoecology 304: 54–73.

Wang, C.W., Hong, H.L., Song, B.W., Yin, K., Li, Z.H., Zhang, K.X.,J.I. J.L. (2011). The early-Eocene climate optimum (EECO) event in the Qaidam basin, northwest China. Clay evidence. Clay Minerals 46: 649–661.

Yao, W., Paytan, A., Wortmann, U.G. (2018). Large-scale ocean deoxygenation during the Paleocene-Eocene Thermal Maximum. Science, 361: 804-806.

Zachos, J. C., Röhl, U., Schellenberg, S. A., Sluijs, A., Hodell, D. A., Kelly, D. C., Thomas, E., Nicolo, M., Raffi, I., Lourens, L. J., McCarren, H., Kroon, D. (2005). Rapid Acidification of the Ocean during the Paleocene-Eocene Thermal Maximum, Science 308 (5728): 1611- 1615.

Zachos,J.C., Lohmann, K.C., Walker, J.C.G., Wise, S.W. (1993). Abrupt Climate Change and Transient Climates during the Paleogene: A Marine Perspective. The Journal of Geology 101(2):191-213, DOI: 10.1086/648216.

Zeebe, R.E. (2013) What caused the long duration of the Paleocene-Eocene Thermal Maximum? Paleoceanography 28, 440-452.

Zeebe, R.E., and Lourens, L.J. (2019). Solar System chaos and the Paleocene–Eocene boundary age constrained by geology and astronomy. Science 365: 926–929.

Zhang, Q., Dinga, L., Kitajimac, K., Valleyc, J.W., Zhangd, B., Xua, X., Willems, H., Klügelb, A. (2019). Constraining the magnitude of the carbon isotope excursion during the Paleocene-Eocene thermal maximum using larger benthic foraminifera. Global and Planetary Change 184 (2020) 103049.

JJEES

JJEES (2020) 11 (2): 146-156
ISSN 1995-6681

Jordan Journal of Earth and Environmental Sciences

A Re-evaluation of the Stratigraphic and Palaeogeographic Evolution of the Paleogene Sedimentary Successions of the Niger Delta

Ogechi Ekwenye[1*], Kingsley Okeke[1], Gloria Otosigbo[2], Ogechukwu Onyemesili[3]

[1]University of Nigeria, Department of Geology, Nigeria.
[2] Alex Ekwueme Federal University, Department of Geology, Nigeria.
[3]Chukwuemka Odumegwu Ojukwu University, Department of Geology, Nigeria.

Received 4 January 2020; Accepted 1st March 2020

Abstract

A critical evaluation of the stratigraphic and paleogeographic evolution of the Paleogene sedimentary successions shows three cycles of sedimentation that are controlled by coastal morphology, basin bathymetry, sediment supply, hydrodynamic processes (dominantly tidal and wave/storm actions), and relative sea-level changes. Early Eocene Imo Formation is of a shallow-marine tidally-influenced environment. Middle Eocene – Late Eocene Ameki Group indicates a continental-marginal marine (estuarine) setting, and Oligocene Ogwashi Formation represents a tidally-influenced coastal-plain environment. Sequence stratigraphic models indicate four major depositional sequences of fluvial, estuarine, coastal-plain and shallow-marine environments that were bounded by unconformities linked to type-1 sequence boundaries (SB1 to SB4), during the Cenozoic. Four systems tracts consisting of the falling-stage systems tract (FSST), the low-stand systems tract (LST), the transgressive systems tract (TST) and the high-stand systems tract (HST) were established. The sequences and systems tracts indicate dominant progressive progradation with periodic retrogradation and aggradation of the Niger Delta Basin sediments. The Paleogene relative sea-level movements in south-eastern Nigeria indicate relative sea-level changes around southern Africa suggesting global relative sea-level fluctuations.

Keywords: Sequence stratigraphy, depositional environments; relative sea-level changes; paleogeography; Paleogene, Niger Delta.

1. Introduction

Several studies which encompass sedimentology, palynology, biostratigraphy, geochemistry, clay and heavy mineral analyses of the Paleogene sedimentary successions in south-eastern Nigeria showed that the strata are mainly of marginal to shallow-marine environments, with occasional fluvial deposition (Reyment, 1965; Adegoke, 1969; Arua, 1986, 1980; Nwajide, 1980, 2013; Anyanwu and Arua, 1990; Oloto, 1984; Oboh-Ikuenobe et al., 2005; Ekwenye et al., 2014, 2015, 2017; Ikegwuonu and Umeji, 2016; Okeke and Umeji, 2016; Ekwenye and Nichols, 2016). However, there are few documented papers on detailed paleogeographic and sequence stratigraphic evolution of the Cenozoic Niger Delta Basin (Oboh-Ikuenobi et al., 2005; Odunze and Obi, 2011; Ekwenye et al., 2017). Oboh-Ikuenobi et al. (2005) focused their study on the Umuahia and environs which is part of the southern region of the study area. Their work focused on the five depositional sequences of the Paleogene and the influence of relative sea- level fluctuations on the depositional cycles. However, no depositional models and relative sea- level curves were constructed to give a visual and deep understanding of the Paleogene paleogeography. Odunze and Obi (2011); Ekwenye et al. (2017) documented and reconstructed the sequence stratigraphic framework of the Imo Formation and Ameki Group respectively.

The need to understand the paleogeography from Paleocene to Oligocene has necessitated a new insight into the stratigraphic successions of Paleogene sediments of south-eastern Nigeria which includes a systematic review of the environment of deposition, palaeocurrent and heavy mineral analyses. In this regard, a paleogeographic evolution is reconstructed, and the relative sea-level changes and the sequence stratigraphic framework of the Paleogene strata are established.

2. Tectonic Setting of The Niger Delta Basin

Tectonic evolution of the Niger Delta basin is closely related to that of the Nigerian Benue. The Niger Delta Basin is geographically situated in the Gulf of Guinea and delineated by latitudes 3° and 6°N and longitudes 5° and 8°E (Nwajide, 2013; Figure 1). The basin is bounded to the west by the Okitipupa Ridge and demarcated from the Anambra Basin to the north by an unconformity. The eastern limit is defined by the Cameroun volcanic line, while the southern limit is the Guinea Abyssal plain. The establishment of the Niger Delta Basin followed the subsidence of the southern area of the Benue Trough during the Danian as a result of thermal contraction of the lithosphere (Sleep, 1971, Turcotte, 1977, Onuoha, 1981, Nwajide, 2013). According to Nwajide (2013), this subsidence induced major marine transgression of the Early Paleocene that paved the way for the accumulation of the basal beds of the Niger Delta basin.

* Corresponding author e-mail: ogechi.ekwenye@unn.edu.ng

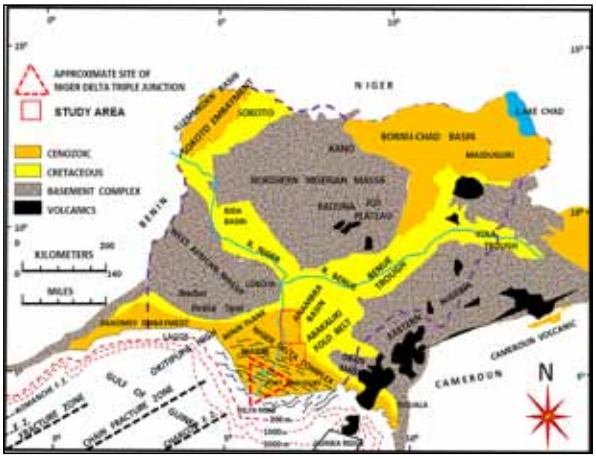

Figure 1. Structural map of the Nigerian Sedimentary Basin showing the chain and Charcot oceanic fracture zone (modified after Murat, 1972).

3. Stratigraphic Setting

The stratigraphic history of south-eastern Nigeria is characterized by three sedimentary phases (Short and Stäuble, 1967; Murat, 1972; Obi et al., 2001) during which the axis of the sedimentary basin shifted. These three phases are: (a) the Abakaliki-Benue phase (Aptian-Santonian), (b) the Anambra-Benin phase (Campanian- Early Palaeocene), and (c) the Niger Delta phase (late Paleocene-Pliocene). The resulting succession of the Niger Delta consists of the Paleogene system which is comprised of the Imo Formation, Ameki Group, and Ogwashi Formation (Figure 2), with a composite thickness of about 3,500 m. The succession begins with the transgressive Imo Formation (Paleocene) consisting of blue-grey clays, shallow-marine shale and sandstone, limestone and calcareous sandstone. The Imo Formation (Reyment, 1965) is the oldest outcropping lithostratigraphic unit of the Niger Delta Basin which is laterally equivalent to the Akata Formation in wells. The type locality of the Imo Formation is at the Imo River with a thickness estimated as 1000 m (Reyment, 1965).

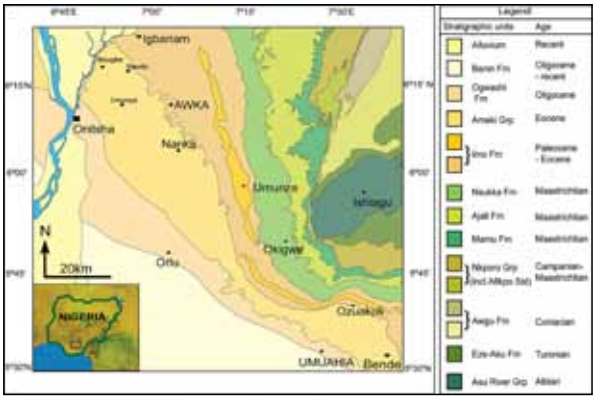

Figure 2. Geologic map of south-eastern Nigeria showing the Paleogene formations.

The Ameki (Ibeku Formation of Ekwenye, 2014), Nanka and Nsugbe formations are the lateral equivalents of the Ameki Group (Nwajide, 1980) the formation conformably overlies the Imo Formation. Reyment (1965) described the type locality of the formation between miles 73 to 87 along the section left behind during the eastern railway construction at Ameki Town. The Ameki Formation, which is composed of rapidly alternating shale, sandy shale, mudstone, clayey sandstone (Adegoke et al., 1980; Arua, 1980; Anyanwu and Arua, 1990) and fine-grained fossiliferous sandstone with thin limestone beds (Reyment, 1965; Arua, 1986), represents most of the Eocene. The age of the formation has been variously considered to be Early Eocene (Reyment, 1965) and Early Middle Eocene (Lutetian) (Berggren, 1960; Adegoke, 1969).The depositional environment has been interpreted as estuarine, lagoonal, and open marine, based on the faunal content. White (1926) interpreted an estuarine environment for the formation because of the presence of certain fish species of a known estuarine affinity. Adegoke (1969), however, indicated that the fish were probably washed into the Ameki Sea from inland waters, and preferred an open marine depositional environment. Nwajide (1980) and Arua (1986) suggested environments that ranged from nearshore (barrier ridge-lagoonal complex) to intertidal and subtidal zones of the shelf environments, whereas Fayose and Ola (1990) suggested that the sediments were deposited in marine waters of depths between 10 m and 100 m. Ekwenye et al. (2017) used the concept of facies analysis and sequence stratigraphy to suggest a tide-dominated estuarine system for the Ameki Group.

The Ogwashi Formation, previously known as Lignite Series (Parkinson, 1907), overlies the Ameki Group conformably with a type locality in Delta State. The Formation correlates with the upper Agbada Formation which is regarded as the down-dip extension of the outcropping Ogwashi Formation, while the lower Agbada Formation correlates with the Ameki Group (Short and Stäuble, 1967). The Ogwashi Formation (Eocene-Oligocene) is comprised of an alternation of coarse-grained sandstone, lignite seams, and light-colored clays of continental origin (Kogbe, 1976). Although Reyment (1965) suggested an Oligocene-Miocene age for the formation, a palynological study by Jan du Chêne et al. (1978) yielded a Middle Eocene age for the basal part of the Ogwashi Formation. Ekwenye and Nichols (2016) proposed a tidally-influenced coastal-plain deposit for the Ogwashi Formation due to the high degree of bioturbation in the basal matrix-supported conglomerate and sandstone facies.

4. Palaeoenvironment of Deposition

The palaeoenvironments of the Paleogene successions of the Niger Delta Basin reveal the interplay of sea-level fluctuations, sediment supply, tide, wave, and storm dynamics during the sedimentation of the Imo Formation, Ameki Group, and the Ogwashi Formation (Figure 3). Although, many variable palaeoenvironmental interpretations exist in the literature for the Paleogene strata; there is a need to harmonise them by integrating research studies on the sedimentology, palynology, and stratigraphy of the Paleogene successions.

The Imo Formation: Littoral to neritic conditions were suggested by Arua, 1980; Anyanwu and Arua, 1990 based on faunal assemblages; foreshore and shoreface zones of beaches and bars (Stevens et al., 2011), while a middle to outer neritic-zone conditions were deduced by Okeke and Umeji (2016) based on the abundance of gonyaulacacean cysts for the Imo Formation. The Costacalista adabionensis

(Adegoke, 1977) along with other foraminiferal and ostracod species (Reyment, 1965; Nwajide, 2013) as well as a shelf to shoreface (shallow marine) setting (Oboh-Ikuenobi et al., 2005) support a neritic environment. A littoral zone is a marginal-marine environment, while the neritic zone is a shallow-marine environment extending from mean low water down to 200-metre depth. Doust and Omatsola, (1990) indicated a high occurrence of microflora and marine planktonic foraminifera, in which foraminifera constitute more than 50% of the microfaunal assemblages suggestive of a shallow-marine shelf deposition. A dominantly shallow-marine shelf deposit for the Imo Formation is also supported by (Ekwenye et al., 2014) who recognized four depositional styles for all the lithofacies components of the formation viz offshore (shelf) shale (Facies association (FA) 1,5), tidal sand waves sandstone (FA 2), shoreface–foreshore (FA 3), and fluvial sandstone (FA 4) (Figure 4).

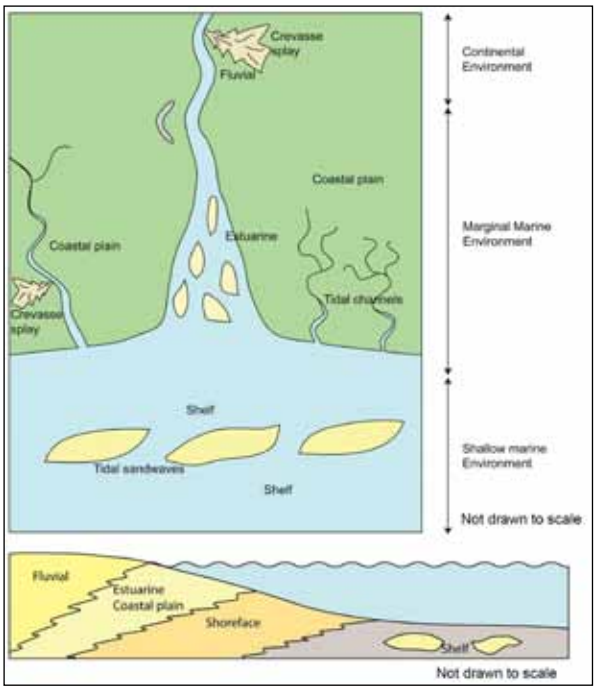

Figure 3. Conceptual model of the various depositional environments that dominated the Niger delta Basin (surface outcrop) during the Paleogene.

Ameki Group: Reyment (1965) suggested a partly marine and partly non-marine to estuary setting, and Adegoke (1969) suggested a shallow-marine setting for the Ameki Formation. This was supported by Ekwenye et al. (2017) who interpreted the Ameki Group as the tide-dominated estuarine system. Similarly, Nwajide, 1980 and Nwajide and Reijers, 1996 unravel the tidal sedimentation of the Ameki and suggested a tidal-influenced environment. The presence of the Pappocetus lugardi invertebrate fauna, foraminifera with Turritella and Siphonochelus nigeriensis invertebrate gastropods exemplifies a tropic shallow marine for the Ameki Formation (Nwajide, 2013). Alternating coastal and inner neritic conditions was recorded by (Okeke and Umeji, 2016) due to the diversity and abundance of terrestrial over marine palynomorph taxa in the formation. According to Okeke and Umeji (2016), the middle to outer neritic taxa are Adnatosphaeridium multispinosum, Hystrichokolpoma rigaudiae, Heteraulacysta pastulata, Eocladopyxis peniculata, Achilleodinium biformoides, Muratodinum fimbriatum. Alternating coastal and inner neritic conditions confirms the partly-marine and partly non-marine settings which are typical of estuarine environments. The dominance of tidal actions during the Eocene implies a tide–dominated estuarine for the Ameki Group.

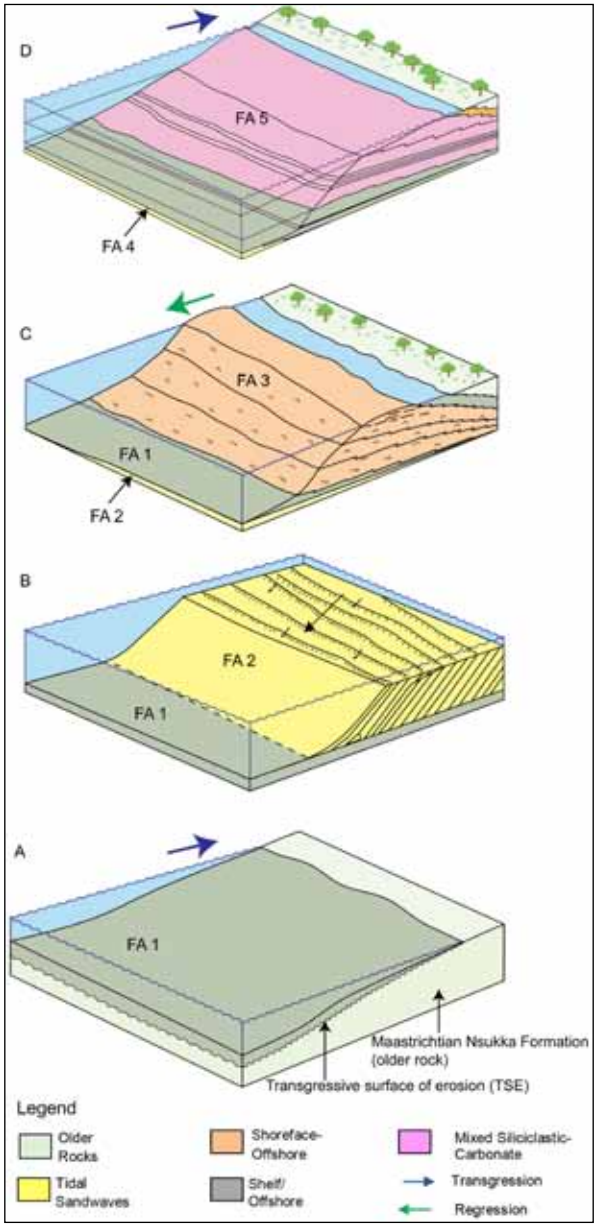

Figure 4. Depositional stages of the Imo Formation showing the **(A)** offshore shale facies (FA 1) which represented a major transgression in the Late Paleocene. **(B)** Tidal sandwaves (FA 2) deposited by an unidirectional tidal current in an offshore environment, whereby the sandwave deposit is encased by the offshore shale (FA 1) (see figure 4c). **(C)** The prevalence of wave action over tides led to the deposition of progradational coarsening-upward succession. Medium to pebbly sandstone. A lagoonal deposit occurs at the backshore. **(D)** A return to transgression is obvious with the deposition of mixed siliciclastic–carbonate sediments in a shelf setting, followed by a highly bioturbated sandstone with mono-specific Thalassinoides boxwork pattern (modified after Ekwenye, 2014; Ekwenye et al., 2015).

Ogwashi Formation: The integrated palynological and sedimentological analysis of the Ogwashi Formation (Umeji, 2003) is indicative of progradational shoreline palaeoenvironments; oscillating between the lower brackish water and upper (fresh water) deltaic plain. Detailed

lithofacies and outcrop studies of exposures (Ekwenye and Nichols, 2016) illustrate tidally influenced coastal-plain environments for the formation. Sub-environments such as fluvio-estuarine channels, tidal channels, tidal flats, coastal-plain channels, and coastal flood plain with mire are deposited in the tidally-influenced coastal-plain settings. An upper flood-plain environment was assigned by Nwajide (2013) while Okezie and Onuogu, 1985 attributed the lignite as a product of tropical to semi tropical plants with palm particles. In the southern part of the Ogwashi Formation around Umuahia (Ikegwuonu and Umeji, 2016) noted the occurrence of Monoporites anulatus a savannah pollen, Psilastephanocolporites laevigatus of tropical lowland evergreen forest and Proxapertites operculatus, Longapertites marginatus and Psilatricolporites crassus palmae pollen of brackish water swamp. These indicate palynomorph assemblages of the upper deltaic and lower deltaic-plain environment in conformity with the works of Umeji, (2002). The basal units of Ogwashi Formation is bioturbated matrix-supported conglomerates or conglomeritic sandstones which are typical of coastal-plain channels that are tidally-influenced. Reyment (1965) referred the Ogwashi Formation to coastal-plain deposits. Typically, a delta coarsens upward from prodelta shales to the delta front and delta-plain channels and bay-fills, but these depositional facies were not observed in the Ogwashi lithologic succession.

5. Discussion

5.1 Paleogeographic Evolution of the Paleogene Strata

The paleogeography of the south-eastern Nigeria is linked to the Cretaceous sedimentation that ended with the Maastrichtian-Paleocene Nsukka Formation, also referred to as the upper Coal Measures. Sedimentation ended in the Anambra Basin with the Nsukka Formation (Nwajide, 2005), and this is marked by the Paleocene unconformity.

Stage 1: Paleocene - Early Eocene

During the Paleocene, marine conditions were created due to a major relative sea-level rise (Nwajide, 2005; Oboh-Ikuenobe et al., 2005; Whiteman, 1982), which resulted in an increased accommodation, but the low supply of siliciclastic sediments led to the deposition of the offshore shales of the Imo Formation (Figure 5A) that is considered to be the oldest strata in the Niger Delta sedimentary Basin regime (Petters, 1991). Evamy et al. (1978) noted the deposition of marine shales in most of the southern Nigerian basin during the Paleocene to early Eocene times. The Paleocene transgression is further supported by the presence of nontronite (clay mineral) in the offshore shales (Ekwenye, 2014), which signifies low sedimentation and sea level rise (Thiry and Jacquin, 1993). Furthermore, the presence of dinoflagellates, acritarchs, and foraminiferal test linings in the offshore shales are good indicators of shallow-marine conditions (Ekwenye, 2014). Terrestrial input is indicated by the occurrence of sporomorphs and freshwater algal cysts (Ekwenye, 2014). Subsequently, the predominance of tidal process, and the increase in sediment supply during the Paleocene are indicated by the deposition of thick tidal sand waves (Figure 4B). The tidal currents were strong enough to rework fluvio-deltaic sediments of the Nsukka Formation which formed the sand waves (Ekwenye et al., 2014). The large-scale cross bed foresets (10 - 20 m thick) trend dominantly towards a northwest direction, reflecting sand waves' migration related to the dominant tidal current. The sand waves are classified as quartz arenite, with the dominance of rounded to subrounded quartz grains (Ekwenye et al., 2014). The Cretaceous sedimentary rocks of the Anambra and Afikpo basins are considered to constitute a major recycled sedimentary source (Mode et al., 2019). Mode et al. (2019) demonstrated the presence of heavy minerals such as zircon, tourmaline and apatite, and medium to high-grade metamorphic minerals, which suggest a contribution from igneous and metamorphic sources as well. Kreisa et al. (1986) interpreted similar giant–scale (3 - 12 m) cross-bed sets such as the tidal sand waves' deposit of Rancho Rojo Sandstone in Arizona which they further suggested to be a tide-dominated transgressive shallow-marine environment.

Cessation of the incoming clastic sediments is indicated by the presence of intense bioturbation of the topmost unit of the tidal sand-wave deposit. The presence of monospecific Thalassinoides horizontalis (Ekwenye et al., 2014) suggests a stressed shallow-marine condition. These events may have occurred as a result of a pause in sedimentation and probably lowering of the sea level which ended the deposition of the sand waves. Similar relationships are recorded by Bottjer (1985), where the lowering of the sea level with a pause in sedimentation during the Cretaceous resulted in monospecific Thalassinoides burrow system at the contact between Marlbook Formation and Saratoga Formation in South western Arkansas. A subsequent rise in relative sea level and reduced clastic supply-initiated deposition of the offshore shale of the Imo Formation (Ekwenye et al., 2014) which encased the tidal sand waves. The interplay between sediment supply, relative sea-level changes and hydrodynamic processes affected the stratigraphic succession of the Imo Formation. The deposition of a coarsening upward succession of well-sorted, rippled laminated sandstone suggests a predominance of a wave action and influx of siliciclastics, which indicates progradation. Heavy mineral assemblages (Ekwenye et al., 2015; Mode et al., 2019) suggest a mixed provenance, and that sediments probably originate from pre-existing sedimentary and metamorphic rocks, most probably from the Oban massif (Figure 5B); input may also be derived from the West African massif. This substantiates Dickinson (1985) QtFL and the QmFLt ternary diagrams' interpretation which illustrate that the Paleogene sandstones are a product of mixed sources of cratonic interiors, transitional continental blocks, and recycled orogen, and transitional continental as well as transitional recycled and quartzose recycled origins respectively.

A lagoonal deposit capped the first depositional sequence of the Imo Formation as a result of progradation. The second sequence commenced with coarse-grained sandstone (indicating regression) which is overlain by shale, marl and a thin limestone layer. This suggests the presence of a transgressive period, which may have occurred during the early Eocene. At the onset of the transgression, the Niger Delta Basin became a shelf in which a marine succession (marl, fossiliferous shale facies and structureless calcareous sandstone with subordinate structureless non-calcareous

sandstone, bioturbated sandstone and non-fossiliferous dark grey shale facies) was deposited; the deposition of these sediments suggested a pause in sedimentation due to a relative rise in sea level. According to Ekwenye et al. (2014), clay mineral analysis of the Imo Formation indicates the presence of nontronite, illite and kaolinite. Nontronite and illite are common in marine environments, while kaolinite indicates a terrestrial input during transgression. The relatively moderate occurrence of palygorskite suggests a Ca-rich water condition which resulted in the deposition of marl, limestone and fossiliferous sandstone. Palygorskite occurs in a wide range of environments (Weaver, 1989); it is common in alkaline lakes and perimarine environments under arid to semi-arid conditions. It is also documented in deep ocean sediments, brackish-water conditions, and marine sediments.

Shallow-marine conditions prevailing with the deposition of fossiliferous sandstone with fossiliferous limestone layers in the upper Sandstone Member of the Imo Formation indicates the availability of clastic sediments during a gradual relative sea-level rise which created accommodation for clastic accumulation. The occurrence of marl and the fossiliferous nature of the clastic sediments are restricted to the southern part of the study area (Umuahia-Bende region) which indicates variability in sediment supply. Results of the heavy mineral analysis indicate that the most probable source area would be the Oban massif. The high occurrence of coarse-grained garnets is associated with a schistose lithologic unit of the Oban massif that includes quartz-mica schist, garnet-mica schist, garnet-sillimanite schist and kyanite-sillimanite schist (Ekwueme et al., 1991).

A strongly bioturbated fine-grained sandstone capped the Imo Formation in the Umuhia-Bende region. The burrows are dominated by monospecific Thalassinoides paradoxicus (Ekwenye et al., 2014). This suggests a gradual fall in relative sea level and a pause in clastic input that enabled the unit to be colonized by burrowing decapod crustaceans. The top of the horizon forms a major discontinuity surface (Bottjer, 1985; Pemberton et al., 2004) that demarcated the Imo Formation from the Ameki Group.

Stage 2: Middle Eocene – Late Eocene

The Ameki Group which consists of the Nsugbe, the Nanka and the Ameki (Ibeku) formations (that are lateral equivalent) were deposited from the Middle-Late Eocene. During the Middle Eocene, a relative sea-level fall resulted to incision, obvious in the north-eastern part of the study area, and subsequent infill led to deposition of multistorey channels (Ugwu-Nnadi quarry, Nsugbe (Ekwenye et al., 2017). The conglomerate to sandstone of the Nsugbe Formation may have originated from the Western Nigerian massif and pre-existing sedimentary rock: as indicated by the high proportion of euhedral and prismatic ultrastable heavy-mineral suites such as zircon, tourmaline and apatite (Ekwenye et al., 2015) associated with the Nsugbe Formation which suggests a close-by acidic igneous or plutonic source and a basic igneous source (Figure 5C). However, the presence of rounded grains indicates multiple cycles of reworking which was common with the pre-existing sediments. The trough and planar cross-stratified sandstone units have a general trend of south-west palaeoflow direction, indicating a northeast provenance. A subsequent rise in relative sea-level and a strong influence of tidal process created estuarine (brackish-water) conditions (Figure 5C) characterised by tidally-influenced fluvial channels, tidal channels, tidal flats, supratidal, and tidal sand bars in the Ameki Group (Ekwenye et al., 2017). Palynological studies record terrestrial and marine influences in the estuarine deposits. The palynology from the Nanka Formation is nearly barren, with only a terrestrial influence. However, results from Ibeku Formation shows a mixed terrestrial and a shallow-marine input. Furthermore, outcrops around the Aguchi and Awgbu area has Proxapertites spp., Longerpertites marginatus and Echiperiporites species, Wilsonidium nigeriense and Phthanoperidinium alectrolophum Homotryblium tenuispinosum, Homotryblium abreviatum at the onset of the Nanka Formation suggesting a low-saline neritic environment (Okeke and Umeji, 2016).

A similar incised valley succession is recorded in the Aspelintoppen Formation, Eocene Central Basin of Spitsbergen, where fluvial deposits pass upwards into macrotidal tide-dominated estuarine deposits (Plink-Björklund, 2005). Eriksson et al. (2006) also observed fluvial-tidally influenced estuarine sedimentation in high-relief zones of tectonic origin, in the Mesoarchean Moodies Group, South Africa, and they related the succession to absolute sea-level fluctuations. Modern macrotidal estuaries with similar depositional facies are recorded in Seine estuary and Mont-Saint-Michel Bay, English Channel, NW France (Tessier et al., 2011); Minas Basin (Yeo and Risk, 1981) and Cobequid Bay, Bay of Fundy (Dalrymple et al., 1990).

In the study area, the Nsugbe Formation is interpreted as a fluvial channel deposit and marine inundation which occurred over the fluvial deposits resulting in the deposition of tidally- influenced point bar deposits (Nanka Formation). The inclined heterolithic strata of this point bar deposit (Nanka Formation) trend in an eastward direction (with low dip angle of 7°-10°). The eastward direction signifies a dominance of flood tidal current, whereas a minor westward trending inclined heterolithic strata shows a subordinate ebb tidal current. The dominance of flood tidal current over the ebb current supports the interpretation as a tide-dominated estuarine system (Hovikoski et al., 2008). Heavy-mineral analysis (Table 1) of the tidally-influenced point bar suggests that more than 68-78% of the clastics are of acidic igneous or plutonic origins, whereas 20-32% of the clastics suggest a metamorphic origin (Ekwenye et al., 2017). This may imply that more sediment is shed from the granitic unit of the Western Nigeria massif, or that the ultrastable heavy minerals are more resistant to weathering and alteration. Tidal channels exhibit palaeocurrent trends in south-east and north-west directions. The sandstones are quartzarenites to lithicarenites. Heavy minerals (Table 1) from the tidal channel sandstones also show higher clastic input from the acidic igneous bodies. Tidal sand bar units are dominated by southwest trending paleocurrent directions. The sands are dominantly quartzarenites and the heavy-mineral interpretation suggest a more clastic input from the metamorphic source (65-68%) than the acidic igneous source

(25-32%). Variation in the proportion of the heavy-mineral suite may also be attributed to grain-size and hydraulic conditions (heavy minerals occur more in finer grain-size fractions), as well as differential weathering from the source areas.

The changes observed in the clay minerals in the tide-dominated estuarine complex probably suggest an interaction between the terrigenous source and marine-source clay minerals. Clay minerals from the Nanka Formation consist mainly of kaolinite and a mixed illite layer. Insignificant palygorskite and very a limited occurrence of montmorillonite (only observed in one sample) are present. The dominance of kaolinite and a mixed illite layer suggest a greater influence of terrigenous input. The presence of montmorillonite as well as chlorite in minor amounts signifies a marine influence due to a rise in sea level (Thiry and Jacquin, 1993; Weaver, 1989). The composition and distribution of these clay minerals is similar to those of the estuaries along the east coast of the United States though the abundances of the clay minerals differ (Weaver, 1989).

Table 1. Summary of the heavy minerals and their provenances (adapted from Ekwenye et al., 2015).

Formation	Environment of Deposition	Heavy Minerals (Zrn, Tur, Apt, Px) %	Heavy Minerals (Rt, Sil, Kyn, St, Ep)%	Source Area
Nsugbe	Fluvial channel	64.7-66.6%	33.4-35.3%	Mixed sources, but dominantly igneous origin
Nanka	Tidally influenced fluvial channel	68.2-78.5%	20.9-31.8%	Mixed sources, but dominantly igneous origin
Nanka	Tidal channel	54.4-66.8%	33.1-45.6%	Mixed sources, but dominantly igneous origin
Nanka	Tidal Flat	53.6-82.3%	17.2-46.4%	Mixed sources, but dominantly igneous origin
Nanka	Tidal sand bar	28.8-32.5%	67.5-67.8%	Mixed sources, but dominantly metamorphic origin

Stage 3: Oligocene

During the late Eocene, the estuary was filled up with the Ameki Group sediments, leaving a low topography and a low-relief landscape. Probably, the activation of the paleo-Niger River or a relative sea-level fall may have resulted in the fluvial incisions on the low topography coastal-plain environment during the Oligocene. The tidally-influenced coastal plain is considered to be controlled by relative sea-level changes based on the vertical variation in the facies and facies associations from marine to non-marine conditions. The clay mineral suites in the Ogwashi Formation are dominated by kaolinite and mixed layer illite which signifies a continental input. A similar composition, but with varying amounts of kaolinite and illite, which occurs in the Early to Middle Cenomanian sediments of the Iberian strait (Northern Spain) is interpreted as fluviatile and littoral deposits (Floquet, 1991). Results from heavy mineral interpretation indicate mixed proportions of suites of minerals from metamorphic and igneous rocks which suggests the dominant source area to be the Oban Massif, which is comprised of basement rock (metamorphic rock) and granite (igneous rock) with contributions probably from the Western Nigeria basement, as well as recycled sedimentary rocks based on the occurrence of rounded and subrounded grains.

Oboh-Ikuenobe et al. (2005) demonstrated from palynlogical studies that the Ogwashi Formation contains 20-60% unstructured phytoclasts, 14-21% structured phytoclasts, <10% amorphous organic matter (AOM), and 5% fungal remains, but contains no marine palynomorphs. In contrast, Okeke and Umeji (2016) and Okeke (2017) recorded dinoflagellate and acritarch dominated by "Homotryblium tenuispinosum (1%) at Ogbunike, H. abbreviatum, in association with Operculodunium centrocarpum, Cleistosphaeridium? aciculare, Leiosphaeridea sp. and trochospiral foraminiferal test lining from the Ogwashi Formation sections at the conspicuous Ogbunike section (formerly Ogbunike Tollgate). According to Okeke and Umeji, 2016, the marine species are indicative of low salinity near shore or a brackish water environment. However, palynological analysis of the Ogwashi Formation around Umuahia yielded pollen and spore species of Monoporites annulatus, Psilastephanocolporites laevigatus and Psilastephanocolporites, Pachydermites diederixiProxapertites operculatus, Longapertites marginatus and Psilatricolporites crassus. Alnipollenites verus, Schizosporis parvus (Spirogyra), Schizophacus spriggi, Ovoidites parvus, and Ulvella nannie suggestive of fresh-water upper deltaic to the lagoon and or brackish-water lower deltaic plain within the tropical lowland rainforests (Ikegwuonwu and Umeji, 2016). The depositional environment interpretation of Ikeguonwu and Umeji op.cit confirmed the non-marine influences documented by Oboh-Ikuenobe et al. (2005). It seems that the marine influences recorded in the Ogbunike domain by Okeke and Umeji Op.cit were absent around the Umuahia-Bende area or the strata were completely missed by the authors during the geological mapping. The high occurrence of unstructured phytoclasts dominated by AOM may be due to the influence of nearshore marine water. Oboh-Ikuenobe et al. (2005) further suggested that the Oligocene Ogwashi Formation is a non-marine succession. They disregard the presence of low diversity, but a high abundance of Skolithos ichnofacies was found in the basal conglomerate and coarse-grained sandstone of the Ogwashi Formation. The occurrences of Skolithos ichnofacies and the ensued paleoenvironmetal interpretation were validated by the marine taxa recorded by Okeke (2017). Okeke and Umeji (2016) which indicate marine influences in the Ogwashi Formation around the vicinity. MacEachern and Hobbs (2004) indicated that the presence of bioturbation in coarse- grained strata is indicative of a marine influence. Thus, the regressive Ogwashi Formation (Figure 5D) had minor marine inundation that resulted in the high level of bioturbation found in the basal units.

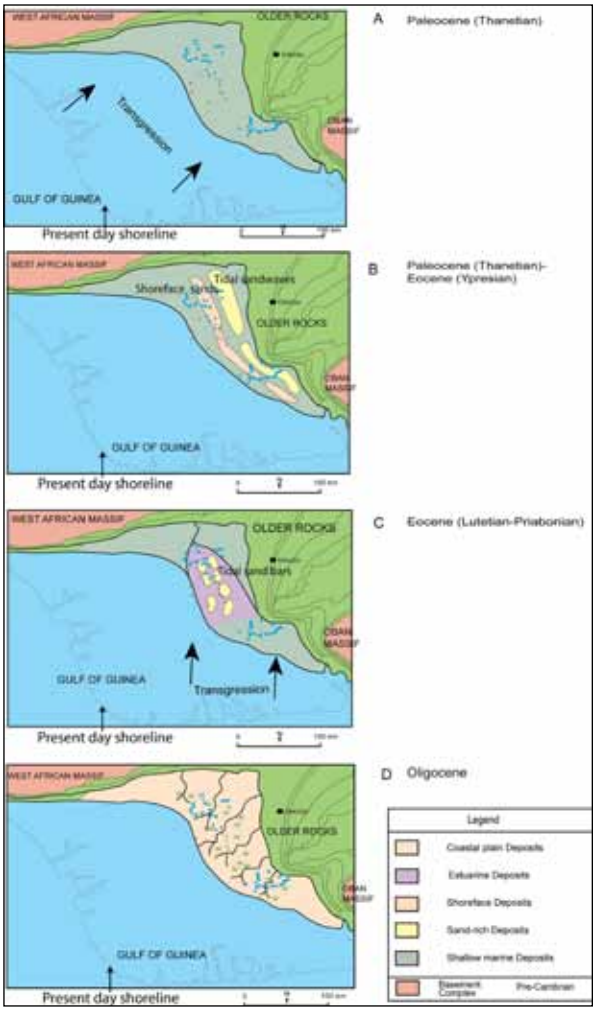

Figure 5. Paleogeographic evolution of the Paleogene strata, south-eastern Nigeria from Paleocene to Oligocene. **(A)** Paleocene transgression resulted in a shallow-marine condition that led to the deposition of bluish to dark grey shale facies interpreted as offshore shale (FA1). **(B)** Sediment influx from most probably pre-existing sedimentary rocks and Oban massif may have resulted in deposition of tidal sandwaves, shoreface/foreshore sandstone and fluvial channel in the Imo Formation. **(C)** Eocene sediments of the Ameki Group are dominantly derived from West African massif and recycled sedimentary rocks. A sea-level rise created an estuarine condition during the Eocene. **(D)** The Oligocene period witness a minor regression that resulted in coastal plain deposits with a minor transgression that led to the deposition of fluvio-estuarine sediments.

5.2 Sequence Stratigraphic Framework

Four depositional sequences are recorded for the Paleogene fluvial, estuarine, coastal-plain and shallow-marine depositional environments (Figure 3). The stratigraphic distribution and the facies' characteristics of the four depositional sequences are controlled by relative sea-level changes, as well as other controlling factors such as sediment supply, tidal processes and basin bathymetry. The cycle chart of the sea-level fluctuations is based mainly on the study of the stratigraphic succession of outcrops (Figure 6) and also contributions from other research works (Avbovbo and Ayoola, 1981; Oboh-Ikuenobe et al., 2005; Nwajide, 2005; Short and Stäuble, 1967). Four systems tracts were delineated: the falling-stage systems tract (FSST), the low-stand systems tract (LST), the transgressive systems tract (TST), and the high-stand systems tract (HST). However, the FSST deposits are not observed; the FSST corresponds to the sequence boundaries (SB 2 - 4).

The stratigraphic sequences are bounded by unconformities (type-1 sequence boundaries) as a result of relative sea-level changes. These sea-level changes can be correlated to other parts of the world (Figure 7). This is not an easy task though, due to the inadequacy of high-resolution chronological data for the study area. Despite this, the timing of the Paleogene sea–level movements around southern Africa (Siesser and Dingle, 1981) is observed to be approximately close to the timing established for sea-level changes in south-eastern Nigeria (Reyment, 1980; Reijers et al., 1997; Petters, 1995). Attempts have been made by Oboh-Ikuenobe et al. (2005) and Odunze and Obi (2011) to analyse the sequence stratigraphy in terms of the global sea- level curve of south-eastern Nigeria, but there are still inconstancies in the location of sequence boundaries, the interpretation of depositional facies and systems tracts.

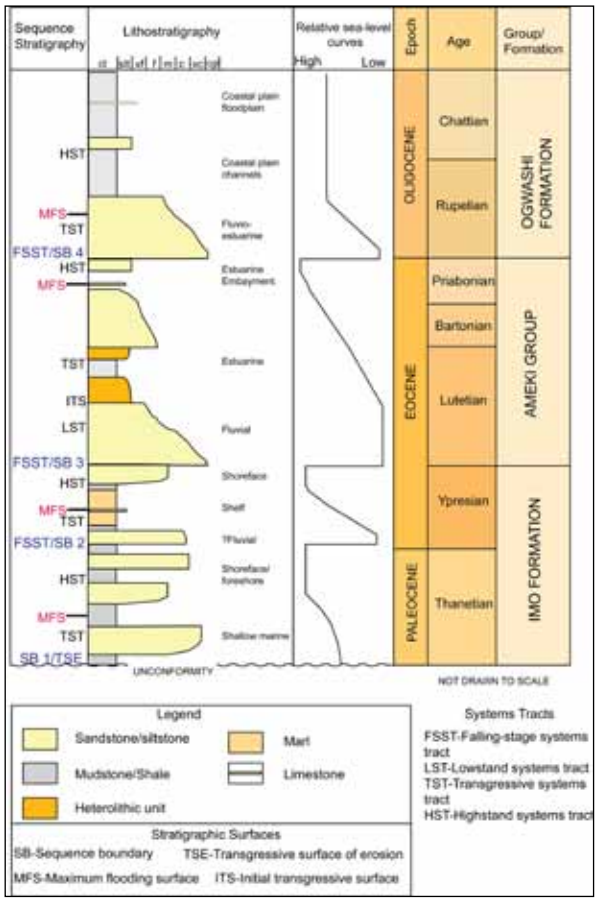

Figure 6. Sequence stratigraphic interpretation and relative sea-level changes of the Paleogene strata in south-eastern Nigeria.

5.2.1 Paleocene-Early Eocene Sequence

The first sequence boundary (SB1) occurs as an unconformity between the Nsukka Formation and the overlying Imo Formation (Avbovbo and Ayoola, 1981). The unconformity coincides with the transgressive surface of erosion which heralded the onset of a relatively rapid sea-level rise during the Paleocene. This Paleocene transgression initiated with the deposition of the offshore/shelf shale/mudstone of Imo Formation. The transgressive surface of erosion (TSE) coincides with the first sequence boundary (SB1) (Figure 6). The lowstand deposit is absent in the first depositional sequence. The offshore/shelf shale/mudstone

and tidal sand wave deposits signifies the transgressive systems tract, while the highstand systems tract is represented by shoreface-foreshore and lagoonal deposits. The Paleocene transgression in the study area is correlated to other regions of the world such as north-western and western Africa (Reyment, 1980), Argentina (Bertels, 1969), Brazil (Ponte and Asmus, 1978), South Africa (Siesser and Dingle, 1981) as well as in the northern and southern areas of eastern Europe and West Siberia as evidenced by the Peri-Tethys (Radionova et al., 2003). The Paleocene transgressions in southern Nigeria and South Africa are suggested to be as a result of tectono-eustacy or relative sea-level changes (Reyment, 1980; Reyment and Mörner, 1977; Siesser and Dingle, 1981; Oboh-Ikuenobe et al., 2005). The Imo Formation succession suggests that the Paleocene transgression continued into probably early Eocene times, with a minor regression pulse that resulted to the second sequence boundary (SB2). This long-term sea-level rise is related to the global sea-level fluctuations (Figure 7) as observed in the South African sea-level curve illustrated by Siesser and Dingle (1981). The regression resulted in a thin bedded, coarse to medium-grained sandstone (that represents fluvial deposits) which reflects a lowstand systems tract. An increase in relative sea-level resulted in the deposition of a thick succession of shale, marl with limestone layers (that represents shelf deposits) which represents the transgressive systems tract. The highstand systems tract is typified by coarsening upward fossiliferous sandstone (that represents shoreface deposits).

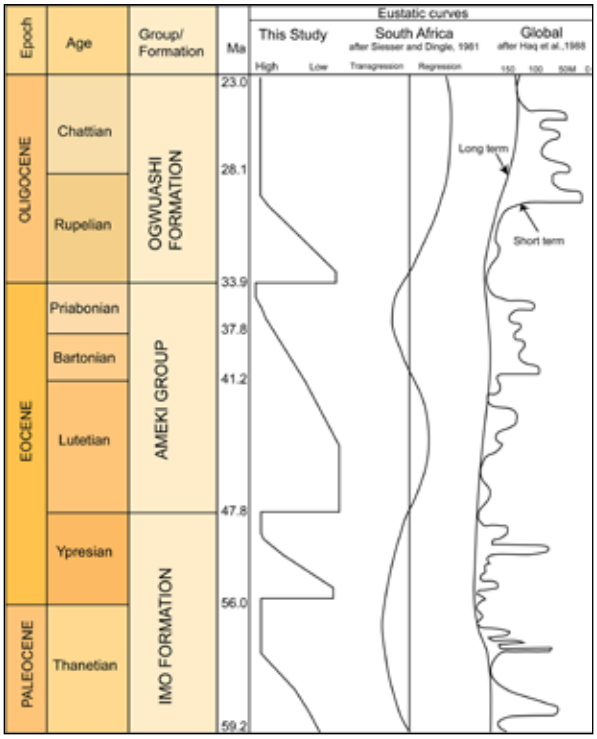

Figure 7. Comparison of south-eastern Nigerian and South African (Siesser and Dingle, 1981).

5.2.2 Middle-Upper Eocene Sequence

Siesser and Dingle (1981) recorded a series of transgressions and regressions during the Paleogene in South Africa and these events correlate approximately to the relative sea-level changes in south-eastern Nigeria (Figure 7). During middle Eocene times (Kogbe, 1976; Oloto, 1984), the Ameki Group was deposited and this corresponds to a regressive pulse which occurred during the middle Eocene in Southern Africa (Siesser and Dingle, 1981). The Ameki Group commenced with an initial regressive fluvial deposit of the Nsugbe Formation which forms the third sequence and the sequence boundary occurs at the base of the fluvial channel (SB3) or tidally influenced fluvial deposit in areas (such as Nando) where the tidal deposits rest directly on the Imo Formation deposits. The regression was followed subsequently by transgression that resulted in the estuarine condition and deposition of the Nanka Formation and the Ibeku Formation. The marine incursion marks the marine flooding surface and landward movement of the bayline which separates the regressive fluvial deposit from the transgressive estuarine deposits. The transgressive systems tract (TST) consists of thick successions interpreted as tidally influenced fluvial channels, tidal channels, tidal flats and tidal sand bars. This implies the availability of accommodation and sediments' supply, which may be due to regional subsidence and eustasy. Major global transgression in the Eocene is recorded by Flemming and Roberts (1973) and Siesser and Dingle (1981). This Eocene transgression may have affected sediments of the surface outcrop in the Niger Delta Basin, resulting in the estuarine conditions of the Ameki Group. The highstand systems tract is more pronounced in the Umuahia-Bende region. It is characterised by marine influence as the sea level gradually increases, which forms an inner tidal sand bar in the Enugwu-Ukwu region and estuarine embayment deposits in the Umuahia-Bende area. Siesser and Dingle, (1981), likewise suggested a regressive pulse during the middle Eocene in Southern Africa, which is represented by intense erosion that led to the absence and scarcity of middle Eocene rocks and subsequent transgression in late Eocene times.

5.2.3 Oligocene Sequence

The Oligocene strata in south-eastern Nigeria are characterised by tidally-influenced coastal- plain deposits which suggest a period of regression. The fourth sequence boundary (SB4) is marked by an unconformity, typified by basal erosive channels that are filled with fluvio-estuarine deposits. The fluvio-estuarine deposit constitutes the transgressive systems tract, while the tidal channel and coastal-plain deposits sensu stricto which include mud-filled channels and floodplain/mire form the highstand systems tract. Likewise, Siesser and Dingle (1981), recorded regression throughout the Oligocene time; marine influence was also noted in the Oligocene strata (Flores, 1973). This sequence is similar to the Oligocene Ogwashi deposit in southern Nigeria that commenced with regressive sequence of thick conglomerate, which was later reworked by shallow-marine infaunal organisms that indicate a marine influence.

6. Conclusions

The Paleogene succession in south-eastern Nigeria includes the Paleocene-Eocene Imo Formation, the Eocene Ameki Group and the Oligocene Ogwashi Formation which were deposited in a shallow-marine environment, a continental-marginal marine (estuarine) setting and a coastal-plain environment respectively. Three major

paleogeographic stages were established based on the stratigraphic distribution of the sediments, sedimentation pattern and presence of regional scale discontinuities. These include:

1) The Paleocene-Early Eocene stage during which marine conditions were created due to a major relative sea-level rise. This resulted in increase in accommodation, low siliciclastic influx and the deposition of the offshore facies of the Imo Formation. The presence of thick tidal sand waves within the Imo Formation indicates that tidal processes were active.
2) The middle Eocene-late Eocene stage, during which a relative sea-level fall resulted to incision and subsequent deposition of multi-storey channelized, trough and planar cross-stratified sandstone with general south-west and northeast-directed palaeocurrent patterns. A subsequent rise in relative sea-level and a strong influence of tidal process created estuarine (brackish-water) conditions characterised by tidally-influenced fluvial channels, tidal channels, tidal flats, supratidal and tidal sand bars in the Ameki Group.
3) The late Eocene-Oligocene stage, during which a tidally-influenced coastal-plain regime prevailed, leading to the accumulation of the coastal-plain sands of the Ogwashi Formation.
4) Four depositional sequences characterized by four systems tracts were delineated: the falling-stage systems tract (FSST), the low-stand systems tract (LST), the transgressive systems tract (TST), and the high-stand systems tract (HST). The internal arrangement of these depositional sequences reflect a progressive progradation with periodic retrogradation and aggradation of the Niger Delta Basin sediments during the Paleogene.

References

Adegoke, O.S. (1969). Eocene stratigraphy of Southern Nigeria. Colloque sur l' Eocene, 3, Bueau de Recherché Geologiques et Minieres Memoir 69: 23-48.

Adegoke, O.S. (1977). Stratigraphy and paleontology of the Ewekoro Formation (Paleocene) of southwestern Nigeria. Bull. American Paleont. 71, 295p.

Adegoke, O.S., Arua, I., Oyegoke, O. (1980). Two new nautiloids from Imo Shale (Paleocene) and Ameki Formation (Middle Eocene), Anambra State, Nigeria. J. Mining and Geology 17: 85 – 89.

Anyanwu, N.P.C., and Arua, I. (1990). Ichnofossils from the Imo Formation and their palaeoenvironmental significance. Journal of Mining and Geology 26: 1–4.

Arua, I. (1980). Palaeocene Macrofossils from the Imo Shale in Anambra State, Nigeria. Journal of Mining and Geology 17: 81–84.

Arua, I. (1986). Paleoenvironment of Eocene deposits in the Afikpo Syncline, southern Nigeria. Journal of African Earth Sciences 5: 279–284.

Avbovbo, A.A., and Ayoola, E.O. (1981). Petroleum prospects of southern Nigeria's Anambra Basin. Oil and Gas Journal 79: 334 – 347.

Berggren, W.A. (1960). Paleocene biostratigraphy and planktonic foraminifera of Nigeria (W. Africa). Proceedings 21st Intern'l Geol. Congress, Copenhagen, p. 41 – 55.

Bertels, A. (1969). Micropaleontologia y estratigrafia del limite Cretacico-Terciario en Huantrai-Co (Provincia de Neuquen). Ameghiniana, 6, 253-280 not seen, cited in Reyment, R.A. 1980. Paleo-oceanology and paleobiogeography of the Cretaceous South Atlantic Ocean. Oceanologica Acta 3 (1): 127-133.

Bottjer, D.J. (1985). Trace fossils and paleoenvironments of two Arkansas Upper Cretaceous discontinuity surfaces. Journal of Paleontology 59: 282-298.

Dalrymple, R.W., Knight, R. J., Zaitlin, B.A., Middleton, G. V. (1990). Dynamics and facies Model of a macrotidal sand-bar complex, Cobequid Bay–Salmon River Estuary (Bay of Fundy). Sedimentology 37: 577–612.

Dickinson, W.R. (1985). Interpreting provenance relations from detrital modes of sandstone. In: Zuffa, G.G., (Ed.), Provenance of Arenites. Dordrecht, Holland, D. Reidel Publishing Company, pp. 333-361.

Doust, H. and Omatsola, E. (1990). Niger Delta. In: Edwards, J.D., Santogrossi, P.A. (Eds.), Divergent/Passive Margin Basins. American Association of Petroleum Geologists Memoir 48: 201–238.

Ekwenye, O.C. (2014). Facies architecture, sedimentary environment and palaeogeographic evolution of the Paleogene stratigraphy. Unpublished Ph.D thesis, Royal Holloway, University of London, South-eastern Nigeria, 544.

Ekwenye, O.C., and Nichols, G.J. (2016). Depositional facies and ichnology of a tidally influenced coastal plain deposit: The Ogwashi Formation, Niger Delta Basin. Arab. J. Geosci. 9 (18): 1–27. https://doi.org/10.1007/s12517-016-2713-2.

Ekwenye, O.C., Nichols, G., Mode, A.W. (2015). Sedimentary petrology and provenance interpretation of the sandstone lithofacies of the Paleogene strata, south-eastern Nigeria. J Afr. Earth Sci. 109: 239– 262.

Ekwenye, O.C., Nichols, G.J., Collinson, M., Nwajide, C.S., Obi, G.C. (2014). A paleogeographic model for the sandstone members of the Imo Shale, South-eastern Nigeria. J Afr. Earth Sci. 96: 190–211.

Ekwenye, O.C., Nichols, G.J., Okogbue, C.O., Dim, C.I.P., Onyemesili, O.C. (2017). Facies architecture and reservoir potential of a macrotidal estuarine system: Eocene Ameki Group, south-eastern Nigeria. In: Onuoha K. M. (Ed.) Advances in Petroleum Geoscience Research in Nigeria Chapter 20: 369–405.

Ekwueme, B.N., Caen-Vachette, M., Onyeagocha, A.C. (1991). Isotopic ages from the Oban Massif and southeast Lokoja: implications for the evolution of the Basement Complex of Nigeria. Journal of African Earth Sciences 12 (3): 489-503.

Eriksson, K.A., Simpson, E.L., Mueller, W. (2006). An unusual fluvial to tidal transition in the mesoarchean Moodies Group, South Africa: a response to high tidal range and active tectonics. Sedimentary Geology 190: 13–24.

Evamy, B.D., Haremboure, J., Kamerling, P., Knaap, W.A., Molloy, F.A., Rowlands, P.H. (1978). Hydrocarbon habitat of Tertiary Niger Delta. American Association of Petroleum Geologists Bulletin 62: 1–39.

Fayose, E.A. and Ola, P.S. (1990). Radiolarian occurrences in the Ameke type section, eastern Nigeria. J. Mining and Geol. 26: 75 – 80.

Flemming, N.C. and Roberts, D.G. (1973). Tectono-eustatic changes in sea level and sea-floor spreading. Nature 243: 19-22.

Floquet, M. (1991). La plate-forme nord-castillane au Crétacé supérieur (Espagne): arrière-pays ibérique de la marge passive basco-cantabrique. Sédimentation et vie Centre des Sciences de la Terre, l4, 925 pp not seen, cited in Thiry, M., Jacquin, T., 1993. Clay mineral distribution related to rift activity, sea-level changes and paleoceanography in the Cretaceous of the

Atlantic Ocean. Clay Minerals 28: 61-84.

Flores, G. (1973). The Cretaceous and Tertiary sedimentary basins of Mozambique and Zululand. In: Bland, G., (Ed.). Sedimentary Basins of the African Coasts. Association of Africa Geological Surveys 81-111.

Haq, B.U., Hardenbol, Jr, J.S., Vail, P.R. (1988). Mesozoic and Cenozoic chronostratigraphy and cycles of sea level changes. In: Wilgus, C.K., Hastings, B.S., Kendall, C.G. St. C., Posamentier, H.W., Ross, C.A. and Van Wagoner, J.C., (Eds.), Sea Level Changes – an Integrated Approach. SEPM Sp. Publ. (42): 71 – 108.

Hovikoski, J., Rasanen, M., Gingras, M., Ranzi, A., Melo, J. (2008). Tidal and seasonal controls in the formation of Late Miocene inclined heterolithic stratification deposits, western Amazonian foreland basin. Sedimentology 55: 499-530.

Ikegwuonu, O.N.and Umeji, O.P. (2016). Palynological age and palaeoenvironment of deposition of Mid-Cenozoic sediments around Umuahia, Niger Delta Basin, southeastern Nigeria, Journal of African Earth Sciences 117: 160-170 doi: 10.1016/j.jafrearsci.2016.01.010.

Jan du Chêne, R., Onyike, M.S., Sowumi, M.A. (1978). Some new Eocene pollen of the Ogwashi-Asaba Formation, Southeastern Nigeria. Revista de Espanol Micropaleontologie 10: 285–322.

Kogbe, C.A. (1976). The Cretaceous and Paleogene sediments of Southern Nigeria. In: Kogbe, C. A., (Ed.). Geology of Nigeria. Elizabethan Publishing Company, Lagos, pp. 273-282.

Kreisa, R.D., Moiola, R.J., Nottvedt, A. (1986). Tidal sand wave facies, Rancho Rojo Sandstone (Permain) Arizona In: Knight, R.J., and McLean, J.R. (Eds.), Shelf Sands and Sandstones: Canadian Society of Petroleum Geologists, Memoir 11: 277-291.

MacEachern, J.A., and Hobbs, T.W. (2004). The ichnological expression of marine and marginal marine conglomerates and conglomeratic intervals, Cretaceous Western Interior Seaway, Alberta and northeastern British Columbia. Bulletin of Canadian Petroleum Geology 52 (1): 77-104.

Mode, A.W., Anidobu, T.M., Ekwenye,O.C., Okwara, I. C. (2019). A Provenance Study of the Paleogene Lithostratigraphic Units of the Niger Delta: An Insight into the Plate-Tectonic Setting. Jordan Journal of Earth and Environmental Sciences 10 (4): 234-246.

Murat, R.C. (1972). Stratigraphy and paleogeography of the Cretaceous and Lower Tertiary in southern Nigeria. In: Dessauvagie, T.F.J. and Whiteman, A.J. (Eds.), African Geology. University of Ibadan Press, Nigeria, pp. 251–266.

Nwajide, C. S. (2013). Geology of Nigeria's Sedimentary Basins. CSS Bookshops Limited, Lagos. 565 pp.

Nwajide, C.S. (1980). Eocene tidal sedimentation in the Anambra Basin, Southern Nigeria. Sedimentary Geology 25: 189-207.S

Nwajide, C.S. (2005). Anambra Basin of Nigeria: Synoptic basin analysis as a basis for evaluating its hydrocarbon prospectivity. In: Okogbue, C.O. (Ed.) Hydrocarbon potentials of the Anambra basin: geology, geochemistry and geohistory perspectives. Proceedings of the 1st seminar organized by Petroleum Technology Development Fund Chair in Geology, University of Nigeria, Nsukka, pp.1-46.

Nwajide, C.S., and Reijers, T.J.A. (1996). Geology of the Southern Anambra Basin. In: Reijers, T.J.A. (Ed.), Selected Chapters on Geology. Shell Petroleum Development Company, Warri, pp. 133–148.

Obi, G.C., Okogbue, C.O., Nwajide, C.S. (2001). Evolution of the Enugu Cuesta: a tectonically driven erosional process. Global Journal of Pure Applied Sciences 7: 321-330.

Oboh-Ikuenobe, F.E., Obi, C.G., Jaramillo C.A. (2005). Lithofacies, palynofacies and sequence stratigraphy of Paleogene strata in Southeastern Nigeria. Journal of African Earth Sciences 41: 79-102.

Odunze, S.O., and Obi, G.C. (2011). Sequence stratigraphic framework of the Imo Formation in the southern Benue Trough. J Min Geol 47(2):135–146.

Okeke, K.K., and Umeji, O.P. (2016). Palynostratigraphy, palynofacies and palaeoenvironment of deposition of Selandian to Aquitanian sediments, southeastern Nigeria, Journal of African Earth Sciences 120: 102-124. DOI: 10.1016/j.jafrearsci.2016.04.020.

Okeke, K.K., (2017). Stratigraphic and palynological studies of the Paleocene to Early Micoene sediments in Awka-Onitsha Area, Niger Delta Basin, south-eastern Nigeria, 240 pp.

Okezie, C.N., and Onuogu, S.A. (1985). The lignites of Southeastern Nigeria. A summary of available information. Geological Survey of Nigeria Occasional Paper 10, 28 pp.

Oloto, I.N. (1984). A Palynological Study of the Late Cretaceous and Tertiary boreholes from Southern Nigerian Sedimentary Basin, Doctoral dissertation, University of Sheffield, Department of Geology.

Onuoha, K.M. (1981). Sediment loading and subsidence in Niger Delta sedimentary basin. Journal of Mining and Geology 18(1): 138 -140.

Parkinson, J. (1907). The post-Cretaceous stratigraphy of Southern Nigeria. Q. J. Geol. Soc. London 63: 311 – 320.

Pemberton, S.G., MacEachern, J.A., Saunders, T. (2004). Stratigraphic applications of substrate-specific ichnofacies: delineating discontinuities in the rock record. In: McIlroy, D. (Ed.) The application of ichnology to palaeoenivronmental and stratigraphic analysis. Geological Society Special Publications 228: 29-62.

Petters, S.W. (1991). Regional Geology of Africa (Lecture Notes in Earth Sciences). Springer-Verlag, Berlin 40, 722.

Petters, S.W. (1995). Foraminiferal biofacies in the Nigerian rift and continental margin deltas. In: Oti, M.N. and Postma, G. (Eds.), Geology of Deltas. A.A. Balkema, Rotterdam, p. 219 – 235.

Plink-Björklund, P. (2005). Stacked fluvial and tide-dominated estuarine deposits in high frequency (fourth-order) sequences of the Eocene Central Basin, Spitsbergen. Sedimentology 52: 391–428.

Ponte, F.C., and Asmus, H.E. (1978). Geological framework of the Brazilian continental margin. Geologische Rundschau 61: 201-235.

Radionova, E.P., Beniamovski, V.N., Iakovleva, A.I., Muzylöv, N.G., Oreshkina, T.V., Shcherbinina, E.A., Kozlova, G.E. (2003). Early Paleogene transgressions: stratigraphical and sedimentological evidence from the northern Peri-Tethys. In: Wing, S.L., Gingerich, P.D., Schmitz, B., Thomas, E. (Eds.), Causes and consequences of globally warm climates in the Early Paleogene. Geological Society of America, Special Papers, pp. 239-262.

Reijers, T.J.A., Petters, S.W., Nwajide, C.S. (1997). The Niger Delta basin. In: Selley, R.C. (Ed.), African Basins. Sedimentary Basins of the World 3. Elsevier Science B.V., Amsterdam, pp. 151 – 172.

Reyment, R.A. (1965). Aspects of the Geology of Nigeria: The stratigraphy of the Cretaceous and Cenozoic deposits, Ibadan University Press, Ibadan, 145 pp.

Reyment, R.A. (1980). Biogeography of the Saharan Cretaceous and Paleocene epicontinental transgressions. Cretaceous Research 1 (4): 299-327.

Reyment, R.A., and Mörner, N.A. (1977). Cretaceous transgressions and regressions exemplified by the South

Atlantic. Palaeontology Society Japan, Special Papers 21: 247-261.

Short, K.C., and Stäuble, A.J. (1967). Outline of geology of Niger Delta. American Association of Petroleum Geologists Bulletin 51: 761-779.

Siesser, W.G., and Dingle, R.V. (1981). Tertiary sea-level movements around southern Africa. The Journal of Geology 89 (4): 523-536.

Sleep, E.H. (1971). The thermal effects of the formation of Atlantic continental margins by continental break up. Geophysical Journal Royal Astronomical Society 24: 325 – 350.

Stevens, N.J., Eastman, J.T., Odunze, S.O., Cooper, L.N., Obi, G.C. (2011). Paleocene Ichthyofauna and palaeoenvironmental setting, Imo formation, southern Nigeria.Neues Jahrb. fur Geol. Palaontologie-Abh. 260 (3): 289-296.

Tessier, B, Billeaud, I., Sorrel, P., Delsinne, N., Lesueur, P. (2011). Infilling stratigraphy of macrotidal tide-dominated estuaries. Controlling mechanisms: sea-level fluctuations, bedrock morphology, sediment supply and climate changes (The examples of the seine estuary and the Mont-Saint-Michel Bay, English Channel, NW France), Sedimentary Geology 297: 62-73. doi: 10.1016/j.sedgeo.2011.02.003.

Thiry, M., and Jacquin, T. (1993). Clay mineral distribution related to rift activity, sea-level changes and palaeoceanography in the Cretaceous of the Atlantic Ocean. Clay Minerals 28: 61-84.

Turcotte, D.L. (1977). The thermal and subsidence history of sedimentary basins. Journal of Geophysical Research 82: 3762 -3766.

Umeji, O.P. (2002). Mid-Tertiary (Late Eocene – Early Miocene) Lignites from Mpu Formation, Abakaliki Basin, southeastern Nigeria. J. Mining and Geol. 38: 111–117.

Umeji, O.P. (2003). Palynological data from the road section at the Ogbunike toll gate, Onitsha, southeastern Nigeria. Journal of Mining and Geology 39: 95–102.

Weaver, C.E. (1989). Clays, muds, and shales (Developments in Sedimentology 44). Elsevier Science Publishers, Netherlands, 818 pp.

White, E.I. (1926). Eocene Fishes of Nigeria. Bulletin of the Geological Survey of Nigeria 10, 78 pp.

Whiteman, A. (1982). Nigeria: its petroleum geology, resources and potential. Graham and Trotman 2, 394.

Yeo, R.K., and Risk, M.J. (1981). The sedimentology, stratigraphy, and preservation of intertidal deposits in the Minas Basin system, Bay of Fundy. Journal of Sedimentary Petrology 51: 245-260.

المملكة الأردنية الهاشمية

صندوق دعم البحث العلمي

الجامعة الهاشمية

المجلة الأردنية
لعلوم الأرض والبيئة

JJEES

مجلة علمية عالمية محكمة

المجلد (١١) العدد (٢)

http:// jjees.hu.edu.jo/

ISSN 1995-6681

المجلة الأردنية لعلوم الأرض والبيئة

مجلة علمية عالمية محكمة

المجلة الأردنية لعلوم الأرض والبيئة: مجلة علمية عالمية محكمة ومفهرسة ومصنفة، تصدر عن عمادة البحث العلمي في الجامعة الهاشمية وبدعم من صندوق البحث العلمي - وزارة التعليم العالي والبحث العلمي، الأردن.

ترسل البحوث إلكترونيا إلى البريد الإلكتروني التالي:

رئيس تحرير المجلة الأردنية لعلوم الأرض والبيئة

jjees@hu.edu.jo

لمزيد من المعلومات والأعداد السابقة يرجى زيارة موقع المجلة على شبكة الانترنت على الرابط التالي:

www.jjees.hu.edu.jo

المملكة الأردنية الهاشمية صندوق دعم البحث العلمي الجامعة الهاشمية

JJEES

المجلة الأردنية لعلوم الأرض والبيئة

المجلد (١١) العدد (٢)

مجلة علمية عالمية محكمة تصدر بدعم من صندوق دعم البحث العلمي

ISSN 1995-6681 jjees.hu.edu.jo حزيران ٢٠٢٠